

Lecture notes on Gasdynamics, AE4-140

by

Prof. Peter Bakker (Delft University of Technology)

and

Prof. Bram van Leer (University of Michigan)

September 3, 2019

Contents

1	Introduction	7
1.1	Introductory comments	7
1.2	Notations, definitions, relations for gases	8
1.3	Equation of state (EOS)	8
1.4	Conservation laws	14
1.4.1	Integral form of the conservation laws	14
1.4.2	Differential form of the flow equations	16
1.5	Euler equations	17
1.6	Entropy	18
1.7	Discontinuities in compressible flow	19
1.7.1	Shock wave	19
1.7.2	Shear wave discontinuity	20
1.7.3	Contact discontinuity	21
1.7.4	Examples of discontinuities in steady flows	21
1.8	One-dimensional unsteady jump equations	22
1.9	Multi-dimensional form of the jump relations	24
1.10	Conservation law of entropy	26
1.11	Too many jump equations	27
1.12	Moving shocks; (t, x) -plane, entropy condition II	28
1.12.1	(t, x) -plane	28
1.12.2	Shock speed	31
1.12.3	Entropy condition II	33
1.13	Numerical approach	33
2	Linearized flow equations	37
2.1	1D acoustics	37
2.1.1	Relation with the wave equation	38
2.1.2	Riemann invariants	39
2.2	Method of Characteristics, M.O.C.	40
2.2.1	Forward M.O.C	40
2.2.2	Backward M.O.C	41
2.2.3	Initial value problem for the wave equation	41
2.2.4	Discontinuities	43
2.3	Piston problem	46
2.3.1	Specific Example: A sinusoidal excursion of the piston for only one single period.	48

2.3.2	Example: a tube with two pistons	50
2.4	Riemann's initial-value problem	50
2.4.1	Example 1: a density discontinuity; (M, \tilde{S}) -diagram	52
2.4.2	Example 2: two colliding flows	55
2.4.3	Example 3: gas streams running away from each other	55
2.4.4	Example 4: Moving piston	57
3	One-dimensional unsteady non-linear flows	61
3.1	Characteristic equations	61
3.2	Simple waves, non-linear	65
3.3	Simple waves created by a moving piston	66
3.4	Centered expansion wave	70
3.4.1	Flow variables in the centered expansion wave	70
3.4.2	Particle path in a centered simple wave	72
3.5	Riemann problem, non-linear	73
3.5.1	Shock moving into a gas; Hugoniot curve	74
3.5.2	Expansion moving into a gas; Poisson curve	76
3.5.3	Example of a Riemann problem	77
3.5.4	Properties of Hugoniot and Poisson curves	77
3.5.5	Solving Riemann problems with a (p, u) -graph	80
3.6	The Method of Characteristics for one-dimensional unsteady flow	82
3.7	Simple compression waves	84
3.8	Wave interactions	89
3.8.1	Two right running shocks	89
3.8.2	Two right running expansion waves	91
3.8.3	Shock interacting with expansion	92
3.8.4	Shock interacting with expansion	93
3.8.5	Interaction of shocks of different family	93
3.8.6	Interaction of two expansions of different family	95
4	Burgers' equation for simple waves	97
4.1	Shock description	97
4.2	Shock formation	99
4.3	Shock formation from a triangular wave	102
4.4	Shock formation from a parabolic curve	104
4.5	Entropy conditions revisited	105
4.6	Wave interaction	109
5	Traffic waves	115
5.1	Definitions, traffic equation	115
5.2	Characteristics and Discontinuities	117
5.3	Traffic light	119
5.4	A chain collision	120

6 Two-Dimensional Inviscid Flow	123
6.1 Governing flow equations	123
6.2 Characteristic form for 2D unsteady flow	126
6.3 Wave propagation in two-dimensional flow	130
7 Steady Two-Dimensional Flow	141
7.1 Characteristic directions	141
7.2 "Time-like" and "space-like"	144
7.3 Equations in flow aligned coordinates	147
7.4 Characteristic equations, compatibility relations	148
7.5 Method of Characteristics; M.O.C.	154
7.6 Method of Waves; M.O.W.	159
7.6.1 Description of the method, simple waves.	159
7.6.2 Interaction of waves	162
7.6.3 M.O.W. for isentropic flows, a calculation scheme	164
7.6.4 Design of a supersonic windtunnel nozzle by M.O.W.	167
8 Two-dimensional steady potential flows	171
8.1 Crocco's Theorem, Velocity Potential, Potential Equation.	171
8.2 Linearized flow; the Prandtl-Glauert equation	174
8.2.1 Linearized pressure coefficient	175
8.2.2 Linearized boundary condition	176
8.2.3 Example 1: a subsonic flow along a wavy wall	177
8.2.4 Example 2: Supersonic flow along a wavy wall.	179
8.3 Characteristics and compatibility relations for potential flow	180
8.3.1 Prandtl-Glauert equation	181
8.3.2 The Full Potential Equation	183
8.4 Two-dimensional flow in the throat of a Laval nozzle	184
8.4.1 Mass flow through a two-dimensional nozzle	190
8.4.2 Literature on the subject	193
9 The 'first non linear' description of steady two dimensional supersonic flow	195
9.1 Inviscid Burgers equation	195
9.2 Discontinuities of the inviscid Burgers equation	197
9.3 Shock pattern created by a biconvex airfoil	202
9.4 Wave interactions	207
9.4.1 Shock-expansion interaction	208
9.4.2 Backward facing slope	209
10 Steady one-dimensional viscous flow	211
10.1 Channel flow: assumptions and basic equations	211
10.2 Constant-area channel flow; Fanno line	215
10.3 A channel with a variable cross-sectional area	219
10.4 Internal structure of a shock wave	224
10.4.1 Introductory comments	224
10.4.2 Navier-Stokes equations for one-dimensional flow	224
10.4.3 Equations of shock structure	225

10.4.4 An estimate for the shock-thickness	226
10.4.5 Entropy production in the shock zone	228
10.4.6 More about the shock structure	228
10.4.7 Special solutions for the shock structure problem	231
10.4.8 Entropy behaviour in the shock zone	234

Chapter 1

Introduction

1.1 Introductory comments

Compressibility of the fluid \implies density is variable
Density = mass/unit volume

What makes compressibility of real importance?

Incompressible flow : fluids (water)
gases (low speed $M \leq 0.3$)

Compressible flow : propagation of sound
wave drag
shock waves
high temperature
combustion
re-entry aerodynamics
high speed flows ($M \gg 1$)

Energy needed to accelerate fluid particles is extracted from two sources:

1. work done by pressure forces
2. decrease of internal energy resulting in a decrease in temperature

1.2 Notations, definitions, relations for gases

Quantity	Symbol	Comment
Density	ρ	mass/unit volume
Specific volume	$v = \frac{1}{\rho}$	volume/unit mass
Pressure	p	
Velocity	\bar{V}, \bar{q}	momentum/unit mass $ \bar{V} \equiv V$ $ \bar{q} \equiv q$
Specific internal energy	e	energy/unit mass
Specific enthalpy	h	$h = e + \frac{p}{\rho}$
Specific total energy	E	$E = e + \frac{1}{2}q^2$
Specific total enthalpy	H	$H = h + \frac{1}{2}q^2 = E + \frac{p}{\rho}$
Specific total entropy	s	probability of state
Temperature	T	
Specific heat at const v,p	c_v, c_p	$c_v = \left(\frac{\partial e}{\partial T}\right)_v$ $c_p = \left(\frac{\partial h}{\partial T}\right)_p$
Ratio of specific heats	γ	$\gamma = \frac{c_p}{c_v}$ ($= 1.4$ for air)
Specific gas constant	R	$R = 287 \frac{\text{J}}{\text{kg K}}$ (air)

1.3 Equation of state (EOS)

- "State principle" (empirically found):

"If the chemical composition of the fluid is fixed then the local thermodynamic state is determined completely by two independent thermodynamic variables".
So, for example:

$$p = f(\rho, e) \quad \text{or} \quad p = f(\rho, h). \quad (1.1)$$

- Thermally perfect gas: c_v and c_p only depend on T , so

$$c_v = c_v(T) \quad \text{and} \quad c_p = c_p(T).$$

Equation of state:

$$p = \rho R T \quad (1.2)$$

R is constant for a particular gas.

Since $c_v = (\frac{\partial e}{\partial T})_v$:

$$e = \int c_v(T) dT \quad (1.3)$$

and $c_p = (\frac{\partial h}{\partial T})_p$:

$$h = \int c_p(T) dT \quad (1.4)$$

Thus $h = e + \frac{p}{\rho}$:

$$\begin{aligned} \int c_p(T) dT &= \int c_v(T) dT + RT \\ R &= c_p(T) - c_v(T) \end{aligned} \quad (1.5)$$

$$c_v(T) = \frac{R}{\gamma(T) - 1}, \quad c_p(T) = \frac{\gamma(T)R}{\gamma(T) - 1} \quad (1.6)$$

- Calorically perfect gas: c_v and c_p are constants
EOS: $\frac{p}{\rho} = RT$, $R = c_p - c_v$

$$e = c_v T = \frac{RT}{\gamma-1} = \frac{p}{\rho(\gamma-1)} \implies$$

$$p = (\gamma - 1)\rho e \quad (1.7)$$

$$h = c_p T = \frac{\gamma R}{\gamma-1} T = \frac{\gamma}{\gamma-1} \frac{p}{\rho} = \gamma e \implies$$

$$p = \frac{\gamma - 1}{\gamma} \rho h \quad (1.8)$$

Air is perfect for temperatures up to 2500 K

For $T < 800$ K air is calorically perfect.

For 800 K $< T < 2500$ K air is thermally perfect.

- Molecular degrees of freedom

From kinetic gas theory we know that the energy is divided according to the “*Principle of Equipartition*”. This means that: “Internal energy of a gas is equally distributed over the available degrees of freedom”. Let n be the number of degrees of freedom, then

$$e = \frac{1}{2}nRT; \quad (1.9)$$

If n is constant, e.g. n is no function of the temperature T , then:

$$c_v = \left(\frac{\partial e}{\partial T} \right)_v = \frac{1}{2}nR \quad (1.10a)$$

$$c_p = R + c_v = \left(\frac{1}{2}n + 1 \right)R \quad (1.10b)$$

When combining (1.10a) and (1.10b), we find that the specific heat ratio is directly related to the degrees of freedom:

$$\gamma = \frac{c_p}{c_v} = \frac{n+2}{n} \quad (1.11)$$

Examples:

1. monatomic gas (He , dissociated gas):
3 degrees of freedom, $n = 3$ so $\gamma = 5/3$.
2. diatomic gas (O_2 , N_2 , air at standard conditions):
a diatomic gas has 5 degrees of freedom: 3 translational and 2 rotational. Then $n = 5$ and $\gamma = 7/5 = 1.4$.

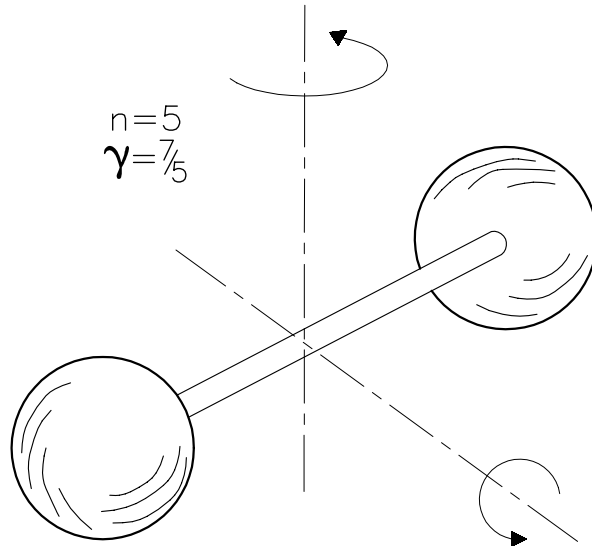


Figure 1.1: Diatomic gas with 5 degrees of freedom, halter model

At higher temperatures due to vibrational excitation two extra degrees of freedom (in the form of a potential and kinetic contribution) become available such that $n = 7$ and $\gamma = 9/7$, see NACA report 1135.

3. monatomic gas in one-dimensional world (only of mathematical interest!):
here there is only one degree of freedom possible, so $n = 1$ and $\gamma = 3$.

- Influence of chemistry on R

The value of R depends on the type of gas because of the different number of particles (molecules, atoms and ions) per unit mass. Multiplying the perfect gas law by the molecular weight μ yields:

$$\mu p v = \mu R T,$$

or,

$$p V = \mathfrak{R} T,$$

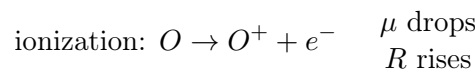
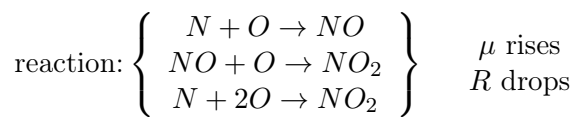
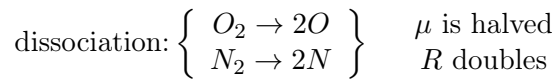
where V is the volume of a mole of gas and \mathfrak{R} is the universal gas constant (gas constant of Regnault):

$$\mathfrak{R} = 8314 \text{ J/(mole K)}$$

The specific gas constant R then becomes: $R = \mathfrak{R}/\mu$.

For air (78% N_2 , 21% O_2 , 1% Ar) with $\mu = 29$ kg/mole it follows that $R = 8314/29 = 287.04$ J/(kg K).

When chemical reactions occur, the value of R changes. Some examples are:



- Entropy

To derive expressions for the entropy we start with the First Law of Thermodynamics:

$$de = dQ + dW$$

For a closed system (no mass transfer!) the increase of internal energy de is found as the sum of heat added to the system dQ and the work performed on the gas in the system dW .

Here the notation d indicates that the increments dQ and dW depend on the type of process (e.g. isothermal, isobaric, isochoric, etc) thus Q and W are *no* state variables! However, entropy *is* a state variable, the entropy difference Δs between two states *only* depends on the thermodynamical (state) properties of the gas in both states.

The first law

$$de = dQ + dW$$

may be written as

$$de = dQ - pdv.$$

For reversible processes $dQ = Tds$ and the First Law can be rewritten as:

$$Tds = de + pdv.$$

For caloric perfect gasses $de = c_v dT$ such that:

$$\begin{aligned} Tds &= c_v dT + pdv \\ ds &= c_v \frac{dT}{T} + \frac{pdv}{T} \\ &= c_v \left(\frac{dp}{p} + \frac{dv}{v} \right) + \frac{R}{v} dv \\ &= c_v \frac{dp}{p} + c_p \frac{dv}{v} \end{aligned}$$

$$ds = c_v \left(\frac{dp}{p} + \gamma \frac{dv}{v} \right) \quad (1.12)$$

This equation can be integrated, resulting in:

$$s - s_0 = c_v \ln \left(\frac{pv^\gamma}{p_0 v_0^\gamma} \right)$$

If the process is also adiabatic : $dQ = 0 \implies ds = 0 \implies s = \text{constant}$.

A reversible adiabatic process is called an isentropic process having :

$$s = \text{constant} \implies pv^\gamma = \text{constant}$$

or

$$p = C\rho^\gamma \quad (1.13)$$

which is called Poisson's relation.

For an irreversible process: Second Law of Thermodynamics $\implies Tds > dQ$. This implies for adiabatic flow ($dQ = 0$) that $ds > 0$.

- Speed of sound

The propagation of sound waves through a gas is a reversible adiabatic process. The speed of sound is denoted by a .

For sound waves it is assumed that:

- perturbations in density, pressure and temperature are infinitely small, and
- the propagation is reversible and adiabatic \Rightarrow isentropic.

Although it is mentioned here as an assumption, one can actually prove that when considering small perturbations, a soundwave is actually isentropic.

The speed of sound is defined by:

$$a^2 = \left(\frac{\partial p}{\partial \rho} \right)_s ; \quad (1.14)$$

where the subscript 's' expresses that sound propagation is assumed to be an isentropic process.

Theorem

$$a^2 = \left(\frac{\partial p}{\partial \rho} \right)_e + \frac{p}{\rho^2} \left(\frac{\partial \rho}{\partial e} \right)_\rho \quad (1.15)$$

If the equation of state is given as $p = p(\rho, e)$ then it is logical to have an equation for the sound velocity wherein ρ and e are the independent variables.

Proof

Sound propagation is isentropic, so $ds = 0$, therefore we can write that

$$de + pd \left(\frac{1}{\rho} \right) = 0.$$

$$de + pd \left(\frac{1}{\rho} \right) = \left(\frac{\partial e}{\partial p} \right)_\rho dp + \left(\frac{\partial e}{\partial \rho} \right)_p d\rho - \frac{p}{\rho^2} d\rho = 0,$$

or

$$\left(\frac{\partial e}{\partial p} \right)_\rho dp + \left\{ \left(\frac{\partial e}{\partial \rho} \right)_p - \frac{p}{\rho^2} \right\} d\rho = 0,$$

so

$$\frac{dp}{d\rho} = \left(\frac{\partial e}{\partial p} \right)_\rho^{-1} \left\{ - \left(\frac{\partial e}{\partial \rho} \right)_p + \frac{p}{\rho^2} \right\} \quad (*)$$

Since we have assumed that $ds = 0$ we may conclude that $\frac{dp}{d\rho}$ is actually $\left(\frac{dp}{d\rho} \right)_{ds=0}$ or $\left(\frac{dp}{d\rho} \right)_s$. Which results in the following equation:

$$\left(\frac{\partial p}{\partial \rho} \right)_s = \left(\frac{\partial e}{\partial p} \right)_\rho^{-1} \left\{ - \left(\frac{\partial e}{\partial \rho} \right)_p + \frac{p}{\rho^2} \right\}$$

Multivariable calculus teaches us that if p , ρ and e are constrained by $f(p, \rho, e) = 0$ then

$$\left(\frac{\partial p}{\partial e} \right)_\rho \cdot \left(\frac{\partial e}{\partial \rho} \right)_p \cdot \left(\frac{\partial \rho}{\partial p} \right)_e = -1,$$

from which we can derive

$$\left(\frac{\partial e}{\partial \rho} \right)_p = \frac{-1}{\left(\frac{\partial p}{\partial e} \right)_\rho \left(\frac{\partial \rho}{\partial p} \right)_e},$$

Inserting $\left(\frac{\partial e}{\partial \rho} \right)_p$ in $(*)$ results into

$$a^2 = \left(\frac{\partial p}{\partial \rho} \right)_s = \left(\frac{\partial p}{\partial \rho} \right)_e + \frac{p}{\rho^2} \left(\frac{\partial p}{\partial e} \right)_\rho,$$

So equation (1.15) is proven. \square

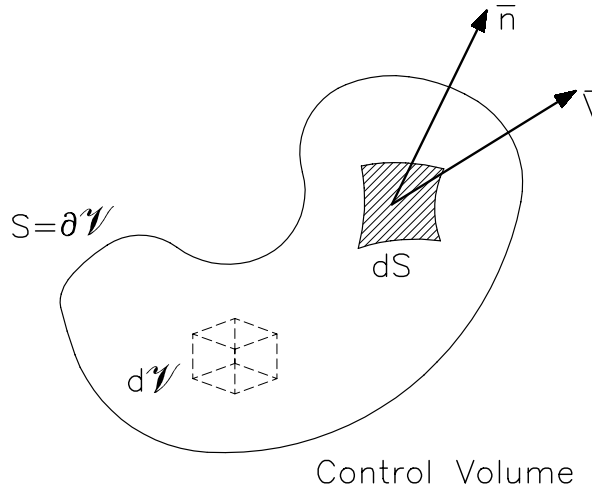


Figure 1.2: Control volume

Using the equation of state in the form

$$p = (\gamma - 1)\rho e$$

we can now easily determine the sound velocity from equation (1.14):

$$\begin{aligned} a^2 &= (\gamma - 1)e + \frac{p}{\rho^2}(\gamma - 1)\rho \\ &= (\gamma - 1) \left(e + \frac{p}{\rho} \right) \\ &= (\gamma - 1)h \\ &= (\gamma - 1)c_p T \\ &= \gamma R T \\ &= \frac{\gamma p}{\rho} \end{aligned}$$

1.4 Conservation laws

1.4.1 Integral form of the conservation laws

Consider a control volume V fixed in space with surface $S = \partial V$, see figure 1.2. Let dV be a small volume element and let dS be a small surface element. Let \bar{n} be the outward unit normal on dS . The integral form of the conservation laws for mass, momentum and energy are then written as follows.

- Mass conservation

$$\underbrace{\frac{d}{dt} \iiint_V \rho dV}_{\text{time rate of change of mass inside } V} + \underbrace{\iint_S \rho \bar{V} \cdot \bar{n} dS}_{\text{net mass flow out } V \text{ through surface } S} = 0 \quad (1.16)$$

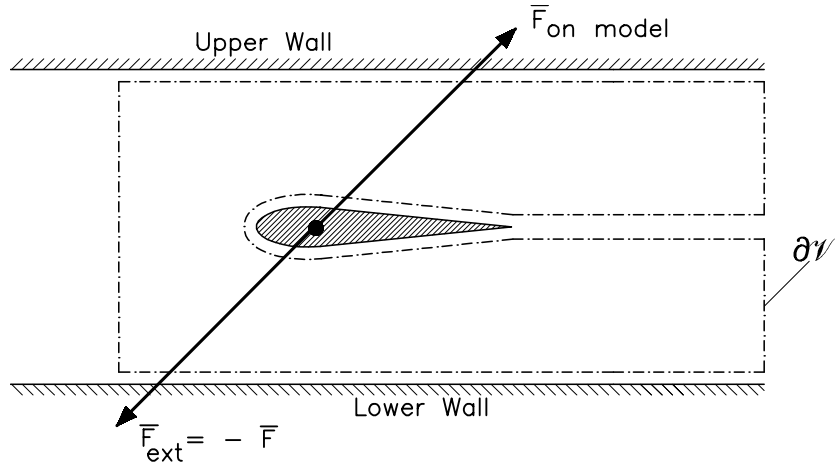


Figure 1.3: Example of an external force ($\bar{F}_{\text{external}}$) on a control volume

- Momentum conservation

$$\begin{aligned}
 & \underbrace{\frac{d}{dt} \iiint_V \rho \bar{V} dV}_{\text{time rate of change of momentum inside } V} + \underbrace{\iint_S \rho \bar{V} \bar{V} \cdot \bar{n} dS}_{\text{net flow of momentum across } S} + \\
 & \underbrace{\iint_S p \cdot \bar{n} dS}_{\text{surface force due to pressure}} = \underbrace{\iiint_V \rho \bar{f} dV}_{\text{body forces}} + \underbrace{\bar{F}_{\text{external}}}_{\text{external forces (strut force, enclosure force)}} + \quad (1.17)
 \end{aligned}$$

viscous forces

Comments

1. Example of $\bar{F}_{\text{external}}$

Consider a windtunnel model as shown in figure 1.3. The force \bar{F} on the model acts as an external force $\bar{F}_{\text{external}} = -\bar{F}$ on the control volume V . The force $\bar{F}_{\text{external}} = -\bar{F}$ is also formed as the integral of the surface forces (both due to pressure as well due to viscous stresses) along the profile contour.

2. \bar{F}_{visc} contains the contribution of the viscous forces

$$\bar{F}_{\text{visc}} = \iint_{\partial V} \bar{\tau} \cdot \bar{n} dS \quad (1.18)$$

where $\bar{\tau}(\bar{x}, t)$ is the viscous stress tensor.

For a Newtonian fluid we have

$$\tau_{ij} = \mu \left(\frac{\partial u_i}{\partial x_j} + \frac{\partial u_j}{\partial x_i} \right) + \lambda \delta_{ij} \frac{\partial u_k}{\partial x_k} \quad (1.19)$$

here μ and λ are viscosity coefficients which in general depend on temperature.

- Energy equation

$$\begin{aligned}
 & \underbrace{\frac{d}{dt} \iiint_V \rho E dV}_{\text{time rate of change of energy inside } V} + \underbrace{\iint_S \rho E \bar{V} \cdot \bar{n} dS}_{\text{net flow of energy across } S} + \\
 & = \underbrace{\iiint_V \rho \bar{f} \cdot \bar{V} dV}_{\text{work done by body forces}} + \\
 & + \underbrace{\dot{W}_{\text{visc}} + \dot{W}_{\text{ext}}}_{\text{work done by viscous and external forces}}
 \end{aligned} \tag{1.20}$$

heat added to the fluid; conduction, radiation, condensation

Comments

1. Since the control volume is fixed in space, the time derivative can be brought into the integral as $\frac{\partial}{\partial t}$.
2. If $\bar{f} = -\nabla\Phi(\bar{x})$ then we have a conservative force field. In that case the body force term in the energy equation can be accounted for by including the potential energy $\Phi(\bar{x})$ in E and H .
3. \dot{Q} has a volume (e.g. combustion) and a surface component (e.g. conduction).

$$\dot{Q} = \underbrace{\iiint_V \rho c dV}_{\text{volumetric heating}} - \underbrace{\iint_S \bar{q} \cdot \bar{n} dS}_{\text{heat flux due to conduction}} \tag{1.21}$$

Fouriers law:

$$\bar{q} = -k \nabla T \tag{1.22}$$

with k as heat conduction coefficient.

The integral forms of the conservation laws have a wide range of applicability. Actually the only assumption to be made is that the integrals are integrable in V and over ∂V . The integrands may be discontinuous.

1.4.2 Differential form of the flow equations

To derive the differential form of the flow equations (PDE's) the surface integrals in the integral form have to be transformed into volume integrals. This can be done by applying the divergence and the gradient theorem.

Divergence theorem:

$$\iiint_V \nabla \cdot \bar{A} dV = \iint_S \bar{A} \cdot \bar{n} dS. \tag{1.23}$$

Gradient theorem:

$$\iiint_V \nabla p dV = \iint_S p \bar{n} dS. \tag{1.24}$$

Combining the volume integrals and recalling that V is fixed in space and arbitrarily chosen, the integrand has to be zero for all points in space. When the contributions of viscosity and heat transfer are omitted, the following set of partial differential equations results:

Continuity equation

$$\frac{\partial \rho}{\partial t} + \nabla \cdot \rho \bar{V} = 0 \quad (1.25)$$

Momentum equation

$$\frac{\partial}{\partial t} \rho \bar{V} + \nabla \cdot \rho \bar{V} \bar{V} + \nabla p = \rho \bar{f} \quad (1.26)$$

Energy equation

$$\frac{\partial}{\partial t} \rho E + \nabla \cdot \rho \bar{V} E + \nabla \cdot p \bar{V} = \rho \bar{V} \cdot \bar{f} \quad (1.27)$$

With $H = E + \frac{p}{\rho}$ we have $\nabla \cdot \rho \bar{V} E + \nabla \cdot p \bar{V} = \nabla \cdot \rho H \bar{V}$.

1.5 Euler equations

The equations (1.25), (1.26) and (1.27) describe a mathematical model of compressible flows where the effects of viscosity, heat conduction and external heating have been neglected. If also external forces are neglected ($\bar{f} = 0$) the Euler equations result:

$$\frac{\partial \rho}{\partial t} + \nabla \cdot \rho \bar{V} = 0 \quad (1.28)$$

$$\frac{\partial}{\partial t} \rho \bar{V} + \nabla \cdot \rho \bar{V} \bar{V} + \nabla p = 0 \quad (1.29)$$

$$\frac{\partial}{\partial t} \rho E + \nabla \cdot \rho H \bar{V} = 0 \quad (1.30)$$

These equations can also be written in the compact form:

$$\frac{\partial \tilde{U}}{\partial t} + \frac{\partial \tilde{F}}{\partial x} + \frac{\partial \tilde{G}}{\partial y} + \frac{\partial \tilde{H}}{\partial z} = 0 \quad (1.31)$$

with

$$\tilde{U} = \begin{pmatrix} \rho \\ \rho u \\ \rho v \\ \rho w \\ \rho E \end{pmatrix}, \quad \tilde{F} = \begin{pmatrix} \rho u \\ p + \rho u^2 \\ \rho uv \\ \rho uw \\ \rho uH \end{pmatrix}, \quad \tilde{G} = \begin{pmatrix} \rho v \\ \rho vu \\ p + \rho v^2 \\ \rho vw \\ \rho vH \end{pmatrix}, \quad \tilde{H} = \begin{pmatrix} \rho w \\ \rho wu \\ \rho wv \\ p + \rho w^2 \\ \rho wH \end{pmatrix}.$$

\tilde{U} is the vector of state quantities and \tilde{F} , \tilde{G} and \tilde{H} are flux vectors.

Equation (1.31) gives the Euler equations in the so-called conservative form.

Non-conservative forms of the Euler equations follow by expanding the derivatives and introducing the substantial derivative:

$$\frac{D}{Dt} = \frac{\partial}{\partial t} + \bar{V} \cdot \nabla. \quad (1.32)$$

Which results in:

$$\frac{D\rho}{Dt} + \rho \nabla \cdot \bar{V} = 0, \quad (1.33)$$

$$\rho \frac{D\bar{V}}{Dt} + \nabla p = 0, \quad (1.34)$$

$$\rho \frac{DE}{Dt} + \nabla \cdot p\bar{V} = 0. \quad (1.35)$$

1.6 Entropy

For a compressible flow governed by the Euler equations it can be shown that the entropy s is constant when moving with a particle.

The first law of thermodynamics $dQ = Tds$ gives

$$Tds = de + pd \left(\frac{1}{\rho} \right).$$

When following a fluid particle, $\frac{Ds}{Dt}$ determines the value of s when time progresses and the particle is convected with the flow,

$$\frac{Ds}{Dt} = \frac{1}{T} \left(\frac{De}{Dt} - \frac{p}{\rho^2} \frac{D\rho}{Dt} \right).$$

Using (1.33) and (1.35) follows

$$\frac{Ds}{Dt} = \frac{1}{T} \left\{ -\frac{1}{\rho} \nabla \cdot p\bar{V} - \bar{V} \cdot \frac{D\bar{V}}{Dt} + \frac{p}{\rho^2} \rho \nabla \cdot \bar{V} \right\}.$$

Introducing (1.34) for $\frac{D\bar{V}}{Dt}$:

$$\frac{Ds}{Dt} = \frac{1}{T} \left\{ -\frac{p}{\rho} \nabla \cdot \bar{V} - \frac{\bar{V}}{\rho} \cdot \nabla p + \bar{V} \cdot \frac{\nabla p}{\rho} + \frac{p}{\rho} \nabla \cdot \bar{V} \right\}.$$

or

$$\frac{Ds}{Dt} = 0 \quad (1.36)$$

So the entropy is constant when moving with a fluid particle. For steady flows this implies that the entropy is constant along a streamline.

The fact that entropy is convected with a fluid particle is a typical result for Euler flows where non-adiabatic processes (external heating), heat conduction and viscous effects are absent.

1.7 Discontinuities in compressible flow

The Euler equations allow for the appearance of discontinuities which are the so called '*weak solutions*'. Across such a discontinuity, certain jump relations hold. These jump relations will be derived in section 1.8, in this paragraph the physical aspects of three different types of discontinuities will be first discussed on a more qualitative basis. They are represented as plane waves appearing in a two-dimensional unsteady flow. The following discontinuities can be identified:

- Shock wave
- Shear wave
- Contact discontinuity

1.7.1 Shock wave

First we consider the shock wave discontinuity, see figure 1.4.

We see a shock wave that moves with velocity c_s . The shock separates the flow domain into

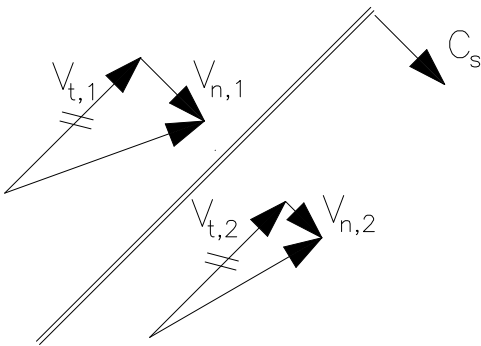
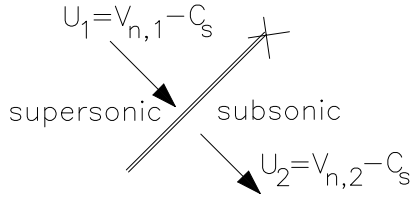
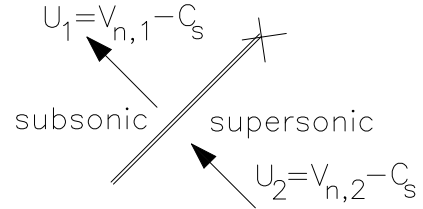


Figure 1.4: Shock wave (viewed in laboratory frame)

two parts having different fluid velocities: V_1 (components V_{n1} and V_{t1}) and V_2 (components V_{n2} and V_{t2}). The velocities are defined w.r.t a fixed reference frame called the '*laboratory frame*'. For steady shocks it can be shown that the tangential velocity component is constant over the shock while the normal component decreases in flow direction, whereas the thermodynamic variables p , ρ , e , T and s increase in flow direction. For steady normal shocks the pre-state is always supersonic and the post-state is always subsonic.

For moving shocks this poses a problem. Take the general situation of a moving shock as depicted in figure 1.4. Where do we find the pre and post-state?

To answer this question the shock is brought into a reference frame that moves with the shock; this frame is called the '*shock frame*'. Figures 1.5 and 1.6 show the situation for a steady flow and a non-moving shock. Viewing figures 1.5 and 1.6, the normal velocities in domain ① and ② are respectively $U_1 = V_{n1} - c_s$ and $U_2 = V_{n2} - c_s$. Two different possibilities occur.

Figure 1.5: $U_1 > 0$, 1 is pre-stateFigure 1.6: $U_1 < 0$, 1 is post-state**Case 1: $U_1 > 0$ (figure 1.5)**

If $U_1 > 0$ then the steady shock relations tell us that also $U_2 > 0$. Thus domain ① appears to be the pre-state where the normal flow component is supersonic; so $U_1 > a_1$ and the thermodynamic variables satisfy: $p_2 > p_1$, $\rho_2 > \rho_1$, $T_2 > T_1$, $e_2 > e_1$ and $s_2 > s_1$.

Case 2: $U_1 < 0$ (figure 1.6)

If $U_1 < 0$ then domain ① appears to be the post-state of the shock and domain ② is now the pre-state of the shock. This means that domain ② is supersonic and domain ① is subsonic ($|U_1| < a_1$). The thermodynamic variables satisfy: $p_2 < p_1$, $\rho_2 < \rho_1$, $T_2 < T_1$, $e_2 < e_1$ and $s_2 < s_1$.

The tangential velocities V_{t1} and V_{t2} are equal, so $V_{t1} = V_{t2}$ both in the steady and in the unsteady situation.

1.7.2 Shear wave discontinuity

A moving shear wave discontinuity is depicted in figure 1.7. The shear wave moves with a velocity c_s normal to its front. The fluid on either side of the shear wave has a normal velocity equal to the shear wave velocity: $V_{n1} = V_{n2} = c_s$. This implies that the shear wave is convected with the fluid. However, there is a tangential velocity jump across the wave: $V_{t1} \neq V_{t2}$. By definition the thermodynamic variables p , ρ , e , T and s are continuous across a shear wave.

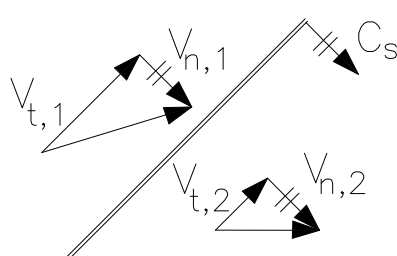


Figure 1.7: Shear wave

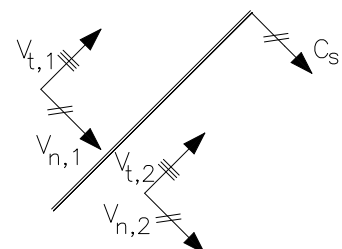


Figure 1.8: Contact discontinuity (may be moving)

1.7.3 Contact discontinuity

A contact discontinuity that moves w.r.t the laboratory frame is shown in figure 1.8. Typical for a contact discontinuity is that ρ , e and s jump across the discontinuity while the velocity and pressure are continuous. This implies that a contact discontinuity convects with the fluid, thus $V_{n1} = V_{n2} = c_s$. Often a contact discontinuity and a shear wave are superimposed.

A summary of the properties of various discontinuities can be found in table 1.1.

Table 1.1: Summary of the properties of various discontinuities

	v_n	v_t	c	p	ρ	e	s
Shock wave	J	C	c_s	J	J	J	J
Shear wave	C	J	v_n	C	C	C	C
Contact discontinuity	C	C	v_n	C	J	J	J
Shear + contact	C	J	v_n	C	J	J	J

1.7.4 Examples of discontinuities in steady flows

Flow over a ramp in a channel

In this flow field an oblique shock reflects on a wall, causing a lambda-shock. At the so-called triple point a superposition of a shear wave and a contact discontinuity occurs. Across this discontinuity the pressure is continuous, the entropy (s), the density (ρ) and the tangential velocity (v_t) jump, see figure 1.9.

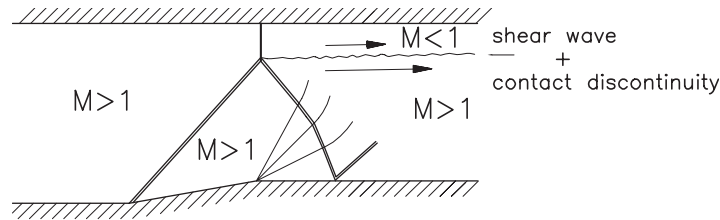


Figure 1.9: Flow over a ramp in a channel

Flow in a channel with two unequal ramps

The ramps generate two shocks which run downstream and intersect (figure 1.10). At

the intersection the shocks interact and again two shocks are produced together with a shear wave/contact discontinuity. This fully supersonic steady 2D flow has a strong analogy in 1D unsteady flow (see next chapters).

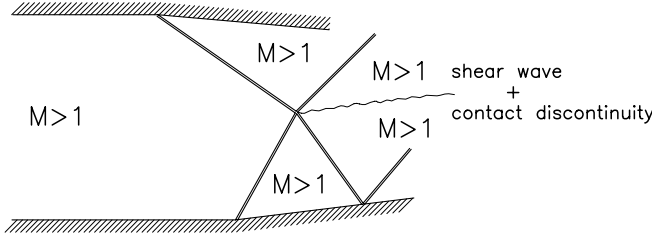


Figure 1.10: Flow in channel with two unequal ramps

Flow over two successive ramps

Due to the presence of the ramps, two shocks of the same family are produced (figure 1.11). They converge and at the intersection a much stronger single shock is formed combined with a shear wave/contact discontinuity. Also in this case a 1D unsteady analogy exists.

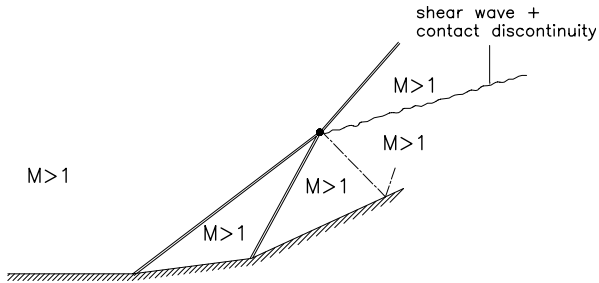


Figure 1.11: Flow over two successive ramps

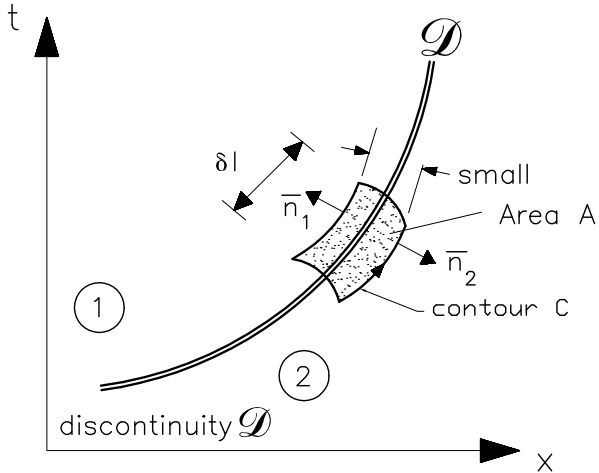
1.8 One-dimensional unsteady jump equations

Now that we have had a qualitative discussion of discontinuities in compressible flows, let's have a closer look at the governing relations for shock waves. To that end, consider a shock discontinuity \mathcal{D} that appears in a one-dimensional unsteady flow. The shock path is depicted by the curve \mathcal{D} in the (t, x) -plane, see figure 1.12. The flow on either side of the discontinuity is governed by the Euler equations (see equation (1.31), omitting the tildes ' \sim '):

$$\frac{\partial U}{\partial t} + \frac{\partial F}{\partial x} = 0, \quad (1.37)$$

where

$$U = \begin{pmatrix} \rho \\ \rho u \\ \rho E \end{pmatrix}, \quad F = \begin{pmatrix} \rho u \\ p + \rho u^2 \\ \rho u H \end{pmatrix}. \quad (1.38)$$

Figure 1.12: Shock discontinuity in the (t, x) -plane

The question is now, which jump corresponds to the continuous solutions in ① and ②. To find the answer we take a small element δl along the shock path and we assume that δl is so small that the shock path can be approximated by a straight line element. This shock element is surrounded by the closed contour C that encloses an area \mathcal{A} . Next we apply the *divergence theorem* to the area \mathcal{A} in the space-time domain:

$$\oint_c \bar{A} \cdot \bar{n} \, dl = \iint_{\mathcal{A}} \nabla \cdot \bar{A} \, d\mathcal{A}$$

with

$$\bar{A} = \begin{pmatrix} U \\ F \end{pmatrix}, \quad \bar{n} = \begin{pmatrix} n_t \\ n_x \end{pmatrix}, \quad \text{and} \quad \nabla = \begin{pmatrix} \frac{\partial}{\partial t} \\ \frac{\partial}{\partial x} \end{pmatrix}.$$

Now we can write

$$\oint_c \begin{pmatrix} U \\ F \end{pmatrix} \cdot \bar{n} \, dl = \iint_{\mathcal{A}} \left(\frac{\partial U}{\partial t} + \frac{\partial F}{\partial x} \right) \, d\mathcal{A} = 0$$

To obtain the jump relations across the discontinuity \mathcal{D} choose the contour C tightly around an element of \mathcal{D} :

$$\begin{pmatrix} U \\ F \end{pmatrix} \cdot \bar{n}_2 \, \delta l + \begin{pmatrix} U \\ F \end{pmatrix} \cdot \bar{n}_1 \, \delta l = 0.$$

Since $\bar{n}_1 = -\bar{n}_2$, we can write

$$\begin{pmatrix} U_2 - U_1 \\ F_2 - F_1 \end{pmatrix} \cdot \bar{n}_2 = 0 \quad \text{or,}$$

$$(U_2 - U_1)n_{2t} + (F_2 - F_1)n_{2x} = 0.$$

where the subscript ‘ t ’ denotes a temporal component of the normal vector, and the subscript ‘ x ’ denotes a spatial component. This can be written as:

$$(U_2 - U_1)\frac{n_{2t}}{n_{2x}} + (F_2 - F_1) = 0$$

and since \bar{n}_2 is normal to \mathcal{D} :

$$\frac{n_{2t}}{n_{2x}} \cdot \left(\frac{dt}{dx} \right)_{\mathcal{D}} = -1.$$

Since $\left(\frac{dt}{dx} \right)_{\mathcal{D}}$ is the shock velocity $V_{\mathcal{D}}$ we finally get that:

$$-V_{\mathcal{D}}(U_2 - U_1) + (F_2 - F_1) = 0,$$

or

$$\mathbf{V}_{\mathcal{D}} [\mathbf{U}] = [\mathbf{F}], \quad (1.39)$$

where $[\cdot] = (\cdot)_2 - (\cdot)_1$ expresses the difference between state 2 and state 1. Equation (1.39) is the jump relation for one-dimensional steady flow.

Consider the special case that the discontinuity is steady, i.e. $V_{\mathcal{D}} = 0$. Equation (1.39) then reduces to:

$$[F] = 0, \quad \text{or} \quad F_2 = F_1$$

and if we substitute the elements of F from equation 1.38:

$$\rho_2 u_2 = \rho_1 u_1, \quad (1.40a)$$

$$p_2 + \rho_2 u_2^2 = p_1 + \rho_1 u_1^2, \quad (1.40b)$$

$$\rho_2 u_2 H_2 = \rho_1 u_1 H_1. \quad (1.40c)$$

we get the well-known Rankine-Hugoniot relations (1.40a)–(1.40c) for steady normal shock waves! In the (t, x) -plane this steady situation looks like figure 1.13.

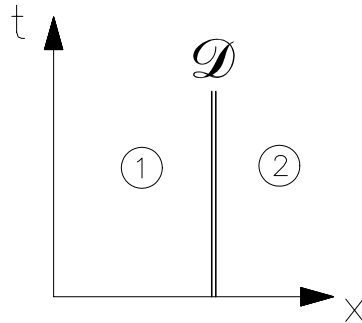


Figure 1.13: Steady shock in the (t, x) -plane

1.9 Multi-dimensional form of the jump relations

Now that we have established the jump relations in 1D we can also have a look at the multi-dimensional form. Consider a discontinuity \mathcal{D} moving with velocity $\bar{V}_{\mathcal{D}}$ in a three-dimensional space. Let $\bar{n}_{\mathcal{D}}$ be the unit vector in space normal to \mathcal{D} pointing from ① to ②, see figure 1.14.

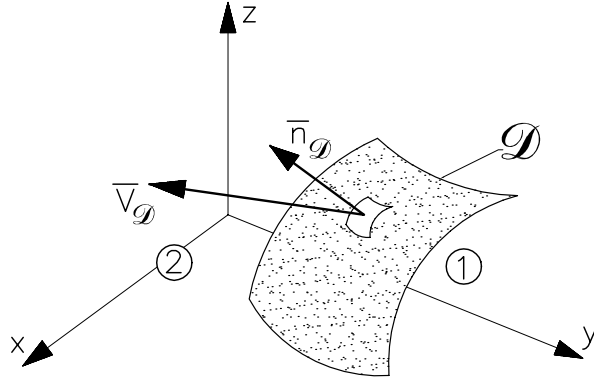


Figure 1.14: Discontinuity in a three-dimensional space

The governing equations for this unsteady three-dimensional problem are

$$\frac{\partial \tilde{U}}{\partial t} + \frac{\partial \tilde{F}}{\partial x} + \frac{\partial \tilde{G}}{\partial y} + \frac{\partial \tilde{H}}{\partial z} = 0.$$

To find the multi-dimensional jump relation, we apply equation (1.39) to an element of \mathcal{D} . This element moves with a velocity $(\bar{V}_D \cdot \bar{n}_D)$ in the direction of its normal, so that

$$(\bar{V}_D \cdot \bar{n}_D) [\tilde{U}] = [\tilde{F}] n_{D_x} + [\tilde{G}] n_{D_y} + [\tilde{H}] n_{D_z}. \quad (1.41)$$

With the definitions of \tilde{U} , \tilde{F} , \tilde{G} and \tilde{H} this can be rearranged into:

$$[\rho(\bar{V} - \bar{V}_D) \cdot \bar{n}_D] = 0 \quad (1.42a)$$

$$[\rho\bar{V}(\bar{V} - \bar{V}_D) \cdot \bar{n}_D + p\bar{n}_D] = 0 \quad (1.42b)$$

$$[\rho E(\bar{V} - \bar{V}_D) \cdot \bar{n}_D + p\bar{V} \cdot \bar{n}_D] = 0. \quad (1.42c)$$

Using discrete algebra:

$$[\bar{a} \cdot \bar{b}] = [\bar{a}] \langle \bar{b} \rangle + [\bar{b}] \langle \bar{a} \rangle,$$

where

$[\bar{a}] = (\bar{a})_2 - (\bar{a})_1$ is the difference and

$\langle \bar{a} \rangle = \frac{1}{2}(\bar{a}_2 + \bar{a}_1)$ is the mean value.

The multi-dimensional jump relations can be brought in the form

$$[\rho(\bar{V} - \bar{V}_D) \cdot \bar{n}_D] = 0 \quad (1.43a)$$

$$[\rho(\bar{V} - \bar{V}_D)(\bar{V} - \bar{V}_D) \cdot \bar{n}_D + p\bar{n}_D] = 0 \quad (1.43b)$$

$$[\rho \left(h + \frac{1}{2} |\bar{V} - \bar{V}_D|^2 \right) (\bar{V} - \bar{V}_D) \cdot \bar{n}_D] = 0. \quad (1.43c)$$

The jump relations given in equations (1.43a)–(1.43c) are again the well-known *Rankine-Hugoniot* relations.

Reversibility of jump conditions

The jump relations are invariant under exchange of states ① and ②. Particularly with regard to shocks, the jump relations cannot distinguish between the *pre-shock state* and the *post-shock state*. Since in a shock irreversible processes (viscous dissipation, heat conduction) take place, a criterion is needed to indicate the direction of time.

When considering a shock wave, we have seen that there is no heat exchange which means that the shock process is *adiabatic*. For an irreversible adiabatic flow we know that $ds > 0$, so entropy can be used to keep track of the direction of time in the process: *a particle that crosses a shock experiences a rise of entropy* so the condition takes the form of an inequality, which we will call “the entropy condition”.

Summary

For the unambiguous description of an inviscid flow we need:

1. PDE's for the flow away from discontinuities, e.g. given as equation (1.31);
2. jump equations, valid across discontinuities e.g. given as equations (1.43a) to (1.43c);
3. an entropy condition; various formulations are in use, the first condition reads as:

Entropy condition I

A fluid particle passing through a shock increases its entropy.

1.10 Conservation law of entropy

For an adiabatic reversible flow we have that:

$$\frac{Ds}{Dt} = 0$$

thus, entropy is convected with a fluid particle (see also section 1.5). In case of a one-dimensional unsteady flow this reduces to:

$$\frac{\partial s}{\partial t} + u \frac{\partial s}{\partial x} = 0 \quad (1.44a)$$

Let us combine this equation with conservation of mass:

$$\frac{\partial \rho}{\partial t} + \frac{\partial \rho u}{\partial x} = 0. \quad (1.44b)$$

Multiply (1.44a) with ρ and (1.44b) with s and add:

$$\frac{\partial(\rho s)}{\partial t} + \frac{\partial}{\partial x}(\rho u s) = 0 \quad (1.45)$$

This equation expresses conservation of the entropy density ρs . Be careful here! (1.45) is not valid for irreversible processes, so it cannot be used to calculate the entropy jump across a

shock. The entropy jump $[s]$ follows from the state variables determined by the other jump relations, e.g. (1.39). Recall: the entropy is *not* a state variable.

In the case of an irreversible flow (1.45) should be replaced by:

$$(\rho s)_t + (\rho u s)_x \geq 0$$

leading to the jump *inequality*:

$$-V_D[\rho s] + [\rho u s] \geq 0. \quad (1.46)$$

Using discrete algebra and the density jump equation

$$V_D[\rho] = [\rho u]$$

we can reduce equation (1.46) to

$$\left(\frac{\langle \rho u \rangle}{\langle \rho \rangle} - V_D \right) [s] \geq 0. \quad (1.47)$$

Check

Assume steady flow, i.e. $V_D = 0$; then forward flow with $\langle \rho u \rangle > 0$ means that $[s] > 0$ or $s_2 > s_1$, a result as expected! Backward flow with $\langle \rho u \rangle < 0$ means $s_2 < s_1$!

1.11 Too many jump equations

For steady flow the jump equation $[F] = 0$ results into the so called *Rankine-Hugoniot* relations:

$$\rho_1 u_1 = \rho_2 u_2 \quad (1.48a)$$

$$p_1 + \rho_1 u_1^2 = p_2 + \rho_2 u_2^2 \quad (1.48b)$$

$$\rho_1 u_1 H_1 = \rho_2 u_2 H_2 \quad (1.48c)$$

From (1.48a)–(1.48c) many useful relations can be derived, e.g.

$$\frac{p_2}{p_1} = 1 + \frac{2\gamma}{\gamma+1} (M_1^2 - 1) \quad (1.49a)$$

$$\frac{\rho_2}{\rho_1} = \frac{(\gamma+1)}{2+(\gamma-1)} \frac{M_1^2}{M_1^2} \quad (1.49b)$$

$$\frac{T_2}{T_1} = \left\{ 1 + \frac{2\gamma}{\gamma+1} (M_1^2 - 1) \right\} \frac{2 + (\gamma-1)M_1^2}{(\gamma+1)M_1^2} \quad (1.49c)$$

$$\frac{u_2}{u_1} = 1 - \frac{2}{\gamma+1} \frac{(M_1^2 - 1)}{M_1^2} \quad (1.49d)$$

where $M_1 = u_1/a_1$ is the Mach number of the flow in the pre-shock state.

For unsteady flows with moving shock waves these relations are less useful since they contain the Mach number M_1 which is not *a priori* known in the moving shock case. Moreover

equations (1.49a) to (1.49d) are only valid for steady flows. In order to use them for a moving shock one has to go to the shock frame, find the appropriate velocities, etc. This is a cumbersome job and not always straightforward.

For moving shocks it is therefore much more convenient to have a jump relation that relates only thermodynamic variables. Starting with

$$V_D[U] = [F]$$

and eliminating V_D one can derive the Hugoniot relation

$$\langle p \rangle \Delta \left(\frac{1}{\rho} \right) + \Delta e = 0. \quad (1.50)$$

The proof is left as a homework problem. For a perfect gas with $e = c_v T$ and $p = (\gamma - 1)\rho e$ we can rewrite equation (1.50):

$$\frac{\rho_2}{\rho_1} = \frac{1 + \frac{\gamma+1}{\gamma-1} \frac{p_2}{p_1}}{\frac{\gamma+1}{\gamma-1} + \frac{p_2}{p_1}}. \quad (1.51)$$

Observe that for strong shocks with $\frac{p_2}{p_1} \rightarrow \infty$, the density ratio remains finite and takes the value

$$\left(\frac{\rho_2}{\rho_1} \right)_{\max} = \frac{\gamma + 1}{\gamma - 1}.$$

The maximum density ratios obtainable depend on γ , for example:

$$\gamma = \frac{5}{3} : \left(\frac{\rho_2}{\rho_1} \right)_{\max} = 4$$

$$\gamma = \frac{7}{5} : \left(\frac{\rho_2}{\rho_1} \right)_{\max} = 6.$$

1.12 Moving shocks; (t, x) -plane, entropy condition II

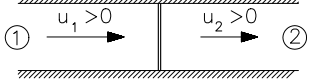
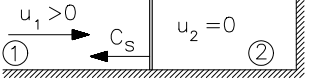
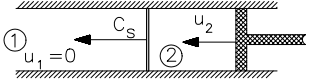
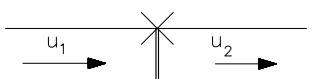
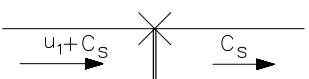
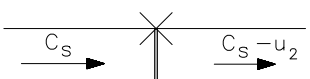
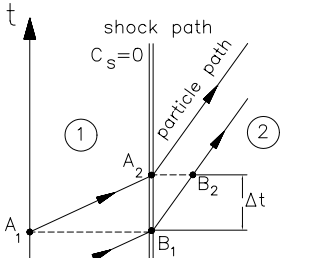
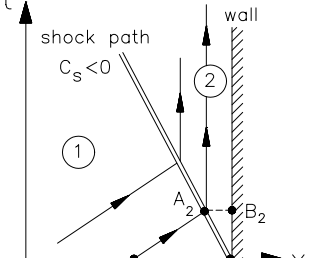
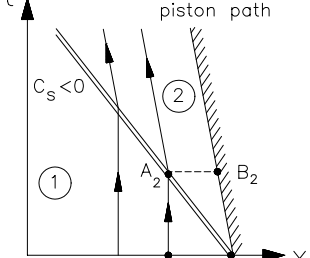
1.12.1 (t, x) -plane

One-dimensional unsteady flow phenomena such as moving shocks can be visualised very well in the (t, x) -plane. To become familiar with this plane, three examples of shocks separating two uniform states are discussed, see table 1.2.

Case A shows a steady shock situation. We notice the following:

- the pictures in the laboratory frame and the shock frame are identical
- in the (t, x) -plane the shock path is a line for which $x = \text{constant}$.
- since $u_1 > u_2$ particles move faster in ①. So $(\frac{dx}{dt})$ of the particle path is larger in ① meaning that the slope $(\frac{dt}{dx})$ of the path is lower.
- a slower particle has a steeper particle path in the (t, x) -plane

Table 1.2: Three examples of shocks

Case A: steady shock	Case B: shock created by gas hitting a wall	Case C: shock created in piston driven gas
 picture in laboratory frame, $c_s = 0$	 picture in laboratory frame, $c_s < 0$, $u_2 = 0$	 picture in laboratory frame, $c_s < 0$, $u_1 = 0$, $u_2 < 0$
 picture in shock frame	 picture in shock frame	 picture in shock frame
 picture in (t, x) -plane	 picture in (t, x) -plane	 picture in (t, x) -plane

- due to conservation of mass, at time t_1 the mass contained between A_1 and B_1 is $\rho_1 u_1 \Delta t$. When this amount of mass is moved to the interval A_2-B_2 at time t_2 , it is equal to $\rho_2 u_2 \Delta t$. So

$$\rho_1 \underbrace{u_1 \Delta t}_{\Delta x_1} = \rho_2 \underbrace{u_2 \Delta t}_{\Delta x_2},$$

therefore

$$\Delta x_1 > \Delta x_2 \Rightarrow \rho_2 > \rho_1$$

When crossing a shock in forward time direction, particle paths get closer!

Case B represents a flow with velocity $u_1 > 0$ that runs into a tube which is closed off at the end. A shock runs into the moving gas bringing it to standstill, i.e. $u_2 = 0$. We notice the following:

- The pictures in the laboratory frame and the shock frame now differ! Calling the pre- and post state velocities in the shock frame v_1 and v_2 respectively, we have:

$$v_1 = u_1 + |c_s|, \quad v_2 = |c_s|.$$

- since $u_1 > 0$, particle paths in region ① have a positive slope; since $u_2 = 0$ particle paths in ② have

$$\left(\frac{dt}{dx} \right)_2 = \infty,$$

therefore in region ② the particle paths are given by $x = \text{constant}$.

- from conservation of mass it follows that particle paths get closer when crossing the shock in forward direction.
- this case has an analogue in steady two-dimensional flow: a shock reflection at a wall, see figure 1.15.

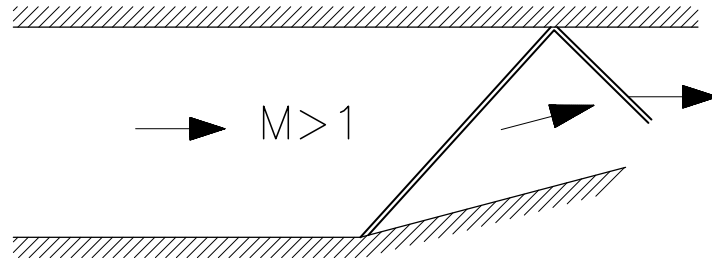


Figure 1.15: Case B two-dimensional analogue; Shock reflection at a wall.

Case C shows a piston with velocity u_p that runs into a tube filled with a gas at rest. The piston creates a shock wave moving with velocity $c_s < 0$ into the gas at rest. We notice the following:

- The pictures in the laboratory frame and the shock frame differ! Calling the pre- and post state velocities v_1 and v_2 respectively, there follows:

$$v_1 = |c_s|, \quad v_2 = |c_s| - u_2.$$

- $u_1 = 0$, therefore

$$\left(\frac{dt}{dx} \right)_1 = \infty$$

so particle paths in ① are given by $x = \text{constant}$.

- in ② u_2 is equal to the velocity of the piston u_p , so the particle paths in ② are parallel to the piston path
- conservation of mass yields again that particle paths get closer when crossing a shock in forward time direction.
- also for this case there is a two-dimensional analogue: a shock induced by a ramp in a supersonic flow, see figure 1.16.

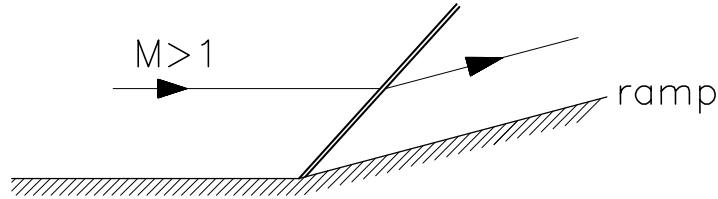


Figure 1.16: Case C two-dimensional analogue; Shock induced by a ramp in a supersonic flow.

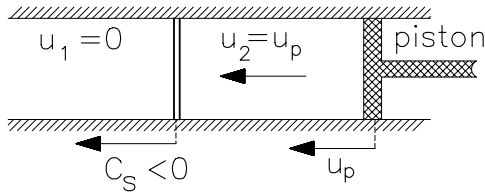
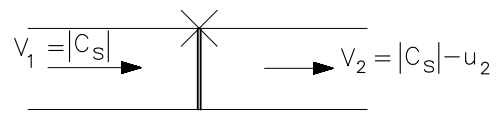
Figure 1.17: Shock moves to the left with velocity c_s 

Figure 1.18: Picture in shock frame

1.12.2 Shock speed

As shown in case C a piston with velocity u_p running into a gas at rest creates a shock that moves with the speed c_s , see figure 1.17. Over the shock a pressure rise $\Delta p = p_2 - p_1$ exists. It is convenient to write the shock speed in terms of the pressure rise $p_2 - p_1$. Recall the already have the relation (1.49a):

$$\frac{p_2}{p_1} = 1 + \frac{2\gamma}{\gamma+1} (M_1^2 - 1); \quad (1.49a)$$

which is only applicable in steady flow. Therefore we view the problem in shock frame, see figure 1.18 where the Mach number in front of the shock is:

$$M_1 = \frac{v_1}{a_1} = \frac{|c_s|}{a_1}.$$

So from equation (1.49a) follows that:

$$\frac{p_2}{p_1} = 1 + \frac{2\gamma}{\gamma+1} \left(\frac{c_s^2}{a_1^2} - 1 \right)$$

Solving for c_s we find

$|c_s| = a_1 \sqrt{1 + \frac{\gamma+1}{2\gamma} \frac{p_2 - p_1}{p_1}}$

(1.52)

Note that $|c_s| > a_1$ so the shock travels faster than the speed of sound!

First consider the **weak shock limit**:

$$\frac{\Delta p}{p_1} \ll 1, \quad \text{where } \Delta p = p_2 - p_1$$

Assuming Δp small w.r.t p_1 in equation (1.52), the shock speed can be approximated by:

$$|c_s| = a_1 \left(1 + \frac{\gamma + 1}{4\gamma} \frac{\Delta p}{p_1} \right) + \mathcal{O}(\Delta p^2) \quad (1.53)$$

Observe from this formula that a sound wave is an infinitesimal small shock ($\Delta p \rightarrow 0$).

Now consider the **strong shock limit**:

$$\frac{\Delta p}{p_1} \gg 1$$

then (1.52) can be approximated by:

$$|c_s| \approx a_1 \sqrt{\frac{\gamma + 1}{2\gamma} \frac{p_2}{p_1}},$$

or

$$\frac{p_2}{p_1} \approx \frac{2\gamma}{\gamma + 1} \frac{c_s^2}{a_1^2}. \quad (1.54)$$

From equation (1.51) we observe that in the strong shock limit the density remains finite and takes the value (also see the previous section):

$$\frac{\rho_2}{\rho_1} = \frac{\gamma + 1}{\gamma - 1},$$

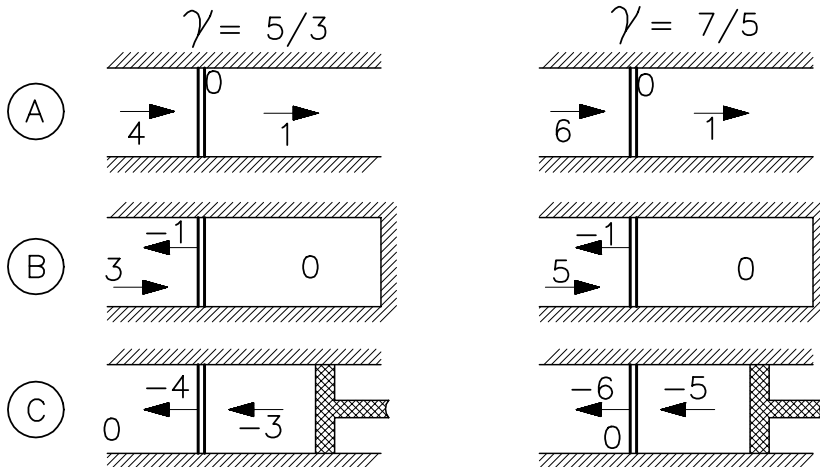
therefore in the strong shock limit the temperature and internal energy behave as:

$$\frac{T_2}{T_1} = \frac{e_2}{e_1} \approx \frac{2\gamma(\gamma - 1)}{(\gamma + 1)^2} \frac{c_s^2}{a_1^2}.$$

So for strong shocks the pressure ratio p_2/p_1 and the temperature ratio T_2/T_1 increase with the square of the shock speed c_s while the density ratio ρ_2/ρ_1 approaches $\frac{\gamma+1}{\gamma-1}$ (in the steady case), so

$$\frac{v_2}{v_1} = \frac{\rho_1}{\rho_2} \rightarrow \frac{\gamma - 1}{\gamma + 1}$$

This implies the following velocity ratios in the cases A, B and C for the strong shock limit:



1.12.3 Entropy condition II

For case A we know from elementary gasdynamics (compressible aerodynamics course) that the flow enters the shock supersonic and exits subsonic, see table 1.2. For a steady shock we therefore have $u_1 > a_1$, $u_2 < a_2$ or

$$(u_1 - a_1) > 0 > (u_2 - a_2). \quad (1.55)$$

This relation is a special case of a more general inequality:

$$(u_1 - a_1) > c_s > (u_2 - a_2)$$

Consider a moving shock in lab frame as shown in figure 1.19 (left) and its transformation in shock frame as shown in figure 1.19 (right). Application of (1.55) for the situation in shock

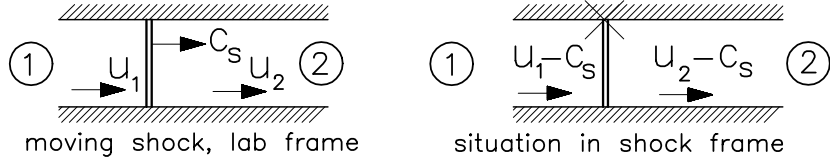


Figure 1.19: Moving shock in lab frame (left) and transformed situation in shock frame (right)

frame gives:

$$(u_1 - c_s - a_1) > 0 > (u_2 - c_s - a_2)$$

or:

$$(u_1 - a_1) > c_s > (u_2 - a_2) \quad (1.56)$$

A moving shock violating this inequality is not physically valid, so we may regard relation (1.56) as another form of the entropy condition, without mentioning the entropy explicitly.

1.13 Numerical approach

Consider the Euler equations for one-dimensional unsteady compressible flows:

$$\frac{\partial U}{\partial t} + \frac{\partial F}{\partial x} = 0$$

For numerically simulating *inviscid* compressible flows, the most popular methods nowadays are *dissipative finite volume methods*. These methods are consistent with the integral conservation laws, so the jump equations are automatically satisfied. To get insight into the derivation and origin of these methods, consider a small domain in (one-dimensional) space–time, see figure 1.20.

Now we integrate the conservation law $U_t + F_x = 0$ over this domain:

$$\int_{x_1}^{x_2} \int_{t_1}^{t_2} U_t \, dt \, dx + \int_{t_1}^{t_2} \int_{x_1}^{x_2} F_x \, dx \, dt = 0,$$

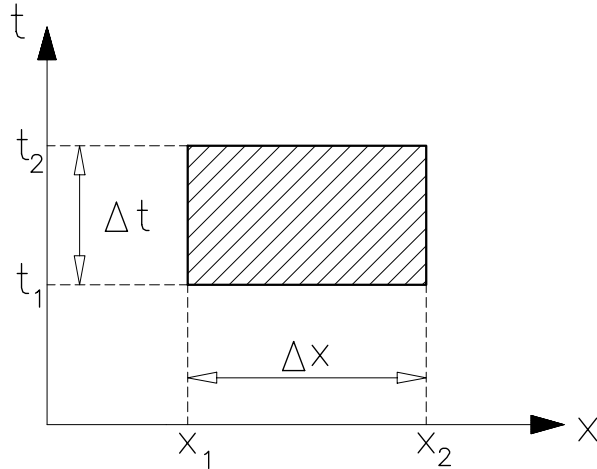


Figure 1.20: A finite domain in space–time

and get

$$\int_{x_1}^{x_2} U \, dx \Big|_{t_1}^{t_2} + \int_{t_1}^{t_2} F \, dt \Big|_{x_1}^{x_2} = 0. \quad (1.57)$$

Furthermore integrate over spatial coordinate to define a spatial mean:

$$\bar{U} = \frac{1}{\Delta x} \int_{x_1}^{x_2} U \, dx,$$

and integrate over time to define a temporal mean:

$$\langle F \rangle = \frac{1}{\Delta t} \int_{t_1}^{t_2} F \, dt.$$

Inserting the spatial mean and the temporal mean in equation (1.57) results in:

$$\frac{\bar{U}(t_2) - \bar{U}(t_1)}{\Delta t} + \frac{\langle F(x_2) \rangle - \langle F(x_1) \rangle}{\Delta x} = 0. \quad (1.58)$$

This looks like a finite-difference approximation of $U_t + F_x = 0$, but this formula is still *exact: no numerical errors have been introduced!* Such errors come into play when the average time-integral of the fluxes is approximately predicted from the solution at the discrete times t_1 and/or t_2 .

Equation (1.58) is an update scheme: once the solution at time level t_1 is known, equation (1.58) yields the solution at time level t_2 , etc., etc. To proceed, one needs to know the fluxes or the flux differences. So, one has to find the flux formulae that are consistent with the equations up to terms of the order $\mathcal{O}(\Delta t, \Delta x)$ or higher, see the works of Prof. B. van Leer and Prof. Ph. Roe.

The update from t to $t + \Delta t$ has to be stable not just if updates are small (in the continuous part of the solution) but also in the presence of strong shock waves, see figure 1.21.

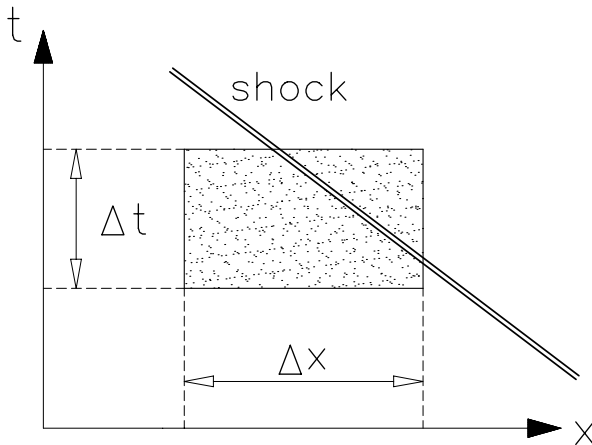


Figure 1.21: A shock intersecting with the finite time-space domain

To achieve this, the flux formulae are designed in such a way that the dominant numerical error produced by the scheme (the ‘truncation’ error) has the appearance of dissipation term. With such an ‘artificial dissipation’ the update is close to equations of the type:

$$U_t + F_x = (D_2 U_x)_x \quad (1.59)$$

or

$$U_t + F_x = (D_4 U_{xxx})_x$$

where

$$D_2 = \mathcal{O}(\Delta t, \Delta x)$$

and

$$D_4 = \mathcal{O}(\Delta t^2, \Delta t^2 \Delta x, \Delta t \Delta x^2, \Delta x^3).$$

Adding dissipation terms ensures time irreversibility, and production of entropy no matter how small Δx and Δt are taken.

For $\Delta x \rightarrow 0$, $\Delta t \rightarrow 0$ the numerical solution approaches the solution of the inviscid equation $U_t + F_x = 0$ including all physically admissible shocks.

Dropping viscosity leads to simpler equations (Euler) but one loses physics (viscous dissipation). To retain flow phenomena related to viscous dissipation (e.g. shocks) dissipation is added artificially to the governing equations; see examples in equation (1.59) by designing appropriate flux formulae in numerical schemes.

This approach is based on the most fundamental form of the *Entropy condition*, which we call ‘Entropy condition III’.

Entropy condition III

Only those inviscid solutions are physically acceptable that can also be obtained from the full viscous and heat conducting equations in the limit of vanishing viscosity and heat conduction.

The limiting process mentioned in entropy condition III is depicted in figure 1.22.

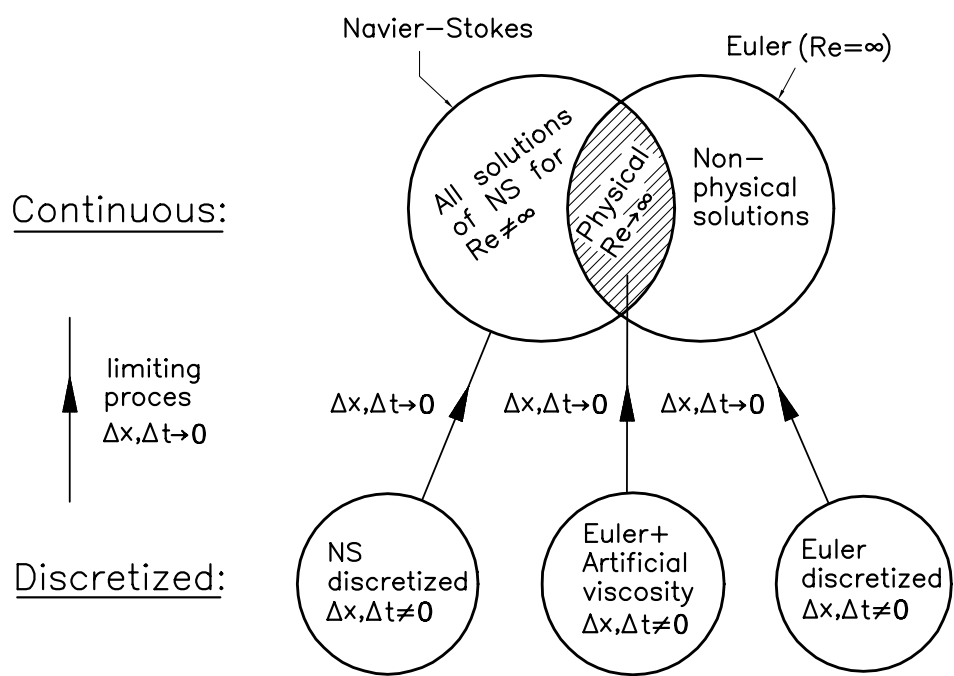


Figure 1.22: Artificial viscosity ensures that only physical solutions of the Euler equations will be obtained.

Chapter 2

Linearized flow equations

2.1 1D acoustics

In this paragraph we will study the physics of acoustic wave propagation in a fluid at rest. In real-life situations fluids occupy a three-dimensional space but the three-dimensional effects are not relevant to understand the principles of acoustics; therefore, it is sufficient to consider the one-dimensional case. All phenomena take place in a constant area tube.

Let the background state in the tube be given by

$$\rho_0, p_0, a_0 \text{ and } u_0 = 0. \quad (2.1)$$

Note that the background state is a fluid state at rest. Let perturbations be denoted by $\Delta\rho$, Δp and Δu , so that

$$\rho = \rho_0 + \Delta\rho, \quad p = p_0 + \Delta p, \quad \text{and} \quad u = u_0 + \Delta u = \Delta u. \quad (2.2)$$

Let the entropy $s = s_0$ be kept constant uniformly in space (x) and time (t). This assumption is justified since acoustic wave propagation is understood to be a reversible process. Thus entropy s is equal to s_0 for all particles at any time and place. Then we have

$$\Delta p = a_0^2 \Delta\rho, \quad (2.3)$$

which is valid not along particle paths only, but for any pair of nearby states! Now introduce the relative density change or “condensation”¹,

$$\tilde{S} = \frac{\Delta\rho}{\rho_0}, \quad (2.4)$$

and the Mach number

$$M = \frac{\Delta u}{a_0} = \frac{u}{a_0}. \quad (2.5)$$

Substitute (2.4) and (2.5) into the governing equations for 1D unsteady flow:

$$U_t + F_x = 0. \quad (2.6)$$

¹Here we will follow the notation from Liepmann & Roshko, don't confuse \tilde{S} with S = entropy.

From the continuity equation follows

$$\frac{\partial \rho}{\partial t} + \frac{\partial(\rho u)}{\partial x} = 0, \quad \frac{\partial}{\partial t}(\rho_0 + \Delta\rho) + \frac{\partial}{\partial x}((\rho_0 + \Delta\rho)u) = 0, \quad (2.7)$$

or

$$\frac{\partial \Delta\rho}{\partial t} + \rho_0 \frac{\partial u}{\partial x} + \underbrace{\frac{\partial}{\partial x}(u\Delta\rho)}_{\text{second order perturbation}} = 0. \quad (2.8)$$

Neglecting second order perturbations, we find

$$\frac{\partial \tilde{S}}{\partial t} + a_0 \frac{\partial M}{\partial x} = 0. \quad (2.9)$$

From the momentum equation there is obtained:

$$\frac{\partial}{\partial t}(\rho u) + \frac{\partial}{\partial x}(p + \rho u^2) = 0.$$

Inserting perturbations:

$$\begin{aligned} & \frac{\partial}{\partial t}(\rho_0 u + u\Delta\rho) + \frac{\partial}{\partial x}(p_0 + \Delta p + \rho_0 u^2 + u^2 \Delta\rho) = 0, \\ & \rho_0 \frac{\partial u}{\partial t} + \frac{\partial \Delta p}{\partial x} + \underbrace{\left(u\Delta\rho + \frac{\partial}{\partial x}(u^2 \rho_0) + \frac{\partial}{\partial x}(u^2 \Delta\rho) \right)}_{\text{2}^{nd} \text{ and } \text{3}^{rd} \text{ order perturbations}} = 0. \end{aligned}$$

Neglecting 2^{nd} and 3^{rd} order terms yields

$$\rho_0 \frac{\partial u}{\partial t} + \frac{\partial \Delta p}{\partial x} = 0,$$

or with equation (2.3):

$$\Rightarrow \frac{\partial M}{\partial t} + a_0 \frac{\partial \tilde{S}}{\partial x} = 0. \quad (2.10)$$

The equation $U_t + F_x = 0$ contains also the energy equation, however this gives no extra information since it is replaced by the assumption of reversibility $ds = 0$.

Equations (2.9) and (2.10) are fundamental for the description of small perturbations appearing in a gas at rest. Actually they govern wave propagation and therefore it may be expected that there is a relation between the well-known wave equation and the two equations (2.9) and (2.10) derived here.

2.1.1 Relation with the wave equation

Differentiate equation (2.9) with respect to time (or space) and differentiate equation (2.10) with respect to space (or time), eliminate cross derivatives and we find:

$$\frac{\partial^2 \tilde{S}}{\partial t^2} - a_0^2 \frac{\partial^2 \tilde{S}}{\partial x^2} = 0, \quad (2.11a)$$

$$\frac{\partial^2 M}{\partial t^2} - a_0^2 \frac{\partial^2 M}{\partial x^2} = 0, \quad (2.11b)$$

i.e. both \tilde{S} and M satisfy a wave equation with a_0 as the wave speed.

The general solution for the wave equation is given by d'Alembert:

$$\tilde{S}(x, t) = F(x - a_0 t) + G(x + a_0 t), \quad (2.12a)$$

$$M(x, t) = f(x - a_0 t) + g(x + a_0 t), \quad (2.12b)$$

where $F(X)$, $f(X)$, $G(Y)$ and $g(Y)$ are arbitrary functions (twice differentiable) of the single arguments $X = x - a_0 t$ and $Y = x + a_0 t$. Equations (2.12a) and (2.12b) show that there are components in the solution which are constant along $X = x - a_0 t$ and others which are constant along $Y = x + a_0 t$; $F(X)$ and $f(X)$ represent the so-called *right-running* waves and similarly $G(Y)$ and $g(Y)$ represent the so-called *left-running* waves. Both waves preserve their exact shape while they propagate with speed a_0 through the fluid along straight lines $X = \text{const}$, or $Y = \text{const}$ in the (t, x) -plane, see figure 2.1.

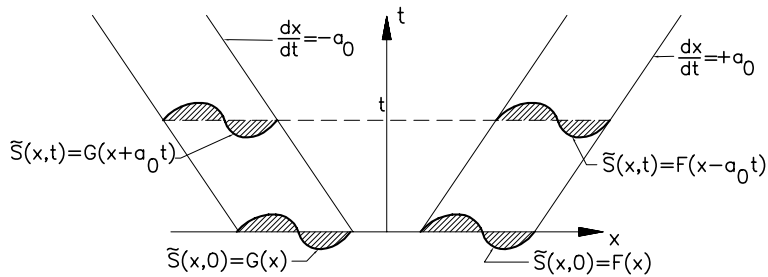


Figure 2.1: Propagation of \tilde{S} in the (t, x) -plane

This phenomenon, so typical for variables satisfying the wave equation can also be observed from the set of equations (2.9) and (2.10).

Adding and subtracting both equations yields:

$$(M + \tilde{S})_t + a_0(M + \tilde{S})_x = 0, \quad (2.13)$$

$$(M - \tilde{S})_t - a_0(M - \tilde{S})_x = 0. \quad (2.14)$$

Hence, $M + \tilde{S}$ is constant along a path in (t, x) -space with $\frac{dx}{dt} = +a_0$, this path is called the ‘characteristic’ Γ^+ , and $M - \tilde{S}$ is constant along a path in (t, x) -space with $\frac{dx}{dt} = -a_0$, this path is called the ‘characteristic’ Γ^- .

These characteristic curves appear to be straight lines in the above case of linear acoustics; for non-linear gasdynamics they are generally curved.

2.1.2 Riemann invariants

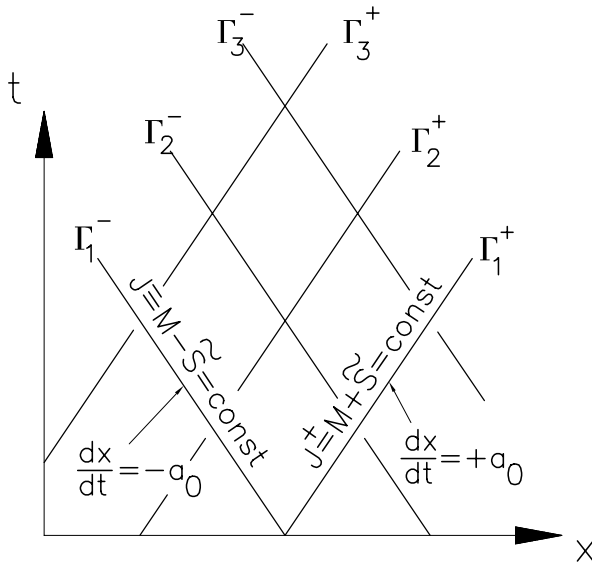
Now we introduce the Riemann invariants J^+ and J^- which are defined as

$$J^+ = M + \tilde{S}, \quad J^- = M - \tilde{S}. \quad (2.15)$$

Equations (2.13) and (2.14) now result into

$$\frac{\partial J^\pm}{\partial t} \pm a_0 \frac{\partial J^\pm}{\partial x} = 0. \quad (2.16)$$

So J^+ is constant along Γ^+ : $\frac{dx}{dt} = +a_0$ and J^- is constant along Γ^- : $\frac{dx}{dt} = -a_0$.

Figure 2.2: Characteristics in the (t, x) -plane

Equations (2.16) will be called the “characteristic equations”. In other texts the equations describing the characteristic curves, i.e.

$$\frac{dx}{dt} = \pm a_0 \quad \text{along } \Gamma^\pm \quad (2.17)$$

are called “characteristic equations” and the conditions on the flow variables, along the characteristics

$$J^\pm = M \pm \tilde{S} = \text{constant along } \Gamma^\pm \quad (2.18)$$

are called “compatibility relations”.

2.2 Method of Characteristics, M.O.C.

The equations (2.13) and (2.14) or (2.15) and (2.16) are very well suited for obtaining solutions whether analytically or, in non-linear cases, numerically. There are two forms, although very similar, of the “method of characteristics”: the *forward* M.O.C. and the *backward* M.O.C.

2.2.1 Forward M.O.C

Assume that on the x -axis ($t = 0$) initial values are given, in particular in the points A and B. Draw the Γ^+ characteristic through A: Γ_A^+ forward (in time) and draw also the Γ^- characteristic through B: Γ_B^- forward (in time). They intersect in P (see figure 2.3). The solution in P follows from the observation that:

$$\text{along } \Gamma_A^+ : (M + \tilde{S})_A = (M + \tilde{S})_P \quad (2.19)$$

$$\text{along } \Gamma_B^- : (M - \tilde{S})_B = (M - \tilde{S})_P \quad (2.20)$$

Solving for the unknowns M_P and \tilde{S}_P we find

$$M(x_p, t_p) = \frac{M_A + \tilde{S}_A}{2} + \frac{M_B - \tilde{S}_B}{2} \quad (2.21)$$

$$\tilde{S}(x_p, t_p) = \frac{M_A + \tilde{S}_A}{2} - \frac{M_B - \tilde{S}_B}{2} \quad (2.22)$$

Observe that the solution in P only depends on the initial data in A and B itself and not on the initial data between A and B.

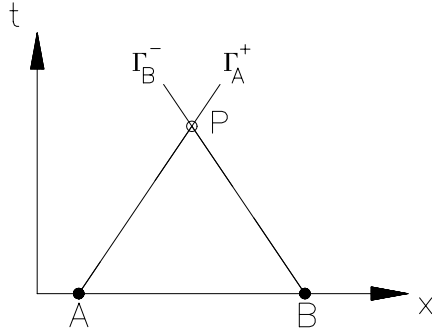


Figure 2.3: Forward method of characteristics

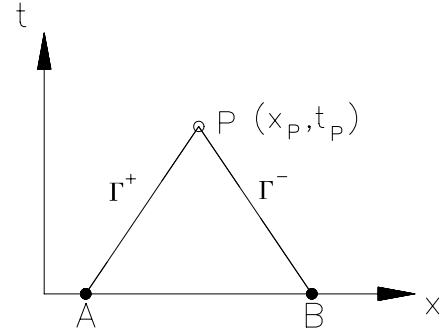


Figure 2.4: Backward method of characteristics

2.2.2 Backward M.O.C

Backward M.O.C. and forward M.O.C. are very similar. In backward M.O.C one has a method that is applicable when one seeks the solution in a particular point $P(x_p, t_p)$, whereas the initial values of M and \tilde{S} are known on the line $t = 0$ (the x -axis in the (x, t) -plane).

Draw Γ^+ and Γ^- backwards through P, intersecting the x -axis in A and B respectively, see figure 2.4. Here the initial data for M and \tilde{S} are given.

The solution in P is now determined by the formulae already given as equations (2.21) and (2.22).

2.2.3 Initial value problem for the wave equation

Consider the wave equation for \tilde{S} :

$$\frac{\partial^2 \tilde{S}}{\partial t^2} + a_0^2 \frac{\partial^2 \tilde{S}}{\partial x^2} = 0, \quad (2.23)$$

and assume that initial conditions are given on the x -axis ($t = 0$) as follows:

$$\tilde{S}(x, 0) = f(x), \quad (2.24)$$

$$\frac{\partial \tilde{S}}{\partial t}(x, 0) = g(x). \quad (2.25)$$

How does the solution $\tilde{S}(x, t)$ depend on the initial data $f(x)$ and $g(x)$?

The solution of d'Alembert, equation (2.12a) and (2.12b) gives

$$\tilde{S}(x, t) = F(x - a_0 t) + G(x + a_0 t), \quad (2.26)$$

$$\tilde{S}_t(x, t) = -a_0 F'(x - a_0 t) + a_0 G'(x + a_0 t) \quad (2.27)$$

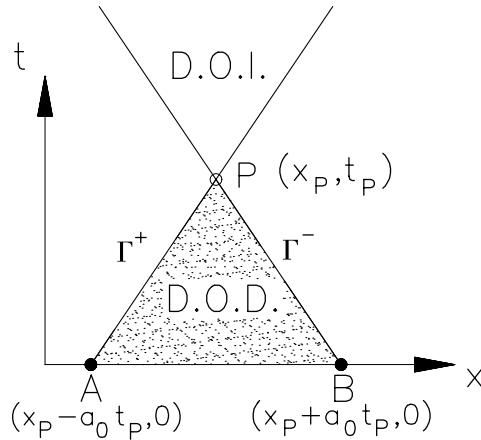


Figure 2.5: Domains of dependence and influence

Evaluating both expressions on the initial data line $t = 0$ yields

$$\tilde{S}(x, 0) = F(x) + G(x) = f(x), \quad (2.28)$$

$$\tilde{S}_t(x, 0) = -a_0(F'(x) - G'(x)) = g(x). \quad (2.29)$$

The last equation can be integrated with respect to x :

$$F(x) - G(x) = -\frac{1}{a_0} \int_0^x g(\xi) d\xi. \quad (2.30)$$

Now there are two equations for the unknown functions $F(x)$ and $G(x)$; they can be solved to give

$$F(x) = \frac{1}{2}f(x) - \frac{1}{2a_0} \int_0^x g(\xi) d\xi, \quad (2.31)$$

$$G(x) = \frac{1}{2}f(x) + \frac{1}{2a_0} \int_0^x g(\xi) d\xi. \quad (2.32)$$

The general solution for $\tilde{S}(x, t)$ is now found as

$$\tilde{S}(x, t) = \frac{1}{2} \{f(x - a_0 t) + f(x + a_0 t)\} + \frac{1}{2a_0} \int_{x-a_0 t}^{x+a_0 t} g(\xi) d\xi. \quad (2.33)$$

Equation (2.33) presents the solutions of $\tilde{S}(x, t)$ in an arbitrary point (x, t) . It depends on the initial data lying on the interval bounded by the intersecting points with the characteristics drawn backward through (x, t) .

In figure 2.5 the initial data between A and B determine the solution in the point $P(x, t)$. The area enclosed by the characteristics Γ^+ , Γ^- and the initial line $t = 0$ is called *the Domain of Dependence* (D.O.D.) of the point P . The area above P between Γ^- and Γ^+ is called *the Domain of Influence* (D.O.I.) of the point P .

In the domain of *dependance* we find all points on which the solution in P *depends*. In the domain of *influence* we find all points whose solution is *influenced* by the solution in P .

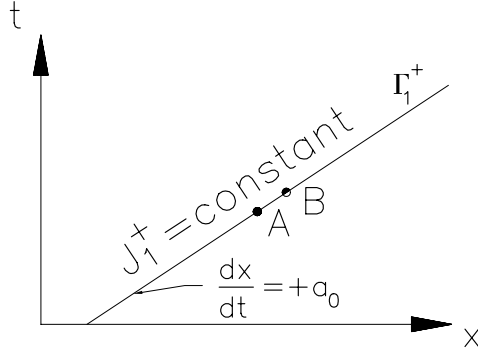


Figure 2.6:

2.2.4 Discontinuities

Linear acoustics is governed by the set of equations

$$\frac{\partial \tilde{S}}{\partial t} + a_0 \frac{\partial M}{\partial x} = 0, \quad (2.9)$$

$$\frac{\partial M}{\partial t} + a_0 \frac{\partial \tilde{S}}{\partial x} = 0, \quad (2.10)$$

whose solutions are characterised by the fact that $M + \tilde{S}$ is constant along Γ^+ and $M - \tilde{S}$ is constant along Γ^- . The solution

$$(M + \tilde{S})(x, t) = (M + \tilde{S})(x - a_0 t, 0), \quad (2.34)$$

$$(M - \tilde{S})(x, t) = (M - \tilde{S})(x + a_0 t, 0), \quad (2.35)$$

obtained from the differential equations, is still valid even when the differentiability of the individual variables M and \tilde{S} is *not* fulfilled.

To show this, consider a characteristic Γ_1^+ in the (t, x) -plane, and let the Riemann invariant on this characteristic have the value J_1^+ . So $J_1^+ = M + \tilde{S}$ and is constant along Γ_1^+ .

Although $M + \tilde{S}$ is constant, the individual variables M and \tilde{S} may vary along Γ_1^+ , and the variations may still contain discontinuities.

Assume that M is discontinuous showing a jump ΔM between A and B , see figure 2.6, so that $M_B = M_A + \Delta M$.

To satisfy the condition J_1^+ is constant, the variable \tilde{S} also jumps between A and B :

$$\tilde{S}_B = \tilde{S}_A + \Delta \tilde{S}, \quad \text{with} \quad \Delta \tilde{S} = -\Delta M. \quad (2.36)$$

This behaviour is sketched in figure 2.7, which shows J_1^+ , M and \tilde{S} along Γ_1^+ .

Discontinuous solutions of the system (2.9) - (2.10) have to satisfy the jump relation

$$\Delta \tilde{S} + \Delta M = 0 \quad \text{on } \Gamma^+, \quad (2.37)$$

and similarly

$$\Delta \tilde{S} - \Delta M = 0 \quad \text{on } \Gamma^-. \quad (2.38)$$

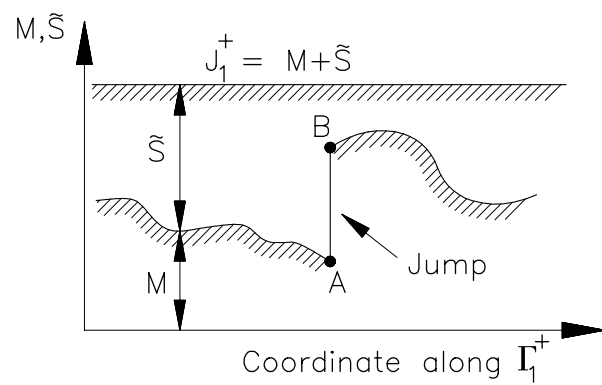


Figure 2.7:

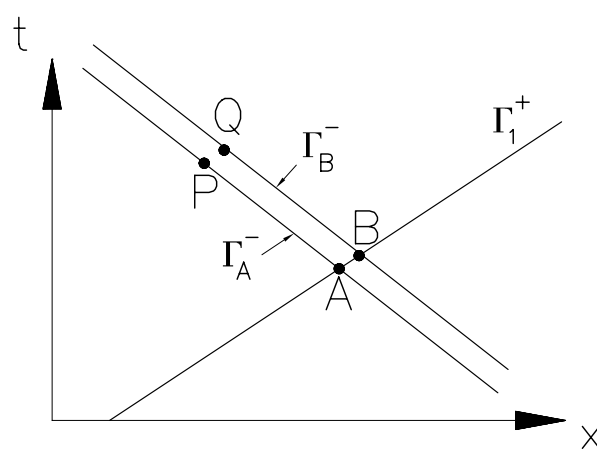


Figure 2.8:

The discontinuity that is observed in point A, B on Γ_1^+ is *not isolated* in the (t, x) -plane but is carried along the Γ^- -characteristic going through A and B , see figure 2.8. This is immediately clear if one applies the condition that $M - \tilde{S}$ is constant along Γ^- characteristics Γ_A^- and Γ_B^- . Take the neighbouring points P and Q on Γ_A^- and Γ_B^- respectively. This gives the following equations:

$$\text{along } \Gamma_A^- \quad M_P - \tilde{S}_P = M_A - \tilde{S}_A, \quad (2.39)$$

$$\text{along } \Gamma_B^- \quad M_Q - \tilde{S}_Q = M_B - \tilde{S}_B = M_A + \Delta M - \tilde{S}_A - \Delta \tilde{S}. \quad (2.40)$$

Subtraction gives:

$$M_Q - M_P - \tilde{S}_Q + \tilde{S}_P = \Delta M - \Delta \tilde{S}. \quad (2.41)$$

Since $\Delta \tilde{S} + \Delta M = 0$, this relation becomes

$$M_Q - M_P - \tilde{S}_Q + \tilde{S}_P = 2\Delta M. \quad (2.42)$$

Since P and Q are on the same Γ^+ -characteristic, we have

$$M_P + \tilde{S}_P = M_Q + \tilde{S}_Q,$$

or

$$M_Q - M_P + \tilde{S}_Q - \tilde{S}_P = 0. \quad (2.43)$$

Combining (2.42) and (2.43), there follows

$$M_Q - M_P = \Delta M, \quad (2.44)$$

and similarly

$$\tilde{S}_Q - \tilde{S}_P = \Delta \tilde{S}. \quad (2.45)$$

Conclusion:

Characteristics serve as discontinuity lines.

To get a formal affirmation of this conclusion consider again the set of equations (2.9) and (2.10), and apply the jump equation for one-dimensional unsteady flow: equation (1.39). The jump equation applied to $\tilde{S}_t + a_0 M_x = 0$ gives:

$$V_D \Delta \tilde{S} = a_0 \Delta M; \quad (2.46)$$

the jump equation applied to $M_t + a_0 \tilde{S}_x = 0$ gives:

$$V_D \Delta M = a_0 \Delta \tilde{S}. \quad (2.47)$$

Combining both equations and solving for the discontinuity velocity V_D yields:

$$V_D^2 = a_0^2, \quad (2.48)$$

or

$$V_D = \pm a_0. \quad (2.49)$$

Conclusion:

In linear acoustics, characteristics are candidates to be discontinuity line \mathcal{D} .

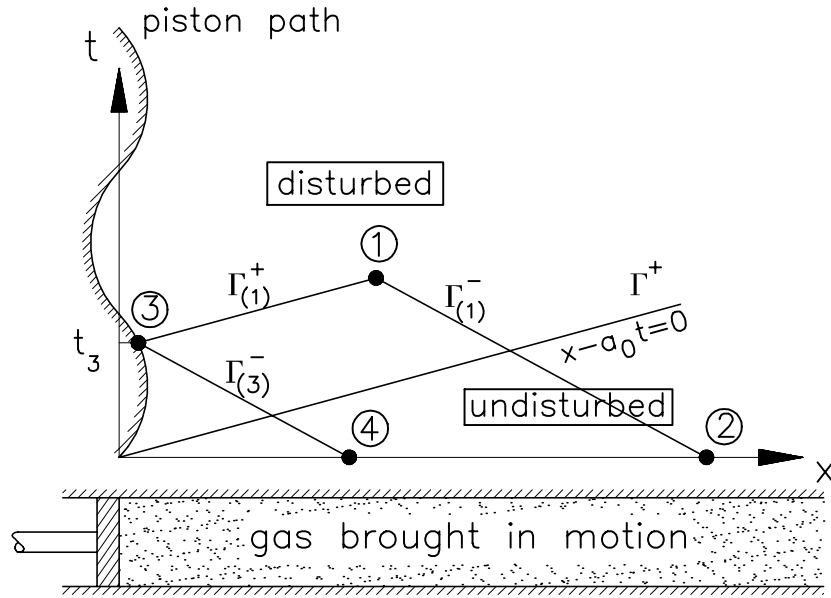


Figure 2.9: Piston problem

2.3 Piston problem

Consider a constant area tube, filled with gas at rest. The rest conditions, labelled with subscript ‘0’ are pressure p_0 , density ρ_0 , sound velocity a_0 , temperature T_0 , etc. The tube is closed off by a movable piston at the left end. The right end of the tube extends to infinity.

The piston, at rest at $t < 0$, starts moving at $t = 0$. The piston velocity $U_p(t)$ and the piston position $X_p(t)$ may depend on time and are assumed to be small. Further, the position of the piston X_p at time t is given by

$$X_p(t) = \int_0^t U_p(\tau) d\tau. \quad (2.50)$$

Problem:

Find for a prescribed piston movement, for example if the piston is oscillating, the impact it has on the gas that was initially at rest. How does the gas come into motion and what is the resulting flow in the tube?

To discuss this problem, draw a picture in the (t, x) -diagram, see figure 2.9. The first message telling the gas at $x > 0$ that the piston has started moving is the sound wave with path $x - a_0 t = 0$.

The gas contained at $x - a_0 t > 0$ is still *undisturbed*, but the gas contained at $x - a_0 t < 0$ experiences the moving (oscillating) piston and is *disturbed*. So in particular on $t = 0$ we have $M = 0$ and $\tilde{S} = 0$.

Let us find the flow variables (M and \tilde{S}) in a point ① in the disturbed zone, using the backward M.O.C. method.

Drawing Γ^- through ① backward in time to $t = 0$ goes as usual, yielding the intersection point ②, but drawing Γ^+ backward in time we hit the piston in point ③. Unlike the x -axis where M and \tilde{S} are known (i.e. $M = 0$ and $\tilde{S} = 0$), at the piston path only one flow variable

is known: the piston velocity U_p or $M_p = \frac{U_p}{a_0}$. Fortunately the missing piece of information is obtained by drawing a Γ^- characteristic through (3) backward in time to $t = 0$ onto point ④ on the initial value line.

This provides enough information to find M and \tilde{S} in point ①. Writing down the equations valid along characteristics:

$$\text{along } \Gamma_{(1)}^-: M_1 - \tilde{S}_1 = M_2 - \tilde{S}_2 = 0 \quad (2.51\text{a})$$

$$\text{along } \Gamma_{(1)}^+: M_1 + \tilde{S}_1 = M_3 + \tilde{S}_3 \quad (2.51\text{b})$$

$$\text{along } \Gamma_{(3)}^-: M_3 - \tilde{S}_3 = M_4 - \tilde{S}_4 = 0 \quad (2.51\text{c})$$

$$\text{on piston path: } M_3 = M_p(t_3) \quad (2.51\text{d})$$

The actual position of the points ② and ④ are immaterial as long as they lie in the undisturbed zone.

The point (x_3, t_3) is the intersection of the piston path: $X_p(t) = \int_0^t U_p(\tau) d\tau$ with the Γ^+ -characteristic going through ①:

$$x - a_0 t = x_1 - a_0 t_1 \quad (2.52)$$

In general, finding (x_3, t_3) results in solving a transcendental equation. Fortunately, we are considering small disturbance theory (linear acoustics) so that it is allowed to assume that the piston excursion x_3 is small. Therefore we may take $x_3 = 0$ and we find from equation (2.52):

$$t_3 = t_1 - \frac{x_1}{a_0}. \quad (2.53)$$

Now, system (2.51a)-(2.51d) can be solved:

step 1: t_3 is inserted in (2.51d) $\Rightarrow M_p \Rightarrow M_3$

step 2: (2.51c) $\Rightarrow \tilde{S}_3 = M_3$

step 3: (2.51a) and (2.51b) $\Rightarrow M_1 - \tilde{S}_1 = 0, M_1 + \tilde{S}_1 = 2M_3$

This leads to the solution $M_1 = M_3, \tilde{S}_1 = M_3$ or,

$$M_1(x, t) = M_p \left(t - \frac{x}{a_0} \right), \quad \tilde{S}_1(x, t) = M_p \left(t - \frac{x}{a_0} \right)$$

which tells us that the values of the state variables at the piston in ③ are *transported without change* along Γ^+ into the gas. In other words, the velocity in a certain position x at time t is just equal to the velocity of the piston at time $t - \frac{x}{a_0}$; $\frac{x}{a_0}$ is precisely the traveling time for a sound wave propagating from the piston to the location x .

Notice that in this case, not just $J^+ = M + \tilde{S}$ is constant along Γ^+ but the individuals M and \tilde{S} are constant too along the Γ^+ -characteristic.

A flow in which there is really only *one* Riemann invariant varying is called a “*simple wave*”. Indeed in the example discussed above we have a simple wave since the Riemann invariant $J^- = M - \tilde{S}$ is constant throughout the flow since all characteristics emanate from the initial line $t = 0$ where the conditions are constant (i.e. $M = 0, \tilde{S} = 0 \rightarrow J^- = 0$). Thus J^- is constant in the whole (t, x) -domain, only J^+ is varying! (More on simple waves may be found in chapter 3 of the lecture notes).

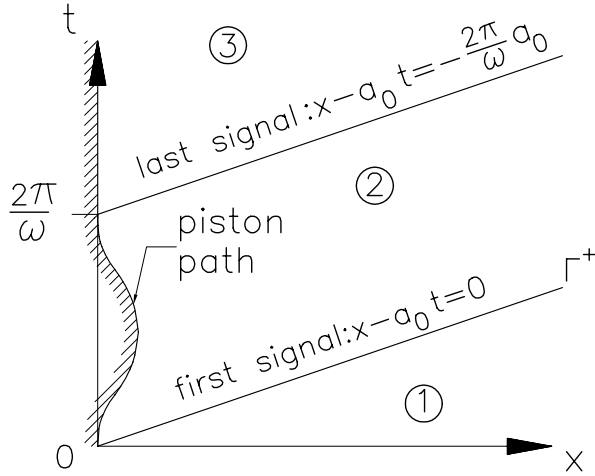


Figure 2.10:

2.3.1 Specific Example: A sinusoidal excursion of the piston for only one single period.

The theory just presented enables us to describe the unsteady gas motion resulting from a prescribed piston movement. To be specific, assume:

$$U_p = \begin{cases} \epsilon a_0 \sin \omega t, & 0 \leq t \leq \frac{2\pi}{\omega}, \\ 0, & \text{for any other time,} \end{cases} \quad (2.54)$$

with ϵ small. Equation (2.54) can be written as

$$M_p = \epsilon \sin \omega t, \quad 0 \leq t \leq \frac{2\pi}{\omega}. \quad (2.55)$$

The piston path

Between $t = 0$ and $t = \frac{2\pi}{\omega}$ the piston path becomes:

$$x_p(t) = \int_0^t u_p(\tau) d\tau = \frac{\epsilon a_0}{\omega} (1 - \cos \omega t). \quad (2.56)$$

The piston moves forward, then backward returning to its starting position at $x = 0$. When the piston stops at $t = \frac{2\pi}{\omega}$, again an undisturbed region (i.e. ③) results, see figure 2.3.1.

The solution in the various domains becomes:

$$\text{domain } ① : \quad (x - a_0 t) > 0 \quad : \tilde{S} = 0, M = 0; \quad (2.57)$$

$$\text{domain } ② : \quad -a_0 \frac{2\pi}{\omega} < (x - a_0 t) < 0 \quad : M(x, t) = \epsilon \sin \omega \left(t - \frac{x}{a_0} \right), \tilde{S} = M; \quad (2.58)$$

$$\text{domain } ③ : \quad (x - a_0 t) < -a_0 \frac{2\pi}{\omega} \quad : M = 0, \tilde{S} = 0. \quad (2.59)$$

Particle paths

Consider a particle ‘*i*’ at the initial position $x_i(0) = x_{i,0}$. The position of the particle can be described by:

$$\text{for } 0 < t < \frac{x_{i,0}}{a_0} : \quad x_i(t) = x_i(0) = x_{i,0} \quad (2.60)$$

$$\text{for } \frac{x_{i,0}}{a_0} < t < \frac{x_{i,0}}{a_0} + \frac{2\pi}{\omega} : \quad x_i(t) = \int_{\frac{x_{i,0}}{a_0}}^t u_i \, ud\tau = \int_{\frac{x_{i,0}}{a_0}}^t a_0 M_i d\tau = \int_{\frac{x_{i,0}}{a_0}}^t a_0 \varepsilon \sin \left[\omega \left(\tau - \frac{x_{i,0}}{a_0} \right) \right] d\tau \quad (2.61)$$

or

$$x_i(t) = x_{i,0} + \frac{a_0 \varepsilon}{\omega} \left[1 - \cos \left(t - \frac{x_{i,0}}{a_0} \right) \omega \right] \quad (2.62)$$

All paths have similar shapes; there is only a time shift. Note that the piston path is found as the path of the particle having $x_{i,0} = 0$.

Disturbed gas motion at $t = 2\pi/\omega$

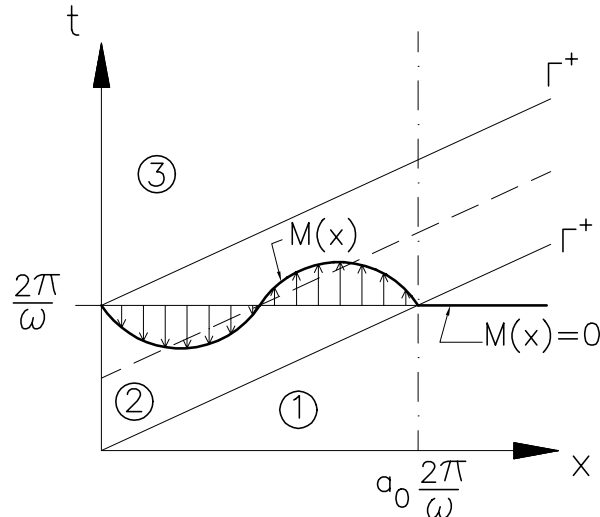


Figure 2.11: Sinusoidal wave introduced by the piston

The piston introduces a sinusoidal wave into the gas at rest; the wave travels to the right with the speed of sound a_0 . This process is depicted in figure 2.11. This figure enables us to describe what an observer located at time $x = a_0 \frac{2\pi}{\omega}$ experiences as time progresses.

Until $t = \frac{2\pi}{\omega}$ the gas is still at rest and the observer is not aware of the fact that the piston has started moving already $\frac{2\pi}{\omega}$ time units ago. However at $t = \frac{2\pi}{\omega}$ things are changing since the gas at $x = a_0 \frac{2\pi}{\omega}$ starts moving. The observer experiences a gas flow moving to the right until $t = \frac{3\pi}{\omega}$. At that particular time instant the gas flow is stopped and now starts moving to the left. Until $t = \frac{4\pi}{\omega}$ the observer experiences this left moving flow. Beyond $t = \frac{4\pi}{\omega}$ the gas is at rest again.

From figure 2.11 we observe the following:

1. discontinuities (in slope) are carried along the characteristics;

2. discontinuities are not smoothed during travelling; there is no physical mechanism such as viscous dissipation that could do that job. In absence of viscous dissipation discontinuities survive.
3. An initial wave, e.g. $t = \frac{2\pi}{\omega}$ cannot be steady; it has to move with the speed a_0 .

2.3.2 Example: a tube with two pistons

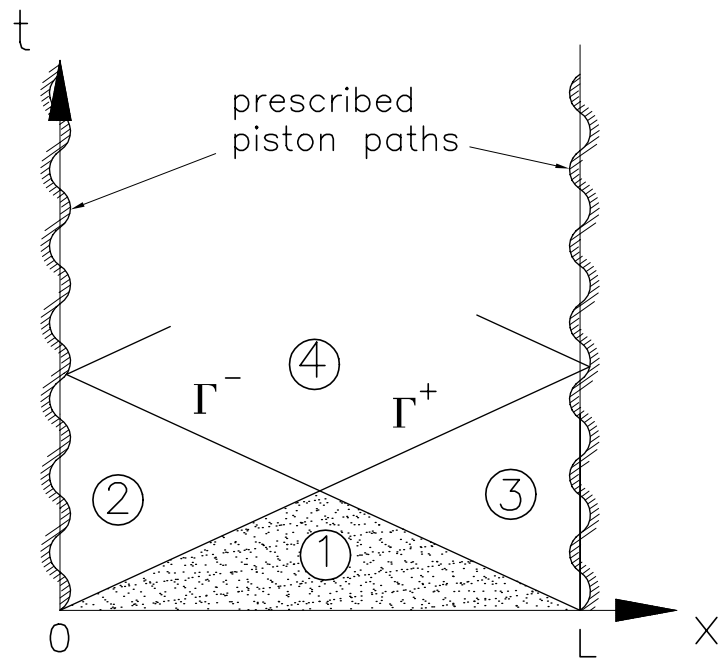


Figure 2.12:

The Method of Characteristics is generally applicable. For example in the case of a finite tube with length L having pistons at both ends. If both pistons follow a prescribed path the motion of the gas between both pistons can be determined using the M.O.C.

In the (t, x) -plane several domains can be distinguished; domain ① is undisturbed; domains ② and ③ are simple waves since J^- and J^+ are constant in ② and ③ respectively. Domain ④ is a non-simple region; here both Riemann invariants J^+ and J^- vary. In a non-simple region the variables M and \tilde{S} are not constant along Γ^+ or Γ^- .

2.4 Riemann's initial-value problem

Riemann's initial-value problem, or Riemann's problem shortly, is one of the most fundamental problems in Gasdynamics and in particular in the description of unsteady gas motions. Apart from its great value to understand these physical phenomena it has also a dominant role in the development of CFD methods to solve these problems.

Riemann's problem is formulated as follows: on the initial line e.g. $t = 0$ two *uniform*

states are separated by a discontinuity, for example at $x = 0$; thus

$$\begin{aligned} x < 0 : M &= M_1, \tilde{S} = \tilde{S}_1; \\ x > 0 : M &= M_4, \tilde{S} = \tilde{S}_4. \end{aligned} \quad (2.63)$$

Take an arbitrary point $P(t, x)$ and use backward M.O.C. to get the solution:

$$\begin{aligned} M_P &= \frac{1}{2}(M + \tilde{S})_A + \frac{1}{2}(M - \tilde{S})_B; \\ \tilde{S}_P &= \frac{1}{2}(M + \tilde{S})_A - \frac{1}{2}(M - \tilde{S})_B, \end{aligned} \quad (2.64)$$

where A and B are points on the initial value line, see figure 2.13.

Let us evaluate this solution in the (t, x) -plane. Depending on the location of P in the (t, x) -plane, we observe three different solutions.

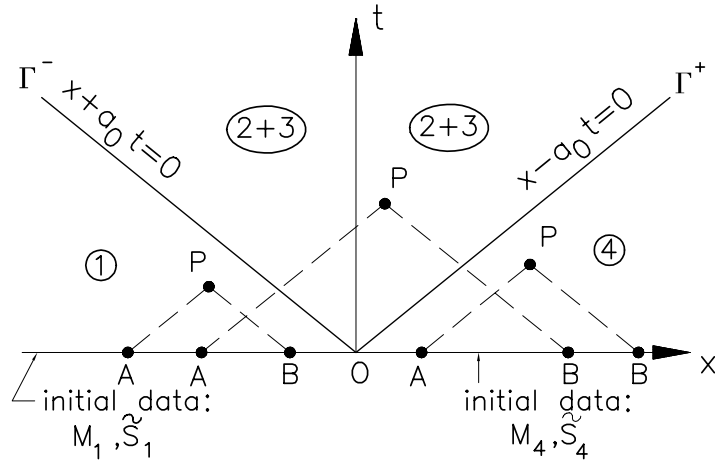


Figure 2.13:

If $P(t, x)$ lies in the domain ① then A and B are both on $x < 0$. This implies:

$$M_A = M_B = M_1$$

and

$$\tilde{S}_A = \tilde{S}_B = \tilde{S}_1.$$

If $P(t, x)$ lies in domain ④ then A and B are both on $x > 0$, implying

$$M_A = M_B = M_4,$$

and

$$\tilde{S}_A = \tilde{S}_B = \tilde{S}_4.$$

Finally if P lies in the domain above the Γ^+ and Γ^- characteristics emanating from the origin $x = 0$, then $x_A < 0$ and $x_B > 0$. Then we have $M_A = M_1$, $\tilde{S}_A = \tilde{S}_1$, $M_B = M_4$ and $\tilde{S}_B = \tilde{S}_4$. The preliminary notation for this domain is ②+③.

Using the general solution given in (2.64) the solution of Riemann's problem becomes:

$$\begin{aligned}
 \text{domain } ① & : M_P = M_1, \\
 & \tilde{S}_P = \tilde{S}_1; \\
 \text{domain } ② + ③ & : M_P = \frac{M_1 + M_4}{2} + \frac{\tilde{S}_1 - \tilde{S}_4}{2}, \\
 & \tilde{S}_P = \frac{\tilde{S}_1 + \tilde{S}_4}{2} + \frac{M_1 - M_4}{2}; \\
 \text{domain } ④ & : M_P = M_4, \\
 & \tilde{S}_P = \tilde{S}_P.
 \end{aligned} \tag{2.65}$$

Let us now discuss some examples of Riemann problems.

2.4.1 Example 1: a density discontinuity; (M, \tilde{S}) -diagram

The first example concerns the time evolution of a density discontinuity in a gas at rest. The initial values at $t = 0$ are shown in figure 2.14.

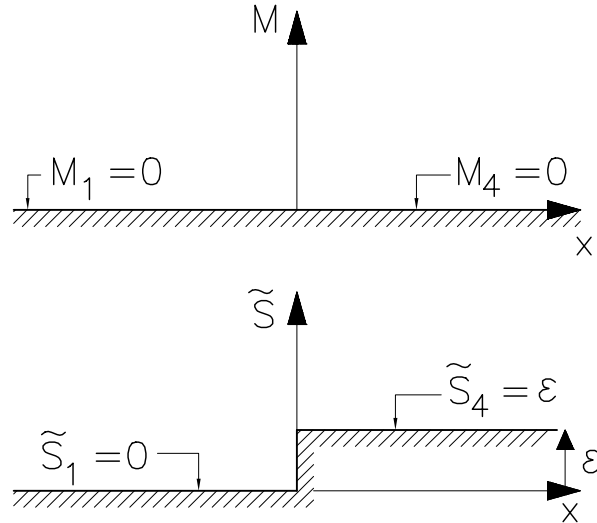
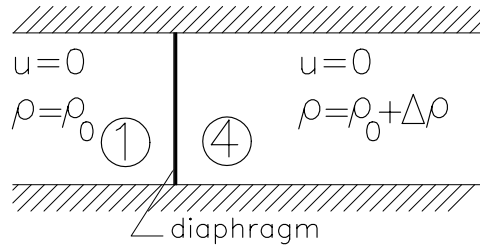


Figure 2.14: Initial values at $t = 0$

These initial data resemble the following physical situation present in a tube at $t \leq 0$ as shown in figure 2.15.

We observe two uniform states in a tube being separated by a diaphragm at $x = 0$, the standard setup for the so-called shock tube problem. Left from the diaphragm the pressure is p_0 and the density is ρ_0 ; right from the diaphragm the pressure is $p_0 + \Delta p$ and the density is $\rho_0 + \Delta \rho$. Because of the assumption of reversibility Δp and $\Delta \rho$ are coupled by $\Delta p = a_0^2 \Delta \rho$. On both sides of the diaphragm the gas is at rest: $u = 0 \Rightarrow M = 0$.

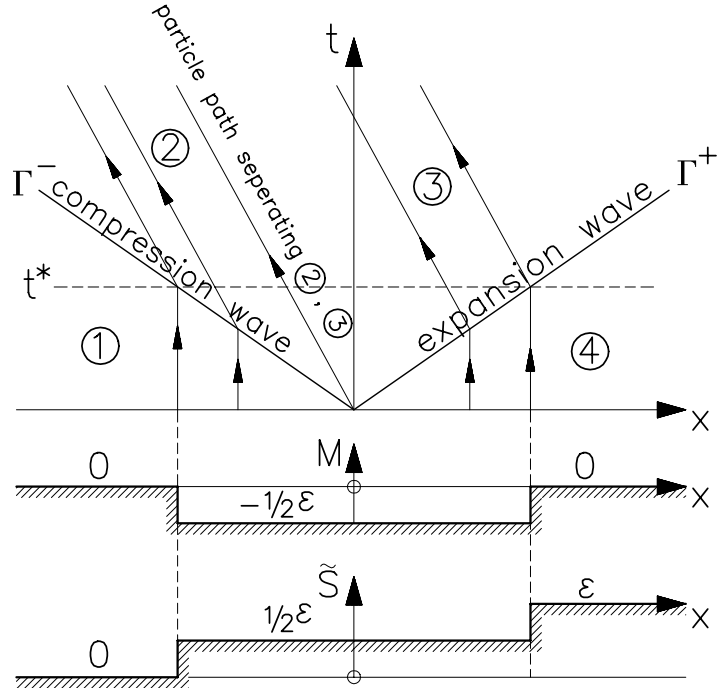
Question: What happens if the diaphragm at $x = 0$ is withdrawn suddenly at $t = 0$?

Figure 2.15: Initial flow situation for $t \leq 0$

Answer: The answer to this question is found by solving the Riemann problem with initial data $M_1 = M_4 = 0$, $\tilde{S}_1 = 0$, $\tilde{S}_4 = \varepsilon$. Using (2.65) one finds:

$$\begin{aligned} \text{domain } ① \quad & M = 0, \quad \tilde{S} = 0; \\ \text{domain } ② \text{ and } ③ \quad & M = -\frac{1}{2}\varepsilon, \quad \tilde{S} = +\frac{1}{2}\varepsilon; \\ \text{domain } ④ \quad & M = 0, \quad \tilde{S} = \varepsilon. \end{aligned}$$

The solution tells us that in domains ① and ④ the gas remains unperturbed with respect to its initial conditions. In domain ② the gas moves with velocity $u = a_0 M = -a_0 \varepsilon / 2$. The (t, x) -diagram together with the behaviour of $M(x)$ and $\tilde{S}(x)$ at a certain time level, t^* , is shown in figure 2.16.

Figure 2.16: Evolution of M and \tilde{S} after diaphragm withdrawal

The figure also shows some particle paths: in ① and ④ the gas is at rest, so the particle paths are straight lines, described by $x = \text{constant}$. In ② the particles move with velocity

$u = a_0 M = -a_0 \varepsilon / 2$ to the left. This makes sense since the pressure drops from right to left. Again we see straight lines but now they are inclined to the left.

The path of the particle initially at the discontinuity $x = 0$ divides ②+③ in separate (sub-) domains ② and ③. Domain ② contains the gas that was originally at $x < 0$. Domain ③ contains the gas that was originally at $x > 0$.

Note that the characteristic (or wave) separating ① and ② is a *compression* wave; it moves to the left into ① and compresses the gas from state ① into state ②. Similarly, the characteristic (or wave) separating ③ and ④ is an *expansion* wave; it moves to the right while expanding state ④ into state ③.

The conditions in the perturbed states ② and ③ are equal; gases in ② and ③ are in the same state. This is a result typical for linear acoustics. In a nonlinear treatment (see chapter 3) the states ② and ③ are generally different and the solution of the Riemann problem then generates *four uniform* domains.

Now we will solve this Riemann problem differently by using (M, \tilde{S}) -diagrams. Let us

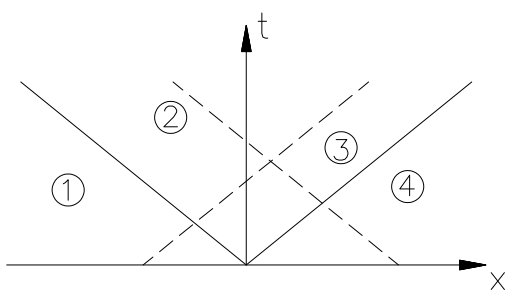


Figure 2.17: (t, x) -diagram

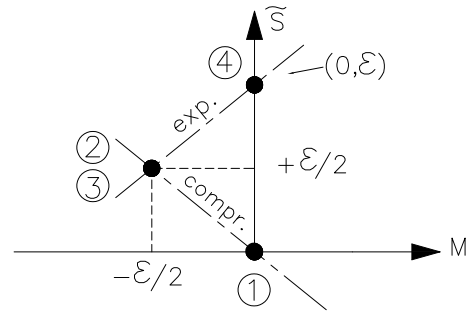


Figure 2.18: (M, \tilde{S}) -diagram

consider the (t, x) -diagram (see figure 2.17), and observe that:

- ①, ②, ③ and ④ are *uniform* states. Uniform means there are no changes of M and \tilde{S} in the same region due to the constant conditions at the initial line.
- Domains ①, ② and ③ are connected by Γ^+ characteristics along which $M + \tilde{S} = \text{constant}$. This implies that the images (locis) of the domains ①, ② and ③ all lie on the same straight line in a (M, \tilde{S}) -diagram. The slope of the line is -1 .
- Similarly, domains ②, ③ and ④ are connected by Γ^- -characteristics on which $M - \tilde{S} = \text{constant}$. Domains ②, ③ and ④ have images (loci) in the (M, \tilde{S}) -diagram that lie on the same straight line with slope $+1$.
- Since we are dealing with homentropic linear theory, the states ② and ③ are equal, so they have the same spot in the (M, \tilde{S}) -diagram.

The solution of the Riemann problem with initial data $M_1 = 0, \tilde{S}_1 = 0, M_4 = 0, \tilde{S}_4 = \varepsilon$ is found as the intersection of the locus of all possible states ② obtainable from ①, with the

locus of all possible states ③ obtainable from ④, see figure 2.18. From the figure the solution is easily obtained as:

$$\begin{aligned} M_2 &= M_3 &= -\frac{1}{2}\varepsilon \\ \tilde{S}_2 &= \tilde{S}_3 &= \frac{1}{2}\varepsilon \end{aligned}$$

2.4.2 Example 2: two colliding flows

Next consider a Riemann problem with initial values at $t = 0$ as shown in figure 2.19:

$$\begin{aligned} \text{State 1: } &x < 0, \quad M_1 = +\varepsilon, \quad \tilde{S}_1 = 0, \\ \text{State 4: } &x > 0, \quad M_4 = -\varepsilon, \quad \tilde{S}_4 = 0, \end{aligned} \quad (2.66)$$

These initial data resemble the flow situation that occurs if two gases in the same state

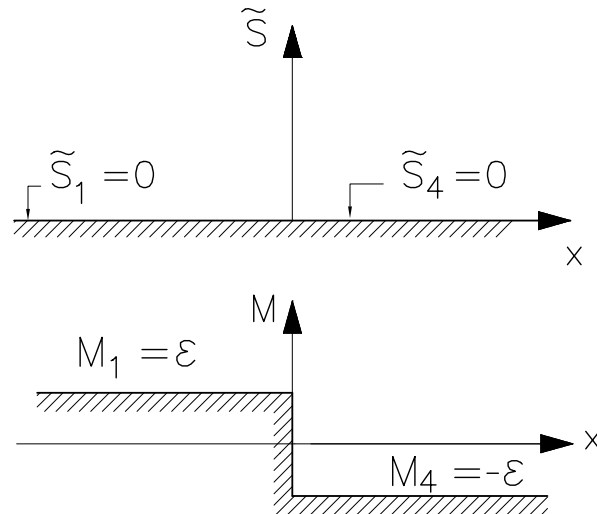


Figure 2.19: Two colliding flows; initial data

$(\tilde{S}_1 = \tilde{S}_4 = 0)$ move toward each other with the 'same' velocity $u_1 = +\varepsilon a_0$, $u_4 = -\varepsilon a_0$, and meet at $x = 0$. This situation can be maintained in a tube for $t \leq 0$ by means of a diaphragm, but it can be created dynamically for one instant ($t = 0$) as explained under example 4. Also the solution of this Riemann problem will be found by using the (M, \tilde{S}) -diagram technique. The initial data $M_1 = \varepsilon$, $\tilde{S}_1 = 0$, $M_4 = -\varepsilon$, $\tilde{S}_4 = 0$ result into the solution $M_2 = M_3 = 0$ and $\tilde{S}_2 = \tilde{S}_3 = \varepsilon$, see figure 2.20. It is seen that the two colliding gas streams create two compression waves; in between these, the motions of the gases cancel each other while the density rises.

2.4.3 Example 3: gas streams running away from each other

This case is similar to example 2, but with the flow velocities reversed; the gases run away from each other with equal speeds but opposite directions.

Initial values (see figure (2.21)):

$$\begin{aligned} \text{State 1: } &x < 0, \quad M_1 = -\varepsilon, \quad \tilde{S}_1 = 0, \\ \text{State 4: } &x > 0, \quad M_4 = +\varepsilon, \quad \tilde{S}_4 = 0, \end{aligned} \quad (2.67)$$

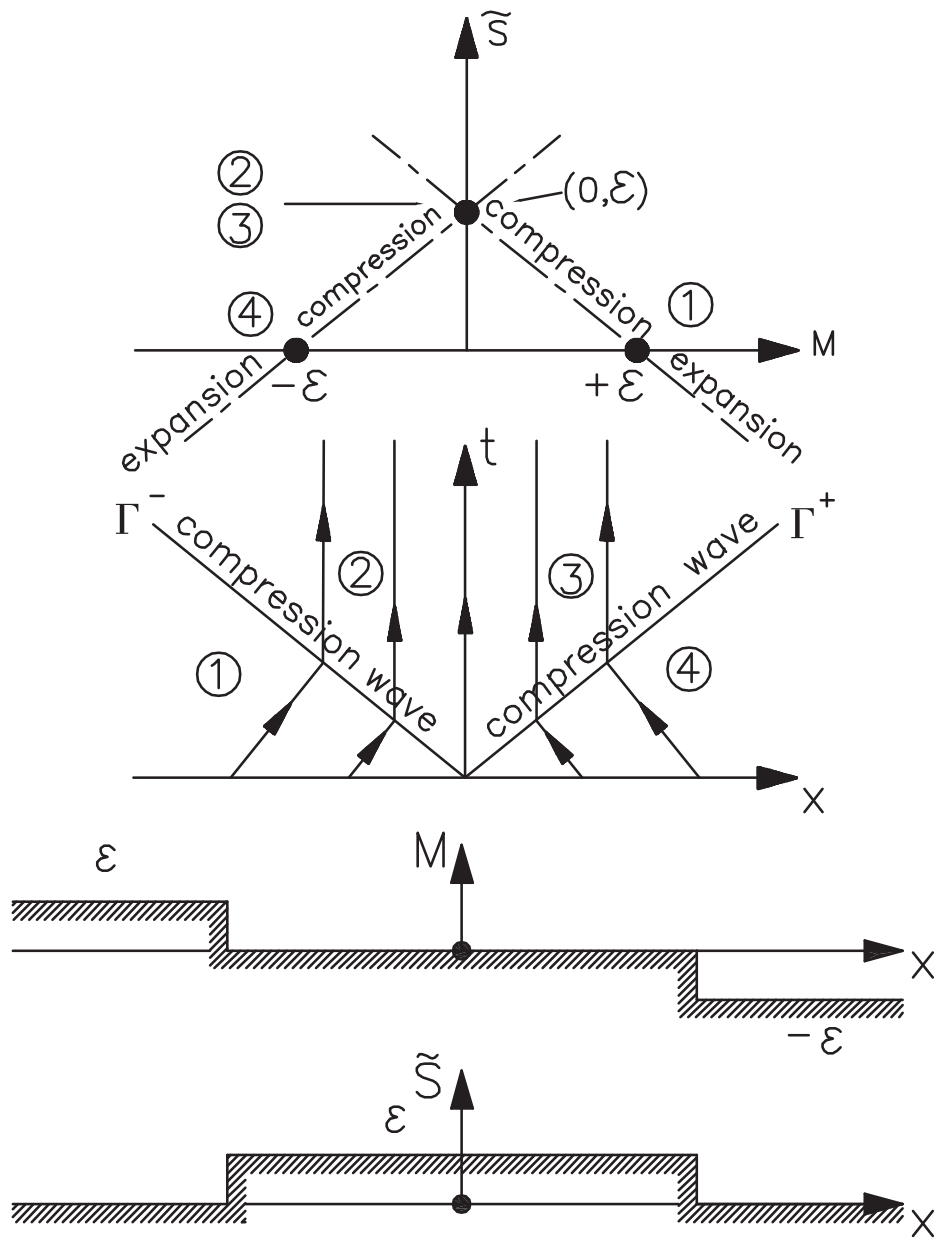


Figure 2.20: Flow collision depicted in (M, \tilde{S}) -diagram

The solution is shown in figure 2.22. The motion of the gases creates two expansion waves; in between these the motions of the gases again cancel each other while the density is now reduced.

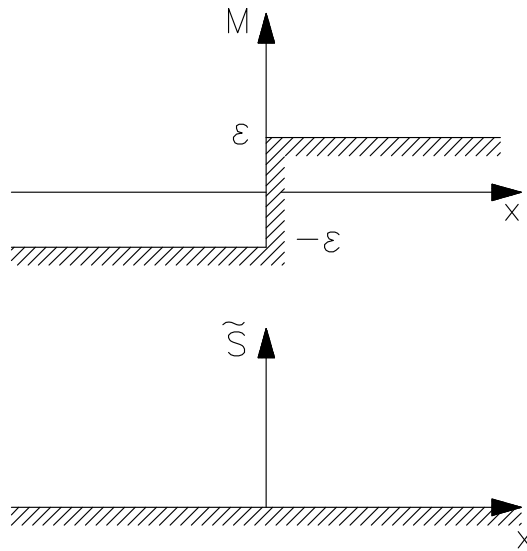


Figure 2.21: Gas streams running away; initial data

2.4.4 Example 4: Moving piston

In this example a Riemann problem is created dynamically in a tube of length l by the action of pistons at both ends of the tube (initially at $x = \pm \frac{l}{2}$). These pistons are set in motion instantaneously at $t = -\frac{l}{2a_0}$. This creates sound waves which meet in the middle of the tube at $t = 0$. At that instant a Riemann problem is created, see figure 2.23. Take for example the left and right piston speeds equal to $U_{P,L} = 2\varepsilon a_0$ and $U_{P,R} = \varepsilon a_0$, acting on an initially uniform fluid at rest. Calling this initial state ① we have $M_0 = 0$, $\tilde{S}_0 = 0$. The states created by the left and the right pistons are labelled ① and ④ respectively, in anticipation of the resulting Riemann problem. The states can be found in the (M, \tilde{S}) -diagram, see figure 2.24 by the intersection of lines. To find state ①, draw the locus of all possible states obtainable from state ① by a right moving wave, and intersect this by the vertical line $M = M_{P,L} = 2\varepsilon$. Similarly, state ④ is found by drawing the locus of all possible states obtainable from ① by a left running wave and intersecting this by the vertical line $M = M_{P,R} = \varepsilon$.

The solution of the ensuing Riemann problem, i.e. finding states ② and ③ can be completed in the same diagram. The results are:

$$\begin{aligned} \text{State 1: } & M_1 = 2\varepsilon, \quad \tilde{S}_1 = 2\varepsilon, \\ \text{State 4: } & M_4 = -\varepsilon, \quad \tilde{S}_4 = -\varepsilon \\ \text{State 2,3: } & M_{2,3} = 3\varepsilon, \quad \tilde{S}_{2,3} = \varepsilon. \end{aligned} \tag{2.68}$$

Note that states ② and ③ have a larger velocity than either piston. This is caused by the extra pressure difference ($p_1 > p_4$) created by the pulsing/pulling actions of the pistons.

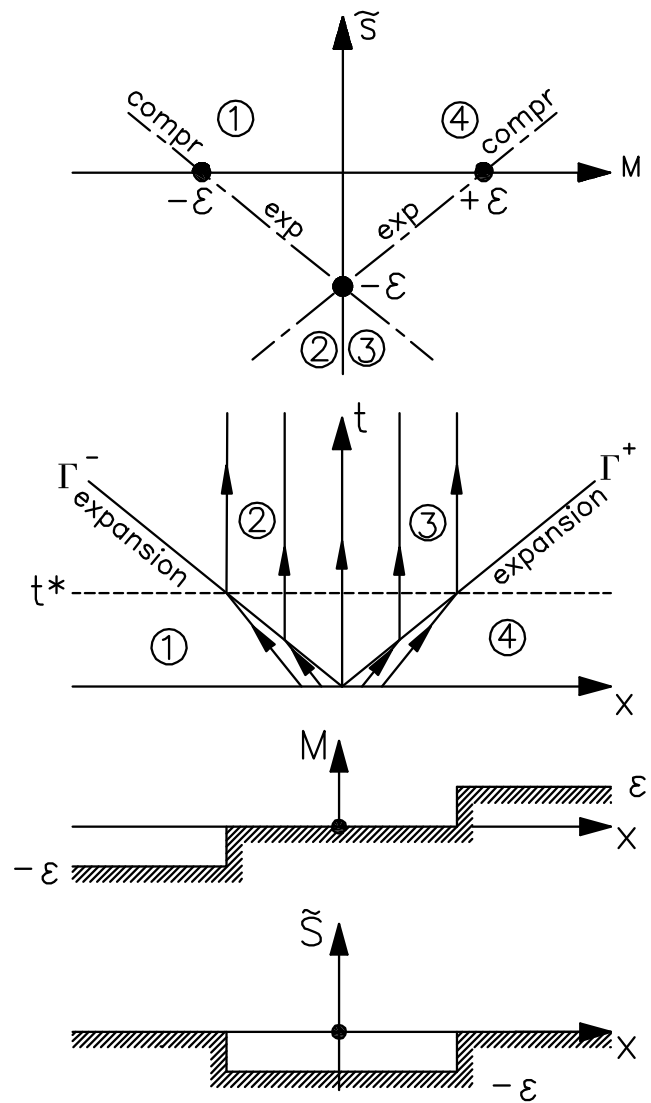
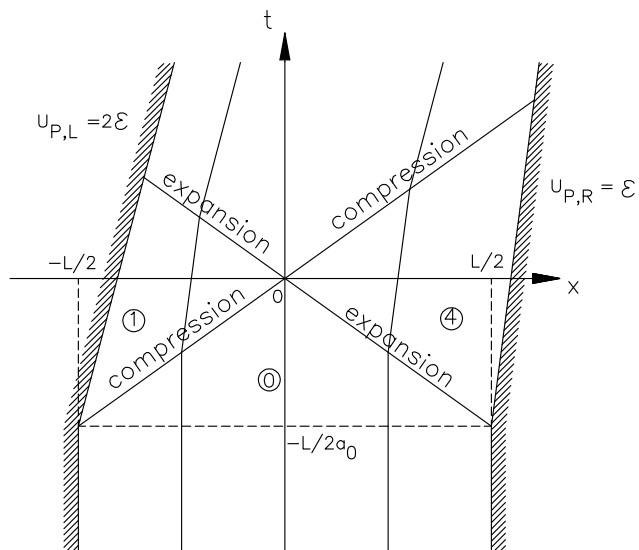
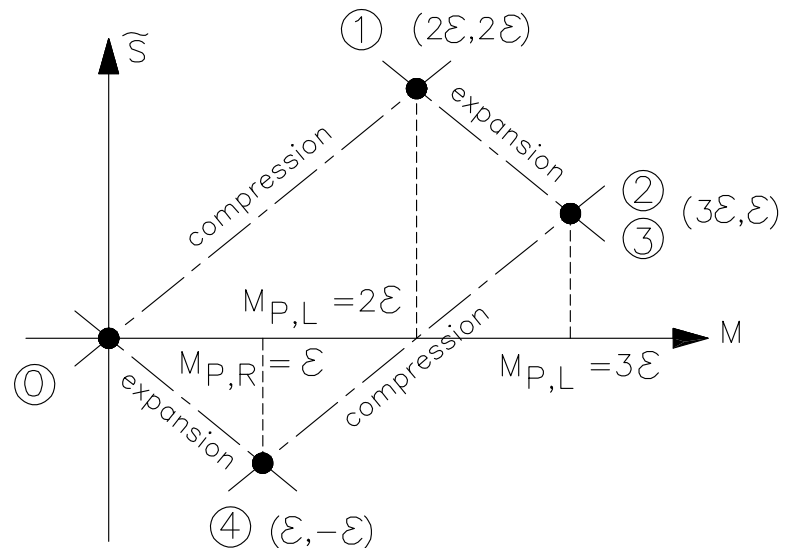


Figure 2.22: Gas streams running away

Figure 2.23: Flow caused by the action of two pistons, (t, x) -diagramFigure 2.24: Flow caused by the action of two pistons; (M, \tilde{S}) -diagram

Chapter 3

One-dimensional unsteady non-linear flows

3.1 Characteristic equations

Let us start from the one-dimensional time-dependent Euler equations in non-conservative form, see (1.33), (1.34) and (1.35). Further, we assume reversibility (smooth flows) so that according to (1.36) the entropy is constant when moving with a fluid particle. Along a particle path the entropy is constant but it may differ from one particle to another. Due to the assumption of reversibility, the energy equation (1.36) is replaced by (1.38) expressing $s = \text{constant}$ along a particle path.

$$\rho_t + u\rho_x + \rho u_x = 0, \quad (3.1)$$

$$u_t + uu_x + \frac{1}{\rho}p_x = 0, \quad (3.2)$$

$$s_t + us_x = 0. \quad (3.3)$$

Since $ds \propto (dp - a^2 d\rho)$, see (1.12), equation (3.3) may be written in terms of p and ρ :

$$p_t - a^2\rho_t + u(p_x - a^2\rho_x) = 0,$$

or

$$p_t + up_x - a^2(\rho_t + u\rho_x) = 0. \quad (3.4)$$

Using (3.1) the ρ -derivatives can be eliminated, yielding

$$p_t + up_x + a^2\rho u_x = 0. \quad (3.5)$$

We would like to make combinations of this equation with (3.2), as we did in the linear case. Therefore, divide (3.5) by ρa , so that it gets the same physical dimension as (3.2), yielding:

$$\frac{p_t}{\rho a} + u\frac{p_x}{\rho a} + au_x = 0,$$

repeat:

$$u_t + uu_x + a\frac{p_x}{\rho a} = 0; \quad (3.2)$$

adding and subtracting these equations yields:

$$u_t + \frac{p_t}{\rho a} + (u + a) \left(u_x + \frac{p_x}{\rho a} \right) = 0, \quad (3.6)$$

$$u_t - \frac{p_t}{\rho a} + (u - a) \left(u_x - \frac{p_x}{\rho a} \right) = 0. \quad (3.7)$$

Introducing the Riemann invariants J^+ and J^- by:

$$dJ^+ = du + \frac{dp}{\rho a}, \quad (3.8)$$

$$dJ^- = du - \frac{dp}{\rho a}, \quad (3.9)$$

then (3.6) and (3.7) become

$$\frac{\partial J^+}{\partial t} + (u + a) \frac{\partial J^+}{\partial x} = 0, \quad (3.10)$$

$$\frac{\partial J^-}{\partial t} + (u - a) \frac{\partial J^-}{\partial x} = 0. \quad (3.11)$$

Apparently there are still two quantities J^+ and J^- transported unchanged along the characteristics Γ^+ and Γ^- respectively; the characteristic speeds are now $(u + a)$ and $(u - a)$, indicating that the signals travel with speeds $\pm a$ with respect to the gas which has a speed u .

J^+ and J^- are the Riemann invariants, in general they cannot be given in integrated form, so we have to regard J^+ and J^- as functions of the *independent* variables x and t ; J^+ and J^- are determined at most by differential relations as given in equations (3.8) and (3.9), Γ^+ and Γ^- are characteristics defined by:

$$\Gamma^\pm : \frac{dx}{dt} = u \pm a. \quad (3.12)$$

Since the characteristic speeds are no longer constant but depend on the solution, the characteristics are generally curved in the non-linear case.

In the *homentropic* case all particles have the same entropy, the relation between pressure and density is given by Poisson's equation (1.13):

$$p = C\rho^\gamma.$$

In that case the term $\frac{dp}{\rho a}$ can be written as

$$\frac{dp}{\rho a} = \frac{2}{\gamma - 1} da.$$

So for homentropic flow equations (3.8) and (3.9) can be integrated:

$$J^\pm = u \pm \frac{2}{\gamma - 1} a. \quad (3.13)$$

Since the entropy equation (3.3) has the same form as the equations for the Riemann invariants, we consider that equation also among the characteristic equations and call the particle path

a characteristic Γ^0 . The total set of characteristic equations may therefore be written as:

$$\left\{ \frac{\partial}{\partial t} + (u - a) \frac{\partial}{\partial x} \right\} J^- = 0, \quad (3.14)$$

$$\left\{ \frac{\partial}{\partial t} + (u) \frac{\partial}{\partial x} \right\} s = 0, \quad (3.15)$$

$$\left\{ \frac{\partial}{\partial t} + (u + a) \frac{\partial}{\partial x} \right\} J^+ = 0, \quad (3.16)$$

or

$$dJ^- = 0 \quad \text{along } \Gamma^- \text{ with } \left(\frac{dx}{dt} \right) = u - a, \quad (3.17)$$

$$ds = 0 \quad \text{along } \Gamma^0 \text{ with } \left(\frac{dx}{dt} \right) = u, \quad (3.18)$$

$$dJ^+ = 0 \quad \text{along } \Gamma^+ \text{ with } \left(\frac{dx}{dt} \right) = u + a. \quad (3.19)$$

The latter equations can also be used if the initial values and also the corresponding solution are $\in C^0$ only in certain points; the entropy distribution may actually contain discontinuities. The characteristics Γ^\pm will abruptly change their slope when they cross a Γ^0 that carries an entropy jump. Three characteristics can be drawn through an arbitrary point in the (t, x) -space, see figure 3.1.

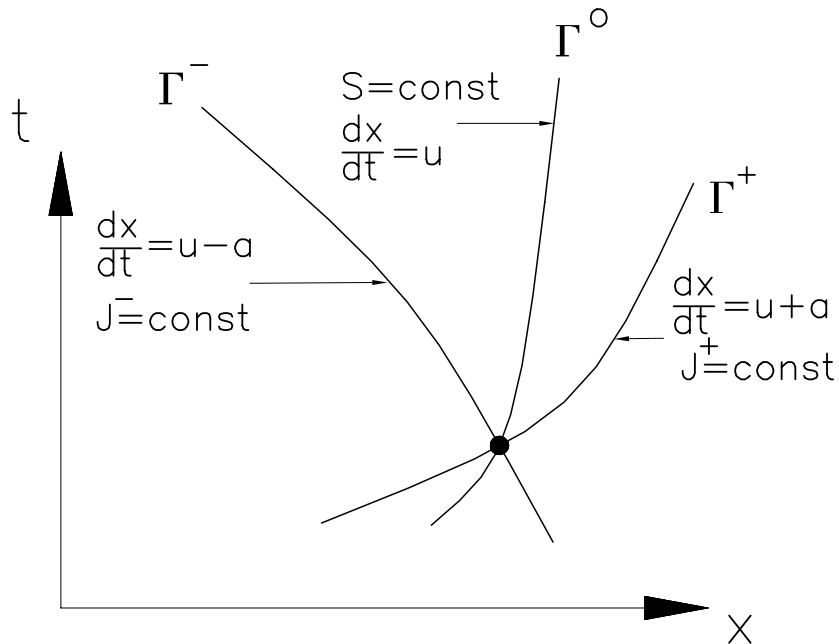
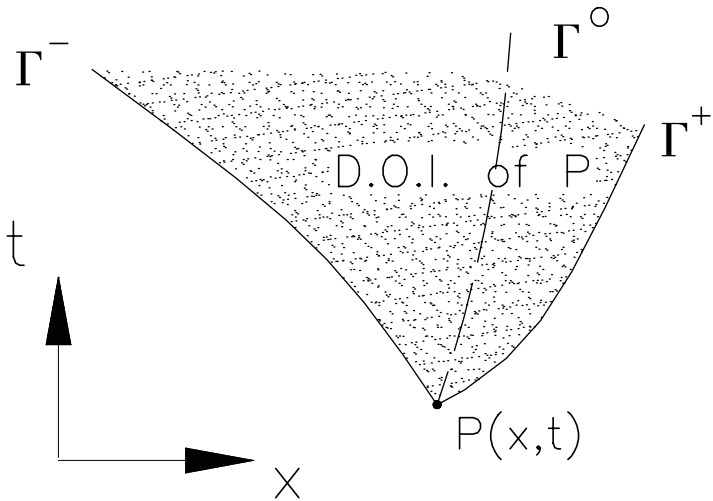
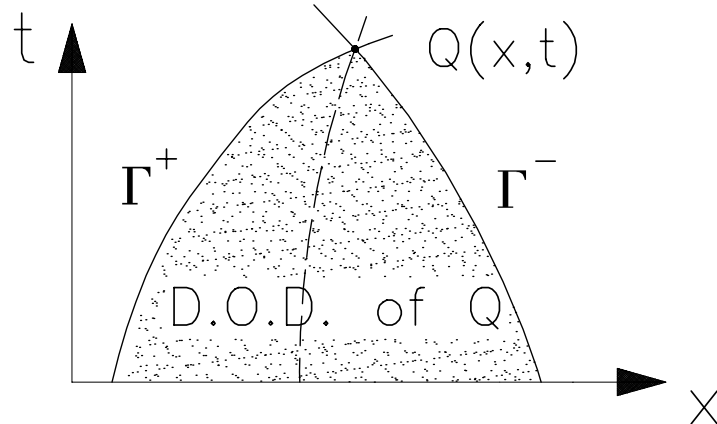


Figure 3.1: The three characteristics

Figure 3.2: Domain of influence of $P(x,t)$

Domain of influence (DOI) and domain of dependence (DOD)

Figure 3.3: Domain of dependence of $Q(x,t)$.

In *linear* acoustics (chapter 2) we have seen that a point in (t,x) -space influences only the solution along the two characteristics Γ^+ and Γ^- through that point. In the *non-linear* case however the influence spreads over a 2-D domain due to the dependence of the characteristic slopes on the solution itself.

Figure 3.2 shows the domain of influence in the (t,x) -space of an arbitrary point $P(x,t)$. Any point in the domain of influence of $P(x,t)$ is affected by an infinitesimal perturbation of variables in P . In figure 3.3 the domain of dependence of an arbitrary point $Q(x,t)$ is shown. Any point in the domain of dependence of $Q(x,t)$ affects the solution in Q .

Both domains are interrelated as follows: the domain of dependence of Q contains all points which have Q in their domain of influence; the domain of influence of P contains all points that have P in their domain of dependence.

3.2 Simple waves, non-linear

Simple waves are a special class of solutions of the characteristic equations. As in linear theory a simple wave appears if one of the Riemann invariants J^+ or J^- is constant in a certain domain. Let us examine some properties of simple waves and assume that $J^- = \text{constant}$; furthermore we assume homentropic flow:

$$J^- = u - \frac{2a}{\gamma - 1} = J_0^- = \text{const.} \quad (3.20)$$

Observe that a linear relation exists between the variables u and a . The Riemann invariant J^+ becomes

$$J^+ = u + \frac{2a}{\gamma - 1} = 2u - J_0^- = \frac{4a}{\gamma - 1} + J_0^-. \quad (3.21)$$

Thus, in a simple wave along the characteristic Γ^+ both u and a must be constant. Hence, along Γ^+ , $u + a$ is constant as well, so we may write:

$$\frac{\partial}{\partial t}(u + a) + (u + a)\frac{\partial}{\partial x}(u + a) = 0, \quad (3.22)$$

which exactly states that in a simple wave having $J^- = \text{constant}$ the state variable $(u + a)$ is constant along curves: $\Gamma^+ : \frac{dx}{dt} = u + a$.

This implies that the characteristic Γ^+ itself must be a straight line.

Conclusion: In a simple wave having $J^- = \text{constant}$ the Γ^+ characteristics are *straight lines* and similarly: in a simple wave having $J^+ = \text{constant}$ the Γ^- characteristics are *straight lines*.

The ' $J^- = \text{constant}$ ' simple waves are called *forward running* waves. The flow variables in the simple wave are governed by equation (3.22). Using the state quantity $v = u + a$, being the characteristic speed of Γ^+ , this equation is the inviscid form of the so called Burgers equation:

$$v_t + vv_x = \nu v_{xx}; \quad (3.23)$$

the right-hand-side expresses the contribution of viscosity.

So in a forward simple wave (J^+ is the only variable) the 1-D Euler equations reduce to a single equation having the form

$$v_t + vv_x = 0. \quad (3.24)$$

The same equation with $w = u - a$ is obtained for a *backward running* simple wave (J^- is variable and J^+ is constant):

$$w_t + ww_x = 0 \quad (3.25)$$

In this case the Γ^- characteristics are straight lines in the (t, x) -plane.

Curiosity In the unrealistic situation that $\gamma = 3$ the characteristic equations (3.14) and (3.16) take the form of two decoupled inviscid Burgers equations because $J^\pm = u \pm a$ in that case. Hence for $\gamma = 3$ the Γ^+ and Γ^- characteristics are all straight lines. (Useful test case for numerical gas dynamics!)

3.3 Simple waves created by a moving piston

Consider a semi-infinite constant area tube filled with a gas at rest, labelled “0”. At the tube’s left end ($x = 0$) a moving piston is located; at the right the tube extends to infinity:

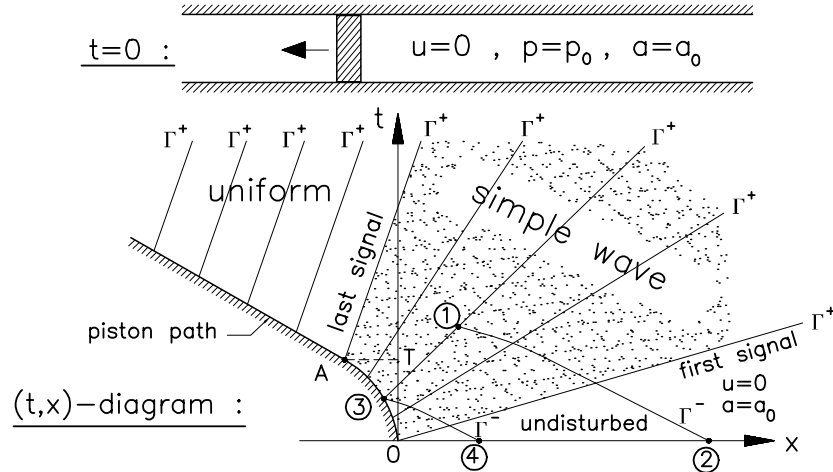


Figure 3.4: Simple wave in a one-dimensional flow

The piston is smoothly accelerated backwards ($x < 0$) from $t = 0$ to $t = T$, at which time it has reached a *negative* speed U_T . From that time on the piston moves with constant speed U_T further backward. Figure 3.4 shows the (t, x) -diagram.

The first signal telling the gas that the piston started to move travels along the Γ^+ -characteristic $x = a_0 t$. The last signal telling the gas that the piston stopped accelerating travels along the Γ^+ characteristic going through the point A (see figure 3.4) located on the path of the piston. This characteristic has a slope $\frac{dx}{dt} = U_T + a_T$. The flow between the first and the last signal is a *simple wave* because J^- is constant in the whole domain.

All Γ^+ -characteristics are straight lines. Beyond the last signal a domain appears having constant conditions: $u = U_T$, $a = a_T$. The value of a_T follows from

$$J^- = u - \frac{2a}{\gamma - 1} = U_T - \frac{2a_T}{\gamma - 1} = -\frac{2a_0}{\gamma - 1},$$

yielding

$$a_t = a_0 + \frac{\gamma - 1}{2} U_T. \quad (3.26)$$

The slope of the Γ^+ -characteristics in the uniform domain is $U_T + a_T$, which yields that

$$\left(\frac{dx}{dt} \right)_{\Gamma^+} = U_T + a_T = a_0 + \frac{\gamma + 1}{2} U_T. \quad (3.27)$$

The solution in the simple wave region is governed by the following set of equations, which is obtained as follows; take an arbitrary point ① in the simple wave and let point ③ be the intersection of the Γ^+ -characteristic through ① and the piston path. Assume that the velocity of the piston $u_p(t)$ is prescribed; so if t_3 should be known then $u_3 = u_p(t_3)$ is also known. We

already knew that u and a are constant along Γ^+ , hence

$$u_1 = u_3 = u_p(t_3) \quad (3.28)$$

$$a_1 = a_3 = a_0 + \frac{\gamma - 1}{2} u_p(t_3) \quad (3.29)$$

The solution given by equations (3.28) and (3.29) depends on the actual value of t_3 .

How to find t_3 for a given point ①? From figure 3.4 we observe that point ③ is found as the intersection of the piston path $x_p(t)$ with the Γ^+ -characteristic through ①: The piston path:

$$x_p(t) = \int_0^t u_p(\tau) d\tau \quad (3.30)$$

The $\Gamma^+(1)$ characteristic is given by:

$$x_p - x_1 = (u_p + a_3)(t_3 - t_1) \quad (3.31)$$

Knowing the prescribed function $u_p(t)$ and using (3.29) (to get a_3) the equations (3.30) and (3.31) can be solved to find t_3 .

Note: if $u_p(t)$ is linear in t , for $0 \leq t \leq T$, then $x_p(t)$ is quadratic in t and one has to solve a quadratic equation to find t_3 . But in general solving (3.30) and (3.31) will require a numerical rootfinder.

In the case $t_3 \geq T$, we always have

$$u_3 = u_p(t \geq T) = U_T, \quad (3.32)$$

$$a_3 = a_T = a_0 + \frac{\gamma - 1}{2} U_T. \quad (3.33)$$

Equation (3.33) leads to the interesting observation that if U_T takes the value

$$U_T = \frac{2}{\gamma - 1} a_0 \quad (3.34)$$

we get $a_3 = 0$ and also $p_3 = 0$ and $\rho_3 = 0$. What does that mean?

The piston has been pulled so fast that the gas has expanded itself to the limit of *vacuum*. Pulling the piston away even faster will create a vacuum between the piston and the gas, since the latter can no longer follow the piston, see figure 3.5.

The speed $\frac{2}{\gamma - 1} a_0$ is the maximum speed that a gas particle from its rest state ($u = 0, a = a_0$) can reach. For air ($\gamma = 1.4$) the maximum speed is $u_{max} = 5a_0$.

Comments

- Piston withdrawal in a tube filled with gas at rest creates an expanding flow being a simple wave. Simple waves can also be created by moving the piston *into* the gas. Then a compression simple wave appears, such a wave would not last for ever but a shock is formed which violates the prerequisites (constant entropy and J^-) for a simple wave.
- A simple wave-region always borders at least a uniform region; the boundary is always a straight characteristic. Notice that in Fig. (3.4) the simple wave is bordered by two uniform regions, i.e. the undisturbed region $u = 0, a = a_0$ and the region beyond the last signal having $u = u_T, a = a_T = a_0 + \frac{\gamma - 1}{2} U_T$.

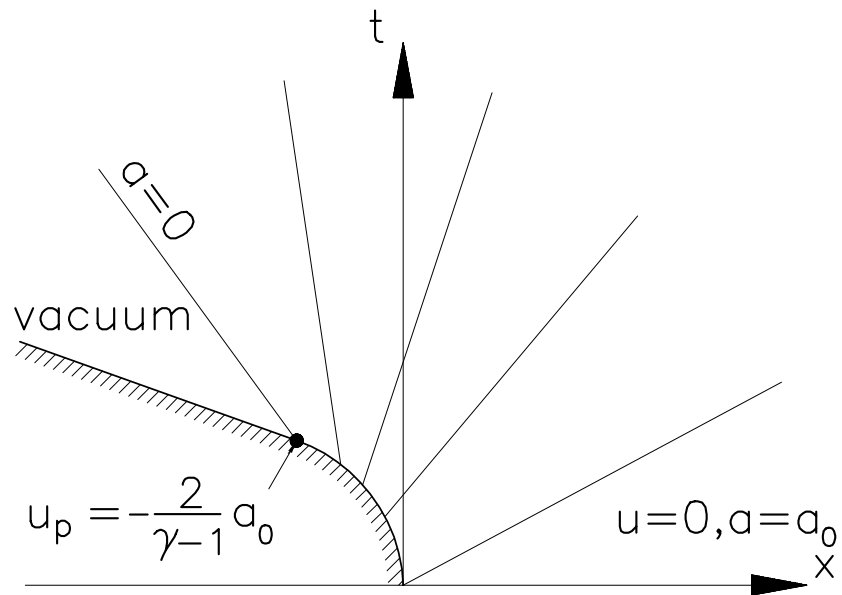
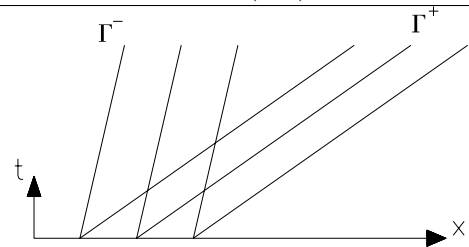
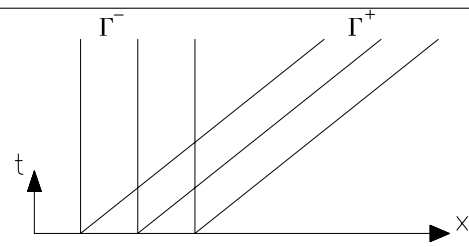
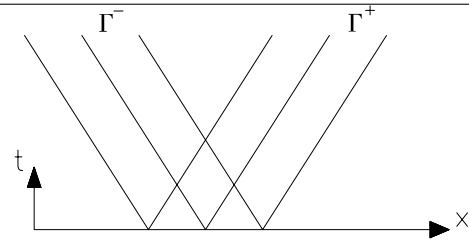
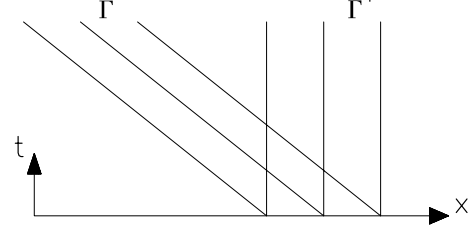
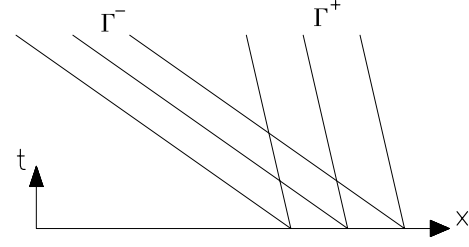


Figure 3.5: Expansion caused by a piston withdrawal

- Uniform regions can be distinguished with respect to Mach number: $M = u/a$ and its influence on the slope of the Γ^\pm characteristics: $\frac{dx}{dt} = u \pm a$ respectively. The various possibilities that can appear in the (t, x) -plane are shown in the following diagram.

Table 3.1: Various uniform flow regions in the (t, x) -plane

Type of flow	u	$u + a$	$u - a$	Characteristics in (t, x) -plane
Supersonic flow to the right	$u > a$	> 0	> 0	
Sonic flow to the right	$u = a$	> 0	$= 0$	
Subsonic flow	$-a < u < a$	> 0	< 0	
Sonic flow to the left	$u = -a$	$= 0$	< 0	
Supersonic flow to the left	$u < -a$	< 0	< 0	

3.4 Centered expansion wave

3.4.1 Flow variables in the centered expansion wave

A *centered* expansion wave results if the piston is withdrawn instantaneously to the speed U_T . The centred expansion may be regarded as the limit case of the previous case when T is small with respect to time intervals we are interested in, i.e. extend figure 3.4 to large x and t and look at the expansion wave from far. Then we observe a picture that is shown in figure 3.6.

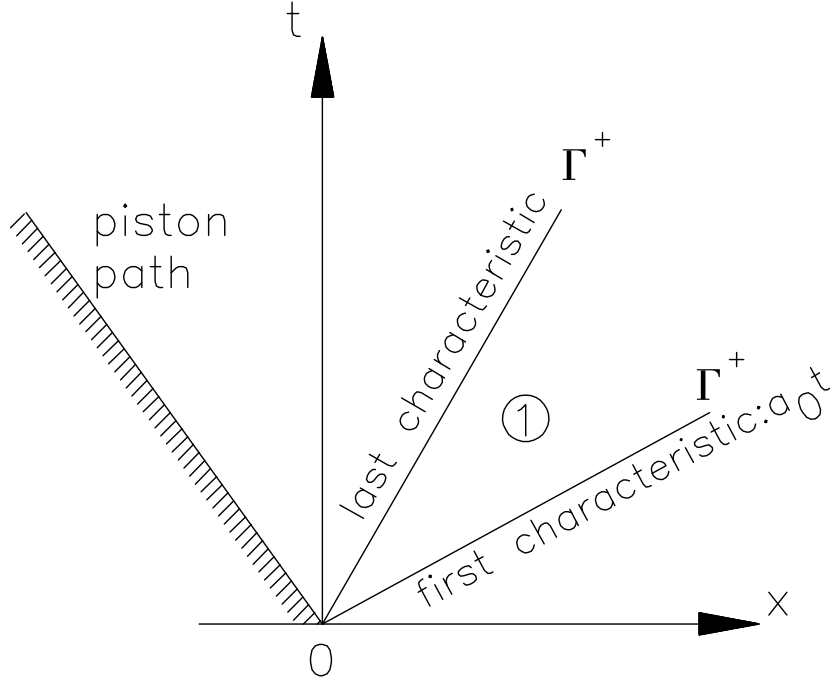


Figure 3.6: Centered expansion wave due to instantaneous piston withdrawal

The center of the wave at O is now a singularity; because J^+ is constant on the Γ^+ characteristics, J^+ is multi-valued in O; together with J^+ also the flow variables u, a, p, ρ are multi-valued.

The solution in the centered wave region, i.e. domain ①, is found by considering a Γ^- -characteristic going through a point 1 in domain ①:

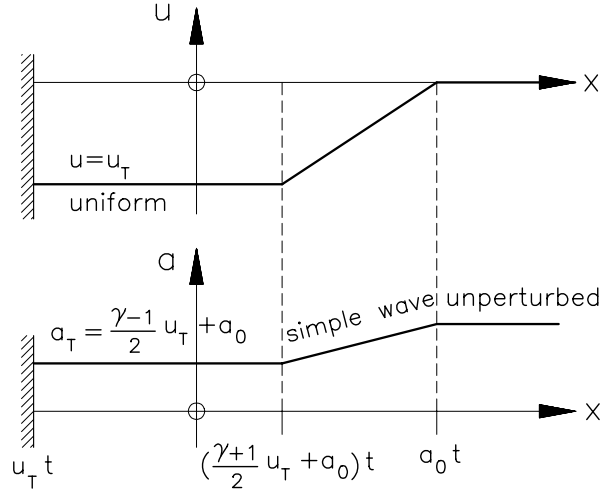
$$\Gamma_{(1)}^- : u_1 - \frac{2}{\gamma - 1} a_1 = \text{constant} = -\frac{2a_0}{\gamma - 1}. \quad (3.35)$$

Furthermore we use the fact that 1 lies on a characteristic Γ^+ having a slope

$$\frac{dx}{dt} = u_1 + a_1 = \frac{x_1}{t_1}. \quad (3.36)$$

From equations (3.35) and (3.36) we find the solution:

$$u_1 = \frac{2}{\gamma + 1} \left(\frac{x_1}{t_1} - a_0 \right). \quad (3.37)$$

Figure 3.7: $u(x)$ and $a(x)$ at constant t

This shows that the disturbance of u is linear in x for constant t . A similar conclusion results for the variable a , see figure 3.7.

For an arbitrary point in domain ① we now omit the subscript 1; the solution for u and also for other flow-variables in terms of x/t becomes:

$$u = \frac{2}{\gamma+1} \left(\frac{x}{t} - a_0 \right) \quad (3.38)$$

$$a = \frac{\gamma-1}{\gamma+1} \frac{x}{t} + \frac{2}{\gamma+1} a_0 \quad (3.39)$$

$$u + a = \frac{x}{t} \quad (\text{slope of } \Gamma^+) \quad (3.40)$$

$$u - a = \frac{3-\gamma}{\gamma+1} \frac{x}{t} - \frac{4}{\gamma+1} a_0 \quad (\text{slope of } \Gamma^-) \quad (3.41)$$

From equation (3.39) and constant entropy we find the distributions for ρ and p :

$$\frac{\rho(x,t)}{\rho_0} = \left(\frac{a}{a_0} \right)^{\frac{2}{\gamma-1}} \quad (3.42)$$

$$\frac{p(x,t)}{p_0} = \left(\frac{a}{a_0} \right)^{\frac{2\gamma}{\gamma-1}} \quad (3.43)$$

The Mach number in the simple wave is now equal to:

$$M = \left| \frac{\frac{2}{\gamma+1} \left(\frac{x}{t} - a_0 \right)}{\frac{\gamma-1}{\gamma+1} \frac{x}{t} + \frac{2}{\gamma+1} a_0} \right| = \left| \frac{2\frac{x}{t} - 2a_0}{(\gamma-1)\frac{x}{t} + 2a_0} \right| \quad (3.44)$$

From this formula it is evident that at

$$\frac{x}{t} = a_0 \quad \Rightarrow \quad M = 0$$

$$\frac{x}{t} = 0 \quad \Rightarrow \quad M = 1$$

$$\frac{x}{t} \leq 0 \quad \Rightarrow \quad M \geq 1$$

3.4.2 Particle path in a centered simple wave

The gas particle residing at x_0 is hit by the first wave of the expansion fan when $t = t_0$ where $t_0 = x_0/a_0$, see figure 3.8.

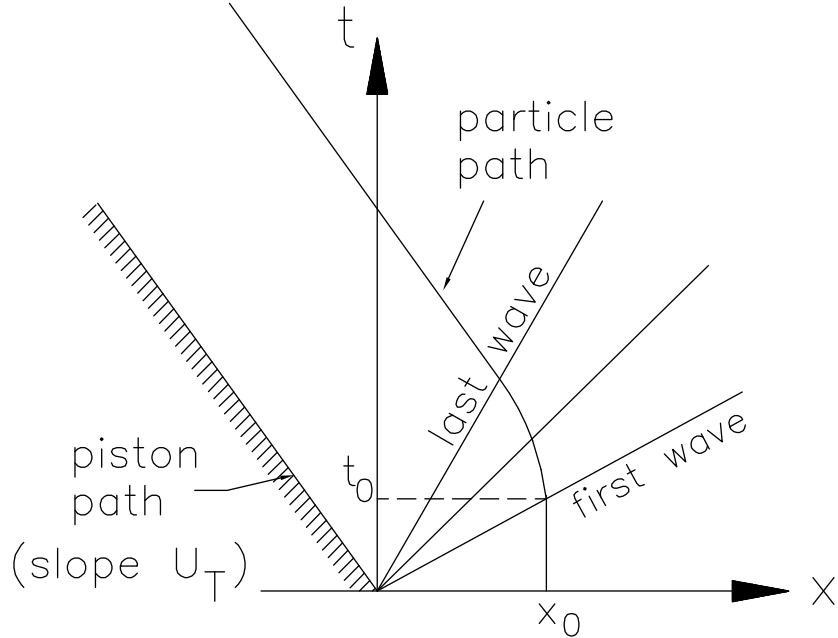


Figure 3.8: Particle path

At that time instant the particle starts to move. As long as the particle is in the expansion wave its path $X : X(t)$ follows from the differential equation:

$$\frac{dX}{dt} = u = \frac{2}{\gamma + 1} \left(\frac{X}{t} - a_0 \right) \quad (3.45)$$

with initial condition

$$X = x_0 \quad \text{at} \quad t = \frac{x_0}{a_0} = t_0.$$

Experience in solving this type of equation teaches us that the solution is a linear combination of linear terms in t (caused by the constant in the right hand side term) and a $t^{2/(\gamma+1)}$ term (caused by the x/t term). Introduce the dimensionless quantities:

$$\xi = \frac{X}{x_0} = X/(a_0 t_0), \quad \tau = \frac{t}{t_0}; \quad (3.46)$$

Equation (3.45) may then be written as:

$$\frac{d\xi}{d\tau} = \frac{2}{\gamma + 1} \left(\frac{\xi}{\tau} - 1 \right). \quad (3.47)$$

To solve (3.47) try the following solution:

$$\xi = \alpha \tau^{\frac{2}{\gamma+1}} + \beta \tau$$

and verify that $\alpha = \frac{\gamma+1}{\gamma-1}$ and $\beta = -\frac{2}{\gamma-1}$ satisfy the initial conditions, $\xi = 1$ and $\tau = 1$.

Hence the particle that starts moving at $t = t_0$ from its position x_0 follows the path:

$$\frac{X(t)}{a_0 t_0} = \frac{\gamma+1}{\gamma-1} \left(\frac{t}{t_0} \right)^{\frac{2}{\gamma+1}} - \frac{2}{\gamma-1} \frac{t}{t_0}. \quad (3.48)$$

This path is followed as long as the Γ^+ -characteristic with slope $U_T + a_T$ is not crossed, or in mathematical terms:

$$\left(\frac{\gamma+1}{2} U_T + a_0 \right) t \leq X(t) \leq x_0. \quad (3.49)$$

After crossing the particle path is a straight line with slope $\frac{dx}{dt} = U_T$.

3.5 Riemann problem, non-linear

We encountered the Riemann problem in the case of linear acoustics. In non-linear theory it is formulated in a similar way and is stated as follows: find the solution of the 1-D, unsteady non-linear flow equations with constant initial conditions except for a single jump discontinuity (say at $t = 0$).

Initial data at $t = 0$:

$$u(x, 0) = \begin{cases} u_1 & \text{for } x < 0 \\ u_4 & \text{for } x > 0 \end{cases}, \quad a(x, 0) = \begin{cases} a_1 & \text{for } x < 0 \\ a_4 & \text{for } x > 0 \end{cases}$$

The solution of the Riemann problem in the full non-linear case differs from the linear case in three aspects:

1. There appears an extra *entropy wave* carrying an entropy jump. This wave travels with characteristic speed u so that its path is a characteristic Γ^0 . There are now really *four* different domains: the pre-state domains ① and ④ and the post-state domains ② and ③. The entropy wave separates ② and ③. Frequently these domains are also labelled:

$$\mathcal{L} \equiv ①, \quad \mathcal{L}^* \equiv ②, \quad \mathcal{R}^* \equiv ③, \quad \mathcal{R} \equiv ④.$$

The entropy wave appears as a contact discontinuity.

2. The two acoustic waves are now non-linear, meaning that they appear either as a shock (discontinuity) or as an expansion.
3. The expansion is a fan occupying some domain in space-time, so it is not a discontinuity.

The solution techniques used for linear and for non-linear Riemann-problems are remarkable similar. In linear theory the (M, \tilde{S}) diagram technique was useful; in the non-linear case the ‘velocity-pressure’ or (u, p) -plane is very appropriate. The reason that we now use (u, p) instead of (M, \tilde{S}) is that the post-states ② and ③ must have the same velocity and the same pressure because ② and ③ are separated by a contact discontinuity.

In preparing ourselves to solve the non-linear Riemann-problem, let us first consider shocks and expansions running into a prescribed ‘pre-state’ (① or ④) and let us look in particular for equations involving the post-wave pressure.

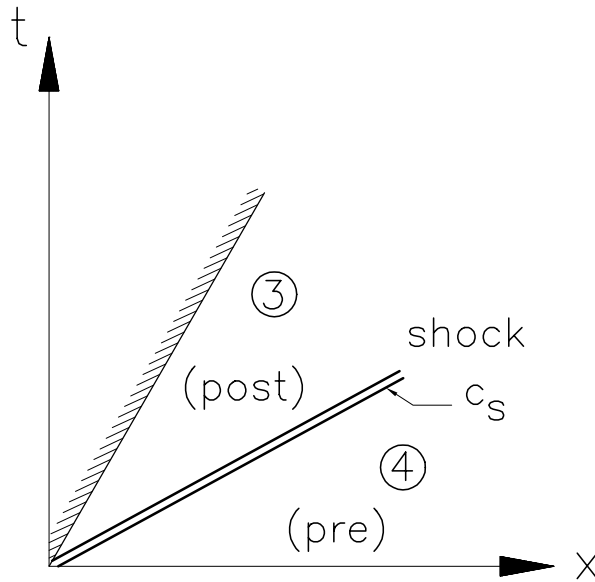


Figure 3.9: Shock advancing in a gas

3.5.1 Shock moving into a gas; Hugoniot curve

Consider a shock wave, for example generated by a moving piston, that advances with speed c_s into a gas which is in the 'pre-state' ④ having prescribed a pressure p_4 and a sound speed a_4 .

Assume for now that the gas in the 'pre-state' ④ is at rest: $u_4 = 0$.

Due to the moving shock, see figure 3.9, the pressure rises and the gas is brought into motion, thus: $p_3 > p_4$ and $u_3 > 0$.

How is the pressure rise $\Delta p = p_3 - p_4$ be related to the velocity increase $\Delta u = u_3 - u_4$?

Consider the process in a shock frame and apply the Rankine-Hugoniot relations for mass and momentum (for now take $u_4 = 0$):

$$\begin{aligned} \text{mass: } & \rho_{\text{pre}} c_s = \rho_{\text{post}} (c_s - u_3) = m; \\ \text{momentum: } & p_{\text{pre}} + \rho_{\text{pre}} c_s^2 = p_{\text{post}} + \rho_{\text{post}} (c_s - u_3)^2. \end{aligned}$$

Inserting the mass flux m into the momentum equation gives:

$$p_{\text{pre}} + m c_s = p_{\text{post}} + m (c_s - u_3),$$

or

$$\Delta p = \pm m \Delta u \quad (3.50)$$

The + sign regards a shock moving to the right and the - sign is for a shock moving to the left.

From equation (1.50) the shock velocity c_s is calculated from the pressure rise as:

$$|c_s| = a_{\text{pre}} \sqrt{1 + \frac{\gamma + 1}{2\gamma} \frac{\Delta p}{p_{\text{pre}}}} \quad (3.51)$$

so that the mass flux m is determined as

$$m = \rho_{\text{pre}}|c_s| = \rho_{\text{pre}}a_{\text{pre}}\sqrt{1 + \frac{\gamma+1}{2\gamma}\frac{\Delta p}{p_{\text{pre}}}} \quad (3.52)$$

Equations (3.50) and (3.52) together describe the relation between Δp and Δu for a shock moving with speed c_s . Thus for a shock moving to the right, with mass flux m_R , we have found:

$$p_3 - p_4 = m_R(u_3 - u_4) \quad (3.53)$$

$$m_R = \rho_4 a_4 \sqrt{1 + \frac{\gamma+1}{2\gamma} \frac{p_3 - p_4}{p_4}}. \quad (3.54)$$

The two relations above give all possible ‘post shock’ states ③ that are obtainable from the ‘pre-shock’ state ④ by passing a shock!

The curve $p_3 = f(u_3; u_4, p_4)$ in the (p, u) -plane is called the *Hugoniot* curve; properties of the Hugoniot curves are discussed in section 3.5.4. Contrary to linear theory only the part of the curve with $p_3 > p_4$ can be used.

Consider the Hugoniot curve in the weak shock limit. Assume a weak shock with $(p_3 - p_4) \ll p_4$; then $m_R \approx \rho_4 a_4$ and therefore

$$\Delta p = \rho_4 a_4 \Delta u,$$

or

$$\Delta u - \frac{\Delta p}{\rho_4 a_4} = 0. \quad (3.55)$$

Notice that equation (3.55) is a discretisation of the characteristic equation along a Γ^- characteristic (see e.g. 3.9) that would cross the shock!!!

Introducing

$$M = \frac{\Delta u}{a_4} \quad \text{and} \quad \tilde{S} = \frac{\Delta \rho}{\rho_4} = \frac{\Delta p}{\rho_4 a_4^2},$$

equation (3.55) can be reduced to

$$a_4 M - \frac{\rho_4 a_4 \tilde{S}}{\rho_4 a_4} = 0,$$

or

$$M - \tilde{S} = 0.$$

In the weak shock limit the shock jump reduces to the condition that the Riemann invariant J^- in the linear theory must be constant crossing the shock.

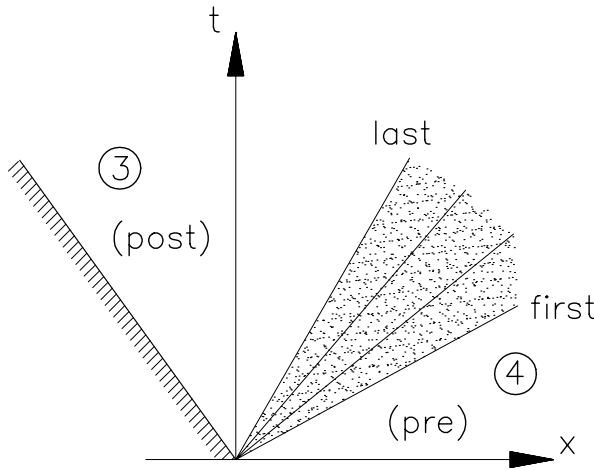


Figure 3.10: Expansion advancing in a gas

3.5.2 Expansion moving into a gas; Poisson curve

Remember we are preparing ourselves to solve the non-linear Riemann problem; to that end we now consider an expansion into a prescribed ‘pre-state’. Consider a right running expansion wave that runs into the gas with prescribed pressure p_4 and prescribed sound speed a_4 , e.g. it runs into ‘pre-state’ ④. The (t, x) -diagram as it is in figure 3.10 shows the process as it is generated by a piston moving to the left.

Note that the expansion is a continuous process that is homentropic because all particles have the same initial entropy s_4 and there are no shocks so that entropy is kept constant at the initial level.

Due to the expansion the pressure decreases and the gas accelerates until it attains the values p_3 and u_3 at the ‘post-state’ respectively. Due to expansion the pressure decreases: $p_3 < p_4$.

As in the shock case, we want to relate the pressure difference $\Delta p = p_3 - p_4$ to the velocity difference $u_3 - u_4$.

Going along a Γ^- -characteristic that runs from state ④ to state ③ we have:

$$u_3 - \frac{2}{\gamma - 1} a_3 = u_4 - \frac{2}{\gamma - 1} a_4,$$

or, with the aid of isentropic relations:

$$u_3 - u_4 = \frac{2}{\gamma - 1} \left\{ \left(\frac{p_3}{p_4} \right)^{\frac{\gamma-1}{2\gamma}} - 1 \right\} a_4. \quad (3.56)$$

This relation can also be brought into the form

$$\Delta p = \pm m \Delta u \quad (3.57)$$

with

$$m = \rho_{\text{pre}} a_{\text{pre}} \frac{\gamma - 1}{2\gamma} \frac{1 - \frac{p_{\text{post}}}{p_{\text{pre}}}}{1 - \left(\frac{p_{\text{post}}}{p_{\text{pre}}} \right)^{\frac{\gamma-1}{2\gamma}}}. \quad (3.58)$$

The + sign is chosen for a right running wave, the – sign for a left running wave. Equations (3.57) and (3.58) together describe the relation between Δp and Δu over an expansion fan; they give all possible ‘post-expansion’ states that are obtainable from the ‘pre-state’ using an expansion process.

The curve $p_{\text{post}} = f(u_{\text{post}}; p_{\text{pre}}, u_{\text{pre}})$ determined by (3.57) and (3.58) in the (p, u) -plane is called the *Poisson curve*.

The mass flux in (3.58) must be regarded as some average over the expansion wave.

3.5.3 Example of a Riemann problem

An example of a Riemann problem with initial conditions $u_L = u_R = 0$, $p_L > p_R$ results into a solution having a left moving expansion and a right moving shock; the corresponding (t, x) -diagram is shown below in figure 3.11.

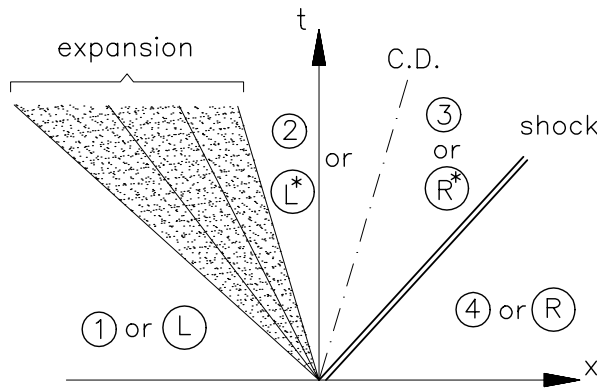


Figure 3.11: Solution of a Riemann problem; $U_{L^*} = U_{R^*}$, $p_{L^*} = p_{R^*}$

3.5.4 Properties of Hugoniot and Poisson curves

When discussing the Riemann problem in section (3.5) we encountered the Hugoniot (H) curve and the Poisson (P) curve. Both are curves in the (p, u) -plane. In short: **Hugoniot** describes shocks and **Poisson** describes expansions.

Both the ‘H-curve’ and the ‘P-curve’ are described formally by the relation

$$\Delta p = m \Delta u,$$

where the mass flux m differs for shocks and expansions — compare (3.52) and (3.58).

Let us write down explicitly the formula for an ‘H-curve’ and a ‘P-curve’ describing all possible ‘post-states’ ③ obtainable from a prescribed ‘pre-state’ ④. That means, let us consider *right* running shocks (H-curve) and right running expansions (P-curve). The formulae are

$$H : \quad p_3 - p_4 = \rho_4 a_4 \sqrt{1 + \frac{\gamma + 1}{2\gamma} \frac{p_3 - p_4}{p_4}} (u_3 - u_4), \quad (3.59)$$

$$P : \left(\frac{p_3}{p_4} \right)^{\frac{\gamma-1}{2\gamma}} = 1 + \frac{\gamma - 1}{2} \frac{u_3 - u_4}{a_4}. \quad (3.60)$$

Figure 3.12 now shows some properties of the Hugoniot and Poisson curves in the (p, u) -plane, both going through the same reference (p_4, u_4) .

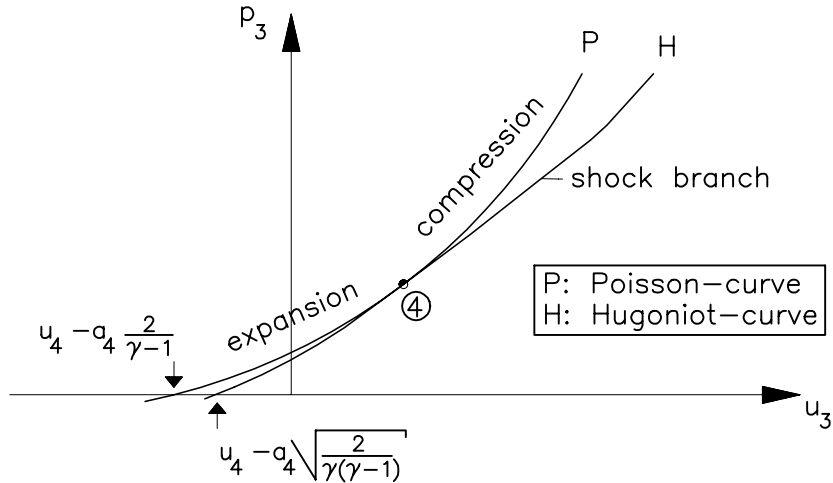


Figure 3.12: Comparison of the Hugoniot and Poisson curve

Some observations:

1. The Poisson curve lies *above* the Hugoniot curve. For the same \$\Delta u\$, isentropic compression is more effective than compression by a shock.
2. In the limit \$p_3 \rightarrow \infty\$ there results for:

$$H : p_3 \propto (u_3 - u_4)^2 \quad (3.61)$$

$$P : p_3 \propto (u_3 - u_4)^{\frac{2\gamma}{\gamma-1}} \quad (3.62)$$

The Hugoniot curve goes less fast to \$\infty\$ than the Poisson curve does.

3. Vacuum conditions: \$p_3 = 0\$ leads to

$$H : u_3 = u_4 - a_4 \sqrt{\frac{2}{\gamma(\gamma-1)}} \quad (3.63)$$

$$P : u_3 = u_4 - a_4 \frac{2}{\gamma-1} \quad (3.64)$$

Since \$\gamma > 1\$ the H-curve intersects the level \$p_3 = 0\$ at higher values of \$u_3\$ than the P-curve does.

4. In the reference point ④ the H-curve and the P-curve have equal slope and equal curvature. A straightforward calculation shows that

$$\left(\frac{dp}{du} \right)_H = \left(\frac{dp}{du} \right)_P = \rho_4 a_4 \quad (3.65a)$$

and

$$\left(\frac{d^2p}{du^2} \right)_H = \left(\frac{d^2p}{du^2} \right)_P = \frac{\gamma+1}{2} \rho_4 \quad (3.65b)$$

The third derivative of the H- and P-curve differ in the reference point which shows that the entropy rise due to a shock is a third-order effect.

5. According to linear theory the pressure change Δp is proportional to Δu : no distinction is made between expansions and real shocks.

In non-linear theory however, there is a substantial difference since both Poisson- and Hugoniot curve share only the slope with the linear graph, see figure 3.13; so the deviation of the pressure from linear theory is $\mathcal{O}(\Delta u^2)$.

From equations (3.65a) and (3.65b) the difference in pressure between Poisson and Hugoniot is $\mathcal{O}(\Delta u^3)$, which reflects the influence of the entropy rise in the Hugoniot case.

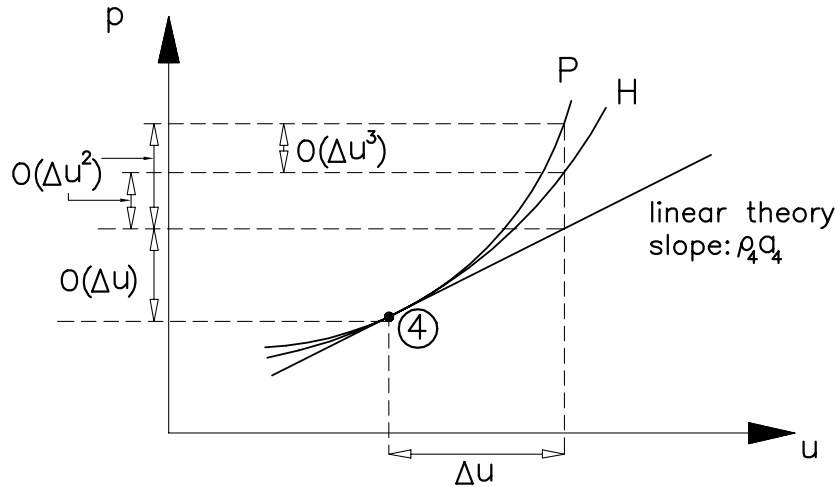


Figure 3.13: Accuracy of linear theory, Poisson and Hugoniot

For an $\mathcal{O}(\Delta u^2)$ accuracy it is still acceptable to use the Poisson-curve for compressions.

6. The expansion branch of the H-curve is not physically valid because expansions are isentropic. If only expansion appear, the P-curve gives a valid description. Since shocks are not isentropic, it is clear that in the case of shocks P-curves can give only an approximate description; for an exact description of shocks, the H-curve has to be used.
7. From the jump equation $\Delta p = \pm m \Delta u$ it follows that m is represented in the (p, u) -graph as the chord between pre- and post-wave states, shown in figure 3.14.

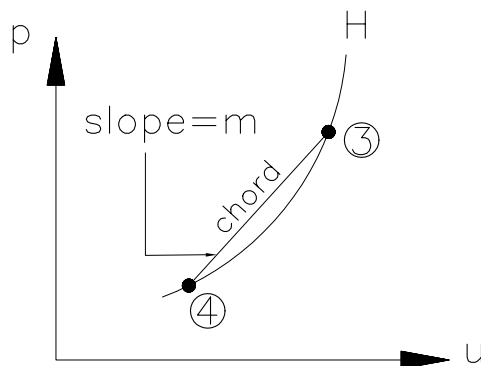


Figure 3.14: Geometrical representation of the mass flux

The properties of right running waves have just been discussed. Shocks are represented by Hugoniot curves in the (p, u) -plane, while expansions are represented by Poisson curves. In the case of left running waves, the graphs in the (p, u) -plane are very similar; they only differ because the velocities change sign. Therefore, the (p, u) -graph for left running waves is just the mirror image of the (p, u) -graph of right running waves. Figure 3.15 summarises the results for both left running and right running waves.

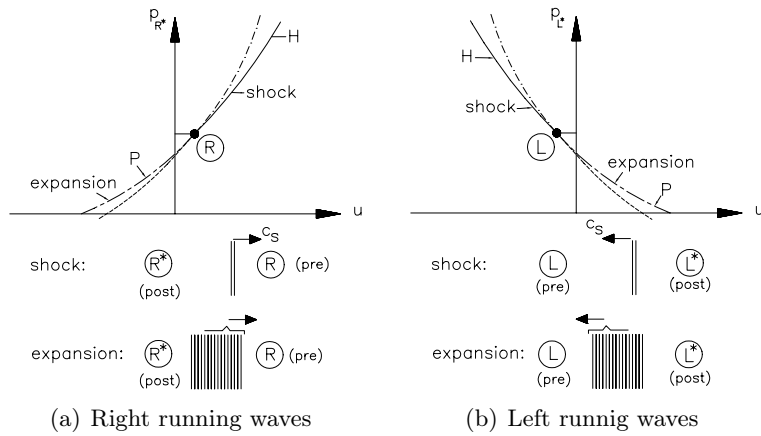


Figure 3.15: (p, u) -graphs for right- and left running waves

3.5.5 Solving Riemann problems with a (p, u) -graph

In the previous sections the necessary tools to solve non-linear Riemann problems were presented. Now, three examples will be given here.

Example 1: two shocks

The states ① and ④, or (L) and (R) respectively, are prescribed as shown in the (p, u) -plane given in figure 3.16.

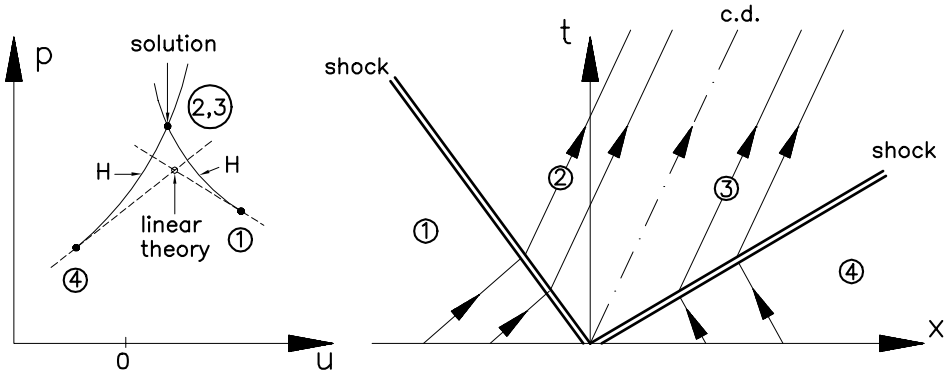
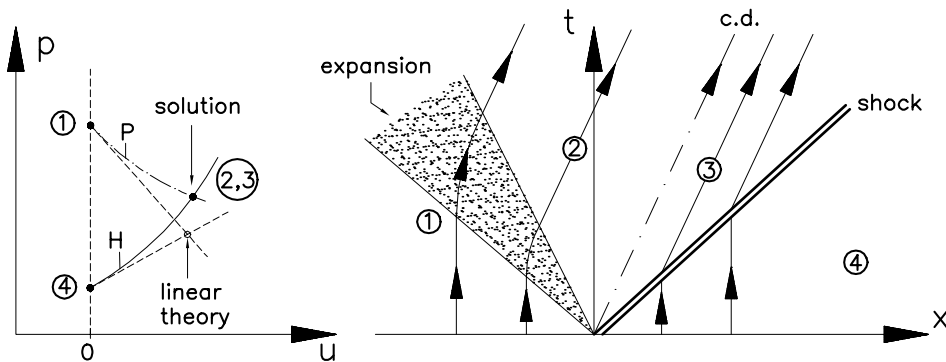
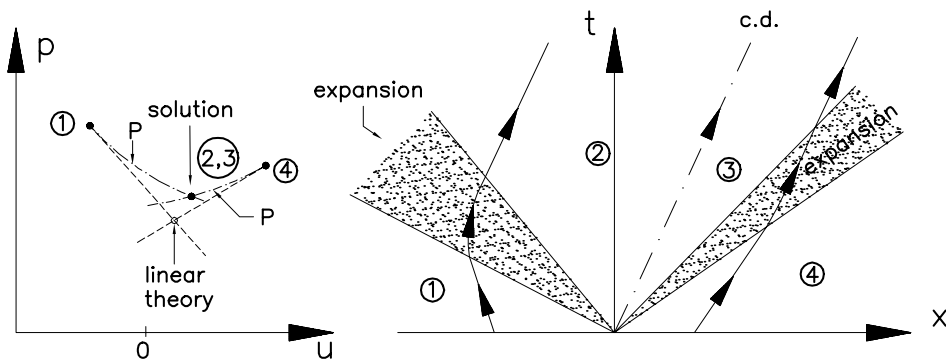


Figure 3.16: Two shocks; (p, u) -plane and (t, x) -plane

The solution of the Riemann problem is found as the intersections of two H-curves, one going through ④ and one going through ①. The intersection point ② = ③ represents the states

Figure 3.17: Expansion and shock; (p, u) -plane and (t, x) -planeFigure 3.18: Two expansions; (p, u) -plane and (t, x) -plane

② and ③ in the (t, x) -plane having equal pressure $p_2 = p_3$ and equal velocity $u_2 = u_3$; states ② and ③ are separated by a contact discontinuity (c.d.) which is parallel to the particle paths in ② and ③.

States ② and ③ have different values for the entropy, density and internal energy, so the contact discontinuity is really a discontinuity. In this example the particle paths in the (t, x) -plane have a positive slope.

Example 2: a shock and an expansion

The states ① and ④ are given in the (p, u) -plane as shown in figure 3.17.

In this example the solution is found by intersecting the H-curve through ④ with the P-curve through ①. The ‘pre-states’ ① and ④ are gases at rest but $p_1 > p_4$. An expansion wave travels into ② and a shock wave travels into ④. The states ② and ③ have equal pressure and equal velocity. The densities, entropy values and internal energy levels are different in ② and ③. This example resembles the flow in a shock tube.

Example 3: a double expansion

The ‘pre-states’ ① and ④ are now given in such a way that two expansion waves appear, see figure 3.18.

The solution is found as the intersection of two P-curves. The flow in the expansion fans itself is also part of the solution and is determined by the P-curves. Since expansions are

isentropic, the entropy jump over the contact discontinuity is equal to the entropy difference between the ‘pre-states’ ① and ④.

It can happen that the ‘pre-states’ ① and ④ are chosen in such a way that the P-curves intersect at a negative value of the pressure. This is physically impossible; if P-curves pass the zero-pressure level, the flow expands to vacuum conditions and *cavitation* occurs.

3.6 The Method of Characteristics for one-dimensional unsteady flow

The same method that we used to obtain the simple-wave solution analytically can be used more generally to obtain solutions numerically on a discrete grid. The grid is built up by characteristics i.e. the grid points are intersections of characteristic curves. Let us start with the homentropic case.

In homentropic flow the entropy is uniform and the Riemann invariants are written in algebraic form:

$$J^\pm = u \pm \frac{2}{\gamma - 1} a. \quad (3.66)$$

The Riemann-invariants J^+ and J^- are constant along the characteristic curves Γ^+ and Γ^- respectively.

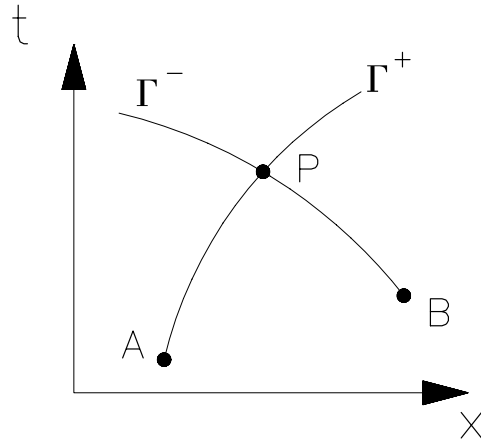


Figure 3.19: M.O.C to find the solution in P , homentropic flow

The solution in a point P in the (t, x) -plane follows entirely from the known solution in the points A and B if P lies at the intersection of Γ^+ going through A and Γ^- going through B (see figure 3.19);

$$\text{along } \Gamma^+(A) : J_A^+ = u_A + \frac{2}{\gamma - 1} a_A = u_P + \frac{2}{\gamma - 1} a_p \quad (3.67)$$

$$\text{along } \Gamma^-(B) : J_B^- = u_B - \frac{2}{\gamma - 1} a_B = u_P - \frac{2}{\gamma - 1} a_p \quad (3.68)$$

Solving for u_P and a_P yields:

$$u_P = \frac{1}{2} (J_A^+ + J_B^-) \quad (3.69)$$

$$a_P = \frac{\gamma - 1}{4} (J_A^+ - J_B^-) \quad (3.70)$$

Now we have the solution in P, but we still have to determine the location of P. The point P can be found, at least approximately, by taking the average direction of Γ^+ in A and P and also the average direction of Γ^- between B and P. Then the approximate location (t_P, x_P) of P follows from the system:

$$x_P - x_A = \left(\frac{dx}{dt} \right)_{\overline{AP}} (t_P - t_A), \quad (3.71a)$$

$$x_P - x_B = \left(\frac{dx}{dt} \right)_{\overline{BP}} (t_P - t_B), \quad (3.71b)$$

where

$$\left(\frac{dx}{dt} \right)_{\overline{AP}} = \frac{u_A + a_A + u_P + a_P}{2},$$

and

$$\left(\frac{dx}{dt} \right)_{\overline{BP}} = \frac{u_B - a_B + u_P - a_P}{2}.$$

Note that the flow variables in the point P are exactly known; on the other hand, the position of P can not be determined exactly. This altogether makes the numerical implementation of the M.O.C. an approximate method in finding the flow variables.

Let us now turn to the non-homentropic case. In non-homentropic flow without shock discontinuities, the entropy s remains constant when following a particle; however, s may differ for different fluid particles. So s is not necessarily uniform in the (t, x) -domain. Due to this non-uniform entropy the Riemann invariants can not be integrated and must be approximated from their differential form.

$$\text{along } \Gamma_A^+: u_P - u_A + \frac{p_P - p_A}{\frac{1}{2}(\rho_P a_P + \rho_A a_A)} = 0 \quad (3.72)$$

$$\text{along } \Gamma_B^+: u_P - u_B - \frac{p_P - p_B}{\frac{1}{2}(\rho_P a_P + \rho_B a_B)} = 0 \quad (3.73)$$

Here we have two equations for the three unknowns u_P , p_P and ρ_P . How to solve this problem? There are several answers; one is explained in figure 3.20.

Observe the particle path through P and *assume* that this path also goes through C being the intersection of Γ_A^- and Γ_B^+ . In other words: it is assumed that the gas particle in P comes from C. Then, the entropy in P has the same value as the entropy in C, so that

$$s_P = s_C,$$

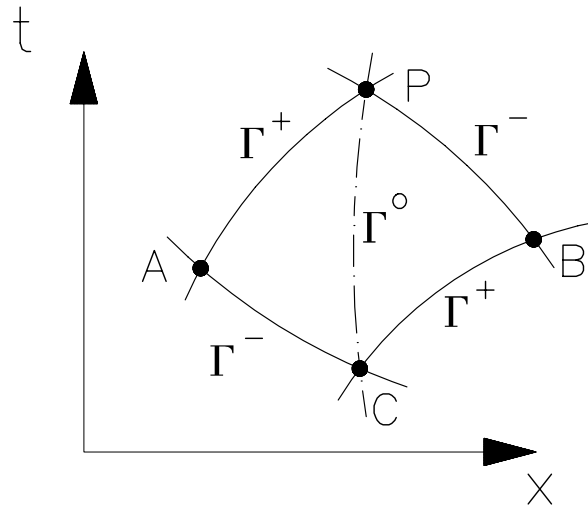


Figure 3.20: M.O.C to find the solution in P , non-homentropic flow

or

$$p_P \rho_C^\gamma = p_C \rho_P^\gamma \quad (3.74)$$

Equation (3.74) is the third equation that closes the system (3.72), (3.73) and (3.74), because the point C and the flow variables in that point are already calculated in a previous step in the computational process.

Comment To close (3.72) and (3.73) with a third equation a possible method is given above. There are other more accurate methods available. But does it make sense to use such a more accurate third equation?

Well, that depends on how each equation contributes to the accuracy of the whole system. Here we touch on the important issue of consistency. To improve the order of accuracy all equations have to be improved in a consistent way. For example in our case: if the order of accuracy of the equations (3.72), (3.73) and (3.74) is the same then it is not useful to look for an improvement of a single equation, e.g. (3.74).

3.7 Simple compression waves

In section 3.5.1 we studied, as part of the non-linear Riemann problem, the instantaneous movement of a piston into a gas at rest. There it was seen, see figure 3.9, that a shock is created moving into a gas with a shock speed c_s that is related to the pressure rise. Since the piston had an infinite acceleration to its final speed $u_p = u_3$, the shock immediately (at $t = 0$) starts moving from the piston's position (at $x = 0$).

Let us now consider the case that the piston is accelerated at a finite rate until the piston has reached its maximum velocity u_{\max} at $t = T$, see figure 3.21.

Considering such a piston that is accelerated and advancing into a gas at rest, a *simple compression wave* will be created.

The characteristics emanating from the piston path are now converging forward in time and sooner or later a fan of neighbouring characteristics will intersect. The solution gradient

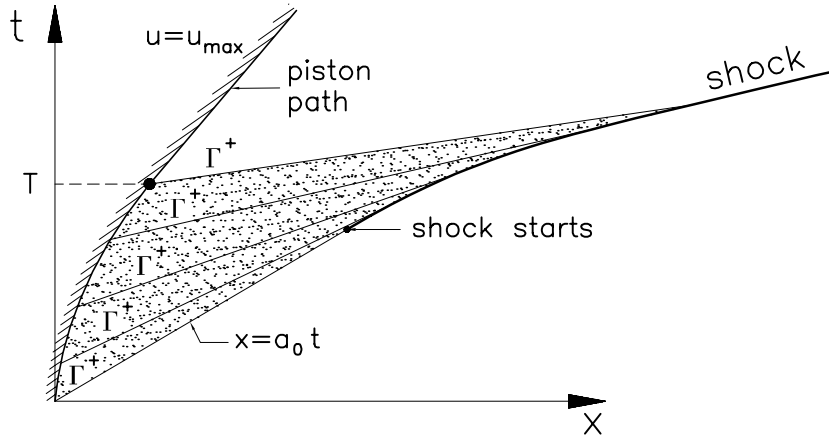


Figure 3.21: Shock development by an accelerating piston

has become infinite at that point; a shock must be introduced now. The shock is building up in strength by characteristics intersecting the shock from behind.

As long as the shock is still absent, the flow is isentropic and since all particles emanate from the rest state (labelled '0') the entropy is uniform. The question now is how long it lasts before the compression waves start intersecting.

To answer this, let us assume that the piston has a constant acceleration, \dot{u}_p :

$$\dot{u}_p = \frac{du_p}{dt},$$

so that

$$u_p = \dot{u}_p t, \quad x_p = \frac{1}{2} (\dot{u}_p) t^2. \quad (3.75)$$

Take a short excursion of the piston to the point A with $x_A = \Delta x$ and $t_A = \Delta t$, Δx and Δt are small, see figure 3.22.

Let point I be the intersection of the two Γ^+ characteristics, one coming from origin and the other coming from A:

$$\text{first characteristic: } x_i = a_0 t_i \quad (3.76)$$

$$\text{characteristic through A: } (x_i - \Delta x) = (u_A + a_A)(t_i - \Delta t) \quad (3.77)$$

The characteristic speed $u_A + a_A$ follows from the fact that the Γ^- -characteristic through A starts in the domain where the gas is at rest. Along Γ_A^- :

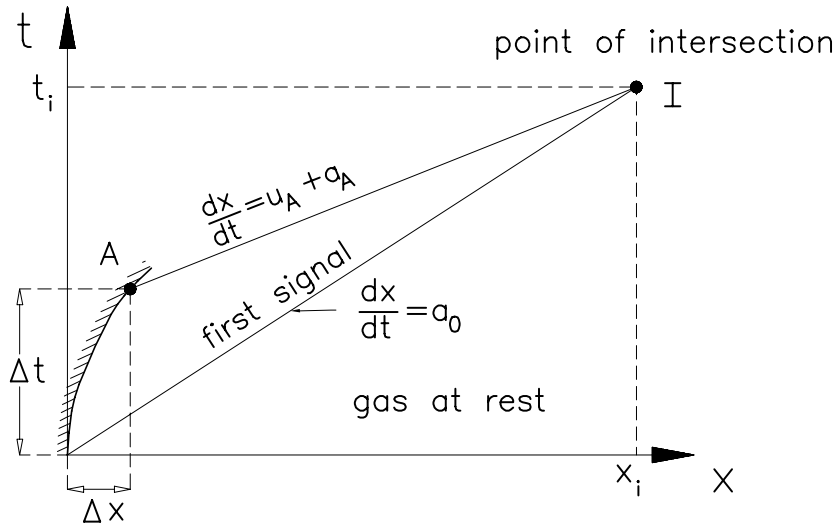
$$u_A - \frac{2}{\gamma - 1} a_A = -\frac{2a_0}{\gamma - 1},$$

or

$$a_A = a_0 + \frac{\gamma - 1}{2} u_A,$$

so that

$$u_A + a_A = \frac{\gamma + 1}{2} u_A + a_0 = \frac{\gamma + 1}{2} \dot{u}_p \Delta t + a_0. \quad (3.78)$$

Figure 3.22: Intersecting Γ^+ characteristics

Then equation (3.77) becomes

$$x_i - \Delta x = \left(\frac{\gamma + 1}{2} \dot{u}_p \Delta t + a_0 \right) (t_i - \Delta t) \quad (3.79)$$

Inserting (3.75) and (3.76) into (3.79) yields

$$a_0 t_i - \frac{1}{2} \dot{u}_p (\Delta t)^2 = \left(\frac{\gamma + 1}{2} \dot{u}_p \Delta t + a_0 \right) (t_i - \Delta t).$$

Solving for t_i yields

$$t_i = \frac{a_0}{\frac{\gamma+1}{2}\dot{u}_p} + \frac{\gamma}{\gamma+1} \Delta t.$$

For $\Delta t \rightarrow 0$, we find that the first signal and its neighbouring characteristic intersect at:

$$t_i = \frac{a_0}{\frac{\gamma+1}{2}\dot{u}_p}. \quad (3.80)$$

The faster the piston accelerates the sooner the characteristics intersect. Equation (3.80) can be interpreted as follows. Therefore we generalize the nominator and denominator of equation (3.80).

Since a_0 is constant, the denominator may be written as:

$$\frac{\gamma + 1}{2} \dot{u}_p = \frac{d}{dt} \left(\frac{\gamma + 1}{2} \dot{u}_p + a_0 \right) = \left(\frac{d}{dt} (u_p + a_p) \right)_0,$$

and since $u_0 = 0$, the nominator may be written as:

$$a_0 = u_0 + a_0,$$

Then equation (3.80) can be interpreted as

$$t_i = \frac{u_0 + a_0}{\left(\frac{d}{dt} (u_p + a_p) \right)_0} = \frac{\text{initial characteristic speed}}{\text{initial } \frac{d}{dt} \text{ characteristic speed}}.$$

A typical example of a simple compression wave appears if the piston path is such that the characteristics Γ^+ all intersect in one focal point. See figure 3.23. Such a compression wave is well known as a centered compression wave.

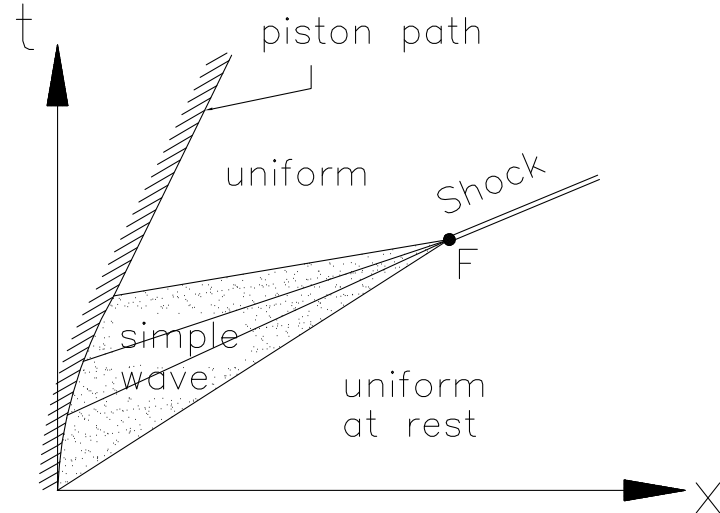


Figure 3.23: Γ^+ characteristics intersecting in one focal point

Let us consider in more detail the various domains that can be distinguished in the (t, x) -plane if an accelerating piston causes the development of a shock wave. The fact that various domains of different properties appear is clear because of shock development and its influence on the entropy in the flow.

Consider now figure 3.24 featuring the shock development process. Domain A represents the fluid at rest. The domains B, C, D, E and F lie left from the particle path Γ^0 going through the starting point of the shock; the domains G, H and I are to the right of this particle path.

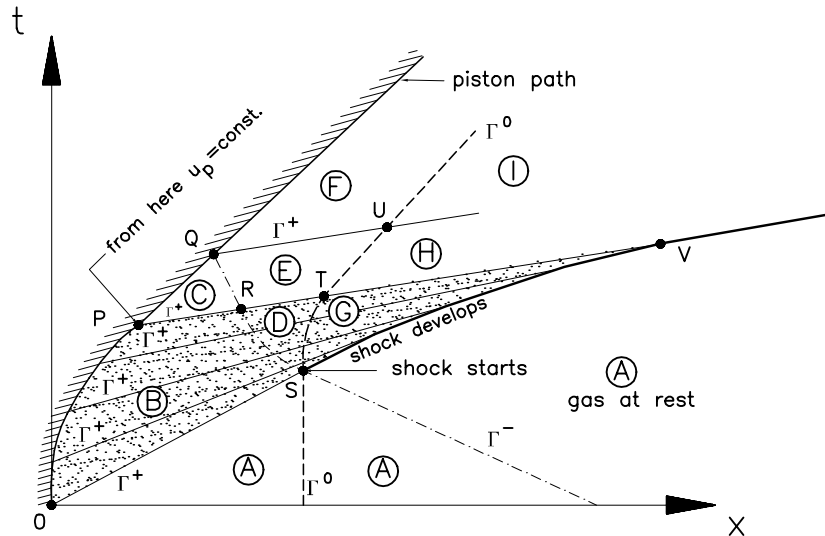


Figure 3.24: Various flow domains under shock development

Domain A: uniform conditions; the gas is at rest. It is bounded by the first signal and the shock curve.

Domain B: is a simple wave because all Γ^- characteristics originate from $t = 0$ and have the same $J_B^- = J_A^-$. All gas particles have the same entropy, so the entropy is uniform and Riemann invariants are integrable. The Riemann invariant J^+ varies from $J^+ = \frac{2a_0}{\gamma-1}$ on the first signal to $J^+ = u_p + \frac{2a_p}{\gamma-1}$ on the Γ^+ characteristic going through P. Domain B is bounded by the Γ^+ characteristic OS, the Γ^- characteristic SR, the Γ^+ characteristic RP and the piston path OP.

Domain C: is bounded by the Γ^+ characteristic PR, the Γ^- characteristic RQ and the piston path QP with $u_p = \text{constant}$. All particles in C start in A and they have crossed no shock, so the entropy is uniform and the Riemann invariants are integrable. All Γ^- characteristics issue from $t = 0$ and do not cross a shock, so $J_C^- = J_A^- = \text{constant}$.

On each Γ^+ characteristic through C the relation $u + \frac{2a}{\gamma-1} = u_p + \frac{2}{\gamma-1}a_p$ is satisfied. Since $J_C^- = \text{constant}$ there is a linear relation between u_p and a_p and since u_p is constant in C, a_p is constant as well. However, u_p and a_p constant implies that J_C^\pm is constant and so u and a are constant in domain C, therefore domain C is uniform.

Domain D: is bounded by the particle path Γ^0 : ST, the Γ^+ characteristic RT and the Γ^- characteristic RS. All particles in D arrive from A without having crossed a shock, therefore the entropy is uniform, so the Riemann invariants J^+ and J^- are integrable. However, $J_D^+ = J_B^+$ and they vary. Also J_D^- varies because the Γ^- characteristics have crossed a shock with varying strength, so domain D is a non-simple domain.

Domain E: is bounded by the Γ^+ characteristics RT and QU and by the particle path TU and the Γ^- characteristic QR. All particles in E arrive from A without having crossed a shock, therefore J^+ and J^- are integrable. $J_E^+ = J_C^+$ is constant. J_E^- varies because the Γ^- characteristics have crossed a shock wave with varying strength. Conclusion: E is a simple wave region.

Domain F: is bounded by the Γ^+ characteristic QU, the particle path Γ^0 and the piston path described by $u_p = \text{constant}$. All gas particles in F start in A and have not crossed a shock, therefore J^+ and J^- are integrable. Since Γ^- characteristics have crossed a shock of varying strength, J_F^- varies. Then a_p (on the piston path) also varies and therefore J_F^+ varies. Conclusion: F is a non-simple region.

Domain G: is bounded by the shock segment SV, the particle path Γ^0 and the Γ^+ characteristic TV. Particles arriving in G must have crossed the shock, therefore the entropy is not uniform and the Riemann invariants are not integrable. Furthermore, J_G^+ is equal to J_B^+ which both vary; J_G^- also varies since the Γ^- characteristics have crossed the shock. Conclusion: G is a non-simple domain.

Domain H: is bounded by Γ^+ characteristics TV and the Γ^+ characteristic through U, and by the particle path TU and a shock segment. Particles in H have crossed a shock, therefore the entropy is not uniform and J^+ and J^- are not-integrable. Furthermore, $J_H^+ = J_C^+$ is constant; J_H^- varies, so domain H is non-simple.

Domain I: is bounded by the particle path Γ^0 , a shock segment and the Γ^+ characteristic through U. Particles in I have crossed a shock, therefore the entropy is not uniform. Furthermore, $J_I^+ = J_F^+$ which varies, and also J_I^- varies. So domain I is a non-uniform, non-simple region.

The properties of each domain just discussed are summarised in table 3.2.

Domain	J^+	J^-	S	comment
A	u	u	u	uniform, i
B	v	u	u	simple wave, i
C	u	u	u	uniform, i
D	v	v	u	non-simple, i
E	u	v	u	simple(!), i
F	v	v	u	non-simple
G	v	v	v	non-simple
H	u	v	v	non-simple
I	v	v	v	non-simple

Table 3.2: Properties of flow domains appearing in the shock development process; key: u: uniform, v: varies, i: integrable

3.8 Wave interactions

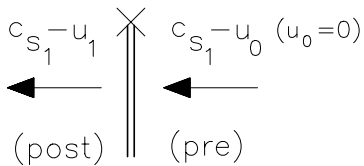
Until now, the one-dimensional unsteady flow phenomena we have encountered were expansion waves, contact discontinuities, compression waves and shocks. In addition, two types of waves were distinguished: left running and right running waves. They always appeared in a single manner, but what if they interact, what can happen? In this section some examples of interactions are discussed.

3.8.1 Two right running shocks

Consider a semi-infinite constant area tube closed off by a piston at its left end and filled with a gas at rest. At $t = 0$ the piston accelerates instantaneously and acquires the speed u_{p1} ; then, at $t = t_1$ it instantaneously switches to the speed u_{p2} with $u_{p2} > u_{p1}$, see figure 3.25. Two shock waves are created; they intersect at time t_2 .

At t_2 a Riemann problem between the states ② (left) and ① (right) appears. The first question is: do shocks really intersect? To answer this, we go to the shock frame and view the first moving shock.

The first moving shock viewed in the shock frame shows the following picture:



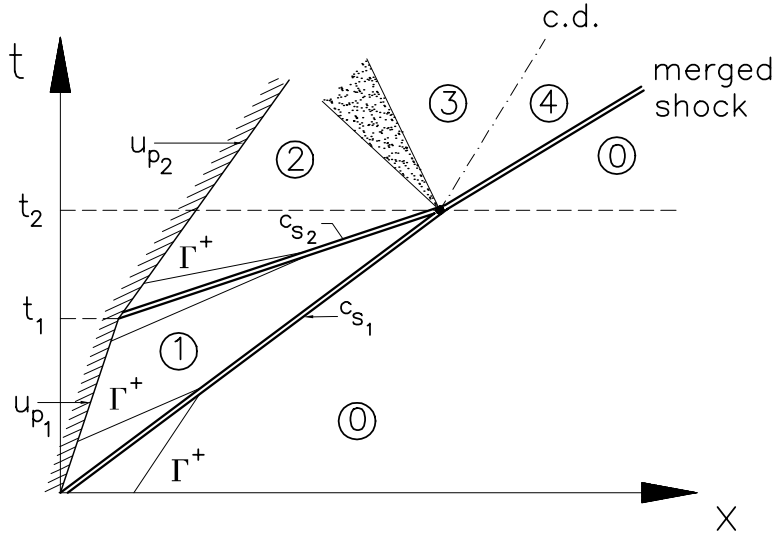
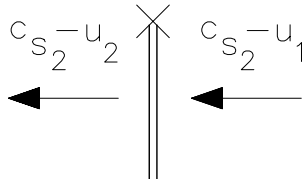


Figure 3.25: Two intersecting shocks of the same family

The entropy condition II states $(a + u)_0 < c_{s_1} < (a + u)_1$. The second moving shock in the shock frame:



The entropy condition II states $(a + u)_1 < c_{s_2} < (a + u)_2$.

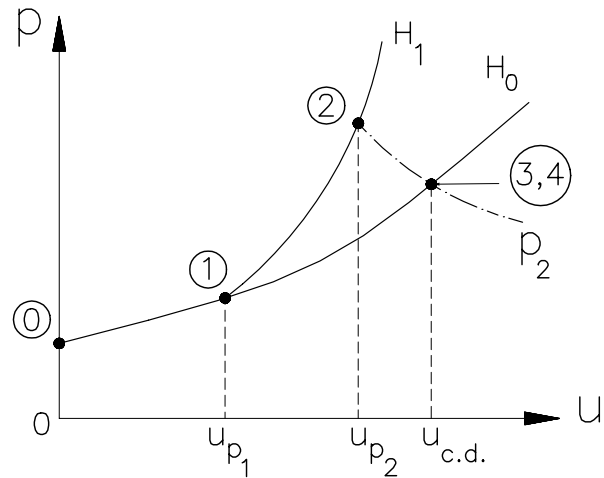
Combining the two inequalities gives $c_{s_1} < c_{s_2}$. Hence the second shock moves faster and reaches the first shock at $t = t_2$.

The entropy condition II also shows that Γ^+ characteristics cannot cross the right running shock. The shock is hit by characteristics from both sides. A shock is a barrier for characteristics, so they terminate there. On the shock the characteristic speed is double valued. One can say that the right running shock belongs to the “+” family. In a similar way one can say that a left running shock belongs to the “-” family implying that Γ^- characteristics cannot cross left-running shocks.

The question we still have is how to solve the Riemann problem appearing at t_2 . The answer can be found by sketching the interaction process in the (p, u) -plane, see figure 3.26.

State ① lies on the Hugoniot curve H_0 going through the point ④. The slope in ④ of the H_0 -curve is $\rho_0 a_0$. State ② lies on the H_1 curve going through ①; the slope of the H_1 curve ① is $\rho_1 a_1$. State ② is found where u_2 has the prescribed velocity u_{p_2} . State ④ also has to lie on the H_0 curve because the merged shock transfers the gas from the ‘pre-state’ ④ to the ‘post-state’ ④. Since H_1 lies above H_0 a Poisson-curve is needed to find a valid solution for state ③. Hence an expansion fan appears between states ② and ③. Furthermore, a contact discontinuity with characteristic speed $u_{cd} > u_{p_2}$ separates ② and ③. That H_1 lies above H_0 can be proved for $1 < \gamma < 2$ by straightforward algebra.

Compare this unsteady interaction with a corresponding 2D steady supersonic flow, sketched

Figure 3.26: (p, u) -plane

in figure 3.27. The weak wave between ③ and ④ can be either an expansion or a shock depending on the free stream Mach number and the two ramp angles δ_1 and δ_2 .

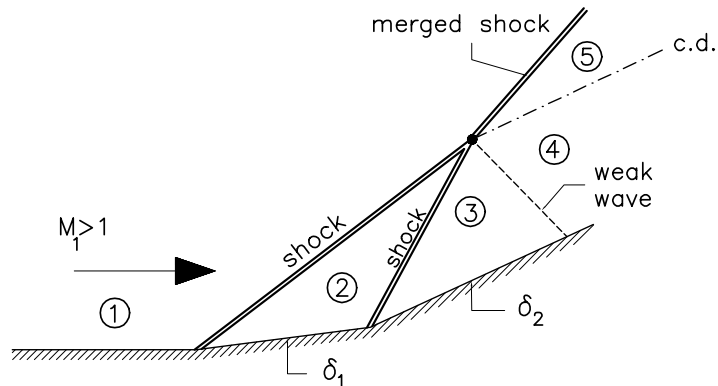


Figure 3.27: Supersonic flow along two successive ramps

3.8.2 Two right running expansion waves

Consider again a semi-infinite constant area tube closed off by a piston at its left end and filled with a gas at rest. At $t = 0$ the piston is instantaneously withdrawn and acquires a speed u_{p1} (< 0), at $t = T$ it instantaneously switches to the speed $u_{p2} < u_{p1} < 0$. Two expansion waves are created, see figure 3.28.

As we see these expansions do not interact. The last signal of the first expansion fan and the first signal of the second expansion fan have the same characteristic speed.

The whole process in the (t, x) domain is mapped onto one single graph in the (p, u) plane: the Poisson curve for the right running waves that starts in the state ①.

Compare this with two subsequent expansions in 2-D steady supersonic flow (see figure 3.29). They also do not interact.

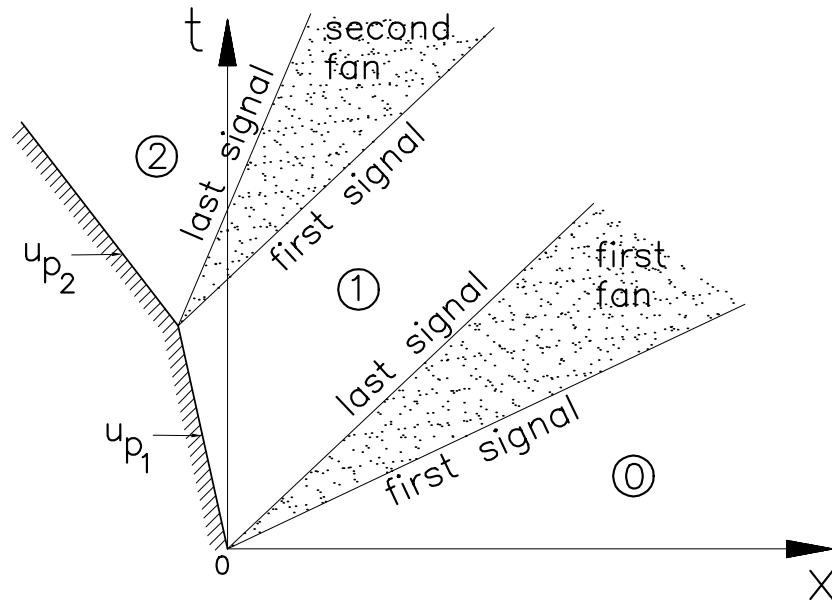


Figure 3.28: Two expansions of the same family

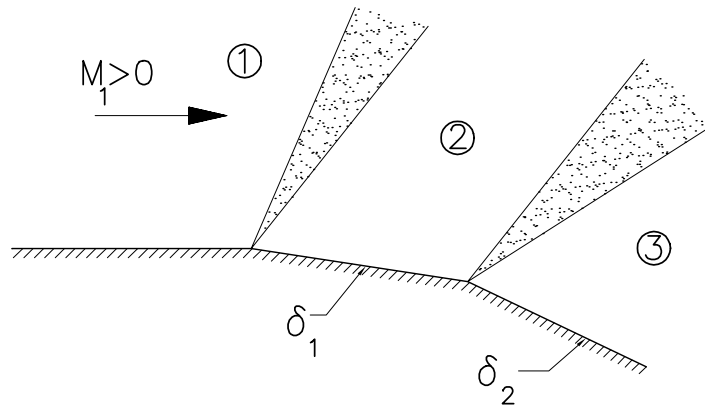


Figure 3.29: Supersonic 2-D steady flow along a plane wall with two successive kinks

3.8.3 Shock interacting with expansion

A piston moves with a constant speed $u_p > 0$ into a gas at rest. At time t_i the piston is instantaneously decelerated to standstill. This creates the interaction of a shock wave and an expansion wave both of the same family. This situation is sketched in figure 3.30.

Interaction starts at (x_i, t_i) . Due to interaction the shock slows down; its strength decreases and its entropy jump decreases too. The particle path going through the point i separates two domains in the expansion fan. On the left the entropy is uniform; on the right of the particle path however, the entropy changes. There is no analytical solution available for this fully non-linear case. Fortunately, there is a first non-linear approximation using the inviscid Burgers' equation (see chapter 4).

Compare this interaction with 2-D steady supersonic flow figure (3.31).

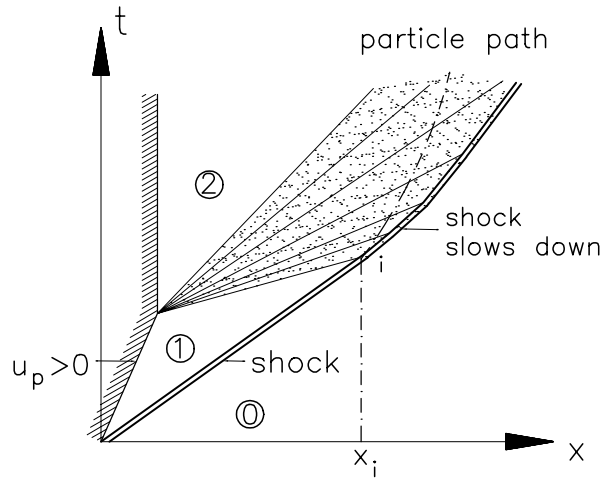


Figure 3.30: Shock-expansion interaction

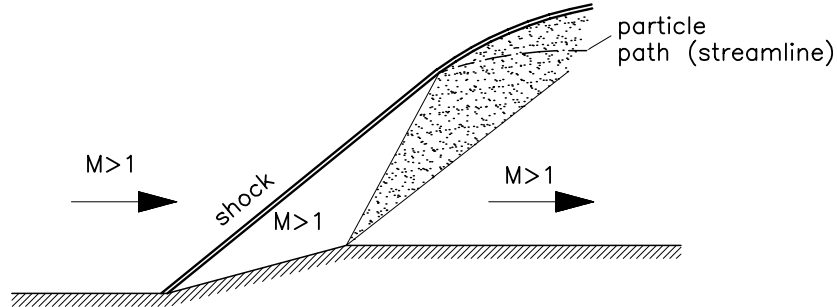


Figure 3.31: Shock-expansion interaction in supersonic flow

3.8.4 Shock interacting with expansion

A second example of shock-expansion interaction where both waves are of the same family (e.g. both are right running waves) appears if the piston is instantaneously withdrawn with speed $u_p < 0$. Later, at time t_i the piston is instantaneously brought to standstill. The initial withdrawal creates an expansion fan, the acceleration to standstill creates a shock wave. Both waves interact at (x_i, t_i) , see figure 3.32.

Due to interaction the shock accelerates. “Behind” the accelerated shock the entropy is non-uniform.

Compare this interaction to the 2D steady supersonic interaction as sketched in figure 3.33.

3.8.5 Interaction of shocks of different family

The interaction of two shocks, one left running and the other right running, is given in figure 3.34. Interactions happen at (x_i, t_i) . At $t = t_i$ a Riemann problem has to be solved between the states ① and ④.

From the (p, u) plane one concludes that after interaction *two* shocks appear. This interaction problem can be solved easily by a numerical Riemann solver.

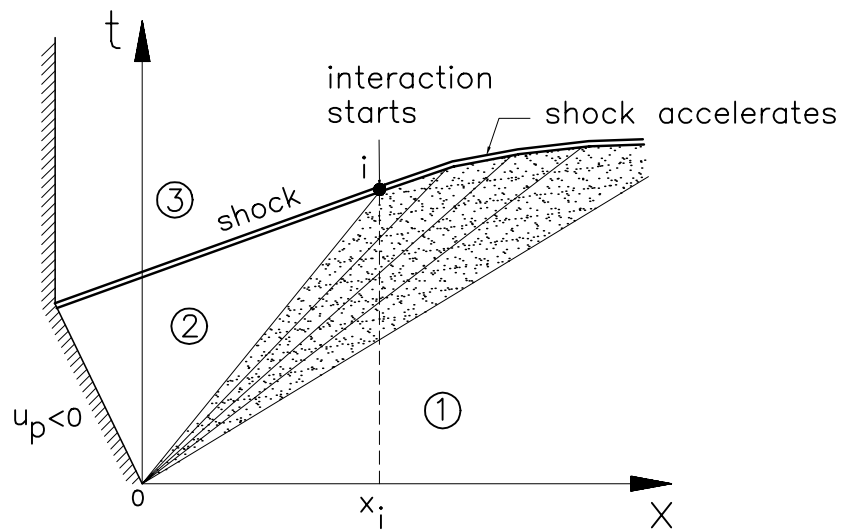


Figure 3.32: Unsteady flow, shock-expansion interaction

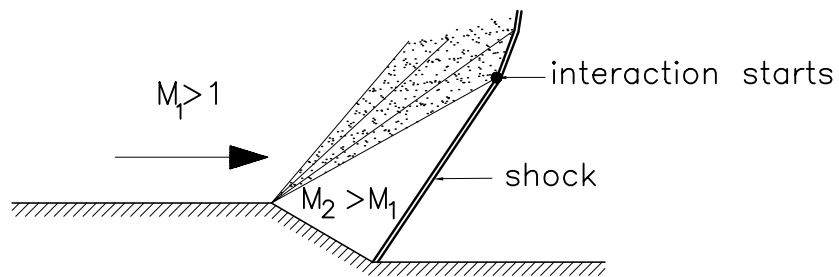


Figure 3.33: steady flow: expansion-shock interaction

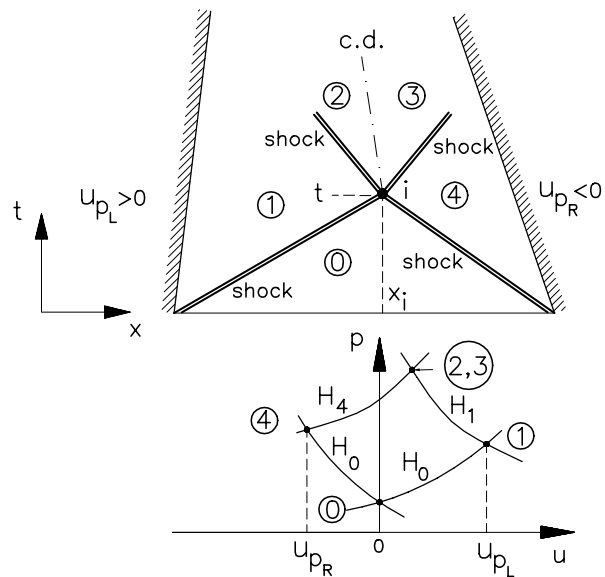


Figure 3.34: Two interacting shocks

3.8.6 Interaction of two expansions of different family

This situation is sketched in figure 3.35. The interaction can be calculated with analytical methods. The interaction pattern displays a non-simple region; both J^+ and J^- vary.

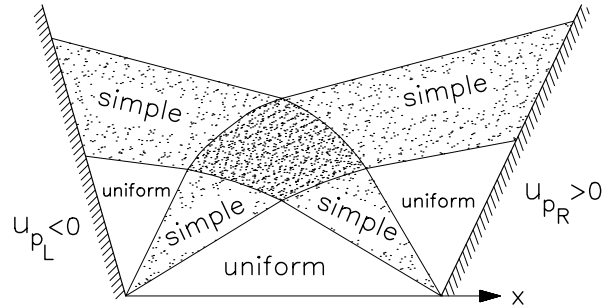


Figure 3.35: Two interacting expansion fans

Chapter 4

Burgers' equation for simple waves

4.1 Shock description

In chapter 3 we encountered the inviscid form of the Burgers' equation

$$v_t + vv_x = 0 \quad (4.1)$$

for the description of a simple wave having $J^- = \text{constant}$; v denotes the characteristic speed $v = u + a$.

In a similar way the Burgers' equation

$$w_t + ww_x = 0 \quad (4.2)$$

is valid for simple waves having $J^+ = \text{constant}$; w denotes the characteristic speed $w = u - a$.

Equations (4.1) and (4.2) are applicable in the continuous part of the flow; once a shock is formed the solutions break down because the assumption that both entropy (s) and one of the Riemann invariants (J^- or J^+) are uniform is violated. For weak shocks however, the error in the solution for v is small: $\mathcal{O}(\Delta v)$ and acceptable.

Consider the conservative form of (4.1):

$$v_t + \left(\frac{1}{2}v^2\right)_x = 0, \quad (4.3)$$

and apply the jump relations. The corresponding jump equation reads:

$$V_{\text{shock}}[v] = \left[\frac{1}{2}v^2\right]. \quad (4.4)$$

With $[v] = v_{\text{post}} - v_{\text{pre}}$ the jump equation becomes

$$V_{\text{shock}} = \frac{1}{2}(v_{\text{pre}} + v_{\text{post}}), \quad (4.5)$$

or

$$V_{\text{shock}} = \frac{1}{2}((u + a)_{\text{pre}} + (u + a)_{\text{post}}), \quad (4.6)$$

Note that the approximate shock speed is equal to the mean of the characteristic speeds of the pre- and post state, see figure 4.1

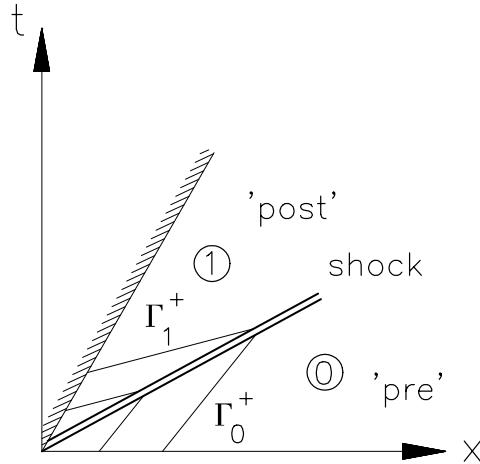


Figure 4.1: Shock running into a gas at rest

Let us determine the order of accuracy in which equation (4.5) or (4.6) approximates the exact value of the shock speed.

For a shock running into a gas at rest (state $u_0 = 0, p_0, \rho_0$) we know from equation (1.50) that the exact speed of the shock in terms of the pressure rise: $p_1 - p_0$ is given as:

$$|c_s| = a_0 \sqrt{1 + \frac{\gamma + 1}{2\gamma} \frac{p_1 - p_0}{p_0}}. \quad (4.7)$$

In terms of the post state velocity u_1 , the shock speed c_s can be written as

$$c_s^2 = a_0^2 + \frac{\gamma + 1}{2} c_s u_1. \quad (4.8)$$

To find this result, consider the flow situation of figure 4.2 in the shock frame and apply conservation of mass and momentum across the shock:

$$\begin{aligned} \rho_0 c_s &= \rho_1 (c_s - u_1) \\ p_0 + \rho_0 c_s^2 &= p_1 + \rho_1 (c_s - u_1)^2. \end{aligned}$$

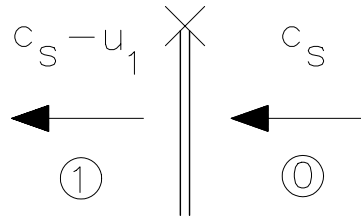


Figure 4.2: Shock in shock frame

Eliminating ρ_1 yields:

$$p_1 - p_0 = \rho_0 c_s u_1 \quad (4.9)$$

Inserting (4.9) into (4.7) gives

$$\begin{aligned} c_s^2 &= a_0^2 \left(1 + \frac{\gamma+1}{2\gamma} \frac{\rho_0 c_s u_1}{p_0} \right) \\ &= a_0^2 + \frac{\gamma+1}{2\gamma} \frac{a_0^2 \rho_0}{p_0} c_s u_1 \\ &= a_0^2 + \frac{\gamma+1}{2} c_s u_1 \end{aligned}$$

For weak shocks ($u_1 \ll c_s$) the exact shock speed (4.8) may be expanded in terms of u_1 as:

$$c_s = a_0 + \frac{\gamma+1}{4} u_1 + \frac{(\gamma+1)^2}{32a_0} u_1^2 + \mathcal{O}(u_1^4). \quad (4.10)$$

The approximate shock speed according to (4.6) with $(u+a)_{\text{pre}} = a_0$ and $(u+a)_{\text{post}} = u_1 + a_1$ becomes

$$c_s \approx V_s = \frac{1}{2}(a_0 + u_1 + a_1). \quad (4.11)$$

From J^- is constant (simple wave!) follows:

$$u_1 - \frac{2a_1}{\gamma-1} = -\frac{2a_0}{\gamma-1},$$

or

$$a_1 = a_0 + \frac{\gamma-1}{2} u_1.$$

Inserting this expression for a_1 in (4.11) we find

$$c_s \approx \frac{1}{2} \left(a_0 + a_0 + u_1 + \frac{\gamma-1}{2} u_1 \right)$$

or

$$c_s \approx a_0 + \frac{\gamma+1}{4} u_1. \quad (4.12)$$

Comparing (4.10) and (4.12) we conclude that using the simple wave approximation the shock speed is accurate to *first* order.

4.2 Shock formation

The Burgers' equation $v_t + vv_x = 0$ has characteristics Γ^+ : $\frac{dx}{dt} = v$ along which v is constant. Consequently, the characteristics of the Burgers' equation are *straight* lines in the (t, x) -plane. Burgers' equations can be used to study the development of a shock wave.

To that end, let us consider an initial value problem where the v -distribution with x is prescribed at $t = 0$. Assume that the initial values of v vary linearly between v_1 at $x = -1$ and v_0 at $x = +1$; take $v_1 > v_0 > 0$. As a consequence of the linear distribution of the initial data the characteristics in the compression domain focus in the single point F, see figure 4.3.

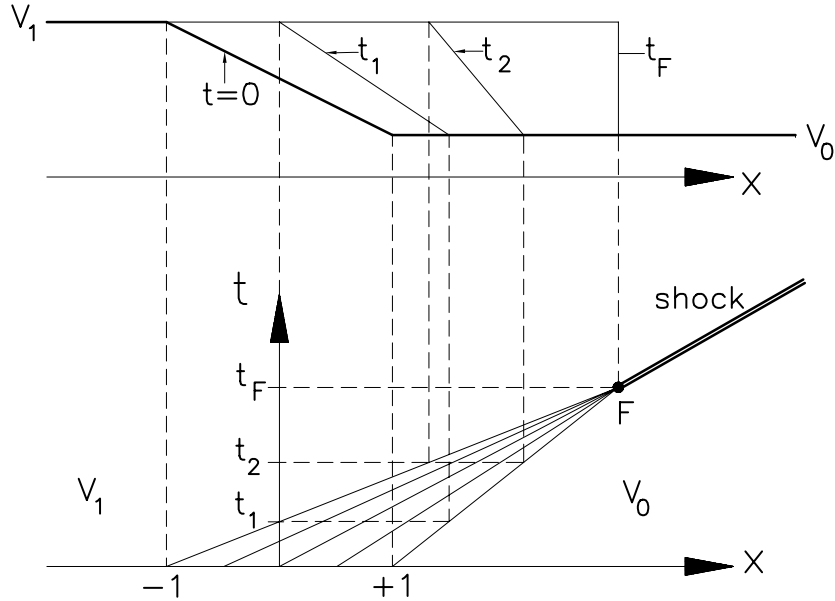


Figure 4.3: Shock development

Let the initial distribution be given by:

$$\begin{aligned} x < -1 : \quad v(x) &= v_1 \\ -1 \leq x \leq 1 : \quad v(x) &= \frac{v_0 + v_1}{2} - \left(\frac{v_1 - v_0}{2} \right) x \\ x \geq 1 : \quad v(x) &= v_0 \end{aligned}$$

Characteristics emanating from x_0 on the initial line $t = 0$, $-1 < x_0 < 1$ are given by:

$$t = \frac{1}{v(x_0)}(x - x_0).$$

The focal point F is located at

$$t_F = \frac{2}{v_1 - v_0}, \quad x_F = 1 + v_0 t_F.$$

At time level $t = t_F$ the shock is developed at its full strength instantaneously. Once it appears it moves to the right with velocity $V_{\text{shock}} = \frac{1}{2}(v_0 + v_1)$ which equals the characteristic speed at $x = 0$.

Now we consider a *non-linear* distribution of the initial value $v(x)$ between v_1 at $x = -1$ and v_0 at $x = +1$. Due to this *non-linearity* a shock develops gradually. The location where shock formation starts depends strongly on the initial data $v(x, 0) = v(x_0)$.

Consider two neighbouring points x_0 and $x_0 + \Delta x_0$ on the initial line. The characteristic through x_0 is given by:

$$\Gamma_{x_0} : \quad t = \frac{1}{v(x_0)}(x - x_0).$$

Similarly the characteristic through $x_0 + \Delta x_0$ is the straight line

$$\Gamma_{x_0+\Delta x_0} : t = \frac{1}{v(x_0) + \frac{dv}{dx_0} \Delta x_0} (x - x_0 - \Delta x_0)$$

Both characteristics intersect at

$$t_i = \frac{-1}{\left(\frac{dv}{dx}\right)_{x_0}} = \frac{-1}{v'(x_0)}.$$

So, shock formation does not occur if $v'(x_0) > 0$. Intersecting characteristics announce shock development, which happens first (in time) at

$$t_F = \frac{-1}{v'(x_0)_{\min}} \quad (4.13)$$

where t_F is the time level at which the shock formation starts. The x position is given by

$$x_F = \hat{x}_0 + t_F v(\hat{x}_0),$$

where \hat{x}_0 denotes the location where $v(x_0)$ attains its largest negative slope.

Example

Case A: Take as initial value at $t = 0$:

$$v(x, 0) = \begin{cases} v_1 = 3, & x < -1, \\ 2 - x + \frac{1}{2}(x^2 - 1), & -1 < x < 1, \\ v_0 = 1, & x > 1, \end{cases}$$

see figure 4.4. The slope $v'(x) = -1 + x$ attains its minimal value at $\hat{x}_0 = -1$; here $v'_{\min} = -2$. Shock formation starts at time level $t_F = \frac{1}{2}$ at position $x_F = \frac{1}{2}$. The initial shock velocity $V_{s,i}$ is just equal to the characteristic speed at $x = -1$, so $V_{s,i} = 3$. The final shock velocity is $V_{s,f} = 2$; it indicates that the shock slows down when moving to the right.

Case B: Take as initial value at $t = 0$:

$$v(x, 0) = \begin{cases} v_1 = 3, & x < -1, \\ 2 - x - \frac{1}{2}(x^2 - 1), & -1 < x < 1, \\ v_0 = 1, & x > 1, \end{cases}$$

see figure 4.5. The slope $v'(x) = -1 - x$ attains its minimum at $\hat{x}_0 = +1$. Here $v'_{\min} = -2$ indicating that shock formation starts at $t_F = +\frac{1}{2}$ and $x_F = \frac{3}{2}$. The initial shock speed is $V_{s,i} = 1$, the final shock speed is $V_{s,f} = 2$, the shock speeds up when moving to the right, see figure 4.5.

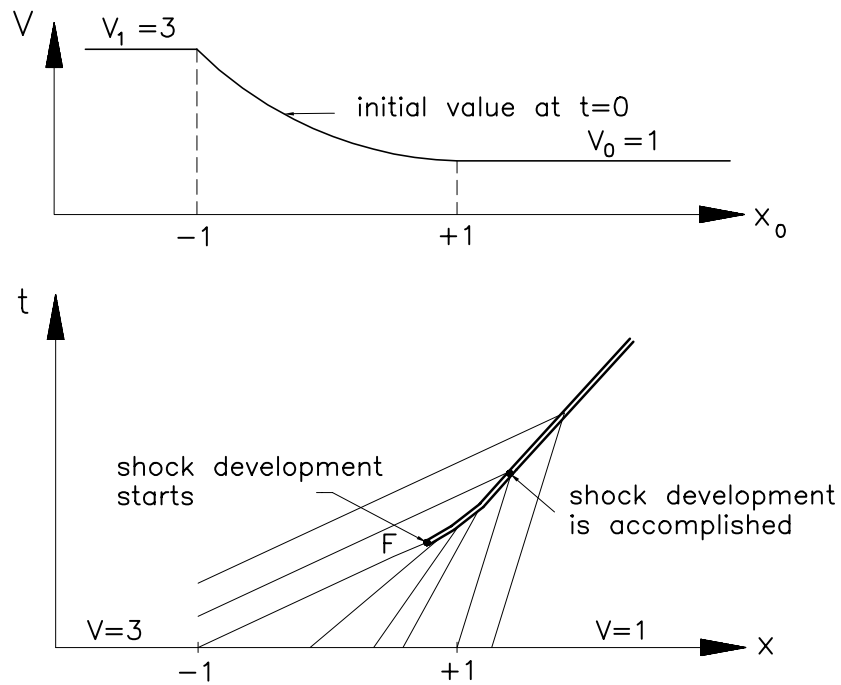


Figure 4.4: Shock development

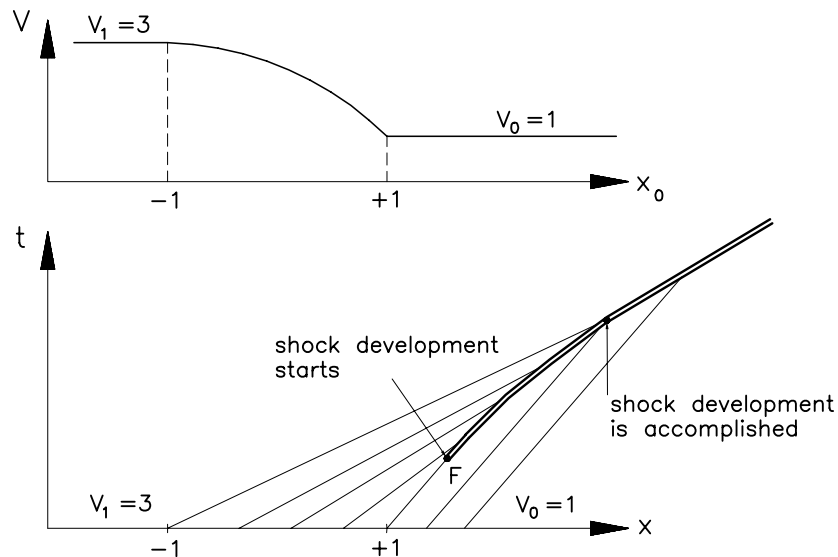


Figure 4.5: Shock development

4.3 Shock formation from a triangular wave

We now look at how the Burgers' equation gives rise to shock development when we start with a triangular wave, see figure 4.6.

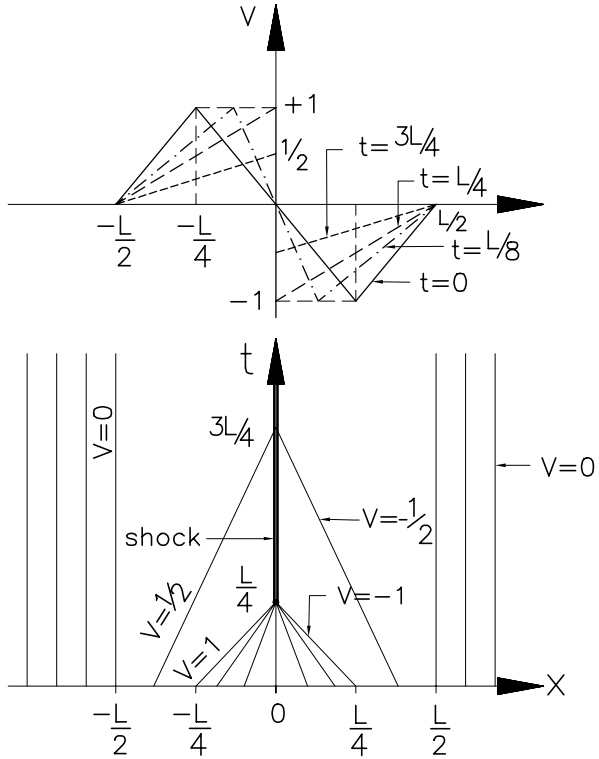


Figure 4.6: Shock formation from a triangular wave

The initial conditions are:

$$v(x, 0) = \begin{cases} 0, & x < -\frac{L}{2}, \\ \frac{4}{L} \left(x + \frac{L}{2} \right), & -\frac{L}{2} < x < -\frac{L}{4}, \\ \frac{-4}{L} x, & -\frac{L}{4} < x < \frac{L}{4}, \\ \frac{4}{L} \left(x - \frac{L}{2} \right), & \frac{L}{4} < x < \frac{L}{2}, \\ 0, & x > \frac{L}{2}, \end{cases}$$

The initial values between $-\frac{L}{4}$ and $\frac{L}{4}$ form a centered compression wave that focuses at $x = 0$, $t = \frac{L}{4}$. After shock formation at $t = \frac{L}{4}$ the shock remains at $x = 0$ and decays due to the expansion fans that arrive at the location $x = 0$. To get the decay we need to know v for increasing time at each side of the shock (say at $x = 0^-$ and $x = 0^+$). Use the method of characteristics to obtain $v(x, t)$ as:

$$v(x, t) = v(x - vt, 0).$$

For the domain covered by the characteristics emanating from $-\frac{L}{2} < x - \frac{L}{4}$ we then find

$$v(x, t) = \frac{4}{L} \left(x + \frac{L}{2} - vt \right)$$

or

$$v(x, t) = \frac{4x + 2L}{L + 4t}.$$

In a similar way for the domain that is covered by the characteristics emanating from $\frac{L}{4} < x \frac{L}{2}$ can be found that:

$$v(x, t) = \frac{4x - 2L}{L + 4t}.$$

So, at a certain time level $t \geq \frac{L}{4}$, the value of v at each side of the shock at $x = 0$ is given by

$$v(0^+, t) = \frac{-2L}{4t + L}, \quad \text{and} \quad v(0^-, t) = \frac{2L}{4t + L}.$$

The shock strength $\Delta v = v(0^+, t) - v(0^-, t)$ becomes:

$$\Delta v = \frac{-4L}{4t + L}.$$

For large t , we have

$$\lim_{t \rightarrow \infty} \Delta v = 0;$$

the shock strength decays asymptotically as t^{-1} .

4.4 Shock formation from a parabolic curve

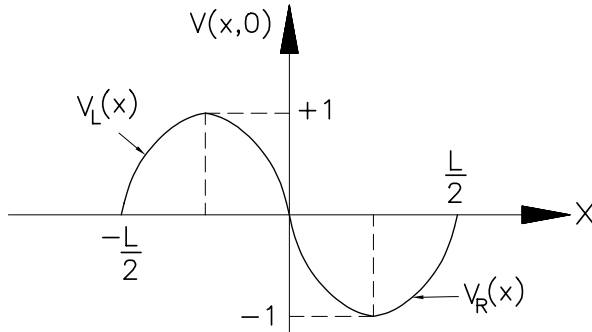


Figure 4.7: Parabolic initial data

Now let us consider initial data that has a parabolic shape. Take initial values $v(x, 0)$ consisting of two parabolic curves defined on the interval $-L/2 \leq x \leq L/2$ as follows:

$$v(x, 0) = \begin{cases} v_L(x, 0) = -\frac{16}{L^2}x(x + \frac{L}{2}) & \text{on } -\frac{L}{2} \leq x \leq 0, \\ v_R(x, 0) = +\frac{16}{L^2}x(x - \frac{L}{2}) & \text{on } 0 \leq x \leq \frac{L}{2}, \\ 0 & \text{outside the interval.} \end{cases} \quad (4.14)$$

The graph of the initial values is shown in figure 4.7. At $x = 0$, $v_L(x)$ and $v_R(x)$ together with their first derivatives match such that $v(x, 0)$ and $\frac{dv}{dx}(x, 0)$ are continuous. The first derivatives:

$$\begin{aligned} \frac{dv_L}{dx} &= -\frac{16}{L^2} \left(2x + \frac{L}{2} \right), \\ \frac{dv_R}{dx} &= +\frac{16}{L^2} \left(2x - \frac{L}{2} \right) \end{aligned}$$

attain their largest minimum value: $-8/L$ at $x = 0$. So shock formation starts at time level $t = \frac{L}{8}$ at $x = 0$. Since $v(x, 0)$ is an odd function, the shock velocity

$$v_s = \frac{1}{2}(v_L + v_R)$$

is zero. The shock remains at $x = 0$ for all $t > \frac{L}{8}$, see figure 4.8.

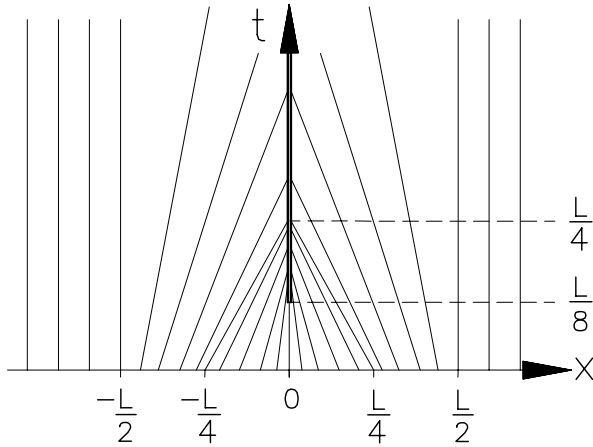


Figure 4.8: Formation of a shock from parabolic initial data

The shock strength defined as $\Delta v = v_L - v_R$ can be found as $\Delta v = \frac{L}{t} - \frac{L^2}{8t^2}$. The shock strength increases until $t = L/4$, thereafter it decays. The maximum shock strength equals $(\Delta v)_{\max} = 2$. Shock decay for large t appears asymptotically: $\Delta v \propto t^{-1}$.

4.5 Entropy conditions revisited

In chapter 1 we discussed the need of an entropy condition in modelling non-viscous discontinuities properly. Three different but equivalent formulations were presented:

I a fluid particle passing through a shock increases its entropy;

II for a physically valid moving shock the inequality $(u_1 - a_1) > c_s > (u_2 - a_2)$ holds;

III only those *inviscid* solutions are physically acceptable that can be obtained also from the fully viscous and heat-conducting equations in the limit of vanishing viscosity and heat conduction.

Condition II was derived for the situation in which the shock velocity c_s of a right running shock is smaller than the gas velocity u_2 in the domain in front of the moving shock. So domain ② is the post-shock state and domain ① is the pre-shock state. Let us rephrase this condition for the case in which a right running shock moves into the pre-shock domain (R); see figure 4.9.

Domain R is the pre-shock state, so it follows that $c_s - u_R > a_R$; similarly, domain L is the post shock state, so $c_s - u_L < a_L$. Combining these conditions there results

$$u_L + a_L > c_s > u_R + a_R \quad (4.15)$$

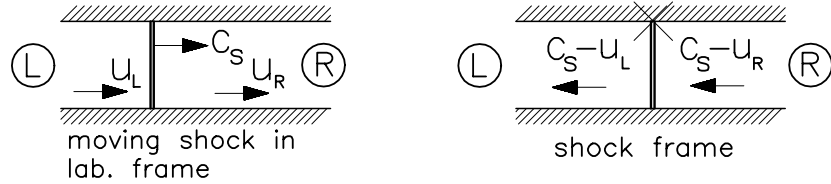


Figure 4.9: Moving shock in laboratory frame (left) and shock frame(right)

or

$$v_L > c_s > v_R.$$

Although the entropy is uniform in the Burgers flow description, we can recognise physical and unphysical shocks by the characteristic pattern in which they appear, see figure 4.10.

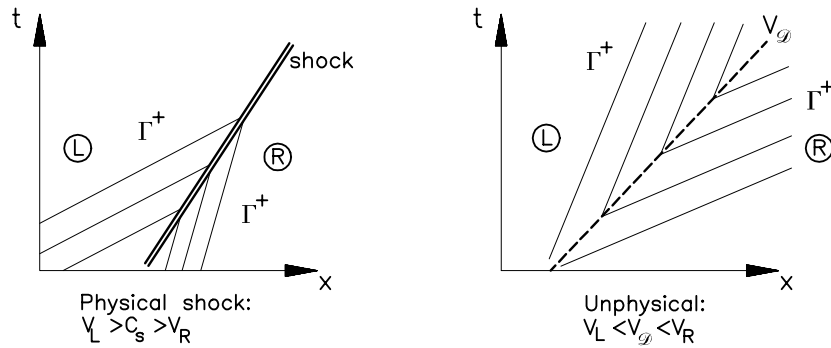


Figure 4.10: Physical and un-physical discontinuities

For physically valid shocks the characteristics of the same family merge or terminate at the shock discontinuity. If characteristics emerge from a discontinuity, an un-physical phenomenon occurs which should be replaced by an expansion fan.

Concerning entropy condition III let us study travelling-wave solutions of the viscous Burgers' equation:

$$v_t + vv_x = \mu v_{xx} \quad (4.16)$$

in the limit \$\mu \rightarrow 0\$ (vanishing viscosity).

We assume two different initial value distributions \$v(x, 0)\$ shown in figure 4.11. There is an interval \$\Delta\$ where \$v(x, 0)\$ varies between \$V_L\$ and \$V_R\$; outside the interval \$\Delta\$, \$v(x, 0)\$ takes the constant value \$V_L\$ or \$V_R\$.

In the non-viscous approximation one finds:

$$\text{case A: } V_{\text{shock}} = \frac{dx}{dt} = \left(\frac{v_L + v_R}{2} \right), \Rightarrow \quad v_L > V_{\text{shock}} > v_R$$

$$\text{case B: } V_{\text{shock}} = \frac{dx}{dt} = \left(\frac{v_L + v_R}{2} \right), \Rightarrow \quad v_L < V_{\text{shock}} < v_R$$

Using (4.15) case A thus evolves into a physically valid shock whereas case B evolves into an unphysical situation.

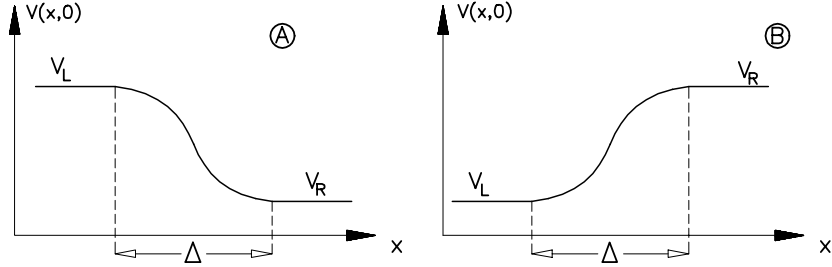


Figure 4.11: Initial values for travelling wave solutions of the viscous Burgers' equations. Case A: $v_L > v_R$, case B: $v_L < v_R$.

Let us now study what happens if viscosity is incorporated into the model. Introduce the new variables:

$$z = x - V_{\text{shock}} \cdot t \quad (4.17)$$

$$w = v - V_{\text{shock}} \quad (4.18)$$

Using

$$\begin{aligned} \left(\frac{\partial}{\partial t} \right)_x &= \left(\frac{\partial}{\partial t} \right)_z - V_{\text{shock}} \left(\frac{\partial}{\partial z} \right)_t, \\ \left(\frac{\partial}{\partial x} \right)_t &= \left(\frac{\partial}{\partial z} \right)_t \end{aligned}$$

it follows that (4.16) becomes

$$w_t + w w_z = \mu w_{zz}. \quad (4.19)$$

The initial condition is transformed into

$$w(x, 0) = v(x, 0) - \frac{v_L + v_R}{2}, \quad (4.20)$$

thus the limit values w_L and w_R are

$$w_L = \frac{v_L - v_R}{2}, \quad w_R = \frac{v_R - v_L}{2}.$$

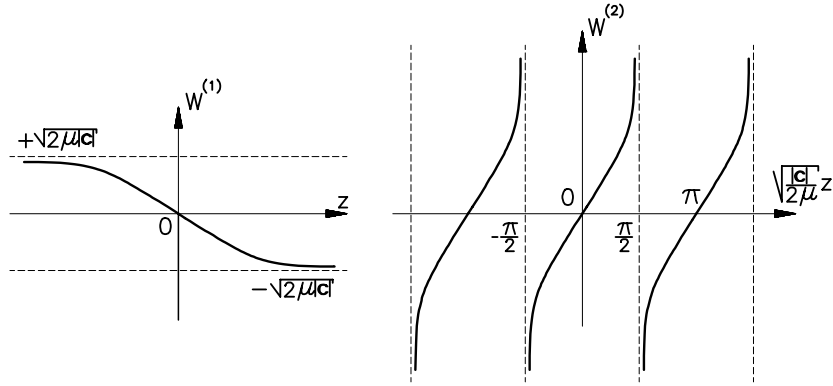
In the non-viscous approximation, the shock velocity becomes

$$\left(\frac{dz}{dt} \right) = \frac{1}{2}(w_L + w_R) = 0,$$

indicating that the shock ultimately evolves into a steady position at $z = 0$. The steady situation happens first at $t = \Delta/(v_L - v_R)$; thereafter the steady shock persists for all time $\Rightarrow w_t = 0$.

To study viscous effects we may also assume $w_t = 0$, then (4.19) can be written as

$$\left(\frac{1}{2} w^2 \right)_z = (\mu w_z)_z \quad (4.21)$$

Figure 4.12: Graph of $w^{(1)}$ and $w^{(2)}$

having the first integral

$$\frac{1}{2}w^2(z) = \mu \frac{dw}{dz} - \mu c \quad (4.22)$$

where c is an integration constant. This differential equation can be written in the form

$$\frac{dw}{w^2 + 2\mu c} = \frac{dz}{2\mu} \quad (4.23)$$

which has *two* different solutions for $c \neq 0$: $w^{(1)}$ and $w^{(2)}$:

$$c < 0 : \quad w^{(1)} = -\sqrt{2\mu|c|} \tanh \sqrt{\frac{|c|}{2\mu}} z; \quad (4.24)$$

$$c > 0 : \quad w^{(2)} = -\sqrt{2\mu|c|} \operatorname{tg} \sqrt{\frac{|c|}{2\mu}} z; \quad (4.25)$$

the integration constant c can be interpreted as the value of $\frac{dw}{dz}$ at $w = 0$. A graph of the solution $w^{(1)}$ and $w^{(2)}$ is given in figure 4.12.

From this figure we observe that $w^{(1)}$ fulfills the boundary conditions:

$$z \rightarrow -\infty : w^{(1)} = +\sqrt{2\mu|c|} = w_L;$$

$$z \rightarrow +\infty : w^{(1)} = -\sqrt{2\mu|c|} = w_R; .$$

If $\sqrt{2\mu|c|}$ is written in terms of w_L and w_R : $\sqrt{2\mu|c|} = \frac{w_L - w_R}{2}$, then the solution for $w^{(1)}$ becomes

$$w^{(1)} = -\frac{w_L - w_R}{2} \tanh \left(\left(\frac{w_L - w_R}{4\mu} \right) z \right). \quad (4.26)$$

In the limit $\mu \rightarrow 0$ $w^{(1)}$ approaches the non-viscous solution with a shock discontinuity where w jumps from w_L to w_R .

Figure 4.12 also makes clear that the $w^{(2)}$ solution cannot satisfy the boundary conditions; thus the assumption that a travelling wave with $w_R - w_L > 0$ exists has been proven to be invalid. ‘Expansion shocks’ do not appear as solutions of the Navier-Stokes equations for decreasing viscosity; so ‘expanding shocks’ must be regarded as unphysical.

4.6 Wave interaction

The inviscid Burgers equation enables us to study various types of wave interactions. Some examples will be elaborated upon in more detail in the sequel.

Example 1: expansion weakens shock

This situation can be viewed in the t, x -plane by uniformly moving a piston into a gas and then stopping it. Assume initial values along the entire x -axis at time $t = 0$ (being the time instant at which the piston stops):

$$v(x, 0) = \begin{cases} 0, & \text{for } x < 0, \\ 1, & \text{for } 0 < x < 1, \\ 0, & \text{for } x > 1, \end{cases}$$

see figure 4.13.

The discontinuity at $x = 1$ represents the shock, the abrupt change in v at $x = 0$ generates a centered expansion created by the stopping piston.

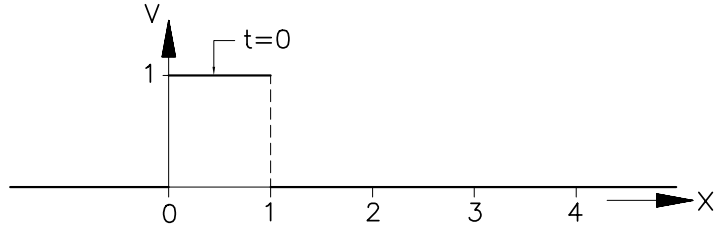


Figure 4.13: Initial values at $t = 0$

The shock produced by the uniformly moving piston has a velocity

$$\left(\frac{dx}{dt} \right)_s = V_s = \frac{1}{2}(v_{\text{pre}} + v_{\text{post}}) = \frac{1}{2}.$$

The first characteristic of the centered expansion wave has a velocity $v = 1$ and hits the shock at $t = 2$. From that instant on the interaction starts. The time evolution of the shock is shown in figure 4.14.

For $t \leq 2$ the shock is a straight line with a slope $\frac{dx_s}{dt} = \frac{1}{2}$. For $t > 2$ the shock is curved. Its shape can be determined from the O.D.E.:

$$\frac{dx_s}{dt} = \frac{1}{2}(v_{\text{pre}} + v_{\text{post}}) = \frac{1}{2}(0 + \frac{x}{t}) = \frac{x}{2t}. \quad (4.27)$$

With the boundary conditions: $x = 2$, $t = 2$ there follows (for $t \geq 2$):

$$x_s = \sqrt{2t} \quad (4.28)$$

The shock has a parabolic shape in the (t, x) -plane. The shock strength for $t \geq 2$ can be calculated as

$$\Delta v = v_{\text{post}} - v_{\text{pre}} = \frac{x}{t}; \quad (4.29)$$

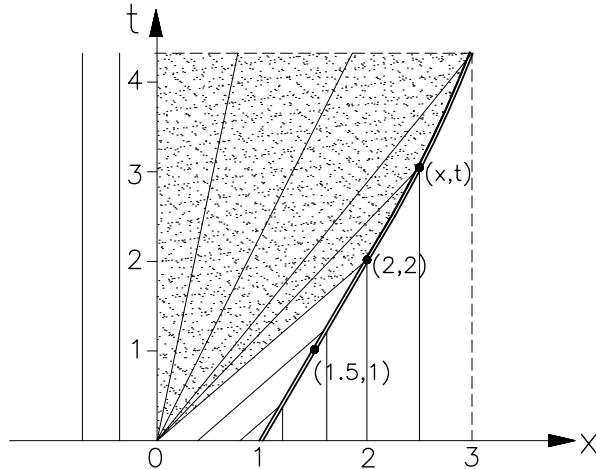


Figure 4.14: Expansion eats shock

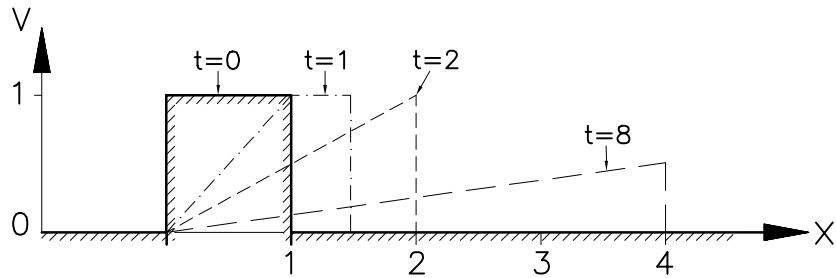


Figure 4.15: Shock development

using (4.28) this becomes

$$\Delta v = \frac{\sqrt{2t}}{t} = \sqrt{\frac{2}{t}}. \quad (4.30)$$

The shock strength decays with increasing time to zero as $1/\sqrt{t}$. The time evolution of $v(x)$ is shown in figure 4.15. Observe that the area A of the v -disturbance is constant in time: $A = \frac{x_s \Delta V}{2} = 1$.

Example 2: a shock accelerated by an expansion

Assume initial conditions $v(x, 0)$ such that:

$$\begin{aligned} x < -1 : \quad & v(x, 0) = 1, \\ -1 \leq x < 0 : \quad & v(x, 0) = 0, \\ x > 0 : \quad & v(x, 0) = 1. \end{aligned}$$

It represents a shock at $x = -1$ and a centered expansion at $x = 0$, see figure 4.16.

The shock at $x = -1$ has a speed $V_s = \frac{1}{2}$. It hits the last characteristic of the expansion fan at $t = 2$. For $t > 2$ the shock weakens and accelerates; its path may be found as a solution of the O.D.E.:

$$\frac{dx_s}{dt} = \frac{1}{2} \left(1 + \frac{x}{t} \right) \quad (4.31)$$

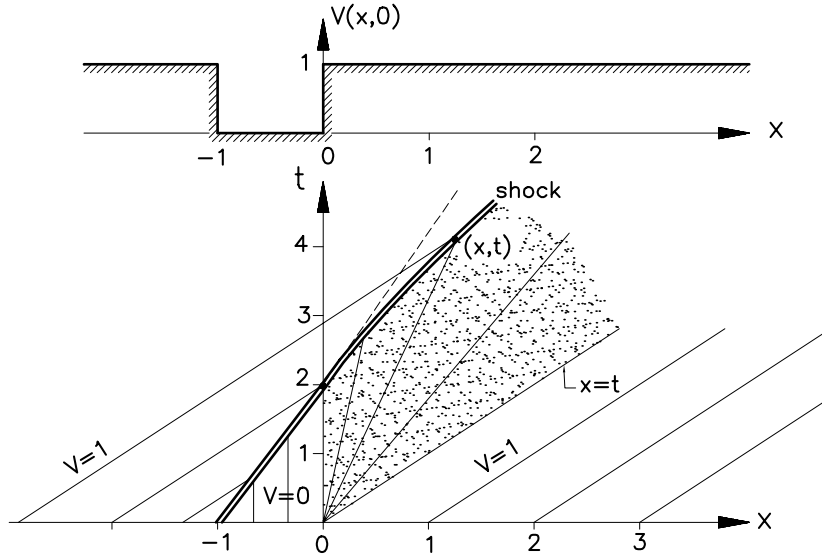


Figure 4.16: Shock accelerated by expansion

with boundary condition

$$x = 0, \quad t = 2.$$

The solution is:

$$x_s = -\sqrt{2t} + t, \quad \text{for } t \geq 2. \quad (4.32)$$

The shock accelerates but it never moves faster than the characteristic speed $v = 1$. The shock strength for $t > 2$ can be calculated as

$$\Delta v = v_{\text{post}} - v_{\text{pre}} = 1 - \frac{x_s}{t} \quad (4.33)$$

With (4.32) this becomes:

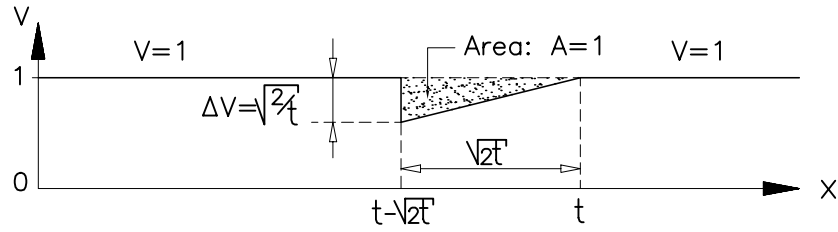
$$\Delta v = \sqrt{\frac{2}{t}}, \quad (4.34)$$

indicating that the shock strength decays asymptotically to zero.

The spatial distance between the shock and the first characteristic of the expansion:

$$x_{\text{char}} - x_{\text{shock}} = t + \sqrt{2t} - t = \sqrt{2t} \quad (4.35)$$

grows with increasing time. At large t the spatial v -distribution at constant t looks as shown in figure 4.17. This figure shows that there is always a weak shock left. The disturbance in the v -distribution has a triangular shape of which the area $A = \frac{1}{2}\sqrt{2t}\sqrt{2/t} = 1$ does not change in time.

Figure 4.17: v -distribution at large t .**Example 3: expansion eats shock**

Assume initial conditions $v(x, 0)$ such that:

$$\begin{aligned} x < 0 : \quad v(x, 0) &= 0, \\ 0 < x < 1 : \quad v(x, 0) &= 2, \\ x > 1 : \quad v(x, 0) &= 1. \end{aligned}$$

It represents a shock at $x = 1$ and a centered expansion at $x = 0$, see figure 4.18.

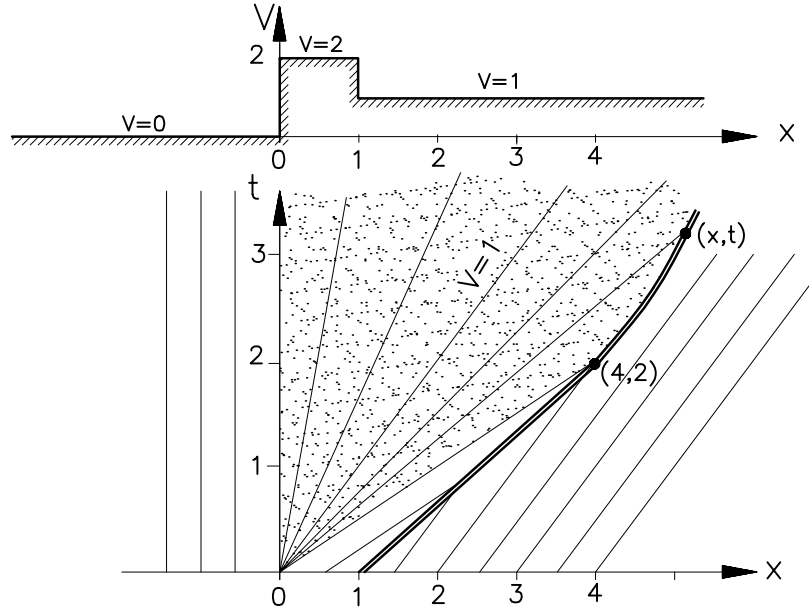


Figure 4.18: Expansion eats shock

The shock at $x = 1$ has a velocity $v_s = \frac{3}{2}$. It meets the first characteristic of the expansion fan at $t = 2$, $x = 4$. For $t = 2$ expansion-shock interaction starts. The path of the shock is found as the solution of the O.D.E.:

$$\frac{dx_s}{dt} = \frac{1}{2} \left(1 + \frac{x}{t} \right) \quad (4.36)$$

with boundary condition $x = 4$, $t = 2$. The solution is (for $t > 2$):

$$x_s = t + \sqrt{2t}. \quad (4.37)$$

The shock slows down, the shock speed is found as

$$\frac{dx}{dt} = V_s = 1 + \frac{1}{\sqrt{2t}}. \quad (4.38)$$

Observe that the shock speed never drops below the value 1. This implies that part of the expansion wave, where $0 < v < 1$, is not affected by the shock.

The shock strength for $t \geq 2$ can be calculated as

$$\Delta v = v_{\text{post}} - v_{\text{pre}} = \frac{x_s}{t} - 1. \quad (4.39)$$

Using (4.37) this becomes:

$$\Delta v = \sqrt{\frac{2}{t}}. \quad (4.40)$$

The shock strength decays asymptotically to zero. For large t the spatial v -distribution is as shown below in figure 4.19. There is always a weak shock travelling to the right.

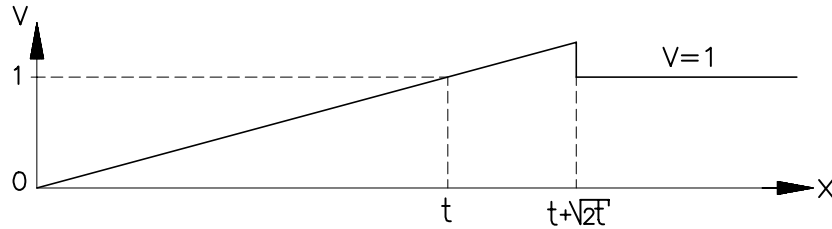


Figure 4.19: Spatial v -distribution for large t

Example 4: shock eats expansion

Assume initial conditions such that:

$$\begin{aligned} x < -1 : \quad v(x, 0) &= 2, \\ -1 < x < 0 : \quad v(x, 0) &= 0, \\ x > 0 : \quad v(x, 0) &= 1. \end{aligned}$$

It represents a shock at $x = -1$ and a centered expansion wave at $x = 0$, see figure 4.20.

The shock at $x = -1$ has a velocity $V_s = 1$. It meets the last characteristic of the expansion wave at $t = 1$, $x = 0$. Due to the interaction the shock accelerates. The shock path $x_s(t)$ is determined by the O.D.E.:

$$\frac{dx_s}{dt} = \frac{1}{2} \left(2 + \frac{x}{t} \right) \quad (4.41)$$

with boundary condition $x = 0$, $t = 1$. The solution is:

$$x_s = -2\sqrt{t} + 2t \quad (4.42)$$

which is valid for $2 \leq t \leq 4$. At $t = 4$ the shock meets the first characteristic $v = 1$ of the expansion fan. For $t > 4$ the shock speed is constant having the value $V_s = \frac{3}{2}$. The shock moves uniformly; all information about what happened for $t < 4$ is lost.

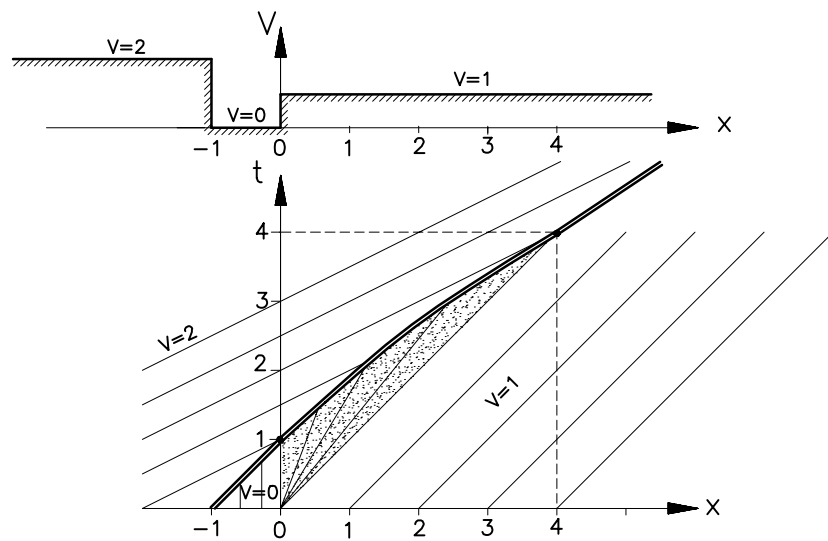


Figure 4.20: Shock eats expansion

The shock strength for $2 < t < 4$ can be calculated as

$$\Delta v = v_{\text{post}} - v_{\text{pre}} = 2 - \frac{x_s}{t}.$$

Using (4.42) there follows:

$$\Delta v = \frac{2}{\sqrt{t}}, \quad (4.43)$$

indicating shock decay from $\Delta v = 2$ at $t = 1$ to $\Delta v = 1$ at $t = 4$.

Chapter 5

Traffic waves

5.1 Definitions, traffic equation

As an application of non-linear unsteady waves we will study traffic flow on a one way, one-lane road. A traffic equation is derived assuming a continuum model of traffic flow.

Consider a one-lane highway with cars having an average length l . Let the traffic speed be $u(x, t)$, depending on time (t) and location (x), see figure 5.1.

The general conservation law for a quantity $f(\bar{x}, t)$ reads

$$\frac{\partial}{\partial t} \iiint_V f(\bar{x}, t) dV + \iint_{\partial V} f(\bar{x}, t) \bar{u} \cdot \bar{n} dS = \dot{s}_f \quad (5.1)$$

\dot{s}_f is a source term denoting the production of f per unit time, V is the control volume fixed in space domain.

In case of a one-dimensional (spatial) problem with $x \in \{x_1, x_2\}$ as control space this results in:

$$\frac{\partial}{\partial t} \int_{x_1}^{x_2} f(x, t) dx + f(x, t) u(x, t) \|_{x_1}^{x_2} = \dot{s}_f. \quad (5.2)$$

Regarding traffic flow $f(x, t)$ is equal to the number of cars per unit length, or the car density: $\rho(x, t)$

$$\rho(x, t) = \frac{\text{number of cars in control space}}{\text{length of control space}}$$

For ρ we have the limit values: $\rho_{\max} = 1/l$ meaning bumper to bumper traffic and $\rho_{\min} = 0$ meaning no traffic.

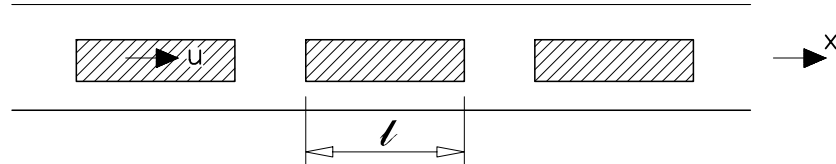


Figure 5.1: Traffic flow on a one-lane road.

If the conservation law of equation (5.2) with $\dot{s}_\rho = 0$ (no cars are destroyed nor created) is applied to an infinitesimal small control space: $x_1 = x$; $x_2 = x + dx$, the result is given by:

$$\frac{\partial \rho}{\partial t} + \frac{\partial}{\partial x} (\rho u) = 0 \quad (5.3)$$

The term ρu is identified as the car flux: the number of cars passing a fixed location per unit time.

To solve the problem a relation between ρ and u is needed. A simple model for the density-speed relation is the linear relation:

$$\frac{u}{V} = 1 - \rho l \quad (5.4)$$

Here V is the speed limit of the cars. If $\rho = 1/l$ there is no free space between the successive cars and the car flow stagnates ($u = 0$); if $\rho \rightarrow 0$ no one else is on the road and cars approach the speed limit.

Of course the density-speed relation can be chose more realistic e.g. by accounting for the fact that the speed limit already appears at $\rho = \rho^* \neq 0$. Another improvement of the density-speed relation follows if one takes the fact into account that the minimum intermediate space between successive cars depends on the velocity. The higher the velocity the larger the necessary intermediate space to decelerate a car to stand still.

Inserting equation (5.4) into (5.3) the traffic equation in dimensional form becomes:

$$\frac{\partial \rho}{\partial t} + \frac{\partial}{\partial x} \{\rho V (1 - \rho l)\} = 0. \quad (5.5)$$

Let us introduce the dimensionless variables

$$\tilde{u} = u/V, \quad \tilde{\rho} = \rho/(1/l),$$

and the dimensionless coordinates

$$\tilde{x} = x/l, \quad \tilde{t} = t/(l/V).$$

Then the traffic eqaution simplifies to

$$\frac{\partial \tilde{\rho}}{\partial \tilde{t}} + \frac{\partial}{\partial \tilde{x}} \{\tilde{\rho}(1 - \tilde{\rho})\} = 0 \quad (5.6)$$

and the speed-density relation becomes

$$\tilde{u} = 1 - \tilde{\rho}. \quad (5.7)$$

This relation is shown in figure 5.2.

Another interesting variable is the car flux: ρu . In dimensionless form we have:

$$\tilde{\rho} \tilde{u} = \tilde{\rho}(1 - \tilde{\rho}). \quad (5.8)$$

The car flux attains a maximum value at $\tilde{\rho} = 1/2$ and $\tilde{u} = 1/2$, (see figure 5.2). So the most efficient speed that allows the highway to be used at its maximum capacity (maximum car flux) is not the speed limit but (in the case of the linear speed-density relation) just the half of this speed limit. (So to use the road at its maximum capacity don't drive at maximum speed!)

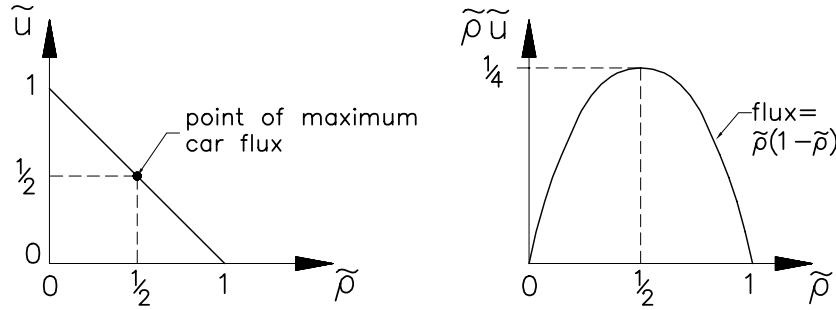


Figure 5.2: Speed-density relation and car flux versus car desity

5.2 Characteristics and Discontinuities

Take the traffic equation in the form of equation (5.6)

$$\frac{\partial \tilde{\rho}}{\partial \tilde{t}} + \frac{\partial}{\partial \tilde{x}} \{ \tilde{\rho}(1 - \tilde{\rho}) \} = 0,$$

and write it in the form of a non-linear convection equation i.e. (omitting tildes):

$$\frac{\partial \rho}{\partial t} + c(\rho) \frac{\partial \rho}{\partial x} = 0, \quad (5.9)$$

where $c(\rho)$ is the characteristics speed given by

$$c(\rho) = 1 - 2\rho. \quad (5.10)$$

Equation (5.9) is interpreted such that along curves $\frac{dx}{dt} = c(\rho)$, ρ is constant.

The curves $\frac{dx}{dt} = c(\rho)$ are characteristics of equation (5.9); since the slope of the characteristics depends solely on ρ they must be straight lines in the (t,x) -plane. This slope, $1 - 2\rho$, depends on the solutions $\rho(x,t)$; so their graph in the (t,x) -plane is not known a priori.

On the interval $0 \leq \rho \leq 1$, $c(\rho)$ varies between the values $c(0) = 1$ and $c(1) = -1$.

Observe that

$$c(\rho) = \frac{d(\rho u)}{d\rho}, \quad (5.11)$$

hence the characteristic speed is found as the slope of the graph $\rho u = f(\rho)$ as shown in figure 5.2. Assume that the initial values of $\rho(x,t)$ are given at: $t = 0$ as $\rho(x,0) = \phi(x)$.

The solution $\rho(x,t)$ is determined as follows; draw the straight characteristic through (x,t) backwards. This line is determined by the equation: $x - c(\rho)t = \text{constant}$, so:

$$\rho(x,t) = \rho(x - ct, 0) = \phi(x - ct).$$

Using $c = 1 - 2\rho$ there follows the implicit expression for $\rho(x,t)$:

$$\rho(x,t) = \phi(x - (1 - 2\rho)t). \quad (5.12)$$

Equation (5.12) describes a closed form solution for continuous traffic flow satisfying the initial conditions $\rho(x,0) = \phi(x)$.

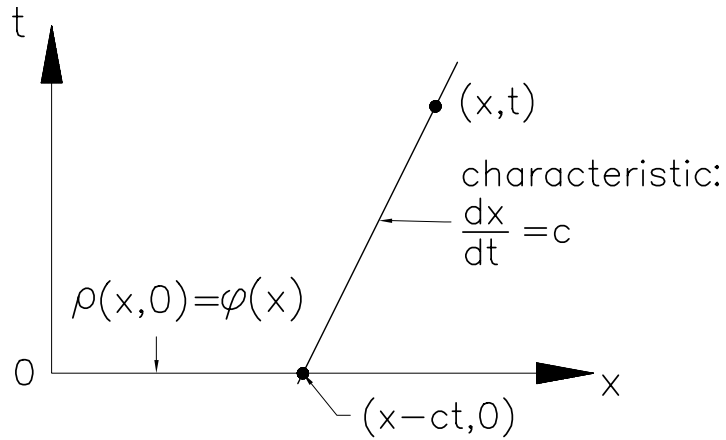


Figure 5.3: Characteristic

Apart from these continuous solutions also discontinuities may appear. Apply the jump relations for 1D steady flow: apply equation (1.39) to equation (5.6) which yields (omitting tildes):

$$c_s[\rho] - [\rho(1 - \rho)] = 0, \quad (5.13)$$

with c_s being the jump velocity and $[-]$ denoting the jump: $(-)_R - (-)_L$, so one finds:

$$\begin{aligned} c_s(\rho_R - \rho_L) &= \rho_R(1 - \rho_R) - \rho_L(1 - \rho_L) \\ &= (\rho_R - \rho_L)(1 - \rho_R - \rho_L), \end{aligned}$$

or

$$c_s = 1 - (\rho_R + \rho_L). \quad (5.14)$$

Now compare the shock velocity c_s with the characteristic speed on either side of the shock discontinuity. At the left side : $c = c_L = 1 - 2\rho_L$; on the right side: $c = c_R = 1 - 2\rho_R$. Expressing c_s in terms of c_R and c_L one obtaines

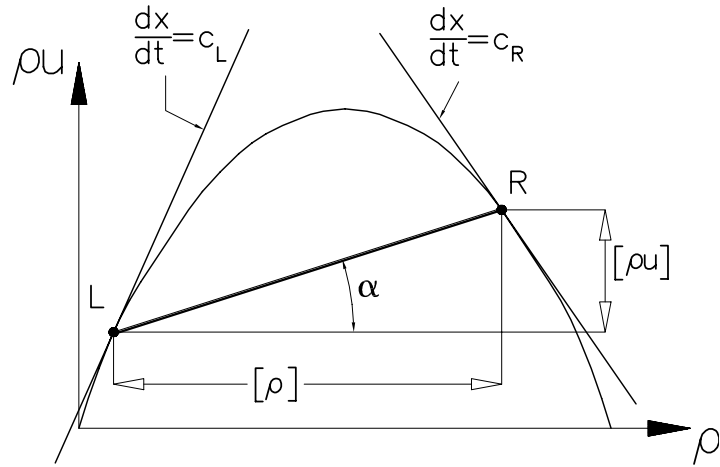
$$c_s = \frac{1}{2}(c_L + c_R), \quad (5.15)$$

reflecting the property that the shock speed c_s is the mean value of the characteristic speeds c_L and c_R .

Returning to equation (5.13) and remembering that $\rho(1 - \rho)$ denotes the car flux ρu , the shock speed c_s can also be viewed as

$$c_s = \frac{[\rho u]}{[\rho]}, \quad (5.16)$$

being the slope of the chord LR in the graph (ρu) vs (ρ) , see figure 5.4; L and R are two points on this graph representing the left- and right side of the discontinuity respectively.

Figure 5.4: Shock speed C_s in graph (ρu) vs ρ

5.3 Traffic light

Consider the traffic situation where a train of cars is lined up at a red traffic light. This situation is modelled by the Riemann problem with initial values ($t \leq 0$):

$$\rho(x, 0) = \begin{cases} 1 & , x < 0 \\ 0 & , x > 0 \end{cases}$$

Let the light turn green at $t = 0$.

View the (t, x) -plane. The characteristics emanating from $x < 0$ ($t = 0$) have the slope $\frac{dx}{dt} = -1$ and those emanating from $x > 0$ ($t = 0$) have the slope $\frac{dx}{dt} = +1$.

From $x = 0$ a fan of straight characteristics appear. Along characteristics the density is constant, so the solution for $t \neq 0$ can be constructed very easily.

Take a certain time level $t = t_1$ and let us find the solution for $\rho(x, t_1)$ and $u(x, t_1)$. A single characteristic in the fan is given as:

$$x = \xi t.$$

The particular value of ξ identifies a particular characteristic. The slope of the characteristic is:

$$\frac{dx}{dt} = \xi = 1 - 2\rho.$$

So the traffic density depends on the slope, yielding

$$\rho = \frac{1 - \xi}{2} = \frac{1 - x/t}{2} = \frac{t - x}{2t}. \quad (5.17)$$

Since $u = 1 - \rho$ one obtaines

$$u = \frac{t + x}{2t}. \quad (5.18)$$

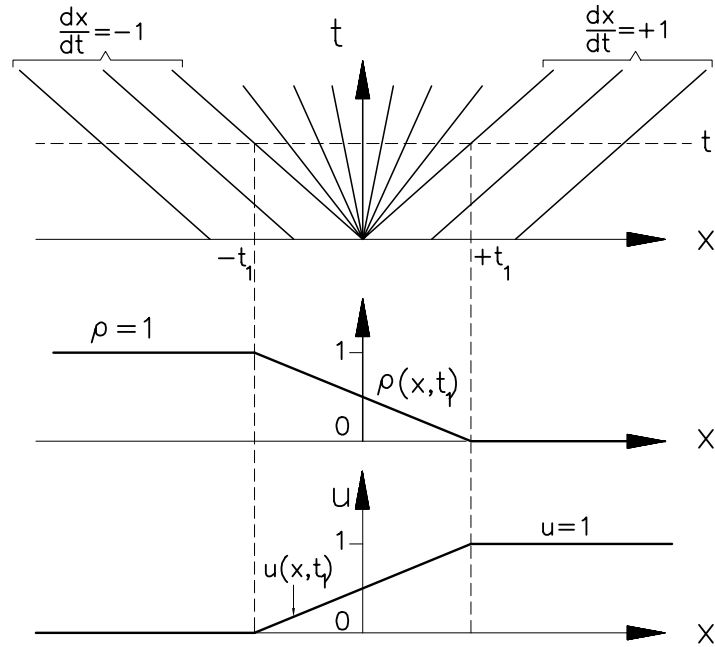


Figure 5.5: Distribution of $\rho(x)$ and $u(x)$ at $t = t_1$

Observe that u and ρ are both linear functions of x at constant t_1 see figure 5.5. When time progresses the original discontinuity at $x = 0$ relaxes into a continuous distribution along the x -axis at an arbitrary time instant.

What is the trajectory of a car? Take the particular car lined up at $x = -1$. This car starts moving at $t = 1$ the time instant that the characteristic $x = -t$ is passed. The trajectory of the car is found as the solution of the ODE

$$\frac{dx_c}{dt} = u = 1 - \rho = \frac{1}{2} \left(1 + \frac{x}{t} \right), \quad (5.19)$$

with the initial conditions $x = 1$, $t = 1$.

The solution of equation (5.19) that satisfies these conditions is

$$x_c(t) = t - 2\sqrt{t}, \quad t \leq 1. \quad (5.20)$$

For $t \rightarrow \infty$ the car path becomes parallel to the characteristics $\frac{dx_c}{dt} = +1$. The car attains its maximum speed ($u = 1$) as $t \rightarrow \infty$. A picture of the car path is shown in figure 5.6.

5.4 A chain collision

Consider the Riemann problem with initial values

$$\rho(x, 0) = \begin{cases} 1/2 & , \quad x < 0 \\ 1 & , \quad x > 0 \end{cases}$$

which models a traffic jam.

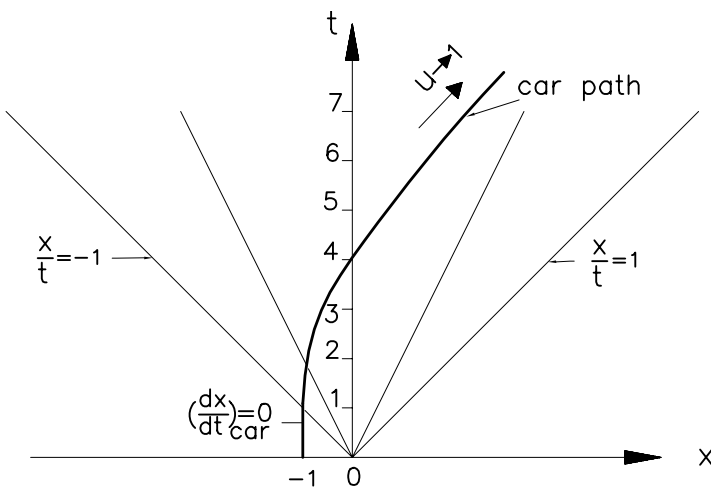


Figure 5.6: Car path

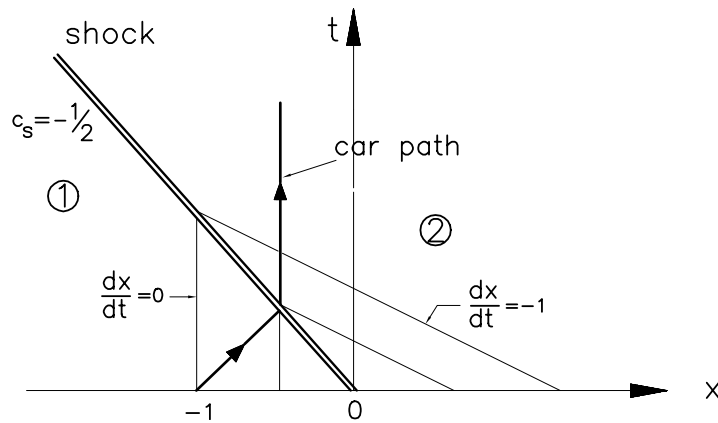


Figure 5.7: Cars backing up

The characteristics emanating from $x < 0$ have a slope $\frac{dx}{dt} = 0$ and those emanating from $x > 0$ have a slope $\frac{dx}{dt} = -1$. Both sets of characteristics intersect; a shock has to be formed. The shock speed is $c_s = 1 - (\rho_L + \rho_R) = -\frac{1}{2}$.

Observe that the shock travels 'upstream'. It acts as a carrier of information telling the on-coming cars that a traffic jam is ahead, see figure 5.7.

Car paths in domain ① are straight lines with slope $\frac{dx}{dt} = u = 1 - \rho = \frac{1}{2}$. When the shock has passed, the cars are decelerated abruptly to stand still. The shock represents the front of cars coming to a stand still.

Chapter 6

Two-Dimensional Inviscid Flow

6.1 Governing flow equations

In paragraph (1.5) we have derived the Euler equations which are the appropriate equations to model compressible flows where the effects of viscosity, heat conduction and external forces have been neglected. These equations for two dimensional flows written in the conservative form (omitting tildes) are

$$\frac{\partial U}{\partial t} + \frac{\partial F}{\partial x} + \frac{\partial G}{\partial y} = 0 \quad (6.1)$$

with

$$U = \begin{pmatrix} \rho \\ \rho u \\ \rho v \\ \rho E \end{pmatrix}, F = \begin{pmatrix} \rho u \\ p + \rho u^2 \\ \rho uv \\ \rho u H \end{pmatrix}, G = \begin{pmatrix} \rho v \\ \rho vu \\ p + \rho v^2 \\ \rho v H \end{pmatrix}$$

U is the vector of state variables, F and G are flux vectors.

The non-conservative form of these equations read

$$\left. \begin{aligned} \frac{\partial \rho}{\partial t} + u \frac{\partial \rho}{\partial x} + v \frac{\partial \rho}{\partial y} + \rho \frac{\partial u}{\partial x} + \rho \frac{\partial v}{\partial y} &= 0 \\ \rho \frac{\partial u}{\partial t} + \rho u \frac{\partial u}{\partial x} + \rho v \frac{\partial u}{\partial y} + \frac{\partial p}{\partial x} &= 0 \\ \rho \frac{\partial v}{\partial t} + \rho u \frac{\partial v}{\partial x} + \rho v \frac{\partial v}{\partial y} + \frac{\partial p}{\partial y} &= 0 \\ \rho \frac{\partial E}{\partial t} + \rho u \frac{\partial H}{\partial x} + \rho v \frac{\partial H}{\partial y} &= 0 \end{aligned} \right\} \quad (6.2)$$

For the analysis of the vector equation (6.1) it is useful to define the Jacobian matrices

$$\left. \begin{aligned} \mathbf{A}_c &= \frac{dF(U)}{dU} \quad \text{with} \quad (A_c)_{i,j} = \frac{\partial F_i}{\partial U_j} \\ \mathbf{B}_c &= \frac{dG(U)}{dU} \quad \text{with} \quad (B_c)_{i,j} = \frac{\partial G_i}{\partial U_j} \end{aligned} \right\} \quad (6.3)$$

Since $F = F(U)$ we can write

$$\frac{\partial F}{\partial x} = \frac{dF}{dU} \frac{\partial U}{\partial x}, \quad (6.4)$$

and in a similar way

$$\frac{\partial G}{\partial y} = \frac{dG}{dU} \frac{\partial U}{\partial y}. \quad (6.5)$$

Inserting (6.4) and (6.5) into (6.1), the last equation can be rewritten as

$$\frac{\partial U}{\partial t} + \mathbf{A}_c \frac{\partial U}{\partial x} + \mathbf{A}_c \frac{\partial U}{\partial y} = 0 \quad (6.6)$$

In order to compute \mathbf{A}_c and \mathbf{B}_c the components of $F(U)$ and $G(U)$ have to be expressed in terms of the components of $U = (U_1, U_2, U_3, U_4)^T$.

A straightforward analysis leads to

$$\left. \begin{aligned} F_1 &= U_2 \\ F_2 &= (\gamma - 1) \left\{ U_4 - \frac{U_2^2}{2U_1} - \frac{U_3^2}{2U_1} \right\} + \frac{U_2^2}{U_1} \\ F_3 &= \frac{U_2 U_3}{U_1} \\ F_4 &= \frac{U_2}{U_1} \left\{ \gamma U_4 - (\gamma - 1) \frac{U_2^2}{2U_1} - (\gamma - 1) \frac{U_3^2}{2U_1} \right\} \end{aligned} \right\} \quad (6.7)$$

and

$$\left. \begin{aligned} G_1 &= U_3 \\ G_2 &= \frac{U_2 U_3}{U_1} \\ G_3 &= (\gamma - 1) \left\{ U_4 - \frac{U_2^2}{2U_1} - \frac{U_3^2}{2U_1} \right\} + \frac{U_3^2}{U_1} \\ G_4 &= \frac{U_3}{U_1} \left\{ \gamma U_4 - (\gamma - 1) \frac{U_2^2}{2U_1} - (\gamma - 1) \frac{U_3^2}{2U_1} \right\} \end{aligned} \right\} \quad (6.8)$$

Equation (6.6) is a non-conservative form of the flow equations expressed in terms of the state vector $\bar{U} = (\rho, \rho u, \rho v, \rho E)^T$. However in a lot of applications it is useful to work with equations expressed in terms of the state vector of primary variables $W = (\rho, u, v, p)^T$. Assume that the equations expressed in terms of W have the form

$$W_t + \mathbf{A}(W)W_x + \mathbf{B}(W)W_y = 0 \quad (6.9)$$

Can we find $\mathbf{A}(W)$ and $\mathbf{B}(W)$?

Considering (6.2) it appears that it is almost expressed in these primary variables apart from the last equation which still contains the non-primary variables E (total energy) and H (total enthalpy).

But this equation can be replaced by the energy equation for adiabatic flow

$$\frac{\partial p}{\partial t} + u \frac{\partial p}{\partial x} + \rho a^2 \frac{\partial u}{\partial x} + v \frac{\partial p}{\partial y} + \rho a^2 \frac{\partial v}{\partial y} = 0 \quad (6.10)$$

Which is a direct consequence of the adiabatic flow assumption:

$$\frac{DS}{Dt} = 0$$

expressing that entropy is constant along a particle path.

From $\frac{DS}{Dt} = 0$ it follows in 2D flows

$$\frac{\partial S}{\partial t} + u \frac{\partial S}{\partial x} + v \frac{\partial S}{\partial y} = 0 \quad (6.11)$$

Since the entropy change dS is proportional to $dp - a^2 d\rho$, equation (6.11) may be written as:

$$\frac{\partial p}{\partial t} - a^2 \frac{\partial \rho}{\partial t} + u \left\{ \frac{\partial p}{\partial x} - a^2 \frac{\partial \rho}{\partial x} \right\} + v \left\{ \frac{\partial p}{\partial y} - a^2 \frac{\partial \rho}{\partial y} \right\} = 0$$

All ρ -derivatives can be eliminated using the unsteady form of the continuity equation

$$\frac{\partial \rho}{\partial t} + u \frac{\partial \rho}{\partial x} + v \frac{\partial \rho}{\partial y} = -\rho \frac{\partial u}{\partial x} - \rho \frac{\partial v}{\partial y}$$

Then equation (6.10) is obtained.

From (6.2) and (6.10) the matrices $\mathbf{A}(W)$ and $\mathbf{B}(W)$ are easily found as

$$\mathbf{A}(W) = \begin{pmatrix} u & \rho & 0 & 0 \\ 0 & u & 0 & \frac{1}{\rho} \\ 0 & 0 & u & 0 \\ u & \rho a^2 & 0 & u \end{pmatrix}, \mathbf{B}(W) = \begin{pmatrix} v & 0 & \rho & 0 \\ 0 & v & 0 & 0 \\ 0 & 0 & v & \frac{1}{\rho} \\ 0 & 0 & \rho a^2 & v \end{pmatrix} \quad (6.12)$$

Of course it is also possible to retrieve the primitive form: (6.9) from the conservative form: (6.1) or (6.6) by noting that from the relation $W = W(U)$ it follows

$$dW = \frac{dW}{dU} dU = \mathbf{T}^{-1} dU, \quad \mathbf{T} = \frac{dU}{dW} \quad (6.13)$$

Formally (6.6) is written as

$$\mathbf{T} \frac{\partial W}{\partial t} + \mathbf{A}_c \mathbf{T} \frac{\partial W}{\partial x} + \mathbf{B}_c \mathbf{T} \frac{\partial W}{\partial y} = 0$$

or, if \mathbf{T} is non-singular

$$\frac{\partial W}{\partial t} + \mathbf{T}^{-1} \mathbf{A}_c \mathbf{T} \frac{\partial W}{\partial x} + \mathbf{T}^{-1} \mathbf{B}_c \mathbf{T} \frac{\partial W}{\partial y} = 0 \quad (6.14)$$

Apparently we can obtain \mathbf{A} and \mathbf{B} from \mathbf{A}_c and \mathbf{B}_c by the relations

$$\mathbf{A} = \mathbf{T}^{-1} \mathbf{A}_c \mathbf{T}, \quad \mathbf{B} = \mathbf{T}^{-1} \mathbf{B}_c \mathbf{T} \quad (6.15)$$

with

$$\mathbf{T} = \begin{pmatrix} 1 & 0 & 0 & 0 \\ u & \rho & 0 & 0 \\ v & 0 & \rho & 0 \\ \frac{u^2+v^2}{2} & \rho u & \rho v & \frac{1}{\gamma-1} \end{pmatrix} \quad (6.16)$$

6.2 Characteristic form for 2D unsteady flow

Now we have the objective to find, if possible, the characteristics and their related invariants for 2D unsteady flow expressed in primary variables.

Remembering for 1D unsteady flows we found

$$\begin{aligned}\frac{\partial J^+}{\partial t} + (u + a)\frac{\partial J^+}{\partial x} &= 0, \\ \frac{\partial S}{\partial t} + u\frac{\partial S}{\partial x} &= 0, \\ \frac{\partial J^-}{\partial t} + (u - a)\frac{\partial J^-}{\partial x} &= 0,\end{aligned}$$

with

$$dJ^\pm = du \pm \frac{dp}{\rho a}.$$

Can we find something similar for 2D unsteady flows?

If so, then it should have the form

$$V_t + \mathbf{A}V_x + \mathbf{B}V_y = 0 \quad (6.17)$$

Where \mathbf{A} and \mathbf{B} are diagonal and V is a new state vector related to W .

Apparently W itself is not a proper state vector because of $\mathbf{A}(W)$ and $\mathbf{B}(W)$ contain some off-diagonal terms. They are definitely not-diagonal.

How to get the proper state vector V and the corresponding matrixes \mathbf{A} and \mathbf{B} ?

Previously in the 1D case we used the "add & subtract" method and we relatively easily found the diagonalized form by trial and error. Using this technique here does not result into a complete success. For instance, try to combine the x-momentum equation (6.2) with the energy equation in the form (6.10); first multiply the latter with $(\rho a)^{-1}$ to get the proper dimensions

$$\begin{aligned}\text{x-momentum : } \frac{\partial u}{\partial t} + u\frac{\partial u}{\partial x} + \frac{1}{\rho}\frac{\partial p}{\partial x} + v\frac{\partial u}{\partial y} &= 0 \\ \text{energy equation : } \frac{1}{\rho a}\frac{\partial p}{\partial t} + \frac{u}{\rho a}\frac{\partial p}{\partial x} + a\frac{\partial u}{\partial x} + \frac{v}{\rho a}\frac{\partial p}{\partial y} + a\frac{\partial v}{\partial y} &= 0\end{aligned}$$

If we add them together we obtain:

$$u_t + \frac{1}{\rho a}p_t + (u + a)\left(u_x + \frac{1}{\rho a}p_x\right) + v\left(u_y + \frac{1}{\rho a}p_y\right) + av_y = 0$$

We observe the appearance of the partial derivatives $\frac{\partial}{\partial t}$, $\frac{\partial}{\partial x}$ and $\frac{\partial}{\partial y}$ of a single term of which $du + \frac{1}{\rho a}dp$ is the total differential, however the extra term av_y has appeared, which destroys the diagonal form. Of course, this was just a first try motivated by our previous success in 1D; we may have overlooked other possibilities.

It is now time to develop a straightforward method of diagonalization.

Let us develop this technique first for the 1D unsteady case; here we already know the outcome!

Diagonalization for unsteady 1D flow The unsteady 1D flow field is governed by (6.9) and (6.12)

$$W_t + \mathbf{A}(W)W_x = 0 \quad (6.18)$$

in which W is the state vector of primary variables $W = (\rho, u, p)^T$ and \mathbf{A} is given by

$$\mathbf{A} = \begin{pmatrix} u & \rho & 0 \\ 0 & u & \frac{1}{\rho} \\ 0 & \rho a^2 & u \end{pmatrix} \quad (6.19)$$

Introduce the change of state variables from W to V by

$$dW = \mathbf{S} dV \quad (6.20)$$

and find S so that it diagonalizes the coefficient matrix in the resulting equation

$$\mathbf{S} V_t + \mathbf{A}(W) \mathbf{S} V_x = 0$$

or if \mathbf{S} is invertible

$$V_t + \mathbf{S}^{-1} \mathbf{A} \mathbf{S} V_x = 0 \quad (6.21)$$

where $\mathbf{S}^{-1} \mathbf{A} \mathbf{S}$ is now a diagonal matrix

$$\mathbf{S}^{-1} \mathbf{A} \mathbf{S} = \Lambda = \begin{pmatrix} \lambda_1 & 0 & 0 \\ 0 & \lambda_2 & 0 \\ 0 & 0 & \lambda_3 \end{pmatrix} \quad (6.22)$$

whose non zero entries lie on the diagonal and follows from the eigenvalues $\lambda_i, i = 1, 2, 3$ of the matrix \mathbf{A} . The eigenvalues of \mathbf{A} are

$$\lambda_1 = u - a \quad (6.23)$$

$$\lambda_2 = u \quad (6.24)$$

$$\lambda_3 = u + a \quad (6.25)$$

From linear algebra we know that the matrix \mathbf{S} is build up by the matrix of right (column) eigenvectors of \mathbf{A} .

Right eigenvectors R_i of \mathbf{A} satisfy the relation

$$\mathbf{A} R_i = \lambda_i R_i \quad (6.26)$$

With the eigenvalues found in (6.23) the eigenvectors (apart from an arbitrary factor) are easily obtained

$$\begin{aligned} \lambda_1 = u - a &\Rightarrow R_1 = (\rho, -a, \rho a^2)^T, \\ \lambda_2 = u &\Rightarrow R_2 = (1, 0, 0)^T, \\ \lambda_3 = u + a &\Rightarrow R_3 = (\rho, a, \rho a^2)^T, \end{aligned} \quad (6.27)$$

So the matrix \mathbf{S} is found as

$$\mathbf{S} = \begin{pmatrix} \rho & 1 & \rho \\ -a & 0 & a \\ \rho a^2 & 0 & \rho a^2 \end{pmatrix}. \quad (6.28)$$

With the help of (6.20) the new state vector V is determined from

$$dV = \mathbf{S}^{-1} dW, \quad (6.29)$$

which shows that the inverse of \mathbf{S} : \mathbf{S}^{-1} has to be determined.
If \mathbf{S} is given by (6.28) then \mathbf{S}^{-1} is

$$\mathbf{S}^{-1} = \frac{1}{2\rho a^2} \begin{pmatrix} 0 & -\rho a & 1 \\ 2\rho a^2 & 0 & -2\rho \\ 0 & \rho a & 1 \end{pmatrix}, \quad (6.30)$$

so that the new state vector V becomes

$$dV \propto \begin{pmatrix} 0 & -\rho a & 1 \\ 2\rho a^2 & 0 & -2\rho \\ 0 & \rho a & 1 \end{pmatrix} \begin{pmatrix} d\rho \\ du \\ dp \end{pmatrix} = \begin{pmatrix} -\rho adu + dp \\ 2\rho a^2 d\rho - 2\rho dp \\ \rho adu + dp \end{pmatrix}$$

or

$$dV \propto \begin{pmatrix} -\rho adJ^- \\ -2\rho (dp - a^2 d\rho) \\ \rho adJ^+ \end{pmatrix} = \begin{pmatrix} -\rho adJ^- \\ \frac{-2\rho p}{c_v} dS \\ \rho adJ^+ \end{pmatrix} \quad (6.31)$$

Here J^- , S and J^+ are the characteristic variables or invariants appearing in 1D unsteady flow.

If the eigenvectors R_1 , R_2 and R_3 are multiplied by an appropriate but inconsequential factor the previously defined state variables dJ^+ , dS and dJ^- are obtained immediately.

Anyhow, the diagonalization technique, just introduced appears to be a straightforward method to find the characteristic speeds and the components of the new state vector (or invariants) dV .

However to attain dV we had to find the inverse \mathbf{S}^{-1} . This gives some labour; a faster method is to go immediately for \mathbf{S}^{-1} which can be accomplished by working with the left (row) eigenvectors of \mathbf{A} . This will be accomplished now

We want to diagonalize the equation

$$W_t + \mathbf{A}W_x = 0,$$

assume

$$dW = \mathbf{L}^{-1}dV, \quad (6.32)$$

where V is the new state vector and \mathbf{L}^{-1} is the matrix that diagonalizes the original equation. Inserting (6.32) into (6.18) one obtains

$$\mathbf{L}^{-1}V_t + \mathbf{A}\mathbf{L}^{-1}V_x = 0$$

or

$$V_t + \mathbf{A}\mathbf{L}\mathbf{L}^{-1}V_x = 0 \quad (6.33)$$

The objective is to find \mathbf{L} such that $\mathbf{A}\mathbf{L}\mathbf{L}^{-1}$ is diagonal,

$$\mathbf{A}\mathbf{L}\mathbf{L}^{-1} = \Lambda. \quad (6.34)$$

From Linear Algebra we know that the rows of \mathbf{L} are the left (row) eigenvectors \mathbf{L}_i of \mathbf{A} satisfying the relation

$$\mathbf{L}_i\mathbf{A} = \lambda_i\mathbf{L}_i \quad (6.35)$$

Proof Arrange the row vectors as the rows of matrix \mathbf{L} , so we have

$$\mathbf{LA} = \Lambda \mathbf{L}_1$$

Multiplying with \mathbf{L}^{-1} there results

$$\mathbf{LAL}^{-1} = \Lambda \mathbf{L}_1 \mathbf{L}^{-1} = \Lambda$$

Q.E.D

When \mathbf{L} is obtained, dV follows explicitly from (6.32).

Let us now demonstrate the left eigenvector method to determine dV directly, e.g. for the unsteady 1D case. Matrix \mathbf{A} is already given in (6.14), its eigenvalues were found (6.23) as

$$\lambda_1 = u - a, \quad \lambda_2 = u, \quad \lambda_3 = u + a$$

The left eigenvectors \mathbf{L}_i (corresponding to λ_i) of \mathbf{A} are obtained as follows.

For $\lambda_1 = u - a$ assume $\mathbf{L}_1 = \{\ell_{11}, \ell_{12}, \ell_{13}\}$.

With (6.35) we have:

$$(\ell_{11}, \ell_{12}, \ell_{13}) \begin{pmatrix} u & \rho & 0 \\ 0 & u & \frac{1}{\rho} \\ 0 & \rho a^2 & u \end{pmatrix} = (\lambda_1 \ell_{11}, \lambda_2 \ell_{12}, \lambda_3 \ell_{13}).$$

or

$$\begin{aligned} \ell_{11}a &= 0 \\ \ell_{12}\rho + \ell_{13}a + \ell_{13}\rho a^2 &= 0 \\ \ell_{12}\frac{1}{\rho} + \ell_{13}a &= 0 \end{aligned}$$

Solving for ℓ_{11} , ℓ_{12} and ℓ_{13} one obtains (apart from an arbitrary factor):

$$\ell_{11} = 0, \quad \ell_{12} = -\rho a, \quad \ell_{13} = 1,$$

making the left eigenvector $\mathbf{L}_1 = (0, -\rho a, 1)$.

In a similar way the left eigenvectors \mathbf{L}_2 and \mathbf{L}_3 can be calculated.

Summarizing the results gives:

$$\begin{aligned} \lambda_1 = u - a &\rightarrow \mathbf{L}_1 = (0, -\rho a, 1) \\ \lambda_2 = u &\rightarrow \mathbf{L}_2 = (-a^2, 0, 1) \\ \lambda_3 = u + a &\rightarrow \mathbf{L}_3 = (0, \rho a, 1) \end{aligned}$$

The matrix \mathbf{L} has the form

$$\mathbf{L} = \begin{pmatrix} 0 & -\rho a & 1 \\ -a^2 & 0 & 1 \\ 0 & \rho a & 1 \end{pmatrix} \quad (6.36)$$

and $dV = \mathbf{L}dW$ gives the result:

$$dV = \begin{pmatrix} 0 & -\rho a & 1 \\ -a^2 & 0 & 1 \\ 0 & \rho a & 1 \end{pmatrix} \begin{pmatrix} d\rho \\ du \\ dp \end{pmatrix} = \begin{pmatrix} -\rho a dJ^- \\ \frac{p}{c_v} dS \\ \rho a dJ^+ \end{pmatrix} \quad (6.37)$$

Observe that for slightly different normalisation of the left eigenvectors, i.e. $\tilde{\mathbf{L}}_1 = -\frac{1}{\rho a} \mathbf{L}_1$, $\tilde{\mathbf{L}}_2 = \frac{c_v}{p} \mathbf{L}_2$ and $\tilde{\mathbf{L}}_3 = \frac{1}{\rho a} \mathbf{L}_3$ will yield the previously defined state variables J^+ and J^- directly. The left eigenvector method is a powerful tool that enables us to find directly the new state variables in the diagonalized formulation. So let us apply this technique now in the case of a two dimensional unsteady flow.

Diagonalization of the 2D flow equations Unsteady 2D inviscid and non-heat conducting adiabatic flow is governed by the vector equation

$$W_t + \mathbf{A}(W)W_x + \mathbf{B}(W)W_y = 0 \quad (6.38)$$

W is the state vector of primary variables $W = (\rho, u, v, p)$ and \mathbf{A} and \mathbf{B} are given by

$$\mathbf{A} = \begin{pmatrix} u & \rho & 0 & 0 \\ 0 & u & 0 & \frac{1}{\rho} \\ 0 & 0 & u & 0 \\ 0 & \rho a^2 & 0 & u \end{pmatrix}, \quad \mathbf{B} = \begin{pmatrix} v & 0 & \rho & 0 \\ 0 & v & 0 & 0 \\ 0 & 0 & v & \frac{1}{\rho} \\ 0 & 0 & \rho a^2 & v \end{pmatrix} \quad (6.39)$$

The objective is to find a transformation of variables $dV = \mathbf{L}dW$ such that the coefficient matrices in the transformed equation are both diagonalized. Substitute in (6.38) now

$$dW = \mathbf{L}^{-1}dV,$$

and multiply with \mathbf{L} ; this gives

$$V_t + \mathbf{L}\mathbf{A}\mathbf{L}^{-1}V_x + \mathbf{L}\mathbf{B}\mathbf{L}^{-1}V_y = 0 \quad (6.40)$$

From linear algebra we remember that \mathbf{A} and \mathbf{B} can be simultaneously diagonalized by the same transformation \mathbf{L} if \mathbf{A} and \mathbf{B} have the same eigenvectors. In that case \mathbf{A} and \mathbf{B} commute, ie $\mathbf{AB} = \mathbf{BA}$.

However from (6.39) where \mathbf{A} and \mathbf{B} are defined it is easily checked that \mathbf{A} and \mathbf{B} do not commute!

This disappointing but important result indicates that no set of equations of the form

$$\frac{\partial}{\partial t} V_i + \lambda_i \frac{\partial V_i}{\partial x} + \mu_i \frac{\partial V_i}{\partial y} = 0 \quad (6.41)$$

exists which is equivalent with the unsteady Euler equations.

Physical experience teaches us the well known fact that sound propagates in all directions. If (6.41) where true then sound would travel only in discrete directions indicated by the velocity vectors (λ_i, μ_i) . In reality there are no such directions; sound propagates omni-directionally.

6.3 Wave propagation in two-dimensional flow

Since we know from the previous paragraph that sound travels in all directions, let us study the behaviour of plane-wave solutions of the Euler-equations.

Assume in two dimensions that plane waves travel with velocity λ in a direction ℓ (having an angle θ with respect to the x -axis) through a fluid which itself moves with a velocity q in the direction s (having an angle φ with respect to the x -axis).

Decomposing q into its components along the x - and y -axis yields $u = q \cos \varphi$, $v = q \sin \varphi$, figure 6.1 shows this wave propagation set up.

The flow situation sketched in figure 6.1 is an unsteady wave phenomenon that has to be a solution of

$$\frac{\partial W}{\partial t} + \mathbf{A} \frac{\partial W}{\partial x} + \mathbf{B} \frac{\partial W}{\partial y} = 0 \quad (6.42)$$

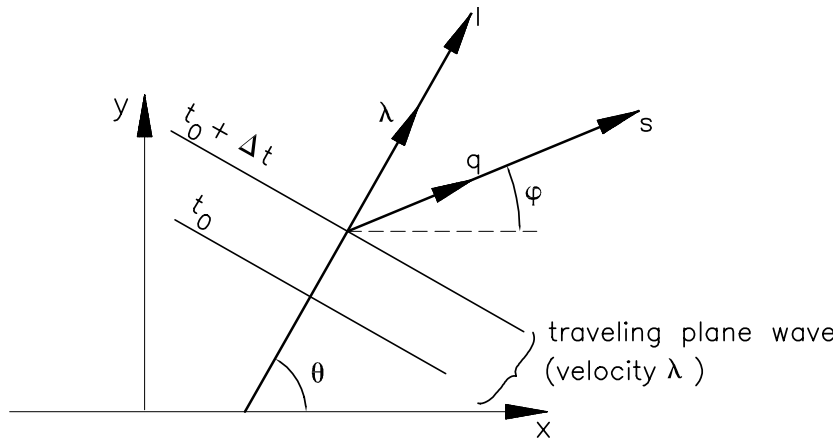


Figure 6.1: Travelling planar acoustic waves

The assumption of plane acoustic waves suggests solutions of the type:

$$W = W_0 f(x \cos \theta + y \sin \theta - \lambda(\theta)t) \quad (6.43)$$

where f is an arbitrary function of the argument $X = x \cos \theta + y \sin \theta - \lambda(\theta)t$. Equation (6.43) represents wave phenomena having W is constant along lines

$$x \cos \theta + y \sin \theta - \lambda(\theta)t = \text{const} \quad (6.44)$$

in the x,y -plane. These straight lines travel with the speed $\lambda(\theta)$ in the direction ℓ when time elapses.

In order to ensure that such waves can exist in the real world they have to satisfy equation (6.42). From equation (6.43) we obtain the partial derivation

$$W_t = -W_0 \frac{df}{dX} \lambda, \quad W_x = -W_0 \frac{df}{dX} \cos \theta, \quad W_y = -W_0 \frac{df}{dX} \sin \theta.$$

Substitution of these expressions in (6.42) yields

$$+W_0 \frac{df}{dX} \left(-\lambda \mathbf{I} + \underbrace{\mathbf{A} \cos \theta + \mathbf{B} \sin \theta}_{\mathbf{A}_\theta} \right) = 0$$

or

$$+W_0 \frac{df}{dX} (\mathbf{A}_\theta - \lambda \mathbf{I}) = 0 \quad (6.45)$$

To have non-trivial solutions of this homogeneous set of equations we need

$$\det(\mathbf{A}_\theta - \lambda \mathbf{I}) = 0 \quad (6.46)$$

or

$$\det \begin{pmatrix} q_\theta - \lambda & \rho \cos \theta & \rho \sin \theta & 0 \\ 0 & q_\theta - \lambda & 0 & \frac{1}{\rho} \cos \theta \\ 0 & 0 & q_\theta - \lambda & \frac{1}{\rho} \sin \theta \\ 0 & \rho a^2 \cos \theta & \rho a^2 \sin \theta & q_\theta - \lambda \end{pmatrix} = 0 \quad (6.47)$$

Where $q_\theta = u \cos \theta + v \sin \theta$ denotes just the projection of the flow speed q in the ℓ direction. Solving (6.47) for λ we obtain

$$(q_\theta - \lambda)^2 \left\{ (q_\theta - \lambda)^2 - a^2 \right\} = 0 \quad (6.48)$$

or

$$\begin{aligned} \lambda_1 &= q_\theta - a \\ \lambda_2 &= \lambda_3 = q_\theta \\ \lambda_4 &= q_\theta + a \end{aligned} \quad \left. \right\} \quad (6.49)$$

This result tells us that physical plane waves propagate either with the acoustic speed with respect to the flow (λ_1 and λ_4) or they propagate with the flow ($\lambda_2 = \lambda_3 = q_\theta$). The first two are just the forward and backward acoustic waves. The last two are convected with the flow; see also the graph in figure 6.2.

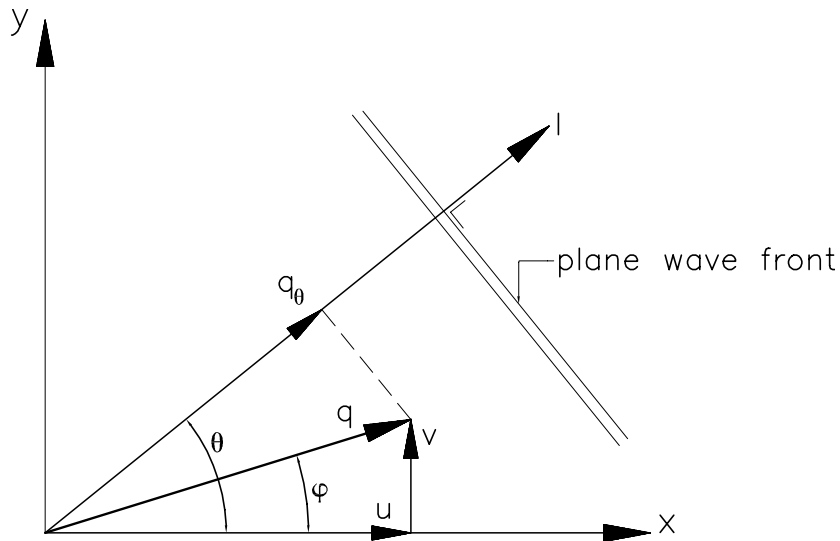


Figure 6.2: Propagation of wave front

Upstream and downstream moving waves (6.49) demonstrates clearly that the travelling speed λ of a plane wave is not just a constant but it depends on the direction e.g. θ in which the wave front travels. Let us study this dependancy, first for acoustic waves and then also for convecting waves.

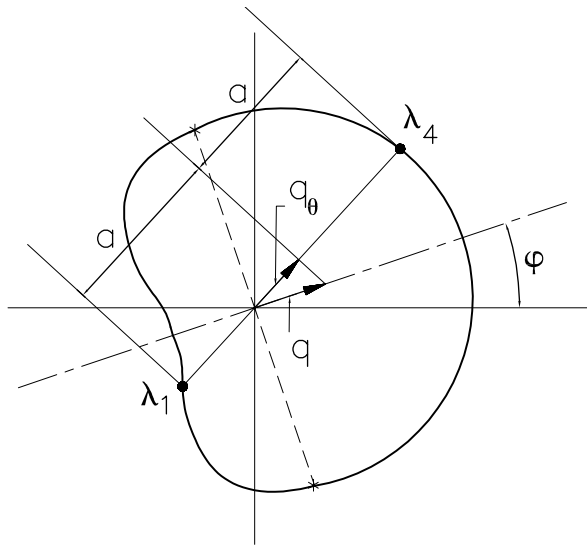
The travelling speed of acoustic signals is given by

$$\lambda_{1,4} = q_\theta \mp a = u \cos \theta + v \sin \theta \mp a$$

Introducing the flow angle φ by $u = q \cos \varphi$, $v = q \sin \varphi$ we found $\lambda_{1,4}$

$$\lambda_{1,4} = q \cos(\varphi - \theta) \mp a \quad (6.50)$$

Depending on the Mach number $M = \frac{q}{a}$, the polar graph $\lambda(\theta)$ shows three distinct graphs, one for $M < 1$, one for $M = 1$ and one for $M > 1$, see figure 6.3.

Figure 6.3: Graphs for $\lambda_{1,4}(\theta)$

The graph of (6.50) is known as the "cardiode", a figure that has the shape of a heart. From figure 6.3 we draw the following conclusions. Acoustic waves always travel with the speed of sound with respect to the fluid.

Since λ_1 and λ_4 are travelling speeds in the laboratory frame we see fast and slow moving waves and also forward and backward moving waves.

Consider figure 6.3 part *a* being the subsonic case. If l and q have the same direction e.g. $\theta = \varphi$ then $\lambda_1 = q - a$ and $\lambda_4 = q + a$. Since $q < a$ this implies $\lambda_1 < 0$ and $\lambda_4 > 0$; λ_1 represents the backward moving waves and λ_4 represents the forward running waves.

If l and q are perpendicular to each other e.g. $\theta = \varphi + \frac{\pi}{2}$ then (6.50) says $\lambda_4 = \mp a$, $\lambda_1 = \pm a$; both waves move transversally w.r.t. the fluid flow with the sound velocity a . Observe that this result is valid irrespective of the fact whether the flow is subsonic, sonic or supersonic.

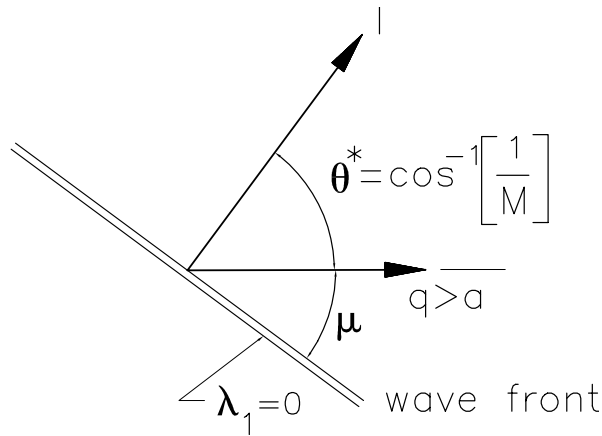
Take for simplicity $\varphi = 0$, then from (6.50) one obtains $\lambda_{1,4} = q \cos \theta \mp a$. Since λ_4 is always positive, it represents forward moving waves regardless the Mach number $M = \frac{q}{a}$. On the other hand λ_1 waves can be either forward moving waves ($q \cos \theta < a$) or backward running waves ($q \cos \theta > a$).

In subsonic flow $q < a$, λ_1 waves move backward but in supersonic flows $q > a$, the λ_1 wave can move backwards also if the propagation direction e.g. the angle θ exceeds a certain value θ^* . In case $\varphi = 0$ we have $\lambda_1 = q \cos \theta - a$. The critical value of θ appears at $\lambda_1 = 0$, so $\theta^* = \cos^{-1}(\frac{1}{M})$. In that case the wave front has an angle $\sin^{-1}(\frac{1}{M})$ with respect to the flow direction. However $\sin^{-1}(\frac{1}{M})$ is just the Mach angle being the angle of a Mach line with respect to the flow direction, see figure 6.4.

Since λ_1 is zero in this perpendicular case, it tells us that wave fronts inclined at the Mach angle μ do not propagate nor upstream nor downstream.

On the other hand if the propagation angle $|\theta| > \theta^*$ then $\lambda_1 < 0$, and λ_1 waves will move upstream (backwards) regardless of the fact that the flow is supersonic.

Based on this observation we may draw the very important conclusion that wave fronts inclined at angles smaller than μ with respect to the flow direction, will travel upstream in a supersonic

Figure 6.4: Wave front inclined at Mach angle $/mu$

flow, see figure 6.5.

A direct result of this phenomenon is the well-known effect that upstream travelling waves

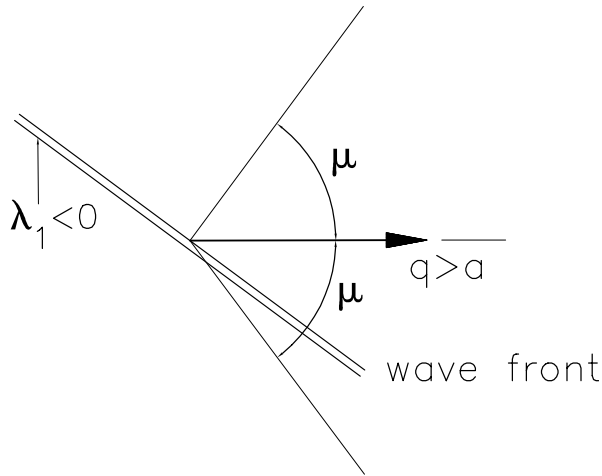


Figure 6.5: Wave front travelling upstream

generated in the wake of an airfoil at supercritical conditions do not necessarily build up a shock wave when entering the local supersonic zone because these waves can travel through this zone provided they are inclined at angles smaller than the Mach angle.

Finally let us consider the convecting (entropy) waves represented by $\lambda_2 = \lambda_3 = q_\theta$, using $u = q \cos \varphi$, $v = q \sin \varphi$ we find for $\lambda_{2,3}$

$$\lambda_{2,3} = q \cos(\theta - \varphi) \quad (6.51)$$

The polar graph of this equation is a circle with radius $(\frac{q}{2})$ having its center at $(\frac{u}{2}, \frac{v}{2})$; the graph is depicted in figure 6.6.

Figure 6.6 shows that the circle goes through the origin $u = 0, v = 0$.

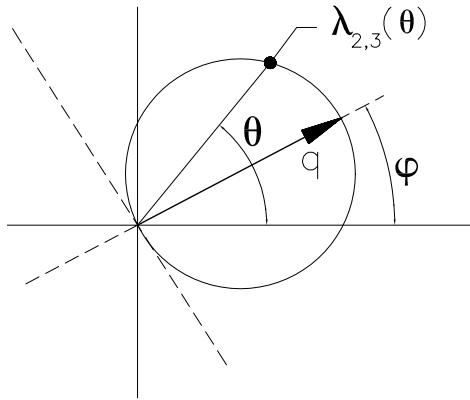


Figure 6.6: Graph $\lambda(\theta)$ for convecting waves and entropy waves

Hyperbolicity Because all plane waves admitted by (6.42) are real for any value of θ e.g. the propagation direction, this equation is truly hyperbolic and the initial value problem is well-posed.

Well-posedness means that the solution has to satisfy the requirements:

1. that a solution exists,
2. that the solution is unique and
3. that the solution depends continuously on the boundary conditions.

Enveloping waves It is a known fact that travelling waves can coalesce to form envelopes. A well-known example is a plane wave which can be regarded as the envelope of circular waves emitted by a row of point sources, figure 6.7. From the plane-wave speeds we can also derive the shape of wave fronts caused by these point disturbances.

According to Huygens' principle, the envelope of all possible plane waves initially going

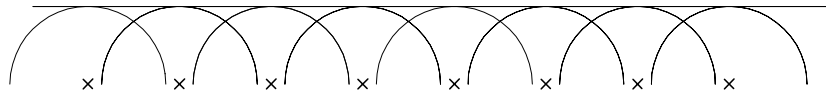


Figure 6.7: Plane wave as envelope

through one point, determine the wave front at later times.

Consider a point source where at $t = 0$ waves in all directions are present.

Let us first pay attention to entropy waves $\lambda_2 = \lambda_3 = q_\theta$. For reasons of simplicity we take $\varphi = 0$; in that case the polar graph $\lambda_{2,3}(\theta)$ is a circle with radius $\frac{q}{2}$ and centre $(\frac{q}{2})$. The entropy wave pattern at $t = 0$ is depicted in figure 6.8.

In particular the waves 1, 2, 3, 4 and 5 are shown all intersecting each other in the common point P . Where do we find these waves one unit of time later? Since we are dealing with entropy waves they are convected with the speed $\lambda(\theta) = q_\theta = q \cos \theta$.

So at $t = 1$ the wave front has travelled a distance $d(\theta) = \lambda(\theta) \times 1$; $d(\theta) = q \cos \theta$.

Consequently at $t = 1$ all waves now intersect each other at the point $Q(q, \theta)$, see figure 6.9.

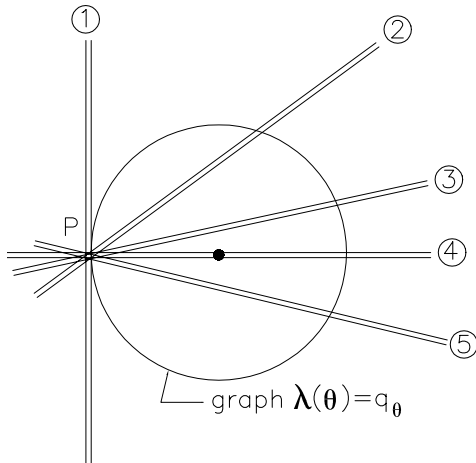


Figure 6.8: Entropy waves at $t = 0$, all intersecting at common point P in the 2D space

The envelope of all plane waves is the point Q ; it reflects the known property that entropy is constant along a particle path. Since $\varphi = 0$ the line PQ is a particle path so the entropy in P at $t = 0$ is equal to the entropy in Q at $t = 1$.

Consider again the point source P at $t = 0$; now the waves which are present in all directions are identified as acoustic waves. These waves travel with the speed $\lambda_{1,4} = q \cos \theta \mp a$; observe that we have again taken $\varphi = 0$. Where do we find these waves one unit of time later? As in the case of the entropy waves we can determine the travel distance of each particular wave front easily by the formula:

$$d^\mp = d_{1,4}(\theta) = q \cos \theta \mp a \quad (6.52)$$

Assume that q is constant in the whole domain then one can proof that the wave fronts build up the envelope:

$$(x - q)^2 + y^2 = a^2 \quad (6.53)$$

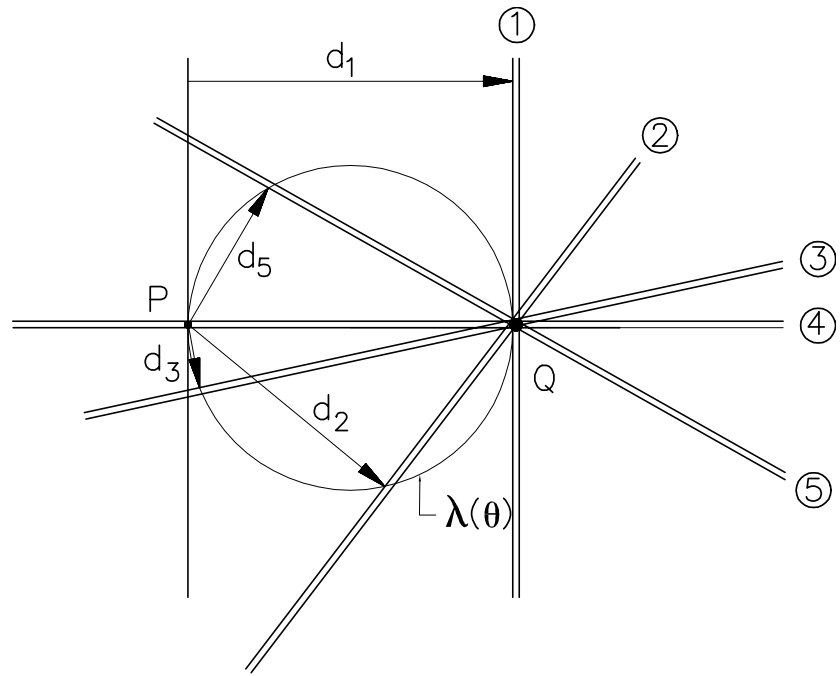
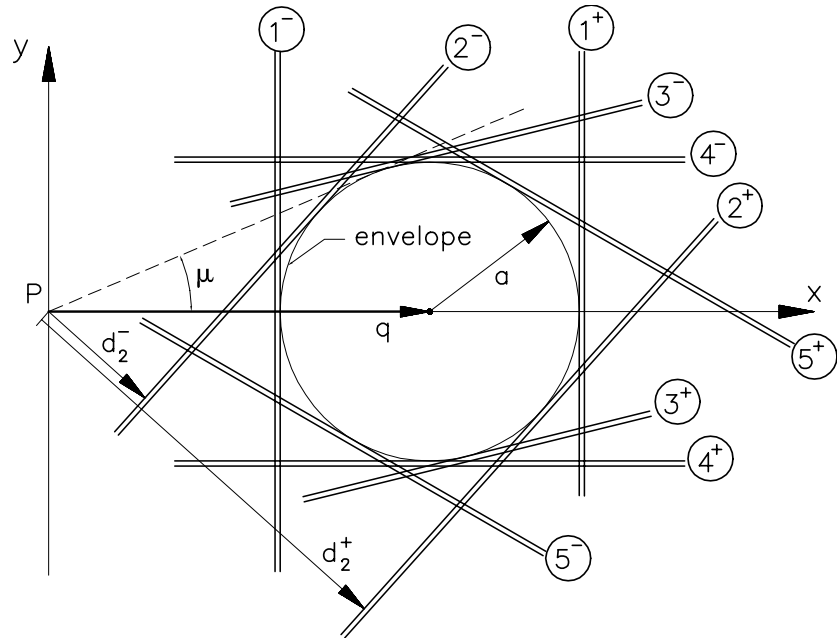
being a circle with radius a and centered at the point $x = q$, $y = 0$.

The proof is left as a homework problem!

Figure 6.10 shows the enveloping wave fronts for the supersonic case $q > a$.

The slow moving waves are indicated with the superscript "-", the fast moving waves carry the superscript "+". The tangent of the circular envelope going through the source point P makes the angle $\mu = \sin^{-1} \left(\frac{a}{q} \right)$ with the flow direction. It is the well known Mach angle. Therefore the envelope that is formed by all planar waves emanating from the point source P (at $t = 0$) is nothing else then the location onto sound is propagated at time $t = 1$. It is the response of the fluid to the point disturbance at P .

Determination of envelopes To determine the geometrical shape of an envelope of 2D plane waves, consider two neighbouring plane wave fronts at time level t . Assume a wave front L_1 that travels with speed $\lambda(\theta)$ in the direction θ ; at time t its position is represented by the

Figure 6.9: Individual entropy wave fronts at $t = 1$ Figure 6.10: Individual acoustic waves at $t = 1$, supersonic main flow $q > a$

graph:

$$L_1 : \quad x \cos \theta + y \sin \theta = \lambda t \quad (6.54)$$

Let wave front L_2 have a slightly different speed $\lambda + d\lambda$ and a slightly different propagation direction $\theta + d\theta$. At time t its position is represented by:

$$L_1 : \quad x \cos(\theta + d\theta) + y \sin(\theta + d\theta) = (\lambda + d\lambda)t \quad (6.55)$$

The intersection point (x_I, y_I) of L_1 and L_2 can be obtained by solving the following two equations:

$$\begin{aligned} x_I \cos \theta + y_I \sin \theta &= \lambda \\ -x_I \sin \theta + y_I \cos \theta &= \frac{d\lambda}{d\theta} = \lambda' \end{aligned} \quad \left. \right\} \quad (6.56)$$

The latter is obtained if (6.54) is subtracted from (6.55) and writing $\cos(\theta + d\theta) = \cos \theta - d\theta \sin \theta$, $\sin(\theta + d\theta) = \sin \theta + d\theta \cos \theta$.

The solution of (6.56) may be written in the vector/matrix form

$$\begin{pmatrix} x_I \\ y_I \end{pmatrix} = \begin{pmatrix} \cos \theta & -\sin \theta \\ \sin \theta & \cos \theta \end{pmatrix} \begin{pmatrix} \lambda(\theta) \\ \lambda'(\theta) \end{pmatrix} \quad (6.57)$$

This is the equation for the wave front envelope.

Another way of finding the point response is to look at the group speed of the plane waves; for this purpose we write the plane wave information as a dispersion relation:

$$\bar{\omega} = \lambda(\theta)\bar{k},$$

here k is the unit vector in the propagation direction (see figure 6.11). $\lambda(\theta)$ is the "phase speed":

$$\lambda(\theta) = \frac{|\omega|}{|k|} = \frac{\omega}{k}$$

To get the "group speed" in polar coordinates take the derivatives

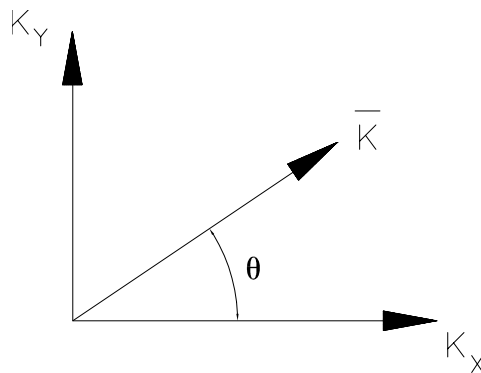


Figure 6.11: k in propagation direction

$$\begin{aligned} v_{g_k} &= \frac{\partial \omega}{\partial k} = \lambda(\theta) \\ v_{g_\theta} &= \frac{1}{k} \frac{\partial \omega}{\partial \theta} = \frac{\partial \lambda}{\partial \theta} = \lambda'(\theta) \end{aligned} \quad (6.58)$$

In Cartesian coordinates:

$$\begin{pmatrix} v_{gx} \\ v_{gy} \end{pmatrix} = \begin{pmatrix} \cos \theta & -\sin \theta \\ \sin \theta & \cos \theta \end{pmatrix} \begin{pmatrix} \lambda(\theta) \\ \lambda'(\theta) \end{pmatrix} \quad (6.59)$$

This is exactly the same formula derived earlier for the wave front. Both procedures are equivalent.

Chapter 7

Steady Two-Dimensional Flow

7.1 Characteristic directions

In chapter 6 we attempted to diagonalize the vector equation:

$$W_t + \mathbf{A}W_x + \mathbf{B}W_y = 0, \quad (7.1)$$

in order to find the characteristic equations equivalent to the unsteady Euler equations; in (7.1) W represents the state vector $W = (\rho, u, v, p)^T$. Unfortunately it turned out that diagonalization was impossible, because of the matrices \mathbf{A} and \mathbf{B} did not commute, e.g. $\mathbf{AB} \neq \mathbf{BA}$.

Now we aim less ambitiously to diagonalize the steady Euler equations, (6.2);

$$u \frac{\partial \rho}{\partial x} + v \frac{\partial \rho}{\partial y} + \rho \frac{\partial u}{\partial x} + \rho \frac{\partial v}{\partial y} = 0, \quad (7.2)$$

$$\rho u \frac{\partial u}{\partial x} + \rho v \frac{\partial u}{\partial y} + \frac{\partial p}{\partial x} = 0, \quad (7.3)$$

$$\rho u \frac{\partial v}{\partial x} + \rho v \frac{\partial v}{\partial y} + \frac{\partial p}{\partial y} = 0, \quad (7.4)$$

$$u \frac{\partial H}{\partial x} + v \frac{\partial H}{\partial y} = 0. \quad (7.5)$$

The last equation is a direct consequence of adiabatic flow and tells that the total enthalpy H is constant on a streamline. Another consequence of the adiabatic flow assumption is that also the entropy is constant along a streamline.

Proof

By definition, the total enthalpy H may be written as

$$H = e + \frac{p}{\rho} + \frac{1}{2}q^2. \quad (7.6)$$

Inserting this into the energy equation (7.5) yields:

$$\frac{\gamma}{\gamma-1}u \left(\frac{p_x}{\rho} - \frac{p}{\rho^2}\rho_x \right) + \frac{\gamma}{\gamma-1}v \left(\frac{p_y}{\rho} - \frac{p}{\rho^2}\rho_y \right) + uqq_x + vqq_y = 0, \quad (7.7)$$

using the momentum equations (7.3) and (7.4):

$$uqq_x + vqq_y = u(uu_x + vv_x) + v(uu_y + vv_y) = -\frac{u}{\rho}p_x - \frac{v}{\rho}p_y$$

Inserting in equation (7.1) and rearranging the terms:

$$u\left(\frac{p_x}{p} - \gamma\frac{\rho_x}{\rho}\right) + v\left(\frac{p_y}{p} - \gamma\frac{\rho_y}{\rho}\right) = 0. \quad (7.8)$$

using $ds = c_v \left(\frac{dp}{p} - \gamma \frac{d\rho}{\rho} \right)$ we obtain from (7.8) the result,

$$u\frac{\partial s}{\partial x} + v\frac{\partial s}{\partial y} = 0. \quad (7.9)$$

telling us that the entropy s is constant along a streamline. \square

Since this result is obtained from the energy equation and the momentum equations it implies that one of them, e.g. the y -momentum equation can be replaced by the entropy equation to keep a closed system.

In order to work with a system that is as simple as possible we continue with the following system:

$$\begin{aligned} u\rho_x + \rho u_x + v\rho_y + \rho v_y &= 0, \\ uu_x + vu_y + \frac{1}{\rho}p_x &= 0, \\ us_x + vs_y &= 0, \\ uH_x + vH_y &= 0. \end{aligned} \quad (7.10)$$

Let us now choose as primary variables the two velocity components u and v and the thermodynamic variables s (entropy) and H (enthalpy) and introduce the new state vector : $W = (u, v, s, H)^T$.

So we have to get rid of the ρ - and p derivatives and try to express them in derivatives of W . From the definition of H (7.6) and s there follows:

$$dH = \frac{\gamma}{\gamma-1} \left(\frac{dp}{\rho} - \frac{p}{\rho^2} d\rho \right) + q dq, \quad (7.11)$$

$$\frac{ds}{c_v} = \frac{dp}{p} - \gamma \frac{d\rho}{\rho} \quad (7.12)$$

From equations (7.11) and (7.12) $d\rho$ and dp can be solved in terms of dH and dq :

$$\frac{d\rho}{\rho} = \frac{-q dq}{a^2} - \frac{d\bar{s}}{\gamma-1} + \frac{dH}{a^2} \quad (7.13)$$

$$\frac{dp}{\rho} = -q dq - \frac{p}{\rho(\gamma-1)} d\bar{s} + dH \quad (7.14)$$

where $d\bar{s} = \frac{ds}{c_v}$.

Observe that equation (7.14) implies the well known result that along a streamline $dp + \rho q dq =$

0. Let the pressure- and density derivatives in (7.10) be expressed in terms of velocity-, entropy- and total enthalpy derivatives then the following system is obtained:

$$\mathbf{A}W_x + \mathbf{B}W_y = 0, \quad (7.15)$$

with

$$\mathbf{A} = \begin{pmatrix} 1 - \frac{u^2}{a^2} & -\frac{uv}{a^2} & -\frac{u}{\gamma-1} & \frac{u}{a^2} \\ 0 & -v & -\frac{a^2}{\gamma(\gamma-1)} & 1 \\ 0 & 0 & u & 0 \\ 0 & 0 & 0 & u \end{pmatrix}, \quad (7.16)$$

$$\mathbf{B} = \begin{pmatrix} -\frac{uv}{a^2} & 1 - \frac{v^2}{a^2} & -\frac{v}{\gamma-1} & \frac{v}{a^2} \\ v & 0 & 0 & 0 \\ 0 & 0 & v & 0 \\ 0 & 0 & 0 & v \end{pmatrix}. \quad (7.17)$$

and W is the state vector $W = (u, v, d\bar{s}, H)^T$. Let us now diagonalize (7.15). Assume \mathbf{A} is not-singular, e.g. \mathbf{A}^{-1} exists then

$$W_x + \mathbf{A}^{-1}\mathbf{B}W_y = 0. \quad (7.18)$$

This equation looks very similar to the unsteady 1-D equations, with x playing the role of time and y playing the role of the space coordinate.

If we want to take advantage of this form we must be sure that x is "time like" and y is "space like", ("space like" and "time like" will be explained in paragraph 7.2).

For the moment we assume that x and y play their intended roles so that the well-known unsteady 1-D analysis is applicable. The objective is to find a transformation of variables $dV = \mathbf{L}dW$ such that equation (7.18) is transformed in the form

$$V_x + \mathbf{\Lambda}V_y = 0. \quad (7.19)$$

where $\mathbf{\Lambda}$ is the diagonal matrix. Get the eigenvalues of $\mathbf{A}^{-1}\mathbf{B}$ from $\det(\mathbf{A}^{-1}\mathbf{B} - \lambda\mathbf{I}) = \det(\mathbf{A}^{-1}(\mathbf{B} - \lambda\mathbf{A})) = 0$. Since \mathbf{A}^{-1} is not-singular this reduces to

$$\det(\mathbf{B} - \lambda\mathbf{A}) \quad (7.20)$$

or,

$$\det \begin{pmatrix} -uv - \lambda(a^2 - v^2) & a^2 - v^2 + \lambda uv & \frac{a^2}{\gamma-1}(-v + \lambda u) & v - \lambda u \\ v & \lambda v & \frac{\lambda}{\gamma} \frac{a^2}{\gamma-1} & -\gamma \\ 0 & 0 & v - \lambda u & 0 \\ 0 & 0 & 0 & v - \lambda u \end{pmatrix} = 0,$$

or,

$$(v - \lambda u)^2 \left\{ -\lambda v \left(\lambda + \frac{u}{a^2} (v - \lambda u) \right) - v \left(\frac{v}{a^2} (\lambda u - v) + 1 \right) \right\} = 0 \quad (7.21)$$

The eigenvalues of $\mathbf{A}^{-1}\mathbf{B}$ are:

$$\lambda_{1,4} = \frac{uv \mp a^2 \sqrt{M^2 - 1}}{u^2 - a^2} \quad (7.22)$$

$$\lambda_{2,3} = \frac{v}{u} = \tan \varphi \quad (7.23)$$

where M is the Mach number: $M = \frac{\sqrt{u^2+v^2}}{a}$.

All the eigenvalues are dimensionless, they represent certain directions in the x,y plane. The eigenvalues $\lambda_{2,3}$ indicate the local flow direction, the eigenvalues $\lambda_{1,4}$ indicate two directions of steady acoustic waves.

$$\lambda_{1,4} = \tan(\varphi \mp \mu) \quad (7.24)$$

where μ is the Mach angle:

$$\sin \mu = \frac{1}{M}, \quad \tan \mu = \frac{1}{\sqrt{M^2 - 1}}$$

The angle μ represents the directions of the Mach lines, e.g. the wave fronts created by an infinitely small pointed obstacle in supersonic flow or those created by a ramp having an infinitely small ramp angle, see figure 7.1.

The angle μ is real only for $M \geq 1$. For $M > 1$, λ_1 and λ_4 represent two different directions;

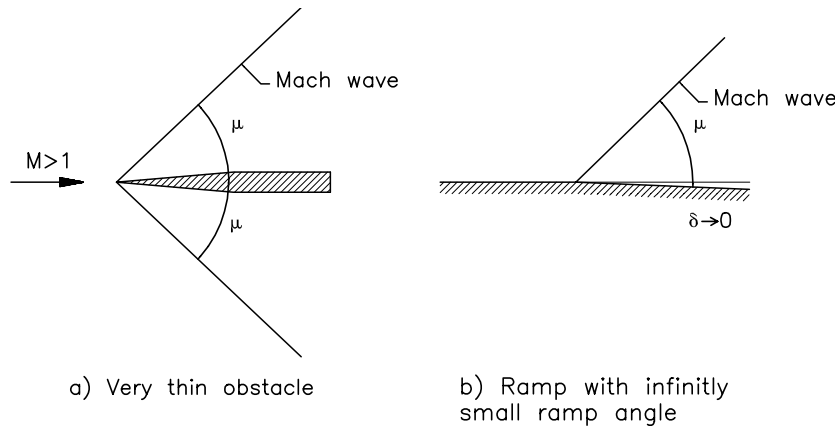


Figure 7.1: Mach lines

for $M = 1$, $\lambda_1 = \lambda_4$ and the directions are parallel. The directions $\lambda_1 = \tan(\varphi - \mu)$, $\lambda_4 = \tan(\varphi + \mu)$ are characteristic directions ; λ_1 representing the direction of the Γ^- characteristics and λ_4 representing the direction of the Γ^+ characteristics. In a supersonic point $P(x, y)$ in the flow one can always draw the fundamental picture shown in figure 7.2.

The flow direction bisects the angle between the two characteristics Γ^- and Γ^+ .

7.2 "Time-like" and "space-like"

For supersonic flow the characteristic directions are real. Unfortunately this does not guarantee that equation (7.6) is the proper form to use; if x is not "time-like" there is no advantage in writing the equation this way. If Γ^+ and/or Γ^- are not pointing downstream the form of (7.6) has no special preference.

To understand what is meant consider the domain of influence (D.O.I.) of a point P in the x,y -plane, as shown in figure 7.3.

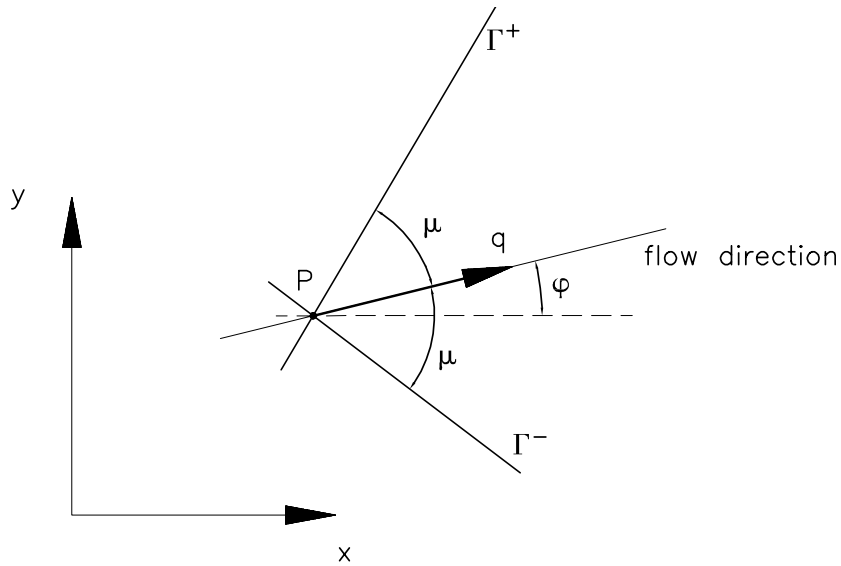


Figure 7.2: Characteristic directions in 2D supersonic flow

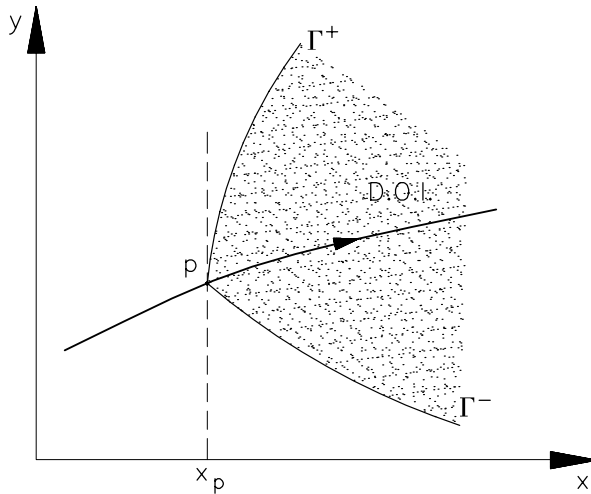


Figure 7.3: Domain of influence

Assume that λ_1 and λ_4 are such that Γ^+ and Γ^- point downstream. Then also the D.O.I. of P points downstream. So we can specify initial values: W , e.g. at $x_p = \text{constant}$ and the solution follows by marching (in space) downstream.

For example the solution at $x = x_p + \Delta x$ can readily be obtained from the formulation $W_x + \mathbf{A}^{-1}\mathbf{B}W_y = 0$. Observe that x acts like a "time-like" parameter and y acts as the "space-like" parameter.

However if one of the characteristic directions points upstream we have not the possibility nor the freedom to specify initial values at x_p is constant and to march downstream (in positive x -direction) to find the solution that satisfies these initial values. The problem is that the initial value line lies partly in the D.O.I. of point P . Figure 7.4 shows this situation in general

and illustrates it with the example of a ramp flow where the ramp angle δ and Mach angle μ_2 are such that $\delta + \mu_2 > \frac{\pi}{2}$.

When there are Mach lines travelling backwards, e.g. Γ^+ in figure 7.4, then the x coordinate

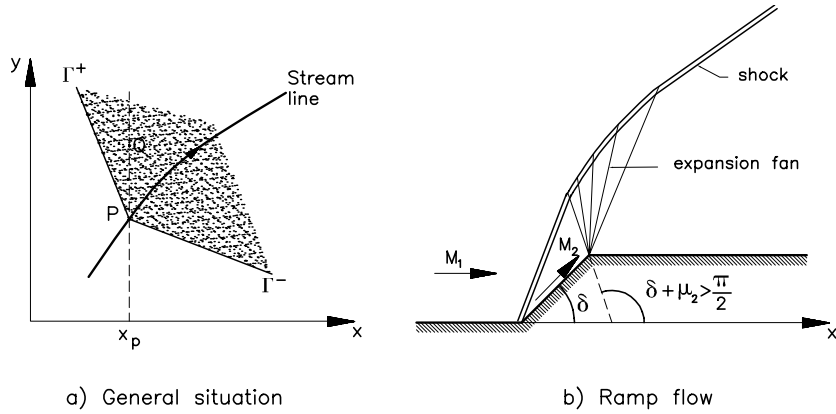


Figure 7.4: Violation of the 'time-like' character of the x coordinate

cannot be a "time-like" parameter because points on $x = x_p$ above P are in the domain of influence of P . So it is not possible to specify initial conditions in P and Q independently. For a coordinate line to be "space-like", it must run nowhere through the domain of influence of any of its own points.

The possibility of Mach lines travelling backwards is nothing else than a projection effect. It can be avoided by changing from the (x, y) -coordinate system to flow aligned coordinates (s, n) ; s being a coordinate along the streamlines and n perpendicular to them, see figure 7.5. From this definition s is always "time-like" and n is always "space-like".

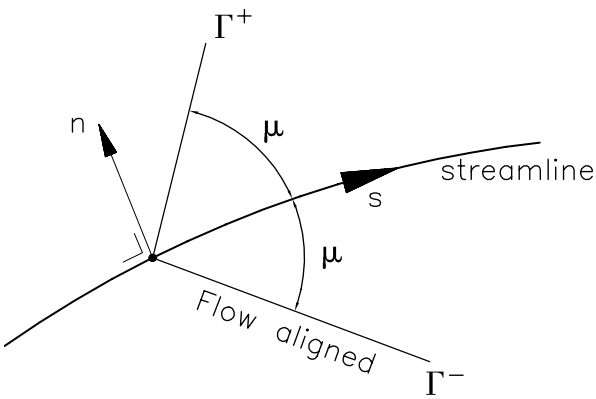


Figure 7.5: Flow aligned coordinates

7.3 Equations in flow aligned coordinates

Take the coordinates (s, n) from:

$$s = x \cos \varphi + y \sin \varphi, \quad (7.25)$$

$$n = -x \sin \varphi + y \cos \varphi, \quad (7.26)$$

where φ is the local flow direction, see figure 7.6. The transformation from (x, y) to (s, n) is a rotation with angle φ .

The partial derivatives $\frac{\partial}{\partial s}$ and $\frac{\partial}{\partial n}$ follow from (7.25) as

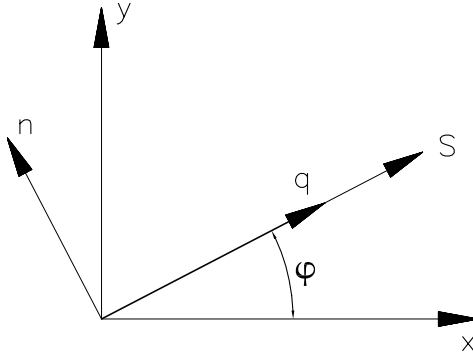


Figure 7.6: Local rotation from (x, y) to (s, n)

$$\frac{\partial}{\partial s} = \cos \varphi \frac{\partial}{\partial x} + \sin \varphi \frac{\partial}{\partial y}, \quad (7.27)$$

$$\frac{\partial}{\partial n} = -\sin \varphi \frac{\partial}{\partial x} + \cos \varphi \frac{\partial}{\partial y}. \quad (7.28)$$

From (7.27) we can also obtain

$$\frac{\partial}{\partial x} = \cos \varphi \frac{\partial}{\partial s} - \sin \varphi \frac{\partial}{\partial n}, \quad (7.29)$$

$$\frac{\partial}{\partial y} = \sin \varphi \frac{\partial}{\partial s} + \cos \varphi \frac{\partial}{\partial n}. \quad (7.30)$$

Let us use the above expressions to transform the flow equations (7.15) to the (s, n) reference frame; this yields

$$\mathbf{A}W_x + \mathbf{B}W_y = (\mathbf{A} \cos \varphi + \mathbf{B} \sin \varphi) W_s + (-\mathbf{A} \sin \varphi + \mathbf{B} \cos \varphi) W_n = 0,$$

or,

$$\mathbf{A}^*W_s + \mathbf{B}^*W_n = 0. \quad (7.31)$$

This system still uses u and v as the velocity variables but it is more natural to use $q = \sqrt{(u^2 + v^2)}$ and $\varphi = \tan^{-1}(\frac{v}{u})$.

To get rid of (u, v) in favour of (q, φ) we introduce the transformation

$$dW = \mathbf{Q}dZ, \quad (7.32)$$

with

$$W = (u, v, \bar{s}, H)^T \quad \text{and} \quad Z = (q, \varphi, \bar{s}, H)^T. \quad (7.33)$$

Z is the new state vector containing (q, φ) as the primary velocity variables. Using (7.32) into (7.31) the state vector Z satisfies:

$$\mathbf{A}^* \mathbf{Q} Z_s + \mathbf{B}^* \mathbf{Q} Z_n = 0. \quad (7.34)$$

The transformation matrix \mathbf{Q} has the form:

$$\mathbf{Q} = \begin{pmatrix} \cos \varphi & -q \sin \varphi & 0 & 0 \\ \sin \varphi & q \cos \varphi & 0 & 0 \\ 0 & 0 & 1 & 0 \\ 0 & 0 & 0 & 1 \end{pmatrix}. \quad (7.35)$$

If we define $\tilde{\mathbf{A}} = \mathbf{A}^* \mathbf{Q}$ and $\tilde{\mathbf{B}} = \mathbf{B}^* \mathbf{Q}$ equation (7.34) becomes

$$\tilde{\mathbf{A}} Z_s + \tilde{\mathbf{B}} Z_n = 0 \quad (7.36)$$

where

$$\tilde{\mathbf{A}} = \begin{pmatrix} 1 - M^2 & 0 & \frac{-q}{\gamma-1} & \frac{q}{a^2} \\ 0 & -q^2 \sin \varphi & -\frac{a^2 \cos \varphi}{\gamma(\gamma-1)} & \cos \varphi \\ 0 & 0 & q & 0 \\ 0 & 0 & 0 & q \end{pmatrix} \quad (7.37)$$

and

$$\tilde{\mathbf{B}} = \begin{pmatrix} 0 & q & 0 & 0 \\ q \sin \varphi & 0 & \frac{a^2 \sin \varphi}{\gamma(\gamma-1)} & -\sin \varphi \\ 0 & 0 & 0 & 0 \\ 0 & 0 & 0 & 0 \end{pmatrix}. \quad (7.38)$$

Equation (7.36) is the desired result. It represents the conservation laws in very compact form expressed in terms of flow aligned coordinates and using primary variables $Z = (q, \varphi, \bar{s}, H)^T$.

7.4 Characteristic equations, compatibility relations

Consider (7.36) and observe that the third and fourth row of matrix $\tilde{\mathbf{B}}$ contain only zeroes. The third and fourth equation of system (7.36) are therefore reduced to

$$q \bar{s}_s = 0, \quad q H_s = 0,$$

respectively. These equations tell us that entropy and total enthalpy are constant in s -direction (streamline). Using this result system (7.36) can be simplified into:

$$\tilde{\mathbf{A}} Z_s + \tilde{\mathbf{B}} Z_n = 0, \quad (7.39)$$

with

$$\tilde{\mathbf{A}} = \begin{pmatrix} 1 - M^2 & 0 & 0 & 0 \\ 0 & -q^2 & 0 & 0 \\ 0 & 0 & 1 & 0 \\ 0 & 0 & 0 & 1 \end{pmatrix}, \tilde{\mathbf{B}} = \begin{pmatrix} 0 & q & 0 & 0 \\ q & 0 & \frac{a^2}{\gamma(\gamma-1)} & -1 \\ 0 & 0 & 0 & 0 \\ 0 & 0 & 0 & 0 \end{pmatrix}.$$

Let us now apply the left-eigenvector methos to diagonalize (7.39) in order to find the characteristic equations. First we have to get the eigenvalues from:

$$\det(\tilde{\mathbf{B}} - \lambda \tilde{\mathbf{A}}) = 0,$$

or

$$\lambda^4(M^2 - 1) - \lambda^2 = 0, \quad (7.40)$$

yielding

$$\lambda_{1,4} = \left(\frac{dn}{ds} \right)_{\Gamma^\mp} = \mp \frac{1}{\sqrt{M^2 - 1}} = \mp \tan \mu \quad (7.41)$$

$$\lambda_{2,3} = \left(\frac{dn}{ds} \right)_{\Gamma^0} = 0 \quad (7.42)$$

The eigenvalues λ_1 and λ_4 represent the directions of the Mach lines in the (s, n) -plane. These directions will be referred to as the characteristic $\Gamma^- : \frac{ds}{dn} = -\tan \mu$ and $\Gamma^+ : \frac{ds}{dn} = +\tan \mu$. The eigenvalues λ_2 and λ_3 are both zero, they represent the direction of the flow.

Let us now get the left (row) eigenvectors L_i of $\tilde{\mathbf{A}}^{-1}\tilde{\mathbf{B}}$ by solving

$$L_i \tilde{\mathbf{A}}^{-1}\tilde{\mathbf{B}} = \lambda_i L_i \quad (7.43)$$

Matrix $\tilde{\mathbf{A}}^{-1}\tilde{\mathbf{B}}$ has the form:

$$\tilde{\mathbf{A}}^{-1}\tilde{\mathbf{B}} = \begin{pmatrix} 0 & \frac{q}{1-M^2} & 0 & 0 \\ \frac{-1}{q} & 0 & \frac{-1}{\gamma(\gamma-1)M^2} & \frac{1}{q^2} \\ 0 & 0 & 0 & 0 \\ 0 & 0 & 0 & 0 \end{pmatrix}. \quad (7.44)$$

The left eigenvectors satisfying (7.43) are,

$$\begin{aligned} \lambda_1 &= -\tan \mu \Rightarrow L_1 = \left(\sqrt{M^2 - 1}, q, \frac{q\sqrt{M^2 - 1}}{\gamma(\gamma-1)M^2}, \frac{-\sqrt{M^2 - 1}}{q} \right), \\ \lambda_2 &= 0 \Rightarrow L_2 = (0, 0, 1, 0), \\ \lambda_3 &= 0 \Rightarrow L_3 = (0, 0, 0, 1), \\ \lambda_4 &= +\tan \mu \Rightarrow L_4 = \left(-\sqrt{M^2 - 1}, q, \frac{-q\sqrt{M^2 - 1}}{\gamma(\gamma-1)M^2}, \frac{\sqrt{M^2 - 1}}{q} \right). \end{aligned}$$

Use these row vectors to form the matrix \mathbf{L}

$$\mathbf{L} = \begin{pmatrix} \sqrt{M^2 - 1} & q & \frac{q\sqrt{M^2 - 1}}{\gamma(\gamma-1)M^2} & \frac{-\sqrt{M^2 - 1}}{q} \\ 0 & 0 & 1 & 0 \\ 0 & 0 & 0 & 1 \\ -\sqrt{M^2 - 1} & q & \frac{-q\sqrt{M^2 - 1}}{\gamma(\gamma-1)M^2} & \frac{\sqrt{M^2 - 1}}{q} \end{pmatrix}. \quad (7.45)$$

The new state quantities now follow from

$$dV = \mathbf{L}dZ \quad (7.46)$$

resulting into

$$\begin{aligned} dV_1 &= \sqrt{M^2 - 1}dq + qd\varphi + \frac{q}{\gamma(\gamma-1)} \frac{\sqrt{M^2 - 1}}{M^2} d\bar{s} - \frac{\sqrt{M^2 - 1}}{q} dH, \\ dV_2 &= d\bar{s}, \\ dV_3 &= dH, \\ dV_4 &= -\sqrt{M^2 - 1}dq + qd\varphi - \frac{q}{\gamma(\gamma-1)} \frac{\sqrt{M^2 - 1}}{M^2} d\bar{s} + \frac{\sqrt{M^2 - 1}}{q} dH. \end{aligned} \quad (7.47)$$

The corresponding characteristic equations are

$$\frac{\partial V_i}{\partial s} + \lambda_i \frac{\partial V_i}{\partial n} = 0. \quad (7.48)$$

So we may conclude from (7.47) and (7.48) and using more convenient notations: V^- instead of V_1 and V^+ instead of V_4 :

$$\text{Along } \Gamma^\mp \text{ with } \left(\frac{dn}{ds}\right) = \mp \tan \mu : dV^\mp = 0,$$

$$\text{Along } \Gamma^0 \text{ with } \left(\frac{dn}{ds}\right) = 0 : dV_2 = V_3 = 0.$$

Equation (7.48) gives the compatibility relations along characteristics for the general case of a non-isentropic flow. Although the flow is assumed to be adiabatic, enthalpy gradients can appear, e.g. due to the fact that the enthalpy specified on the boundary is not uniform. In this general case dV^- and dV^+ cannot be brought in integral form, a direct consequence of the presence of entropy- and/or enthalpy variations.

Let us consider the variables dV^- and dV^+ in terms of the familiar variables q, φ, ρ and p . So we substitute from (7.11) and (7.12):

$$dH = \frac{\gamma}{\gamma - 1} \left(\frac{dp}{\rho} - \frac{p}{\rho^2} d\rho \right) + qdq = \frac{a^2}{\gamma - 1} \left(\frac{dp}{p} - \frac{d\rho}{\rho} \right) + qdq, \quad (7.49)$$

$$d\bar{s} = \frac{dp}{p} - \gamma \frac{d\rho}{\rho}. \quad (7.50)$$

Then we find:

$$dV^- = q \left(d\varphi - \frac{\sqrt{M^2 - 1}}{\gamma M^2} \frac{dp}{p} \right), \quad (7.51)$$

$$dV^+ = q \left(d\varphi + \frac{\sqrt{M^2 - 1}}{\gamma M^2} \frac{dp}{p} \right). \quad (7.52)$$

Compatibility relations in the above form are still valid for the general case of adiabatic non-isentropic ($d\bar{s} \neq 0$) and non-isenthalpic ($dH \neq 0$).

Special case: Homentropic flow ($d\bar{s} = 0, dH = 0$).

In homentropic flow, entropy and total enthalpy are constant throughout the whole flow domain. In the special flowfields the compatibility relations: dV^- on Γ^- and dV^+ on Γ^+ can be simplified considerably. If $d\bar{s} = 0$, the expression for dH (7.49) yields $dH = \frac{dp}{\rho} + qdq$; thus in homentropic flow where we have in any direction $dH = 0$ it implies

$$dp = -\rho q dq \quad (7.53)$$

Therefore, after a suitable renormalisation of eigenvectors:

$$dV^\mp = \frac{\sqrt{M^2 - 1}}{q} dq \pm d\varphi. \quad (7.54)$$

The first term of the right hand side may be recognized as the differential of the Prandtl-Meyer function: $\nu(M)$

$$d\nu = \frac{\sqrt{M^2 - 1}}{q} dq, \quad (7.55)$$

ν is the Prandtl-Meyer angle defined as:

$$\nu(M) = \int_1^M \frac{\sqrt{M^2 - 1}}{q} dq = \sqrt{\frac{\gamma + 1}{\gamma - 1}} \tan^{-1} \sqrt{\frac{\gamma + 1}{\gamma - 1} (M^2 - 1)} - \tan^{-1} \sqrt{M^2 - 1}. \quad (7.56)$$

So the compatibility equations for homentropic flow can now be written as

$$dV^\mp = d\nu \pm d\varphi, \quad (7.57)$$

which can be integrated very easily resulting into

$$V^- = \nu + \varphi \text{ is constant along } \Gamma^- \text{ with slope } \frac{dy}{dx} = \tan(\varphi - \mu)$$

$$V^+ = \nu - \varphi \text{ is constant along } \Gamma^+ \text{ with slope } \frac{dy}{dx} = \tan(\varphi + \mu)$$

with V^- and V^+ being the invariants in homentropic flow.

In figure 7.2 we have presented a fundamental picture of the flow situation in and near an arbitrary supersonic point P .

Since we now have the conditions along characteristics Γ^\mp , this picture can be completed for homentropic flows as depicted in figure 7.7.

Example 1: Centered Prandtl-Meyer expansion A uniform supersonic flow having a Mach number $M_1 > 1$ is deflected abruptly over a turning angle δ such that the gas expands. At the turning point a Prandtl-Meyer expansion fan is centered and emanates from this point into the flow field. Upstream of the fan the flow is uniform with conditions $M = M_1$ and $\varphi_1 = 0$. Downstream of the fan the flow becomes uniform again; the conditions are $M = M_2$ and $\varphi = -\delta$ see figure 7.8.

The expansion fan is build up by Γ^+ characteristics; the first characteristic has an angle μ_1 with the upstream flow direction. The last characteristic has an angle μ_2 with respect to the downstream flow direction.

We aim to determine the flow conditions in domain ② and use characteristics theory. Consider

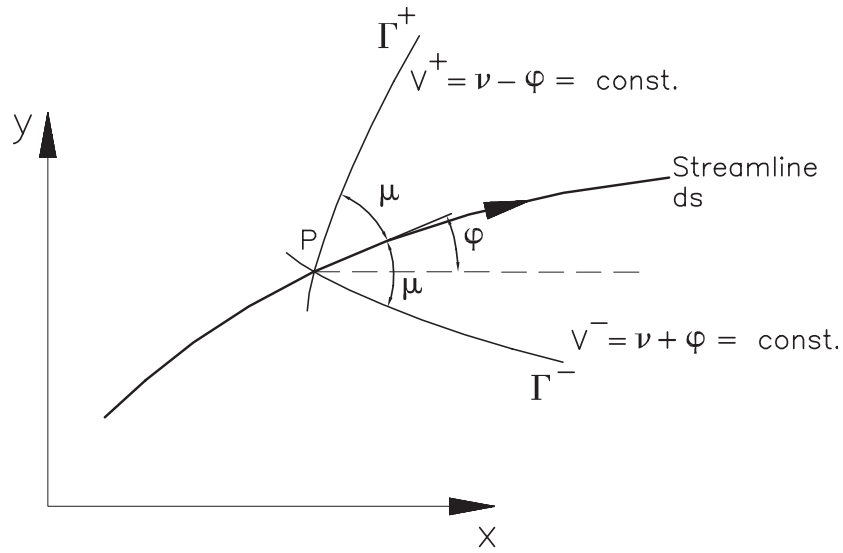


Figure 7.7: Flow properties in 2D supersonic flow; homentropic case

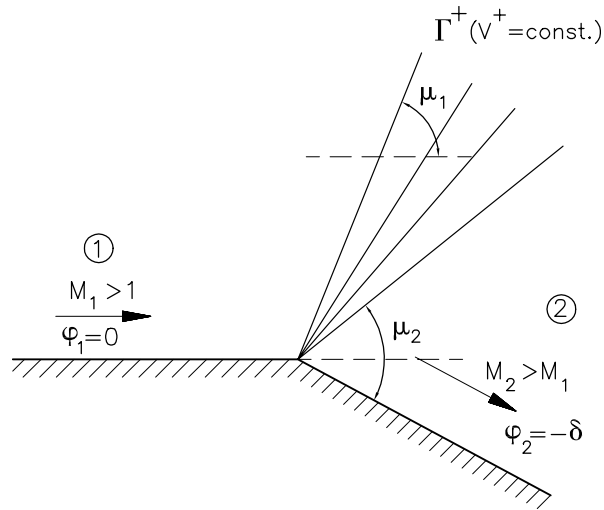


Figure 7.8: Prandtl-Meyer expansion flow

an arbitrary Γ^- -characteristic running from domain ① through the expansion fan into domain ②. Observe that on this characteristic we have $V^- = \nu_1 + \varphi_1 = \nu_2 + \varphi_2 = \text{constant}$. Since $\varphi_1 = 0$ and $\varphi_2 = -\delta$ there results:

$$\nu_2 = \nu_1 + \delta \quad (7.58)$$

The Prandtl-Meyer angle in domain ② is now found and the remaining flow conditions in this domain e.g. Mach number, temperature, pressure, density can be determined using isentropic relations.

The well-known relation,

$$\nu_2 = \nu_1 + \delta$$

finds his origin in the theory of characteristics!

Since all Γ^- -characteristics issue from the uniform domain ① it implies that the invariant $\nu + \varphi$ is a constant in the whole flow field. Thus the expansion wave is a simple wave and the Γ^+ -characteristics are straight lines. The proof is found in the next example.

Example 2: Simple waves Simple waves were already encountered in one-dimensional unsteady flows. They have the property that one of the Riemann invariants J^+ or J^- is uniform. In 2D steady flows also simple waves appear, if one of the invariants V^- or V^+ is uniform.

Let us discuss the simple wave flow that appears if a uniform flow is expanded along a partly curved wall as sketched in figure 7.9. Assume a uniform supersonic flow with Mach number M_1 which flows along the plane part (upstream of s).

Downstream of point S the wall bends away and the gas expands. Since all Γ^- -characteristics

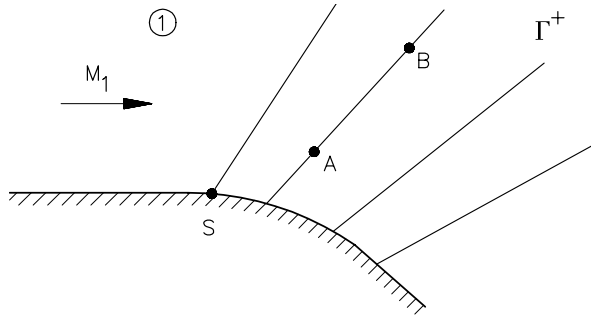


Figure 7.9: Simple wave flow

originate from the same uniform domain ①, V^- is constant throughout the flowfield. This implies

$$\nu_A + \varphi_A = \nu_B + \varphi_B,$$

for two arbitrary points A and B in the expansion region. If A and B are also taken on the same Γ^+ characteristic then the additional relation

$$\nu_A - \varphi_A = \nu_B - \varphi_B,$$

holds. Both relations are satisfied if

$$\nu_A = \nu_B \text{ and } \varphi_A = \varphi_B.$$

Thus along a Γ^+ -characteristic all flow variables are constant. This implies that also $\varphi + \mu$ is constant so that Γ^+ is a straight line. However Γ^- characteristics are curved but each Γ^-

characteristic intersects a particular Γ^+ characteristic at a constant angle. Of course this angle differs from Γ^+ characteristic to Γ^+ characteristic.

Non-simple regions occur if both invariants V^- and V^+ vary in the flow region. Analogous to the 1D unsteady case: uniform regions are bordered by simple waves and simple waves are bordered by either non-simple regions or uniform regions.

7.5 Method of Characteristics; M.O.C.

In 2D steady supersonic flow the characteristics are real curves in the flow domain. This enables the set up of a characteristic method. Consider a flow situation as sketched in figure 7.10 where the flow variables are given on the initial value line.

In each point, for example A and B , we know the slopes of the characteristics Γ^+ and Γ^- ,

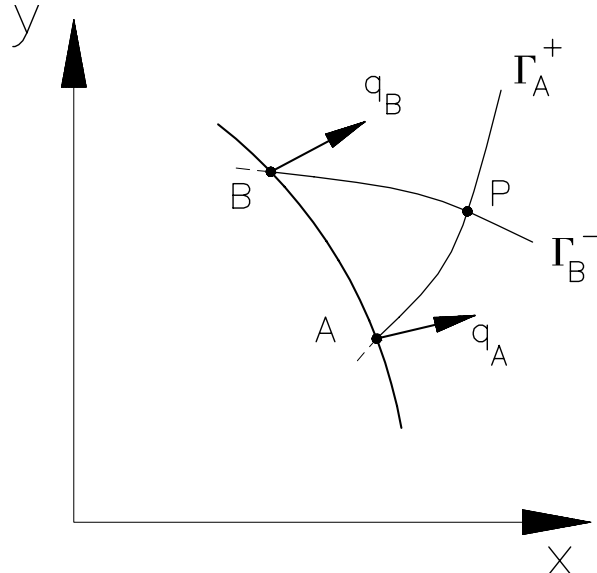


Figure 7.10: Constructing solution in P

the Mach number and the flow direction. Consider the Γ^+ -characteristic emanating from A and the Γ^- -characteristic emanating from B ; they intersect at point P . The solution in P is found by applying the compatibility relations : $V^- = \nu + \varphi = \text{constant}$ along Γ_B^- and $V^+ = \nu - \varphi = \text{constant}$ along Γ_A^+ . This yields two equations:

$$\begin{aligned} \nu_A - \varphi_A &= \nu_P - \varphi_P, \\ \nu_B + \varphi_B &= \nu_P + \varphi_P, \end{aligned}$$

for the unknowns ν_P and φ_P . The solution is

$$\left. \begin{aligned} \nu_P &= \frac{1}{2}(\nu_B + \nu_A) + \frac{1}{2}(\varphi_B - \varphi_A) \\ \varphi_P &= \frac{1}{2}(\varphi_B + \varphi_A) + \frac{1}{2}(\nu_B - \nu_A) \end{aligned} \right\} \quad (7.59)$$

The solution in P is exactly known and, without knowing the position of P in advance! The position of P can be determined most accurately afterwards.

Point	a	b	c	d	e	f	g	i	j	l
ν	10	10	10	10	12	12	12	14	14	16
φ	0	4	8	12	2	6	10	4	8	6

Table 7.1: ν and φ in 2D diffusor

To find P draw straight lines at average angles $\frac{1}{2}(\varphi_A + \mu_A + \varphi_P + \mu_P)$ and $\frac{1}{2}(\varphi_B - \mu_B + \varphi_B - \mu_B)$ through A and B respectively. Intersecting these lines gives P 's location approximately. The larger the distance between A and B the less accurate the position of the point P .

Using this method a set of points can be constructed on which the solution is known. This set of points forms a new initial value line from which the solution process can proceed. The M.O.C. is used in particular for analyzing supersonic windtunnel nozzles or to analyse supersonic jets for example produced by rocket engines.

Example 1: Radial flow in a 2D diffusor Consider a supersonic flow entering a two-dimensional conical diffusor having a certain diverging angle, say $\varphi = 12^\circ$.

The flow enters radially with a constant speed q_0 that corresponds to a Prandtl-Meyer angle $\nu_0 = 10$. The flow expands in the diffusor to higher Mach numbers.

The method of characteristics is appropriate to analyse the expanding flow regime. Assume that the initial value line is part of a circular arc on which $\nu = \nu_0 = 10$ and on which the flow angle φ ranges as $0^\circ \leq \varphi \leq 12^\circ$, see figure 7.11.

Assume points a, b, c and d on the initial value line with $\varphi_a = 0, \varphi_b = 4, \varphi_c = 8$ and $\varphi_d = 12^\circ$.

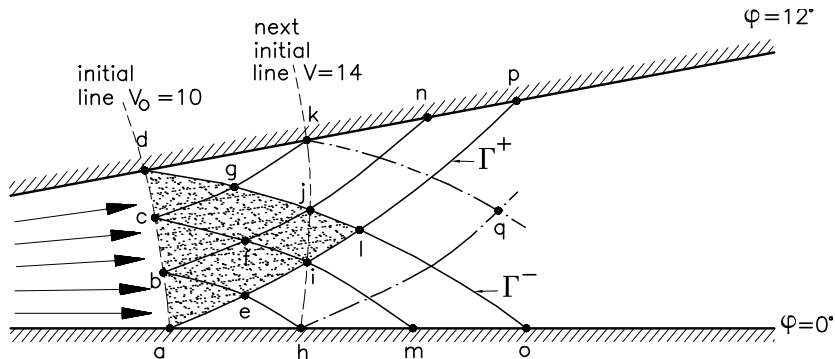


Figure 7.11: Radial flow in diffusor

Using M.O.C. the solution is constructed on all grid points in the characteristic triangle "adl". The results are assembled in table 7.5. But, how to proceed the solution beyond the characteristic triangle "adl"?

To find the solution in the points "h" or "k" we cannot use M.O.C. directly because of the value of one invariant is not known. However in "h" and "k" and also on all points lying on the diffusor walls the flow angle is known. In "h", $\varphi_h = 0^\circ$ and in "k", $\varphi_k = 12^\circ$. This enables us to find the solution in "h" to be $\nu_h = 14, \varphi_h = 0^\circ$ and in "k" to be $\nu_k = 14, \varphi_h = 12^\circ$.

Since "h" and "k" are now also known we have constructed a new initial value curve going

through the points "h", "i", "j" and "k", on this line the Prandtl-Meyer angle is constant: $\nu = 14$ and the flow angle varies from 0° to 12° .

The solution procedure can now be repeated to find the solution in the characteristic triangle "hkq". In this way the whole flow domain downstream of the diffusor can be determined.

Remember: although the solution values are exactly known, the positions of the grid points can only be calculated approximately.

Example 2: Under-expanded jet An under-expanded jet exits from a rocket nozzle. At the exit the flow is parallel ($\varphi = 0$) and has a constant Mach number M_{jet} . The jet exits into quiescent air having an ambient pressure p_a .

The pressure in the nozzle exit is assumed to be $p_e > p_a$ causing a further expansion of the jet when flowing downstream.

A sketch of this flow situation is depicted in figure 7.12. The method of characteristics may now be used to find the development of the jet outside the nozzle.

At the outer lip of the nozzle exit (point A) a centered expansion appears which reflects on

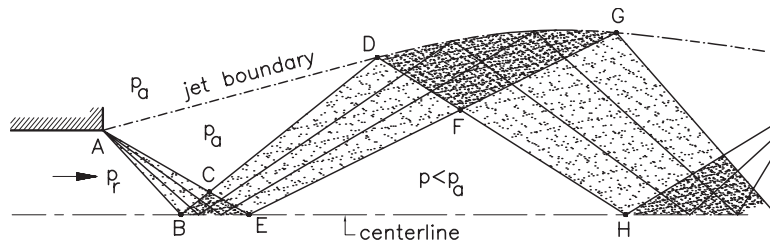


Figure 7.12: Under-expanded jet, $p_{exit} > p_{ambient}$

the opposite jet boundary as a compression wave. In the expansion regime characteristics diverge, in the compression part they converge to each other. Where converging characteristics start to intersect a shock wave will appear and the M.O.C. method breaks down. Consider those parts of the jet where no shocks have been formed yet. The flow is symmetric with respect to the centerline and therefore the discussion can be restricted to the upper part only. We observe several domains having different conditions. Domain ABC is a simple wave with straight Γ^- -characteristics. In domain BCE two simple waves interact and a non-simple region is present here. Domain ACD is uniform with a pressure that is equal to p_a . Domain CDEF is a simple wave with straight Γ^+ -characteristics.

Domain DFG is non-simple because both invariants V^+ and V^- vary. Domain EFH is uniform with a pressure lower than p_a . Domain FGHI is a simple wave with V^+ is uniform; the Γ^- -characteristics are straight. Domain GIJ is uniform with a pressure equal to p_a . In domain HIK two simple waves interact and a non-simple region is formed. Table 7.5 summarizes the typical conditions of each domain.

The jet boundary of the exhausting jet is a line of constant pressure: p_a . There appears a repeated pattern of divergence and convergence of the total jet area.

Well-posed problems (WPP's) When working with the method of characteristics one frequently encounters several so called well-posed problems (WPP's). A WPP is a problem

Domain	V^+	V^-	comment
ABC	u	v	simple wave
BCE	v	v	non-simple
ACD	u	u	uniform
CDEF	v	u	simple wave
DFG	v	v	non-simple
EFH	u	u	uniform
FGHI	u	v	simple wave
GIJ	u	u	uniform
HIK	v	v	non-simple

Table 7.2: Characteristics of exhausting jet, key: u: uniform, v: varies

regarding the solution of a differential equation that fulfils the requirements:

1. uniqueness of the solution,
2. existence of the solution and
3. solution depends continuously on the initial conditions.

The following three WPP's are very common.

WPP 1: Cauchy initial value problem Initial data are given on a non-characteristic curve AB .

The solution can be determined inside the characteristic quadrangle formed by the charac-

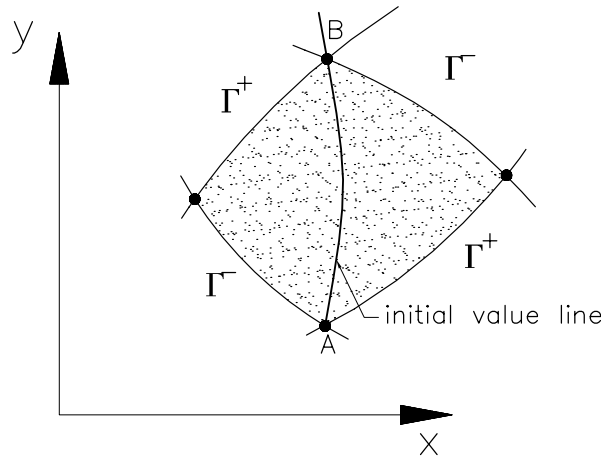


Figure 7.13: Cauchy problem

teristics: Γ^+ and Γ^- going through A and B .

WPP 2: Goursat problem Initial data are given on both characteristics: Γ^+ and Γ^- going through a single point A .

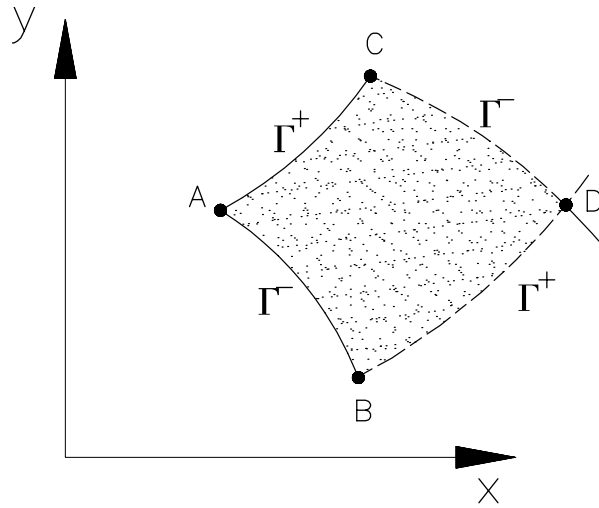


Figure 7.14: Goursat problem

On Γ^+ the data are specified from A to B . On Γ^- the data are specified from A to C . Now the solution can be determined in the characteristic quadrangle $ABCD$, CD is the Γ^- -characteristic emanating from C and BD is the Γ^+ -characteristic that issues from point B . Both characteristics intersect in D .

WPP 3: Combined initial value/boundary value problem In this problem initial data are specified along a characteristic curve AB : ν and φ are known on curve AB , see figure 7.15.

In addition boundary conditions e.g. ν or φ are specified on a non-characteristic curve AC . The solution can be determined in the triangle ABC formed by the characteristic Γ^+ through A and B , the characteristic Γ^- going through BC and the boundary AC . Take a point 1 on the Γ^+ -characteristic through AB close to A . In 1 the variables ν and φ are assumed to be known and consequently also the invariant V_1^- is known. Draw the Γ^- -characteristic through 1 which intersects the boundary curve in 2. Now we have $V_1^- = V_2^- = \nu_2 + \varphi_2$. Since ν_2 or φ_2 is known because of 2 lies on the boundary curve all conditions in 2 can now be determined. So if 2 is known then also V_2^+ and the characteristic direction $\varphi_2 + \mu_2$ is known. This enables us to calculate the Γ^+ -characteristic going through 2 which then acts as a new initial value line like AB . Now the whole calculation process can be repeated until the domain ABC is determined.

Observe that the determination of the radial flow in the diffusor (example 1 fig 7.11) is a combination of a **Cauchy** problem (domain *adl*), a **combined initial value/boundary value** problem (domain *alo* and *alp*) and a **Goursat** problem (domain *olp*).

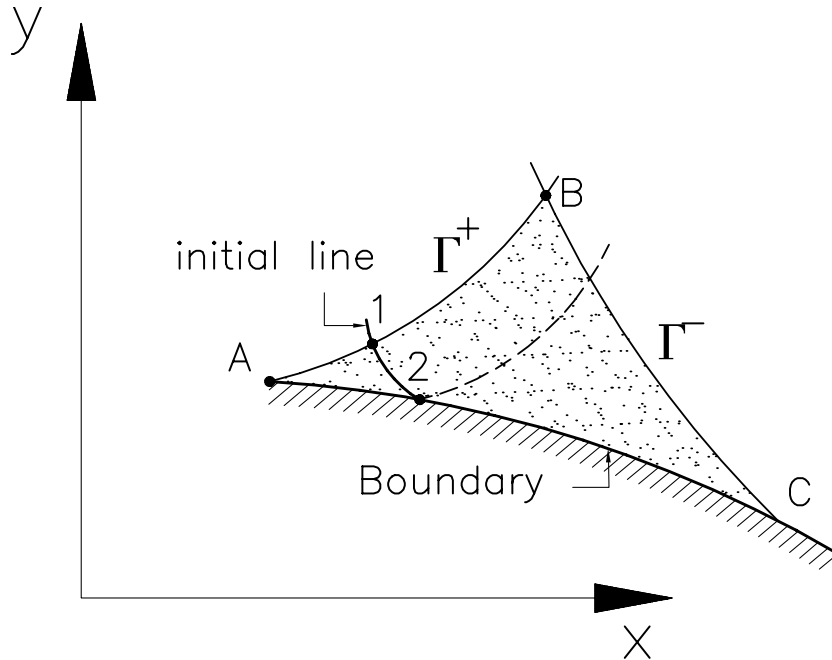


Figure 7.15: Combined IV/BV problem

7.6 Method of Waves; M.O.W.

7.6.1 Description of the method, simple waves.

In contrast to the M.O.C. which provides exact data of the flow variables e.g. ν and φ on grid points, the method of waves is essentially an approximate method that subdivides the flow domain in a great number of small regions having constant properties.

Where the M.O.C. is very suitable for analysis of properties of supersonic flowfields, the M.O.W. however is more favourite for design studies.

The key idea in the M.O.W. is the discretization of a continuous varying flow domain into domains having constant properties. To elucidate the method consider a simple wave that develops along a continuous curved contour.

In figure 7.16 a non-centered expanding simple wave flow is shown in subfigure *a* the wall is continuously curved, the Γ^+ characteristics are straight lines representing that the flow expands in down-stream direction. The flow properties are exactly described by the simple wave condition $\nu + \varphi = \text{constant}$ in the whole domain implying that on a particular Γ^+ characteristic ν is constant and φ is constant. Thus the Γ^+ characteristics issuing from the curved wall form a bundle of diverging straight lines representing an expanding flow.

Hence the flow properties in an arbitrary point follow by considering the Γ^+ characteristic going through this point. This Γ^+ characteristic intersects the boundary at P where the wall has a known inclination φ_p . The flow properties on that particular Γ^+ are then

$$\varphi(\Gamma_P^+) = \varphi_p, \quad \nu(\Gamma_P^+) = \text{const} - \varphi_p. \quad (7.60)$$

Equation (7.60) is the exact solution of the expanding flow as depicted in figure 7.16 part *a*. In the M.O.W. the continuous curved wall is replaced by the geometry shown in figure 7.16

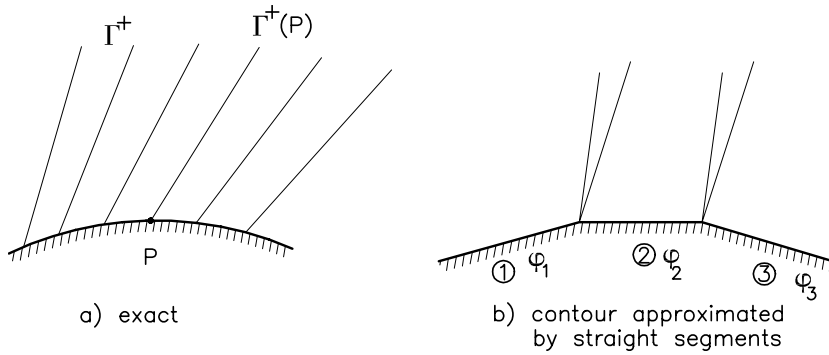


Figure 7.16: Non-centered expansion

part *b*. The wall is approximated by successive straight segments $1, 2, 3, \dots$ having constant direction angles $\varphi_1, \varphi_2, \varphi_3, \dots$ respectively. Here $\varphi_1 > \varphi_2 > \varphi_3 > \dots$. The difference in direction angle between two consecutive wall segments $\varphi_{i+1} - \varphi_i = \Delta\varphi_i$ may differ for different pairs of wall segments. However in many practical applications $\Delta\varphi_i$ is taken constant $\Delta\varphi < 0$ having an absolute value $|\Delta\varphi|$. Now consider the 'exact' flow along the approximate wall contour as depicted in figure 7.16 part *b*.

This flow is characterised by a collection of uniform domains separated by centered Prandtl-Meyer expansion fans. The flow conditions (speed, direction, pressure, etc.) in these uniform regions follow from Prandtl-Meyer theory. If $\Delta\varphi$ ($\Delta\varphi < 0$) is taken constant and the flow in region ① is assumed to be known then the solution along the segmented contour becomes

$$\begin{aligned}\varphi_2 &= \varphi_1 - |\Delta\varphi|, & \varphi_3 &= \varphi_1 - 2|\Delta\varphi| \\ \nu_2 &= \nu_1 + |\Delta\varphi|, & \nu_3 &= \nu_1 + 2|\Delta\varphi|\end{aligned}\tag{7.61}$$

If $\Delta\varphi$ is taken small (e.g. 0.01 rad.) then the Prandtl-Meyer fans are also small meaning that the angle between the first and the last characteristic of the fan is also small ($O(0.01 \text{ rad.})$). Therefore in the M.O.W. Prandtl-Meyer fans will be replaced by single straight lines being called a 'wave'.

The slope of a wave is determined as the average of the slopes of the first and the last characteristic.

For example the wave that separates the domains ① and ② has a slope $\tan \alpha_{12}$, with

$$\alpha_{12} = \frac{1}{2} (\varphi_1 + \mu_1 + \varphi_2 + \mu_2)\tag{7.62}$$

Notice that the waves are not characteristics; they just represent a (weak) Prandtl-Meyer fan. The difference between a characteristic and a wave is apparent in the case of uniform parallel flow with Mach number $M_\infty > 1$. This flow is supersonic so characteristics exist having a slope $\pm \tan \mu$ with respect to the flow direction.

However there are no waves here because the flow is uniform. So waves and characteristics are not identical but they are related. Therefore waves related to Γ^+ characteristics will be called C^+ waves and those related to Γ^- characteristics will be called C^- waves.

We conclude that in the method of waves the continuous expansion is discretized into a number of uniform regions bounded by waves across which the flow properties jump; see figure 7.17.

In order to develop the M.O.W. further, consider an isentropic compressing flow as this is

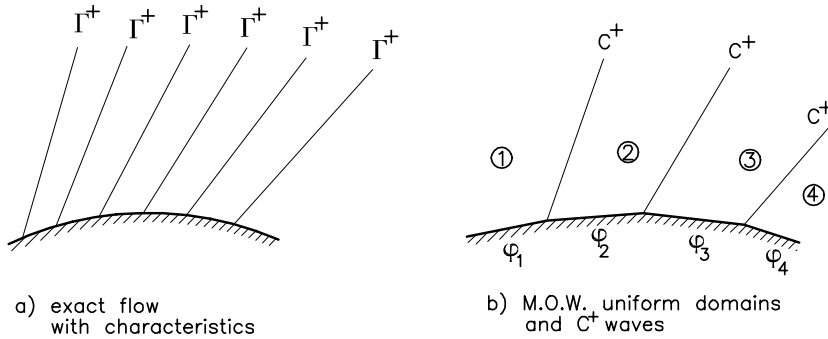


Figure 7.17: M.O.W. applied to a continuous expanding flow

generated by the curved boundary shown in figure 7.18. It presents the exact flow together with the representation in the M.O.W.

In the M.O.W. the treatment of the isentropic compression and the continuous expansion is

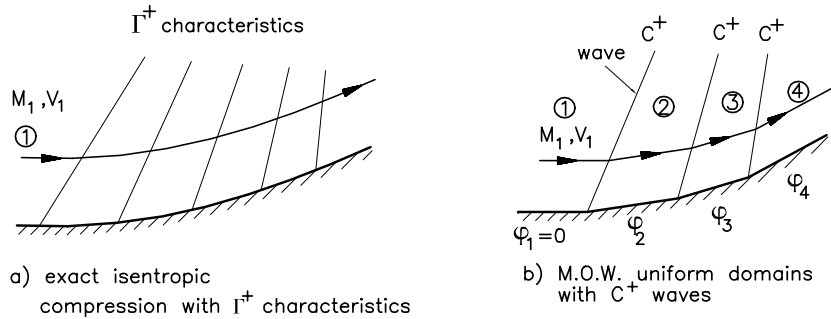


Figure 7.18: M.O.W. applied to a compressing flow

very similar: the curved boundary is approximated by an appropriate number of successive straight segments 1, 2, 3, ... having constant slopes $\varphi_1, \varphi_2, \varphi_3, \dots$ respectively. Again take the difference in slope of the consecutive wall segments $\varphi_{i+1} - \varphi_i = \Delta\varphi_i > 0$ constant. Since φ is counted positive counter clockwise $\varphi_1 < \varphi_2 < \varphi_3$ and $\Delta\varphi > 0$. Using Prandtl-Meyer theory the flow conditions in the various uniform domains are:

$$\begin{aligned}\varphi_2 &= \varphi_1 + |\Delta\varphi|, & \nu_2 &= \nu_1 - |\Delta\varphi| \\ \varphi_3 &= \varphi_1 + 2|\Delta\varphi|, & \nu_3 &= \nu_1 - 2|\Delta\varphi|\end{aligned}\tag{7.63}$$

Across the C^+ wave the flow properties show a jump; $|\Delta\varphi|$ is taken as a measure of the jump and it is called the strength of the wave.

The slope of the C^+ wave follows as the average slope of the Γ^+ characteristics in the domains that have C^+ as the common boundary. For example the C^+ wave between domains ② and ③ has the slope $\tan \alpha_{2,3}$ with

$$\alpha_{2,3} = \frac{1}{2} (\mu_2 + \varphi_2 + \mu_3 + \varphi_3). \tag{7.64}$$

Again observe the difference between waves and characteristics.

	C^+ waves	C^- waves
expansions	<p>$\Delta\nu = + \Delta\varphi$ $\Delta\varphi = - \Delta\varphi$</p>	<p>$\Delta\nu = + \Delta\varphi$ $\Delta\varphi = + \Delta\varphi$</p>
compressions	<p>$\Delta\nu = - \Delta\varphi$ $\Delta\varphi = + \Delta\varphi$</p>	<p>$\Delta\nu = - \Delta\varphi$ $\Delta\varphi = - \Delta\varphi$</p>

Table 7.3: The effect of C^+ and C^- waves on flow properties.

When overlooking the results for C^+ waves having a strength $|\Delta\varphi|$ as given in equations (7.61) and (7.62) we may conclude:

Expanding C^+ waves ($|\Delta\varphi| < 0$) do increase the Prandtl-Meyer angle and do decrease the flow direction by the same amount $|\Delta\varphi|$, so $\Delta\nu = |\Delta\varphi|$, $\Delta\varphi = -|\Delta\varphi|$.

Compressing C^+ waves ($|\Delta\varphi| > 0$) do decrease the Prandtl-Meyer angle and do increase the flow direction both by the amount $|\Delta\varphi|$, so $\Delta\nu = -|\Delta\varphi|$, $\Delta\varphi = |\Delta\varphi|$.

In case of C^- waves we expect to find almost similar results, however there are some minor differences regarding slope and strength. A C^- wave may be related to a Γ^- characteristic and therefore the slope of a C^- wave is found as the average slope of two appropriate Γ^- characteristics. For example a C^- wave lying between domain ① and ② has a slope $\tan\beta_{1,2}$ determined by

$$\beta_{1,2} = \frac{1}{2}(\varphi_1 - \mu_1 + \varphi_2 - \mu_2) \quad (7.65)$$

The difference with equation (7.64) is obvious. Concerning the strength observe that an expanding C^- wave gives an increase in flow direction, thus $\Delta\varphi > 0$ and a compressing C^- wave yields a decreasing flow direction, thus then $\Delta\varphi < 0$.

Very similar to C^+ waves we may now conclude for C^- waves having a strength $|\Delta\varphi|$.

Expanding C^- waves ($|\Delta\varphi| > 0$) do increase the Prandtl-Meyer angle and do increase the flow direction by the same amount $|\Delta\varphi|$, so $\Delta\nu = |\Delta\varphi|$, $\Delta\varphi = |\Delta\varphi|$.

Compressing C^- waves ($|\Delta\varphi| < 0$) do decrease the Prandtl-Meyer angle and do decrease the flow direction both by the amount $|\Delta\varphi|$, so $\Delta\nu = -|\Delta\varphi|$, $\Delta\varphi = -|\Delta\varphi|$.

The results for C^+ waves and C^- waves are summarized in table 7.6.1.

7.6.2 Interaction of waves

Consider a two-dimensional supersonic flow in a diverging channel having the special geometry shown in figure 7.19. Two centered expansions are generated one at the kink B in the top wall and one at the kink A in the bottom wall. Upstream of the kinks the top and bottom wall are parallel and the flow is uniform with conditions ν_1 and $\varphi_1 = 0$. Figure 7.19 part *a* shows

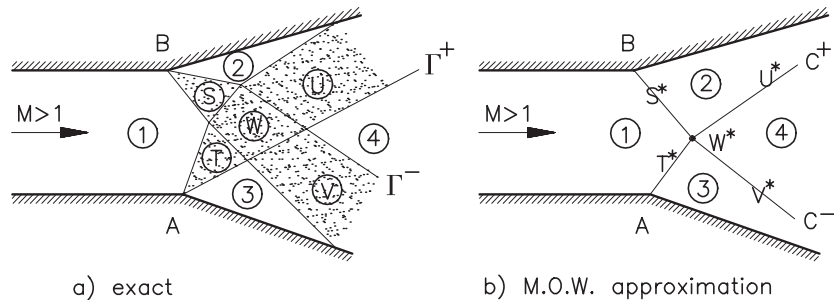


Figure 7.19: Interacting expansion waves

the interacting wave pattern displaying the uniform domains ①, ②, ③ and ④, the simple wave regions S , T , U and V , and the non-simple wave domain W . Assume that the flow deflection at kink B : $\varphi_1 - \varphi_2 > 0$ is known. Let us now apply the method of waves to this flow problem. In the M.O.W. approximation the expansion fan from B is replaced by a C^- wave, see figure 7.19 part b.

Observe that the non-simple domain W is reduced to the intersection W^* of the C^+ wave and the C^- wave. If the deflection angles φ_2 and φ_3 are different (irrespective their signs) the C^+ and the C^- waves will have different strength. The strength of the C^+ wave from A to W^* is $|\Delta\varphi|_A = |\Delta\varphi_3|$, (take $\varphi_1 = 0$) and the strength of the C^- wave from B to W^* is $|\Delta\varphi|_B = |\Delta\varphi_2|$. Taking into account that $\varphi_2 > 0$ and $\varphi_3 < 0$ and recalling table 7.6.1 both the C^+ and the C^- waves have to be expansion waves and therefore one may conclude:

$$\begin{aligned} \nu_2 &= \nu_1 + |\Delta\varphi|_B = \nu_1 + \varphi_2 \\ \nu_3 &= \nu_1 + |\Delta\varphi|_A = \nu_1 - \varphi_3 \end{aligned} \quad \left. \right\} \quad (7.66)$$

This result from M.O.W. is still exact for those points in ② and ③ which lie outside the expansion fans. For points lying inside the fans (7.66) gives an approximation for the flow variables. The accuracy of the solution depends on the wave strength; weaker waves will increase the accuracy. Let us now try to determine the flow variables in domain ④. Domain ④ is uniform and appears when both waves (C^+ and C^-) have interacted. It is obvious that domain ④ can be determined if the strength of the C^+ wave between ② and ④ is known or if the strength of the C^- wave between ③ and ④ is known. However these wave strengths are yet unknown since C^+ and C^- have been interacted at W^* . So the question remains what happens with the wave strength if interaction occurs?

The wave strength of the C^- wave before interaction is $|\Delta\varphi|_{\text{pre}} = |\varphi_2| = \varphi_2$, the wave strength after interaction is $|\Delta\varphi|_{\text{post}} = |\varphi_4 - \varphi_3|$. How are $|\Delta\varphi|_{\text{post}}$ and $|\Delta\varphi|_{\text{pre}}$ related to each other?

Theorem: The strength of a wave (in terms of $|\Delta\varphi|$) is conserved during interaction with waves of the opposite family.

Proof: Consider the 'exact' flow pattern as sketched in figure 7.19 part a and use M.O.C. to find the flow properties in domain ④

$$\text{along } \Gamma_{1 \rightarrow 2}^+ : \quad \nu_1 - \varphi_1 = \nu_2 - \varphi_2, \quad (7.67)$$

$$\text{along } \Gamma_{2 \rightarrow 4}^- : \quad \nu_4 + \varphi_4 = \nu_2 + \varphi_2, \quad (7.68)$$

$$\text{along } \Gamma_{1 \rightarrow 3}^- : \quad \nu_1 + \varphi_1 = \nu_3 + \varphi_3, \quad (7.69)$$

$$\text{along } \Gamma_{3 \rightarrow 4}^+ : \quad \nu_4 - \varphi_4 = \nu_3 - \varphi_3. \quad (7.70)$$

Substracting (7.67) and (7.68) yields:

$$\nu_4 - \nu_1 + \varphi_4 + \varphi_1 = 2\varphi_2. \quad (7.71)$$

Substracting (7.69) and (7.70) yields:

$$\nu_4 - \nu_1 - (\varphi_4 + \varphi_1) = -2\varphi_3. \quad (7.72)$$

Substracting (7.71) and (7.72) yields:

$$2(\varphi_4 + \varphi_1) = 2\varphi_2 + 2\varphi_3,$$

or

$$\varphi_4 - \varphi_2 = \varphi_3 - \varphi_1 \quad (7.73)$$

or

$$\varphi_4 - \varphi_3 = \varphi_2 - \varphi_1 \quad (7.74)$$

Equation (7.73) tells that the strength of the C^+ wave is constant if a C^- is crossed. Similarly, equation (7.74) implies that the strength of the C^- wave is constant if a C^+ wave is crossed. Based on this result the flow properties in domain ④ may be found as

$$\left. \begin{aligned} \nu_4 &= \nu_2 + |\Delta\varphi|_A &= \nu_1 + \varphi_2 - \varphi_3 \\ \varphi_4 &= \varphi_2 - |\Delta\varphi|_A &= \varphi_2 + \varphi_3 \end{aligned} \right\} \quad (7.75)$$

Comment: In the case that both waves: C^+ and C^- have the same strength: $|\Delta\varphi|_A = |\Delta\varphi|_B$ then $\varphi_3 = -\varphi_2$, $\nu_4 = \nu_1 + 2\varphi_2$ and $\varphi_4 = 0$.

Two interacting expansion waves of equal strength and opposite family (C^+ and C^-) will cancel out deflections but strengthens the expansion rate.

7.6.3 M.O.W. for isentropic flows, a calculation scheme

The M.O.W. just introduced and explained for simple flow fields (e.g. a single compression or a single expansion) can be generalized to calculated flows having a more complicated structure. Such flow may be encountered if compression waves together with expansion waves, irrespective of their type (C^+ or C^-) are present in the flow domain. Let us study some examples.

Consider a uniform flow (conditions: $\nu_1 > 0$, $\varphi_1 = 0$) entering a two dimensional diverging channel, not necessarily symmetric. An example is shown in figure 7.20.

Let the walls be discretized so that all waves emanating from corner points have equal strength: $|\Delta\varphi|$. Since the channel is diverging all waves are expansion waves. The pattern of C^+ waves and C^- waves is shown in figure 7.20, they intersect and subdivide the flow domain in a number of uniform subdomains or cells. The flow properties (ν, φ) in a particular cell may now be calculated simply by counting waves. Travelling from domain ① where we have specified the entrance conditions to a particular cell : P one passes several C^+ waves and/or C^- waves. Once a wave is passed (in flow direction!) the Prandtl-Meyer angle (ν) increases

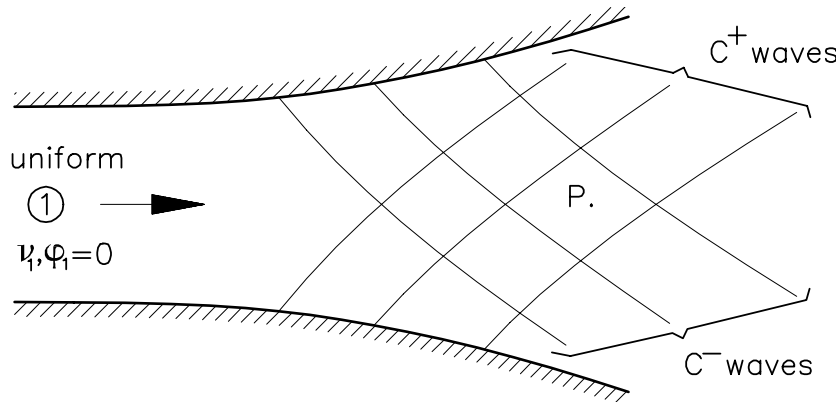


Figure 7.20: Wave pattern in a two-dimensional diverging channel

with the amount $|\Delta\varphi|$; the flow angle (φ) decreases if a C^+ wave is crossed and increases if a C^- wave is crossed both with the amount of $|\Delta\varphi|$.

Assume that for the cell P one has to cross a number of m_p^+ C^+ waves and m_p^- C^- waves. The flow properties in cell P are then determined by

$$\left. \begin{aligned} \nu_p &= \nu_1 + (m_p^- + m_p^+) |\Delta\varphi|, \\ \varphi_p &= \varphi_1 + (m_p^- - m_p^+) |\Delta\varphi|. \end{aligned} \right\} \quad (7.76)$$

The above result holds for expansion waves.

In case only compression waves appear a very similar expression can be derived. Assume that all compression waves have equal strength: $|\Delta\varphi|$. For a particular cell P one has to cross a number of n_p^+ C^+ waves and a number of n_p^- C^- waves. Crossing a compression wave (in flow direction) decreases the Prandtl-Meyer angle with the amount $|\Delta\varphi|$; it also decreases the flow angle if the crossed wave is of C^+ type. Thus for compressing flows we find:

$$\left. \begin{aligned} \nu_p &= \nu_1 - (n_p^- + n_p^+) |\Delta\varphi|, \\ \varphi_p &= \varphi_1 - (n_p^- - n_p^+) |\Delta\varphi|. \end{aligned} \right\} \quad (7.77)$$

The particular results for expanding regimes and compressing regimes may be combined to obtain a general expression for the flow conditions in a particular cell P :

$$\left. \begin{aligned} \nu_p &= \nu_1 + (m_p^- + m_p^+ - n_p^- - n_p^+) |\Delta\varphi|, \\ \varphi_p &= \varphi_1 + (m_p^- - m_p^+ - n_p^- + n_p^+) |\Delta\varphi|. \end{aligned} \right\} \quad (7.78)$$

This expression holds for isentropic supersonic flow domains, shocks may not occur.

Wave reflection on a plane wall In figure 7.20 we see C^+ waves running onto the top wall and C^- waves running onto the bottom wall. If these waves arrive at the opposite wall they will be reflected into waves of the opposite type: C^+ waves will reflect into C^- waves and vice versa.

Let us study some details of the reflection process, for example if a C^- expansion wave enters a plane wall, see figure 7.21.

A C^- expansion wave with strength $|\Delta\varphi|$ is generated by deflecting the top wall at A with an angle $\Delta\varphi$. The C^- wave runs onto the lower wall where it is reflected into a C^+ wave.

Question:

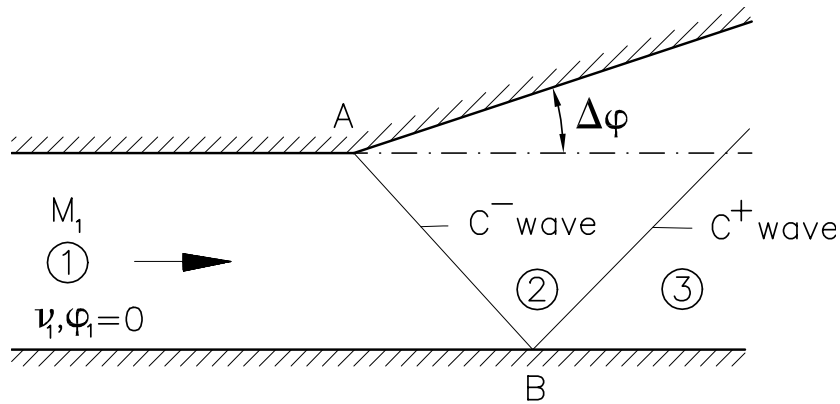


Figure 7.21: Reflection of an expansion wave

What are the flow conditions in domain ③ and what is the character of the reflected wave expanding or compressing?

In domain ③ the flow must be parallel to the wall so $\varphi_3 = \varphi_1 = 0$. Travelling from domain ① to domain ③ we pass one C^- wave and one C^+ wave, this makes $m_3^- = 1$, $n_3^- = 0$ since the character of the C^+ wave is as yet unknown the integers n_3^+ and m_3^+ cannot be determined. Using (7.78) the flow angle φ_3 follows as

$$\varphi_3 = \varphi_1 + (1 - m_3^+ + n_3^+) |\Delta\varphi|.$$

Taking into account the boundary condition $\varphi_3 = \varphi_1 = 0$ there is obtained

$$(1 - m_3^+ + n_3^+) = 0.$$

Since m_3^+ and n_3^+ are non-negative integers there follows $m_3^+ = 1$, $n_3^+ = 0$ implying that the reflected C^+ wave is an expansion wave with strength $|\Delta\varphi|$. The above example leads to the more general observation that: *Expansion waves will reflect on a plane wall as expansion waves; during reflection the wave strength is unchanged.*

A similar treatment for compression waves will lead to the observation that: *Compression waves will reflect on a plane wall as compression waves; during reflection the wave strength is unchanged.*

Wave reflection on a jet boundary Another interesting reflection phenomenon happens if a C^+ wave (expansion or compression) reflects on a jet boundary. A jet boundary is a contact discontinuity separating two flows having different conditions. Across the jet boundary the pressure and the flow direction is continuous but flow velocity (Mach number), density and entropy are discontinuous.

Since the flow direction is continuous the jet boundary is also a streamline. Consider a C^- expansion wave that hits a jet boundary, see figure 7.22. Assume that the jet boundary separates the supersonic flow in domain ① (conditions ν_1 , $\varphi_1 = 0$, p_1) from a gas at rest ($M = 0$) in domain ④. The C^- wave is reflected and a C^+ wave appears emanating from point B. Across the jet boundary the pressure is continuous thus $p_1 = p_4 = p_3$ and because the flow is isentropic $\nu_3 = \nu_1$. Travelling from domain ① to domain ③ one C^- wave and one

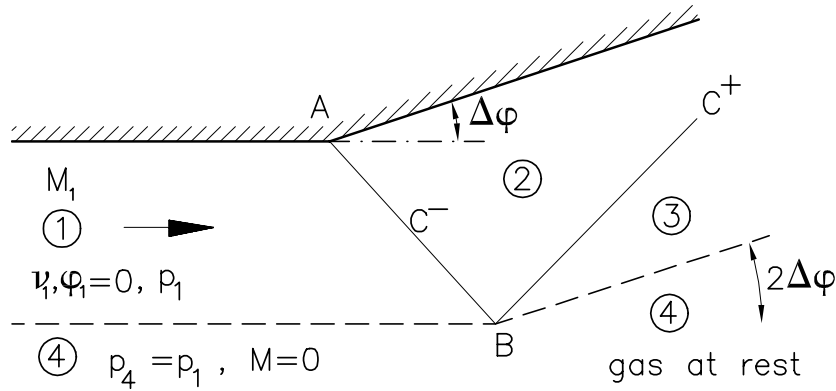


Figure 7.22: Wave reflecting on a jet boundary

C^+ wave is passed, thus $m_3^- = 1$, $n_3^- = 0$. Since the character of C^+ is yet unknown the integers m_3^+ and n_3^+ are left undetermined. From (7.78) we can determine the Prandtl-Meyer angle in domain ③ as

$$\nu_3 = \nu_1 + (1 + m_3^+ - n_3^-).$$

Taking into account the condition $\nu_3 = \nu_1$ and that m_3^+ and n_3^+ have to be zero or positive there is obtained $m_3^+ = 0$, $n_3^+ = 1$. The reflected wave is a compression wave and has strength $|\Delta\varphi|$. The flow direction in region ③ follows (use again (7.78) with $m_3^- = 1$, $m_3^+ = 0$, $n_3^+ = 0$, $n_3^+ = 1$) as

$$\varphi_3 = 2|\Delta\varphi|.$$

Due to the interaction the flow deflection doubles! Conclusion:

Expansion waves will reflect on a jet boundary with a gas at rest as compression waves and compression waves will reflect as expansion waves.

7.6.4 Design of a supersonic windtunnel nozzle by M.O.W.

The main objective of a supersonic windtunnel is the realisation of a steady uniform flow having specified conditions such as Mach number, pressure and temperature. From one dimensional compressible flow theory it is well known that a nozzle throat is needed, for the transition from subsonic to supersonic flow. In the nozzle throat sonic flow conditions appear. Downstream of the throat in the diverging part a supersonic flow may be obtained.

The required steady uniform flow is found in the test section of the windtunnel. The area ratio between test section and throat determines the test section Mach number. To guarantee that the flow in the test section is exactly uniform a special contour between the throat and the test section has to be designed. To obtain such a special contour, the method of waves is a useful technique.

Assume a symmetric nozzle, a sketch of the upper part of the nozzle contour between throat and test section is shown in figure 7.23. The flow enters the throat just at sonic conditions, so the Prandtl-Meyer angle in the throat is $\nu = 0$. To be specific we aim to design a nozzle contour for a supersonic windtunnel with test section Mach number: $M_T = 1.916$, the corresponding

Prandtl-Meyer angle in the test section is $\nu_T = 24$. The nozzle contour is replaced by rectilinear segments, such that at each corner point the flow direction changes by a constant amount of 2° .

Along the diverging part AB the slope angle increases stepwise until the maximum angle of

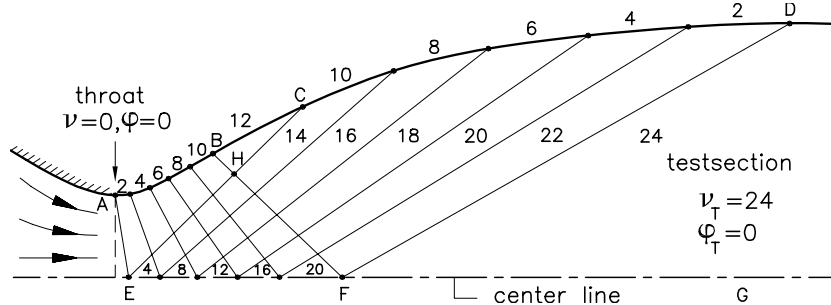


Figure 7.23: Design of a nozzle contour for a supersonic windtunnel. Indicated values in the flow field refer to the values of the Prandtl-Meyer angle ν , values along the contour refer to the contour slope.

12° is reached along BC . From C to D the slope angle decreases until 0° beyond D . From the diverging part AB , C^- expansion waves are generated. Crossing these waves will increase the Prandtl-Meyer angle and the flow direction by an amount of 2° . The C^- waves reflect at the centre line along EF into C^+ waves. The C^+ waves are also expansion waves, crossing them will increase the value of ν but decreases the flow angle, both by the same amount of 2° . Each wave has a strength $|\Delta\varphi| = |2^\circ|$.

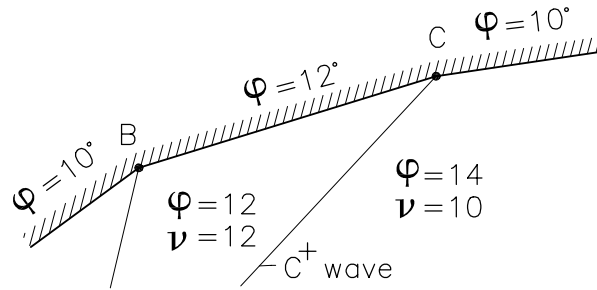
In the actual design the part AB of the nozzle contour may be chosen more or less arbitrary; for example a parabolic curve with zero slope at A . Using M.O.W. the flow conditions in each cell in $ADEF$ can now be determined, just by counting waves! For example the triangular shaped domains along the centre line all have $\varphi = 0$ due to the fact that an equal number of C^+ waves and C^- waves have to be passed when travelling from the throat to a particular domain. But since C^+ waves and C^- waves both do increase the Prandtl-Meyer angle we see $\Delta\nu = 2|\Delta\varphi| = 4^\circ$ between consecutive triangles. We observe that $ABEH$ is a simple wave and that EHF is a non-simple region. Downstream of the C^+ wave FD the test section conditions $\nu = 24$, $\varphi = 0$ are reached. The slopes of the waves in $ADEF$ can now be calculated. For example the slope angle of AE may be determined as

$$\beta_{AE} = \frac{1}{2} (\varphi_{\text{pre}} - \mu_{\text{pre}} + \varphi_{\text{post}} - \mu_{\text{post}}).$$

Now we come to the determination of the shape of contour CD . Consider the flow near C in more detail, see figure 7.24.

The C^+ wave emanating from E intersects the wall segment having $\varphi = 12^\circ$ at point C . When passing this C^+ wave the ν increases from 12° to 14° and the flow angle decreases from 12° to 10° . At C the C^+ wave reflects and a C^- wave runs downstream. This C^- wave is an expansion wave which increases the ν values by an amount of 2° . This process also happens on the centre line downstream of F where the flow conditions already had met the requirements in the test section.

Due to the C^- wave emanating from C the flow conditions in the test section will be disturbed.

Figure 7.24: Wall adaption starting a C

To avoid this disturbing effect the C^- wave reflecting from C has to be suppressed. This can be done by properly adapting the nozzle contour and changing the slope of the nozzle contour at C from 12° to 10° which gives the desired result and cancels the reflected wave. In a similar way all the other C^+ waves arriving at the contour CD will be prevented from reflecting by wall adaption. Along CD the nozzle contour shows a decreasing slope angle until beyond D the angle is 0° . Along part AB of the nozzle contour expansion waves are *generated*, along part CD wave cancellation is accomplished by wall adaption. The arbitrariness in the choice of the shape of nozzle part AB is corrected by a proper design of the nozzle part CD .

Comments:

1. The test conditions $\nu_T = 24$, $\varphi_T = 0$ are realized by passing six C^- waves and six C^+ waves, each of them having a strength $|\Delta\varphi| = 2^\circ$. The nozzle contour obtained in figure 7.23 is not a unique contour but just one of the possible designs that realizes the required test conditions. On the other hand it has the special property that it uses just one reflection of C^- waves on the centre line to acquire the prescribed test conditions $\nu_T = 24$, $\varphi_T = 0$.

Designs having more reflections are very well known, however '*the one reflection nozzle*' gives a short nozzle for a given throat height.

2. For a '*the one reflection nozzle*' the maximum deflection appears at the nozzle contour where all C^- waves and no C^+ waves are passed, thus if just the half of the total number of waves are passed. So the maximum deflection angle φ_{\max} becomes $\varphi_{\max} = 1/2\nu_T$, it increases with increasing Mach number.

Due to viscous effects flow separation is likely to occur certainly if the deflection angle becomes too large. In practice, a maximum deflection angle of $\approx 6^\circ$ is acceptable. Thus supersonic windtunnels designed for Mach numbers $M > 1.5$ ($\nu_T \leq 12^\circ$) are equipped with nozzles showing more than one reflection.

3. The design of a '*one-reflection nozzle*' is a very good starting point to design nozzle contours for the same Mach number but having more reflections because '*multi-reflection nozzles*' are already incorporated in the '*one-reflection nozzle*' design. Such a '*multi-reflection nozzle*' is obtained if one constructs in the '*one-reflection*' solution a streamline going from throat to test section and that crosses the non-simple domain EFH (see figure 7.23). Such a streamline can be viewed as the contour for a new nozzle. Inside the new nozzle the flow is accelerated from throat ($M = 1$, $\nu = 0$) to test conditions ($\nu_T = 24$). Now we observe more reflections of C^- waves along the centre line; the closer the nozzle

contour is chosen to the centre line the more reflections appear and the smaller the maximum deflection angle becomes.

So, once a 'one-reflection nozzle' for a given test Mach number is obtained then a class of 'multi-reflection nozzles' having the same Mach number but different deflection angles are available as part of the 'one-reflection' solution.

4. Figure 7.23 shows the exact nozzle flow of a supersonic nozzle. The flow is definitely two-dimensional in the domain between nozzle throat and test section. One of the consequences of this two dimensional behaviour is that the Mach number at the centre line already attains the test section value upstream of the test section. The test section conditions are found not only in the test section itself but also in the diverging part of the nozzle downstream of the wave FD . So in actual supersonic experiments one may observe that windtunnel models are sometimes placed upstream of the test section.

Chapter 8

Two-dimensional steady potential flows

8.1 Crocco's Theorem, Velocity Potential, Potential Equation.

In chapter 7 we have considered the two-dimensional steady flow of an inviscid, non-heat conducting fluid. Furthermore, we have neglected the influence of external force fields and external heat sources.

So we have assumed adiabatic flow governed by the steady Euler equations (see (7.24)).

$$\text{continuity: } \frac{\partial}{\partial x}(\rho u) + \frac{\partial}{\partial y}(\rho v) = 0 \quad (8.1)$$

$$x\text{-momentum: } \rho u \frac{\partial u}{\partial x} + \rho v \frac{\partial v}{\partial x} + \frac{\partial p}{\partial x} = 0 \quad (8.2)$$

$$y\text{-momentum: } \rho u \frac{\partial v}{\partial x} + \rho v \frac{\partial v}{\partial y} + \frac{\partial p}{\partial y} = 0 \quad (8.3)$$

$$\text{energy: } u \frac{\partial H}{\partial x} + v \frac{\partial H}{\partial y} = 0 \quad (8.4)$$

The last equation expresses that the total enthalpy H is kept constant when travelling along a streamline. A similar result for the entropy could be obtained (see equation (7.9)):

$$u \frac{\partial s}{\partial x} + v \frac{\partial s}{\partial y} = 0. \quad (8.5)$$

In this chapter we will consider the special class of *irrotational* flow fields because they have a wide range of applicability.

In irrotational flows the vorticity ω , defined as

$$\bar{\omega} = \nabla \times \bar{v}, \quad (8.6)$$

is everywhere zero in the flow field.

It is well known that vorticity appears in shear layers and/or boundary layers, thus in flows where viscous effects are present. However, are there, apart from viscosity, other mechanisms that can create vorticity in a flow field? To answer this question combine the momentum equation for *unsteady* inviscid flow:

$$\frac{\partial \bar{v}}{\partial t} + (\bar{v} \cdot \nabla) \bar{v} + \frac{1}{\rho} \nabla p = 0, \quad (8.7)$$

and the first law in the form:

$$T\nabla s = \nabla e + p\nabla \frac{1}{\rho} = \nabla h - \frac{1}{\rho}\nabla p. \quad (8.8)$$

Using the vector identity

$$(\bar{v} \cdot \nabla)\bar{v} = \nabla\left(\frac{1}{2}\bar{v} \cdot \bar{v}\right) - \bar{v} \times \bar{\omega}, \quad (8.9)$$

there follows from equation (8.7):

$$\frac{\partial \bar{v}}{\partial t} + \nabla\left(\frac{1}{2}\bar{v} \cdot \bar{v}\right) - \bar{v} \times \bar{\omega} + \frac{1}{\rho}\nabla p = 0. \quad (8.10)$$

Eliminating $\frac{1}{\rho}\nabla p$ from equation (8.8) there results

$$\frac{\partial \bar{v}}{\partial t} + \nabla\left(\frac{1}{2}\bar{v} \cdot \bar{v}\right) - \bar{v} \times \bar{\omega} + \nabla h - T\nabla S = 0. \quad (8.11)$$

Using the definition of the total enthalpy H :

$$H = h + \frac{1}{2}\bar{v} \cdot \bar{v}, \quad (8.12)$$

Crocco's well-known result is now obtained:

$$\frac{\partial \bar{v}}{\partial t} + \nabla H - T\nabla s = \bar{v} \times \bar{\omega}. \quad (8.13)$$

Crocco's equation relates vorticity ($\bar{\omega}$), entropy (s), total enthalpy (H) and unsteadiness ($\frac{\partial \bar{v}}{\partial t}$) together. It tells that in inviscid flow vorticity is created if entropy gradients, total enthalpy gradients or unsteady effects appear. Three well-known examples of vorticity production are

- curved shocks ($\nabla s \neq 0$),
- jet boundaries ($\nabla H \neq 0$),
- oscillating airfoil ($\frac{\partial}{\partial t} \neq 0$)

From Crocco's Theorem it is obvious that steady flows having uniform entropy and uniform total enthalpy can be treated as irrotational.

If the entropy is uniform then equation (8.5) is identically fulfilled and the flow is called *homentropic*; similarly if the total enthalpy is uniform then equation (8.4) is identically fulfilled, the flowfield is called *isenthalpic*.

So, steady homentropic and isenthalpic flows can be treated as irrotational.

For this class of flows the governing equations (8.1)-(8.3) can be simplified considerably by introducing the velocity potential $\Phi(x, y, z)$ according to

$$\bar{v} = \nabla\Phi(x, y, z). \quad (8.14)$$

In order to derive a simple equation for the potential function Φ we try to eliminate the pressure p and density ρ from the system (8.1)-(8.3). First write the continuity equation in the form

$$\rho \left(\frac{\partial u}{\partial x} + \frac{\partial v}{\partial y} \right) + u \frac{\partial \rho}{\partial x} + v \frac{\partial \rho}{\partial y} = 0. \quad (8.15)$$

Density gradients can be expressed in terms of pressure gradients by differentiating the isenthalpic condition:

$$H = \frac{\gamma}{\gamma - 1} \frac{p}{\rho} + \frac{u^2 + v^2}{2} = \text{constant}, \quad (8.16)$$

with respect to x and with respect to y , yielding

$$\frac{a^2}{\gamma - 1} \frac{1}{\rho} \frac{\partial \rho}{\partial x} = \frac{\gamma}{\gamma - 1} \frac{1}{\rho} \frac{\partial p}{\partial x} + \frac{\partial}{\partial x} \left(\frac{u^2 + v^2}{2} \right), \quad (8.17)$$

$$\frac{a^2}{\gamma - 1} \frac{1}{\rho} \frac{\partial \rho}{\partial y} = \frac{\gamma}{\gamma - 1} \frac{1}{\rho} \frac{\partial p}{\partial y} + \frac{\partial}{\partial y} \left(\frac{u^2 + v^2}{2} \right). \quad (8.18)$$

With equations (8.2) and (8.3) the pressure derivatives can be substituted, yielding:

$$\frac{a^2}{\gamma - 1} \frac{1}{\rho} \frac{\partial \rho}{\partial x} = \frac{-\gamma}{\gamma - 1} \left(u \frac{\partial u}{\partial x} + v \frac{\partial u}{\partial y} \right) + \frac{\partial}{\partial x} \left(\frac{u^2 + v^2}{2} \right), \quad (8.19)$$

$$\frac{a^2}{\gamma - 1} \frac{1}{\rho} \frac{\partial \rho}{\partial y} = \frac{-\gamma}{\gamma - 1} \left(u \frac{\partial v}{\partial x} + v \frac{\partial v}{\partial y} \right) + \frac{\partial}{\partial y} \left(\frac{u^2 + v^2}{2} \right). \quad (8.20)$$

The density derivatives according to equations (8.19) and (8.20) can now be inserted in the continuity equation in the form of equation (8.15); after some rearranging of terms there results

$$(a^2 - u^2) \frac{\partial u}{\partial x} - uv \left(\frac{\partial u}{\partial y} + \frac{\partial v}{\partial x} \right) + (a^2 - v^2) \frac{\partial v}{\partial y} = 0. \quad (8.21)$$

The equation just obtained contains only the velocity components u and v and the sound velocity a , the latter can also be expressed in terms of the velocity components u, v by writing $a^2 = \gamma p / \rho$ and using equation (8.16) leading to the relation

$$\frac{a^2}{\gamma - 1} + \frac{u^2 + v^2}{2} = \text{constant}. \quad (8.22)$$

From the definition of the velocity potential, equation (8.14), the velocity components are expressed as:

$$u = \frac{\partial \Phi}{\partial x}, \quad v = \frac{\partial \Phi}{\partial y}. \quad (8.23)$$

Inserting them in equation (8.21) we find the well-known potential equation:

$$(a^2 - u^2) \frac{\partial^2 \Phi}{\partial x^2} - 2uv \frac{\partial^2 \Phi}{\partial x \partial y} + (a^2 - v^2) \frac{\partial^2 \Phi}{\partial y^2} = 0. \quad (8.24)$$

The velocity potential Φ satisfies a quasi-linear P.D.E. of second order. The equation governs compressible flows ranging from low speeds (subsonic) to high speeds (supersonic) as long as the fluid may be regarded as a perfect gas.

Also the transonic speed regime where the transition from subsonic to supersonic and vice versa appears very well modelled by equation (8.24). Supersonic flows with strong shock

waves cannot be treated since the assumption of constant entropy is violated when crossing a shock wave.

In the exceptional case of incompressible flow: $a^2 \gg (u^2 + v^2)$, equation (8.24) reduces to the Laplace equation

$$\frac{\partial^2 \Phi}{\partial x^2} + \frac{\partial^2 \Phi}{\partial y^2} = 0. \quad (8.25)$$

Obviously incompressible potential flow is just a special case of a compressible flow.

8.2 Linearized flow; the Prandl-Glauert equation

Consider a steady two-dimensional flow and let this flow be described as a perturbation of the uniform flow with velocity U_∞ in x -direction. The velocities of the perturbed flow then become:

$$u(x, y) = U_\infty + u'(x, y), \quad (8.26)$$

$$v(x, y) = v'(x, y). \quad (8.27)$$

The perturbation velocities u' and v' are assumed to be small with respect to the velocity U_∞ :

$$\frac{u'}{U_\infty} \ll 1, \quad \frac{v'}{U_\infty} \ll 1. \quad (8.28)$$

A perturbation velocity potential $\phi(x, y)$ is now defined as:

$$\Phi(x, y) = U_\infty(x + \varepsilon\phi(x, y)), \quad (8.29)$$

yielding the velocity components:

$$\begin{aligned} u &= \Phi_x = U_\infty + \varepsilon U_\infty \frac{\partial \phi}{\partial x}, \\ v &= \Phi_y = \varepsilon U_\infty \frac{\partial \phi}{\partial y}. \end{aligned} \quad (8.30)$$

Obviously the velocity perturbations are small so:

$$\varepsilon \frac{\partial \phi}{\partial x} \ll 1, \quad \text{and} \quad \varepsilon \frac{\partial \phi}{\partial y} \ll 1, \quad (8.31)$$

where ε is a small quantity governing the magnitude of the perturbations.

Taking the magnitude $\mathcal{O}(\varepsilon)$ then

$$\frac{\partial \phi}{\partial x} = \mathcal{O}(1), \quad \frac{\partial \phi}{\partial y} = \mathcal{O}(1). \quad (8.32)$$

The velocity potential equation may now be linearized by taking into account the order esti-

mations:

$$\begin{aligned}\frac{u^2}{U_\infty^2} &= 1 + 2\varepsilon\phi_x + \mathcal{O}(\varepsilon^2), \\ \frac{v^2}{U_\infty^2} &= \mathcal{O}(\varepsilon^2), \\ \frac{uv}{U_\infty^2} &= \varepsilon\phi_x + \mathcal{O}(\varepsilon^2), \\ \frac{a^2}{U_\infty^2} &= \frac{1}{M_\infty^2} - (\gamma - 1)\varepsilon\phi_x + \mathcal{O}(\varepsilon^2), \\ \frac{\partial^2\Phi}{\partial x^2} &= \varepsilon U_\infty \frac{\partial^2\phi}{\partial x^2}, \\ \frac{\partial^2\Phi}{\partial x\partial y} &= \varepsilon U_\infty \frac{\partial^2\phi}{\partial x\partial y}, \\ \frac{\partial^2\Phi}{\partial y^2} &= \varepsilon U_\infty \frac{\partial^2\phi}{\partial y^2}.\end{aligned}$$

Inserting these order estimates into the velocity potential equation: (8.24) and neglecting terms of $\mathcal{O}(\varepsilon^2)$ and higher the Prandtl-Glauert equation:

$$(1 - M_\infty^2) \frac{\partial^2\phi}{\partial x^2} + \frac{\partial^2\phi}{\partial y^2} = 0, \quad (8.33)$$

for the perturbation potential $\phi(x, y)$ is obtained. Here $M_\infty = U_\infty/a_\infty$ and a_∞ is the sound speed of the unperturbed flow.

The Prandtl-Glauert equation is a *linear* second order PDE with constant coefficients. For subsonic free streams ($M_\infty < 1$) the Prandtl-Glauert equation is elliptic, for supersonic free stream ($M_\infty > 1$) this equation is hyperbolic.

For transonic flow ($M_\infty \approx 1$) equation (8.33) *cannot* be used because the term $(1 - M_\infty^2)$ can no longer be viewed as an $\mathcal{O}(1)$ term but has to be considered as an $\mathcal{O}(\varepsilon)$ term if $M \rightarrow 1$.

8.2.1 Linearized pressure coefficient

Once a solution of the Prandtl-Glauert equation is obtained the velocity components u and v are known and the pressure can be calculated; in terms of pressure coefficient c_p it leads to:

$$c_p = \frac{p - p_\infty}{\frac{1}{2}\rho_\infty U_\infty^2} = -2\varepsilon\phi_x + \mathcal{O}(\varepsilon^2), \quad (8.34)$$

which reveals that the first order pressure perturbation only depends on the perturbation velocity in main flow direction.

Expression (8.34) can be verified by using the fact that in isentropic flow the sound velocity is proportional to the pressure as:

$$a^2 \propto p^{\frac{\gamma-1}{\gamma}}. \quad (8.35)$$

If the coefficient of proportionality is evaluated using the uniform flow conditions ($a_\infty, p_\infty, \rho_\infty$) then there is obtained

$$\left(\frac{a}{a_\infty}\right)^2 = \left(\frac{p}{p_\infty}\right)^{\frac{\gamma-1}{\gamma}}, \quad (8.36)$$

with the help of the order estimate of the variable $(a/U_\infty)^2$ one finds

$$\left(\frac{p}{p_\infty}\right)^{\frac{\gamma-1}{\gamma}} = M_\infty^2 \left(\frac{a}{U_\infty}\right) = 1 - (\gamma - 1)M_\infty^2 \varepsilon \phi_x + \mathcal{O}(\varepsilon^2), \quad (8.37)$$

or

$$\frac{p}{p_\infty} = 1 - \gamma M_\infty^2 \varepsilon \phi_x + \mathcal{O}(\varepsilon^2). \quad (8.38)$$

Using the definition of the pressure coefficient the result given in (8.34) is obtained. Notice also the minus sign, velocity increase causes a pressure decrease and vice versa.

8.2.2 Linearized boundary condition

Assume that a solid surface $y = \varepsilon h(x)$ is present in the flow domain. The shape of this surface depends on the small parameter ε . For $\varepsilon = 0$ this surface falls along the x -axis ($y = 0$) being also a streamline of the undisturbed uniform flow. For $\varepsilon \neq 0$ the solid surface induces a perturbation on this uniform flow.

Along the solid surface the boundary condition $\vec{v} \cdot \vec{n} = 0$ has to be fulfilled;

This boundary condition can also be linearized. Applying $\vec{v} \cdot \vec{n} = 0$ on the surface $y = \varepsilon h(x)$ there follows

$$\frac{dy}{dx} = \varepsilon h'(x) = \frac{v(x, y)}{u(x, y)} \quad (8.39)$$

which has to be valid at $y = \varepsilon h(x)$, yielding

$$\varepsilon h'(x) \cdot u(x, \varepsilon h(x)) = v(x, \varepsilon h(x)), \quad (8.40)$$

or in terms of the perturbation potential:

$$\varepsilon h'(x) \{U_\infty + U_\infty \varepsilon \phi_x(x, \varepsilon h(x))\} = \varepsilon U_\infty \phi_y(x, \varepsilon h(x)) \quad (8.41)$$

For small ε the perturbation velocities $\phi_x(x, \varepsilon h(x))$ and $\phi_y(x, \varepsilon h(x))$ may be expanded as:

$$\begin{aligned} \phi_x(x, \varepsilon h(x)) &= \phi_x(x, 0) + \left(\frac{\partial \phi_x}{\partial \varepsilon}\right)_{\varepsilon=0} \varepsilon + \mathcal{O}(\varepsilon^2) \\ \phi_y(x, \varepsilon h(x)) &= \phi_y(x, 0) + \left(\frac{\partial \phi_y}{\partial \varepsilon}\right)_{\varepsilon=0} \varepsilon + \mathcal{O}(\varepsilon^2) \end{aligned}$$

Inserting this expansion into Eq. (8.35) and neglecting terms of $\mathcal{O}(\varepsilon^2)$ the linearized boundary condition

$$h'(x) = \phi_y(x, 0) \quad (8.42)$$

results. Equation (8.42) expresses that the line $y = 0$ (x -axis) experiences an outflow ($\phi_y(x = 0)$) such that at the line $y = 0$ the velocity vector is tangential to the direction of the solid surface ($h'(x)$).

A small perturbation problem for potential flow may be summarized as follows: find a solution of the Prandtl-Glauert equation:

$$(1 - M_\infty^2) \frac{\partial^2 \phi}{\partial x^2} + \frac{\partial^2 \phi}{\partial y^2} = 0$$

which satisfies the boundary conditions

$$\frac{\partial \phi}{\partial y} = \frac{dh}{dx} \quad \text{at} \quad y = 0.$$

When $\phi(x, y)$ is known, the pressure coefficient follows from

$$c_p = -2\varepsilon \frac{\partial \phi}{\partial x}.$$

8.2.3 Example 1: a subsonic flow along a wavy wall

Consider a subsonic flow along an infinite solid surface which is wavy; for example having a sinusoidal shape:

$$y = \varepsilon h(x) = \varepsilon \sin kx, \quad (8.43)$$

k is the so called wave number which counts the number of waves on an interval of 2π length.

Assume that far away of this wall the flow is uniform with velocity $u = U_\infty$ parallel to the x -axis, see figure 8.1. The linearized boundary condition becomes

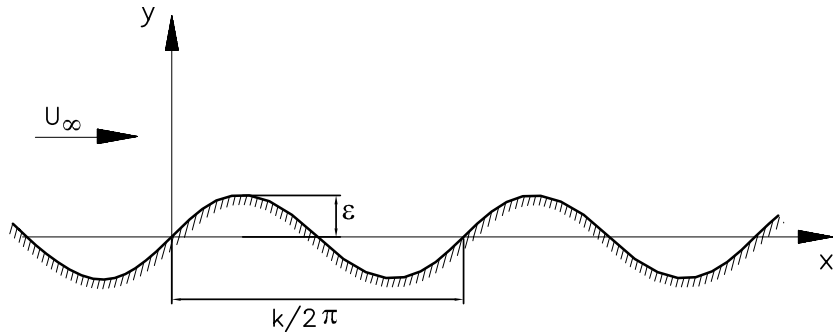


Figure 8.1: Flow along a wavy wall

$$\phi_y(x, 0) = k \cos kx \quad (8.44)$$

This is a Neumann type boundary condition because it specifies the normal derivative (e.g. $\frac{\partial \phi}{\partial y}$).

For subsonic flow $M_\infty < 1$ the Prandtl-Glauert-equation is of elliptic type, implying that boundary conditions have to be specified all along the boundary.

In this example we require that the perturbation potential $\phi(x, y)$ vanishes at large y (say $y \rightarrow \infty$) and further that the solution continues harmonically for $|x| \rightarrow \infty$.

Let us perform the method of separation of variables and try a solution of the form:

$$\phi(x, y) = X(x) \cdot Y(y) \quad (8.45)$$

where $X(x)$ is a function of x and $Y(y)$ is a function of y . Both have to be determined so that $\phi(x, y)$ satisfies the boundary conditions. When (8.45) is substituted in the Prandtl-Glauert equation there results

$$(1 - M_\infty^2) \frac{X''}{X} = -\frac{Y''}{Y}, \quad (8.46)$$

(where a prime indicates differentiation). The left-hand side of equation (8.46) is just a function of x and the right-hand side of it is just a function of y ; consequently both must be equal to the same constant because otherwise a relation between the independent variables x and y appears which is not allowed if x and y have to be independent. So the only possibility left is that both sides are equal to the same constant. Since $\phi(x, y)$ is expected to be periodic in x we propose this constant equal to a negative number, say $-m^2$. Then equation (8.40) leads to the set of second-order ODE's:

$$\begin{aligned}(1 - M_\infty^2)X'' &= -m^2 X \\ Y'' &= m^2 Y\end{aligned}\tag{8.47}$$

The solution that satisfies the boundary conditions reads

$$\phi(x, y) = -\frac{1}{\beta_\infty} \cos kx \exp(-k\beta_\infty y)\tag{8.48}$$

where we have taken

$$\beta_\infty = \sqrt{1 - M_\infty^2}\tag{8.49}$$

The perturbation potential is periodical in x -direction and in y -direction it shows exponential decay for $y \rightarrow \infty$. With the help of (8.34) we can calculate the pressure coefficient at the wall as

$$c_p = -2\varepsilon\phi_x(x, 0) = -2\frac{\varepsilon k}{\beta_\infty} \sin kx.\tag{8.50}$$

We observe a periodic behaviour in x -direction with a wave number equal to that of the wavy wall. The pressure coefficient varies linearly with the perturbation parameter ε . Furthermore it appears that the pressure coefficient is proportional with the *curvature* of the wavy wall.

The solution given in equation (8.50) shows exponential decay in y -direction. Let us introduce a characteristic length L by equating

$$\exp(-k\beta_\infty y) = \exp(-\frac{y}{l})$$

The characteristic length $L = \frac{1}{\beta_\infty k}$ is characteristic for the damping of the perturbations in y -direction. Damping increases with increasing Mach number and increasing wave number. This implies that perturbations induced by a wall with long waves in a low subsonic flow damp slowly.

Equation (8.50) shows that in the limit of incompressible flow ($M_\infty = 0, \beta_\infty = 1$) the pressure coefficient becomes

$$c_{p\text{incompressible}} = -2\varepsilon \sin kx.$$

So if we express the pressure coefficient for incompressible flow ($M_\infty = 0$) in terms of the pressure coefficient for incompressible flow, the well-known Prandtl-Glauert rule results:

$$c_{p_{M_\infty \neq 0}} = \frac{1}{\sqrt{1 - M_\infty^2}} c_{p_{M_\infty = 0}}\tag{8.51}$$

The factor $1/\sqrt{1 - M_\infty^2}$ acts as a compressibility correction. In subsonic flow ($M_\infty < 1$) the pressure coefficient increases due to compressibility effects. For M_∞ close to 1 this correction formula fails, the correction factor becomes very large which violates the small perturbation assumption.

8.2.4 Example 2: Supersonic flow along a wavy wall.

Assume a wavy wall expressed by

$$y = \varepsilon h(x) = \varepsilon \sin kx,$$

and a supersonic flow ($M_\infty > 1$) along it. Since $M_\infty \geq 1$ let us call

$$\beta_\infty^2 = M_\infty^2 - 1, \quad (8.52)$$

so that the Prandtl-Glauert equation takes the form

$$\beta_\infty^2 \phi_{xx} - \phi_{yy} = 0, \quad (8.53)$$

which is typically a 2D wave equation. The general solution is known as d'Alembert's solutions:

$$\phi(x, y) = F(x - \beta_\infty y) + G(x + \beta_\infty y), \quad (8.54)$$

where F and G are arbitrary functions of the arguments $x - \beta_\infty y$ and $x + \beta_\infty y$ respectively. $F(x - \beta_\infty y)$ represents left running waves and $G(x + \beta_\infty y)$ represents right running waves. The straight lines $x - \beta_\infty y = \text{constant}$ and $x + \beta_\infty y = \text{constant}$ are left- and right running characteristics. They represent Mach lines having an angle $\mu = \pm \sin^{-1}(1/M_\infty)$ with respect to the undisturbed flow direction (the x -axis); see figure 8.2.

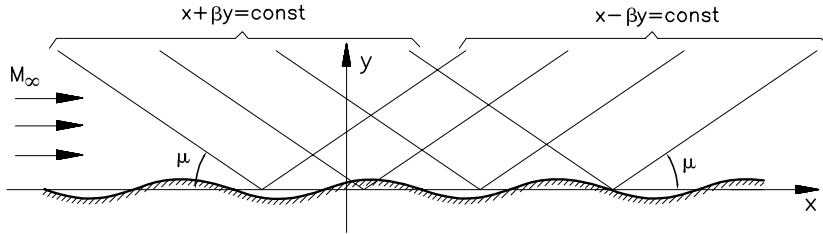


Figure 8.2: Characteristics of a linearized flow along a wavy wall

Since disturbances in a supersonic flow only propagate downstream the right running waves do not carry any information; to account for this effect take $G = 0$ and the solution of the Prandtl-Glauert-equation for the wavy wall problem has to be sought in the form

$$\phi(x, y) = F(x - \beta_\infty y). \quad (8.55)$$

From equation (8.42) the boundary condition that has to be fulfilled reads:

$$\phi_y(x, 0) = h'(x) = k \cos(kx) = -\beta_\infty F'(x). \quad (8.56)$$

Thus there follows

$$F'(x) = -\frac{k}{\beta_\infty} \cos(kx), \quad (8.57)$$

or

$$F(x) = -\frac{k}{\beta_\infty} \sin(kx), \quad (8.58)$$

or

$$F(x - \beta_\infty y) = -\frac{1}{\beta_\infty} \sin(x - \beta_\infty y). \quad (8.59)$$

Hence the perturbation potential $\phi(x, y)$ that satisfies the Prandtl-Glauert equation and that fulfills the boundary condition is then found as

$$\phi(x, y) = -\frac{1}{\beta_\infty} \sin k(x - \beta_\infty y). \quad (8.60)$$

In order to obtain the pressure (e.g. in the form of the pressure coefficient) we have to calculate:

$$\phi_x(x, 0) = -\frac{k}{\beta_\infty} \cos(kx). \quad (8.61)$$

Using equation (8.34) we then find

$$c_p = 2 \frac{\varepsilon k}{\beta_\infty} \cos(kx). \quad (8.62)$$

The pressure coefficient appears to be proportional to the slope of the wall. Everywhere where the wall has a positive slope the pressure is increased with respect to the reference pressure p_∞ . Similarly, at negative slopes the pressure just decreases compared to the reference pressure p_∞ .

From equation (8.62) it can be deduced very easily that also in the supersonic case the Prandtl-Glauert rule can be expressed as

$$c_{p_{M_\infty \neq 0}} = \frac{1}{\beta_\infty} c_{p_{M_\infty = \sqrt{2}}} \quad (8.63)$$

Note that in the transonic region ($M_\infty \approx 1$) the factor $1/\beta_\infty$ becomes unbounded, the Prandtl-Glauert rule becomes invalid and the small perturbation assumption is clearly not justified. A qualitative picture of c_p versus Mach number shows this behaviour very well; see figure 8.3.

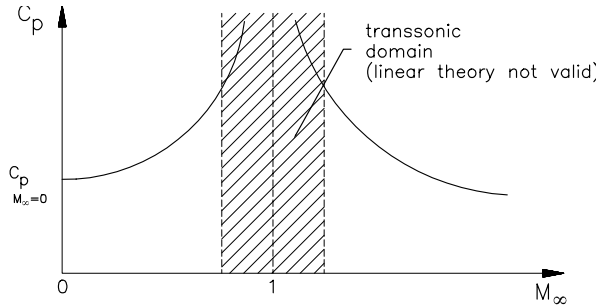


Figure 8.3: Prandtl-Glauert rule

8.3 Characteristics and compatibility relations for potential flow

In the previous section we have discussed the fully non-linear potential model (e.g. equation (8.24)):

$$(a^2 - u^2)\Phi_{xx} - 2uv\Phi_{xy} + (a^2 - v^2)\Phi_{yy} = 0, \quad (8.64)$$

and also the linearized flow model (eg equation (8.33)):

$$(M_\infty^2 - 1)\phi_{xx} - \phi_{yy} = 0. \quad (8.65)$$

The latter was referred to as the Prandtl-Glauert equation.

Both models are in the form of a second-order P.D.E. Now we attempt to find the characteristics and the corresponding compatibility relations of both equations in order to compare them with those of the fully non-linear equations obtained in chapter 7 (eg equation (7.54)).

8.3.1 Prandtl-Glauert equation

In order to obtain the characteristics of the PG equation we will apply the ‘left eigenvector’ method to the system

$$AU'_x + BU'_y = 0 \quad (8.66)$$

which is obtained if the perturbation velocities u' and v' are inserted into the PG equation. Here $U' = (u', v')^T$ is the state vector of the perturbation velocities u' and v' according to

$$\begin{aligned} u' &= \varepsilon U_\infty \phi_x, \\ v' &= \varepsilon U_\infty \phi_y, \end{aligned}$$

and

$$A = \begin{pmatrix} \beta_\infty^2 & 0 \\ 0 & -1 \end{pmatrix}, \quad B = \begin{pmatrix} 0 & -1 \\ 1 & 0 \end{pmatrix} \quad (8.67)$$

where

$$\beta_\infty^2 = M_\infty^2 - 1. \quad (8.68)$$

From $\det(B - \lambda A) = 0$ we obtain the eigenvalues

$$\lambda_1 = -\frac{1}{\beta_\infty} = -1/\sqrt{M_\infty^2 - 1} \quad (8.69)$$

$$\lambda_4 = +\frac{1}{\beta_\infty} = +1/\sqrt{M_\infty^2 - 1} \quad (8.70)$$

The eigenvalues are real only in the case of supersonic main flow ($U_\infty > a_\infty$). The corresponding left eigenvectors L_i (where $i = 1 \dots 4$) are found from

$$L_i A^{-1} B = \lambda L_i. \quad (8.71)$$

Matrix $A^{-1}B$ has the form

$$A^{-1}B = \begin{pmatrix} 0 & -1/\beta_\infty^2 \\ -1 & 0 \end{pmatrix} \quad (8.72)$$

The left eigenvectors satisfying equation (8.71) are found as

$$\lambda_1 = -\frac{1}{\beta_\infty} \Rightarrow L_1 = (\beta_\infty, -1),$$

$$\lambda_4 = +\frac{1}{\beta_\infty} \Rightarrow L_4 = (\beta_\infty, +1),$$

The compatibility relations now follow as:

$$\text{along } \Gamma^- \text{ with } \frac{dy}{dx} = -\frac{1}{\beta_\infty} : \beta_\infty du' + dv' = 0, \quad (8.73)$$

$$\text{along } \Gamma^+ \text{ with } \frac{dy}{dx} = +\frac{1}{\beta_\infty} : \beta_\infty du' - dv' = 0. \quad (8.74)$$

Since β_∞ is a constant, the compatibility relations can be integrated into:

$$\beta_\infty u' + v' = \text{constant along } \frac{dy}{dx} = -1/\beta_\infty = -\tan \mu, \quad (8.75a)$$

$$\beta_\infty u' - v' = \text{constant along } \frac{dy}{dx} = +1/\beta_\infty = +\tan \mu, \quad (8.75b)$$

In the linearized flow model the characteristics appear as two bundles of parallel lines. One bundle is the set of left-running characteristics with slope $+\tan \mu_\infty$, the other bundle represents the set of right running characteristics with slope $-\tan \mu_\infty$. Note that these slopes are exactly the same as those in the undisturbed flow region. *In the linearized flow model it appears that perturbations do not influence the characteristic pattern of the flow field.*

Let us now compare the compatibility relations as found in the linearized model (e.g. equations 8.75a, 8.75b) with those of the fully non-linear model as they are given in equation (7.54):

$$\frac{\sqrt{M^2 - 1}}{q} dq \pm d\phi = 0 \quad \text{along } \frac{dy}{dx} = \tan(\phi \mp \mu).$$

By remembering that $q^2 = u^2 + v^2$ and $\tan \phi = v/u$ the exact compatibility relations take the form

$$(\beta u \mp v)du + (\beta v \pm u)dv = 0, \quad (8.76)$$

with

$$\beta = \sqrt{M^2 - 1}.$$

If we now introduce the perturbations u' and v' according to

$$u(x, y) = U_\infty + u'(x, y), \quad v(x, y) = v'(x, y)$$

and if these perturbations are assumed to be so small that

$$\frac{u'}{U_\infty} \ll 1 \quad \text{and} \quad \frac{v'}{U_\infty} \ll 1 \quad (8.77)$$

then equation (8.76) reduces to

$$\beta_\infty du' \pm dv' = 0 \quad \text{along} \quad \frac{dy}{dx} = \tan(\mp \mu_\infty) \quad (8.78)$$

which are precisely the linearized compatibility relations given in equations (8.75a),(8.75b).

8.3.2 The Full Potential Equation

The full potential equation for two-dimensional steady compressible homentropic flow reads

$$(a^2 - u^2)\Phi_{xx} - 2uv\Phi_{xy} + (a^2 - v^2)\Phi_{yy} = 0 \quad (8.79)$$

In order to obtain the characteristics and corresponding compatibility relations of this equation we will again use the ‘left eigenvector method’. Equation (8.79) can be transformed into the system

$$AU_x + BU_y = 0, \quad (8.80)$$

where the state vector U is defined as

$$U = \begin{pmatrix} u \\ v \end{pmatrix}, \quad (8.81)$$

and where the matrices A and B have the form

$$A = \begin{pmatrix} a^2 - u^2 & -uv \\ 0 & -1 \end{pmatrix}, \quad \text{and} \quad B = \begin{pmatrix} -uv & a^2 - v^2 \\ 1 & 0 \end{pmatrix}. \quad (8.82)$$

From $\det(B - \lambda A) = 0$ we obtain the eigenvalues:

$$\lambda_{1,4} = \frac{uv \mp a^2\sqrt{M^2 - 1}}{u^2 - a^2}, \quad (8.83)$$

which are exactly the same as those of the steady two-dimensional Euler equations, see equation (7.22). This implies that the characteristics of the full potential equation have a slope $\frac{dy}{dx} = \tan(\phi \mp u)$. Physically it means that they have a slope-angle $\mp\mu$ with respect to the flow direction.

The eigenvalues $\lambda_{1,4}$ are real everywhere the *local* Mach number is larger than 1 (which is the case for supersonic flow). In order to obtain the compatibility relations that correspond to the real eigenvalues we have to determine the left eigenvectors L_i (with $i = 1 \dots 4$) from

$$L_i A^{-1} B = \lambda L_i. \quad (8.84)$$

In the full potential flow model the matrix $A^{-1}B$ takes the form

$$A^{-1}B = \frac{1}{a^2 - u^2} \begin{pmatrix} -2uv & a^2 - u^2 \\ -(a^2 - u^2) & 0 \end{pmatrix} \quad (8.85)$$

The left eigenvectors that satisfy equation (8.84) are found to be

$$\begin{aligned} \lambda_1 &= \frac{uv - \beta a^2}{u^2 - a^2} \Rightarrow L_1 = (uv - \beta a^2, -(a^2 - v^2)), \\ \lambda_4 &= \frac{uv + \beta a^2}{u^2 - a^2} \Rightarrow L_4 = (uv + \beta a^2, -(a^2 - v^2)). \end{aligned}$$

From

$$dV = L \ dU, \quad (8.86)$$

with

$$L = \begin{pmatrix} L_1 \\ L_4 \end{pmatrix} \quad (8.87)$$

we obtain the compatibility relations in the full-potential model:

$$dV_{1,4} = (uv \mp \beta a^2) du - (a^2 - v^2) dv = 0 \quad (8.88)$$

along $\frac{dy}{dx} = \lambda_{1,4}$.

Using the definition:

$$q^2 = M^2 a^2 = u^2 + v^2 \quad (8.89)$$

we may write

$$\beta a^2 = \frac{\beta(u^2 + v^2)}{\beta^2 + 1} \quad (8.90)$$

and equation (8.88) gets the form

$$dV_{1,4} = (\beta^2 uv + uv \mp \beta u^2 \mp \beta v^2) du + (\beta^2 v^2 - u^2) dv = 0,$$

or

$$(\beta u \mp v)(\beta v \mp u) du + (\beta v - u)(\beta v + u) dv = 0,$$

so that the compatibility relations for the full potential equation becomes

$$(\beta u \mp v) du + (\beta v \pm u) dv = 0 \quad \text{along } \frac{dy}{dx} = \lambda_{1,4} = \tan(\phi \mp \mu) \quad (8.91)$$

Comparing the results with equation (8.76) leads to the conclusion that the compatibility relations of the full potential equation and those of the Euler model for homentropic flow are exactly the same. This result could be expected since for steady homentropic flow Crocco's theorem implies irrotational flow ($\nabla \times \vec{v} = \vec{0}$) which allows the introduction of potential flow.

8.4 Two-dimensional flow in the throat of a Laval nozzle

The Laval nozzle is an essential device in a supersonic windtunnel to produce supersonic flow conditions downstream of the throat. From a one-dimensional point of view the transition from subsonic to supersonic flow takes place just at the smallest cross-sectional area, the throat of the nozzle. Upstream of the throat in the converging part, the flow is subsonic, whereas downstream of the throat in the diverging part, the flow is supersonic, see figure 8.4. Due to cross sectional area variations of the nozzle the quasi one-dimensional theory is not an exact treatment of the flow problem. The quasi one-dimensional theory accounts for the area effects on the mass flow by using the continuity equation in the form $\rho u A = \text{constant}$ but this theory ignores traversal effects such as transverse pressure gradients (due to streamline curvatures) or transverse velocity variations. In order to get a more realistic view on the flow properties in the nozzle a two-dimensional (planar or axi-symmetric) treatment is necessary.

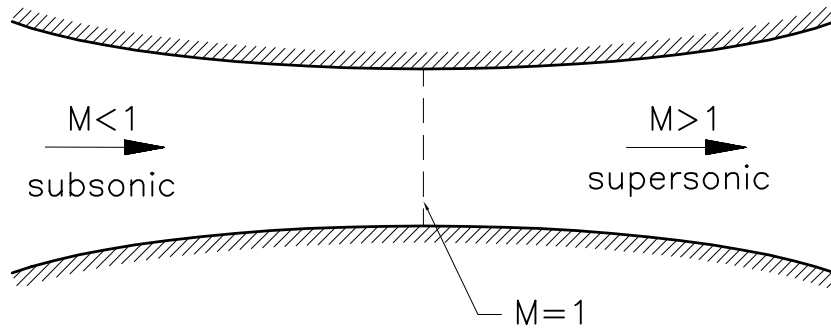


Figure 8.4: Transition of a subsonic flow into a supersonic flow in a Laval nozzle (quasi one-dimensional approximation)

Let us consider here the planar two-dimensional nozzle transporting a gas with ideal fluid properties. Furthermore, we assume steady flow, no frictional effects and no heat transfer. Also the flow is assumed to behave continuously in the sense that flow discontinuities such as shock waves are absent. At the subsonic entrance of the nozzle the flow enters with uniform conditions.

Summing up we are dealing with an isentropic and isenthalpic flow which is governed by the full-potential equation:

$$(a^2 - u^2)\Phi_{xx} - 2uv\Phi_{xy} + (a^2 - v^2)\Phi_{yy} = 0, \quad (8.92)$$

with

$$(u, v) = \nabla\Phi. \quad (8.93)$$

The geometry of the Laval nozzle is shown in figure 8.5; only the upper part of the nozzle

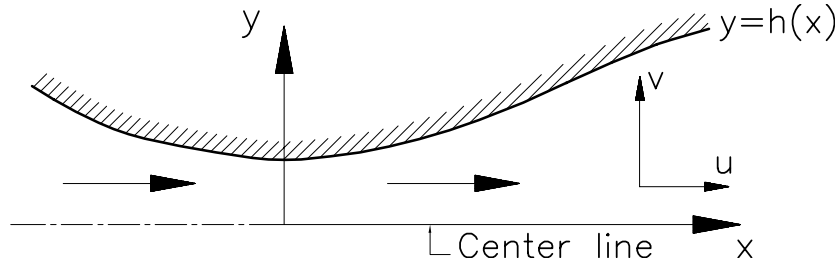


Figure 8.5: Upper part of the symmetric Laval nozzle

contour is depicted because we have assumed a symmetric nozzle configuration. Now we introduce the reference frame (x, y) with the x -axis on the center line of the nozzle. The origin of the (x, y) -system is taken at the *sonic* point on the center line. At this particular point, let the velocity components u and v take the values $u = u^*$ and $v = v^*$. Note that for reasons of symmetry $v^* = 0$, hence u^* is the local sound speed at the origin where the flow is sonic. This specific value of the sound speed is referred to as a^* . So at the origin we may write $u = u^* = a^*$, $v = v^* = 0$.

In order to attain the details of the flow in the transition region we will assume that the flow is a combination of a *uniform* flow ($u = a^*$, $v = 0$) in x -direction and a non-uniform

velocity field $u'(x, y)$, $v'(x, y)$ superimposed on it. Then the velocity field may be written as

$$u(x, y) = a^* + u'(x, y) \quad (8.94)$$

$$v(x, y) = v'(x, y) \quad (8.95)$$

When taken in the neighbourhood of the throat, the perturbation terms $u'(x, y)$ and $v'(x, y)$ are small compared to the sonic sound speed a^* , so that

$$\frac{u'}{a^*} \ll 1 \quad \text{and} \quad \frac{v'}{a^*} \ll 1. \quad (8.96)$$

The transonic throat problem is conceived as a small perturbation of a uniform sonic flow. A perturbation potential $\phi(x, y)$ may be introduced by

$$\Phi(x, y) = a^* (x + \phi(x, y)). \quad (8.97)$$

The perturbation velocities $u'(x, y)$ and $v'(x, y)$ expressed in terms of the perturbation potential become

$$\begin{aligned} u'(x, y) &= a^* \phi_x \\ v'(x, y) &= a^* \phi_y \end{aligned}$$

So ϕ_x and ϕ_y may be seen as dimensionless velocities.

Let us now rewrite the full potential equation (8.92) in terms of u' , v' and the perturbation potential $\phi(x, y)$. The sound speed a may be also expressed in u' and v' ; take the energy equation in the form of equation (8.22) and evaluate the constant at sonic conditions where $u = a^*$ and $v = v^* = 0$:

$$\frac{a^2}{\gamma - 1} + \frac{u^2 + v^2}{2} = \frac{(\gamma + 1)(a^*)^2}{2(\gamma - 1)} \quad (8.98)$$

Now the following expressions can be obtained in a straightforward manner:

$$\left(\frac{a}{a^*} \right)^2 = 1 - \frac{\gamma - 1}{2} (2\phi_x + \phi_x^2 + \phi_y^2), \quad (8.99)$$

$$\frac{a^2 - u^2}{(a^*)^2} = -\frac{\gamma + 1}{2} \left(2\phi_x + \phi_x^2 + \frac{\gamma - 1}{\gamma + 1} \phi_y^2 \right), \quad (8.100)$$

$$\frac{a^2 - v^2}{(a^*)^2} = 1 - \frac{\gamma + 1}{2} \left(\frac{2(\gamma - 1)}{\gamma + 1} \phi_x + \frac{2(\gamma - 1)}{\gamma + 1} \phi_x^2 + \phi_y^2 \right). \quad (8.101)$$

When these expressions are used in the full potential equation, the dominant terms are obtained as

$$-(\gamma + 1)\phi_x \phi_{xx} - 2\phi_y \phi_{xy} + \phi_{yy} + \text{H.O.T.} = 0 \quad (8.102)$$

Equation (8.102) is a second-order P.D.E. for the perturbation potential $\phi(x, y)$. A solution $\phi(x, y)$ is sought in the form of a series expansion in even powers of y :

$$\phi(x, y) = f(x) + g(x)y^2 + h(x)y^4 + \mathcal{O}(y^6). \quad (8.103)$$

To make $\phi(x, y)$ an even function of y is just a consequence of the symmetry of the flow problem. The functions $f(x)$, $g(x)$ and $h(x)$ have to be determined so that equation (8.102) is satisfied to a certain order. A possible solution, valid in the neighbourhood of $x = 0$, is:

$$\begin{aligned} f(x) &= \frac{1}{2}kx^2 + \mathcal{O}(x^3), \\ g(x) &= \frac{\gamma+1}{2}k^2x + \mathcal{O}(x^2) \\ h(x) &= \frac{(\gamma+1)^2}{24}k^3 + \mathcal{O}(x) \end{aligned} \quad (8.104)$$

where k is a free parameter which will be determined later when the contour of the nozzle wall is discussed. Combining equations (8.103) and (8.104), the solution for $\phi(x, y)$ valid near the sonic point reads:

$$\begin{aligned} \phi(x, y) = & \left(\frac{1}{2}kx^2 + \mathcal{O}(x^3) \right) + \left(\frac{\gamma+1}{2}k^2x + \mathcal{O}(x^2) \right) y^2 + \\ & \left(\frac{(\gamma+1)^2}{24}k^3 + \mathcal{O}(x) \right) y^4 + \mathcal{O}(y^6). \end{aligned} \quad (8.105)$$

When omitting the higher order terms $\mathcal{O}(x^3)$, $\mathcal{O}(x^2)y^2$, $\mathcal{O}(x)y^4$ and $\mathcal{O}(y^6)$ this solution satisfies exactly the P.D.E.:

$$-(\gamma+1)\phi_x\phi_{xx} + \phi_{yy} = 0. \quad (8.106)$$

The term $\phi_x\phi_{xy}$ in equation (8.102) appears to be a higher order term as well!

From equation (8.105) the velocity field near $x = 0$, $y = 0$ may be obtained as

$$u = a^*(1 + kx\frac{\gamma+1}{2}k^2y^2) + \mathcal{O}(x^2, xy^2, y^4), \quad (8.107)$$

$$v = a^*\left((\gamma+1)k^2xy + \frac{(\gamma+1)^2}{6}k^3y^3\right) + \mathcal{O}(x^2y, xy^3, y^5). \quad (8.108)$$

Observe that along the center line, where $y = 0$, we have $v = 0$ and $u = a^* \cdot (1 + kx + \mathcal{O}(x^2))$. If $k > 0$ then $u < a^*$ for $x < 0$ and $u > a^*$ for $x > 0$. Obviously the origin is sonic and $k > 0$ implies transition from the subsonic to the supersonic region. Using the velocity field just obtained in equations (8.107) and (8.108), the sonic line where $M = 1$ (or $u^2 + v^2 = (a^*)^2$) may be found as:

$$x_{\text{sonic line}} = -\frac{\gamma+1}{2}ky^2 + \mathcal{O}(y^4). \quad (8.109)$$

The sonic line has a parabolic shape; for $k > 0$ it runs upstream ($x < 0$) if $y \neq 0$, see figure 8.6.

Observe the difference with *one-dimensional theory* which predicts the sonic line as a line $x = \text{constant}$. Another aspect of interest is the curve where the flow is parallel to the x -axis, so where $v = 0$. From equation (8.108) we obtain two solutions: the trivial solution $y = 0$ and the non-trivial one:

$$v = 0 : \quad x = -\frac{\gamma+1}{6}ky^2 + \mathcal{O}(y^4). \quad (8.110)$$

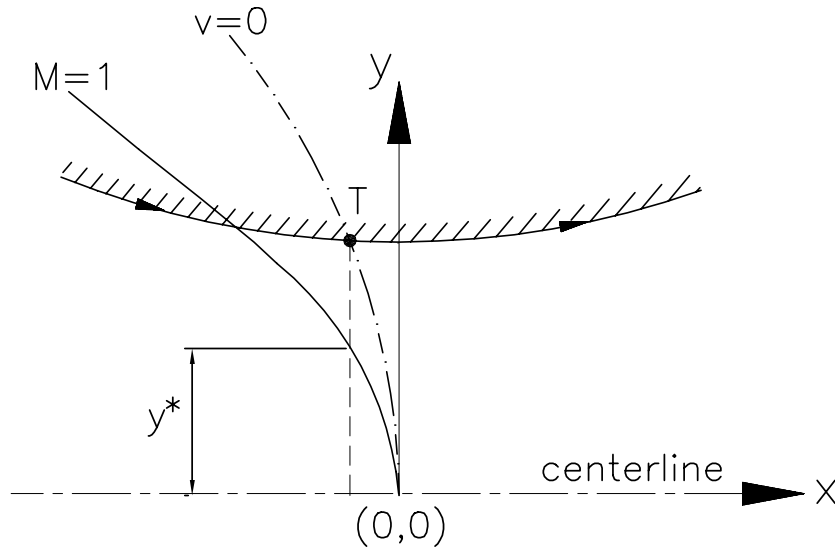


Figure 8.6: Two-dimensional flow in the throat of a Laval nozzle ($k > 0$).

Similar to the sonic line, the $v = 0$ curve is also a parabola running upstream ($x < 0$) if $y \neq 0$, see figure 8.6. Across the $v = 0$ curve the v -component changes sign: upstream of this curve v is negative, downstream v is positive.

This implies a streamline behaviour as sketched qualitatively in figure 8.6. In inviscid flow theory every streamline may be viewed as a solid wall. So we observe now a converging-diverging channel with a throat at $v = 0$! Now take a particular streamline and call the point in the throat as point T . For a prescribed height of the throat y_T the x location of the throat follows from equation (8.110) as

$$x_T = -\frac{\gamma + 1}{6}ky_T^2. \quad (8.111)$$

At this x -location the sonic line has the height y^* ; with equation (8.109) it can be calculated from

$$x_T = -\frac{\gamma + 1}{6}k(y^*)^2. \quad (8.112)$$

The ratio between the height of the throat y_T and the location of the sonic point in the throat is now found to be

$$\frac{y^*}{y_T} = \frac{1}{3}\sqrt{3} \approx 0.577. \quad (8.113)$$

In a two-dimensional planar nozzle the throat appears to be partially subsonic (near and on the center line) and partially supersonic (near the wall contour). There appears only one sonic point in the throat; this is in contrast with the one-dimensional theory, which predicts an entirely sonic throat!

Shape of the wall contour

The transonic throat problem just solved in equation (8.107) and (8.108) still contains the unknown parameter k . When considering the velocity distribution along the center line:

$$u(x, 0) = a^* \cdot (1 + kx + \mathcal{O}(x^2)), \quad (8.114)$$

k can be interpreted physically as the first derivative in streamline direction of the dimensionless velocity u/a^* :

$$\left(\frac{\partial u}{\partial x} \right)_{u=a^*} = a^* k, \quad (8.115)$$

taken at the sonic point: $u = a = a^*$. This is just an interpretation in terms of a local variable and not yet in terms of global variables such as the geometry of the Laval nozzle. To find such a relationship let us calculate the shape of an arbitrary streamline.

Streamlines in the throat area of the nozzle are solutions of the ordinary differential equation

$$\begin{aligned} \frac{dy}{dx} &= \frac{v(x, y)}{u(x, y)} \\ &= \frac{(\gamma + 1)k^2xy + \frac{(\gamma+1)^2}{6}k^3y^3 + \mathcal{O}(x^2y, xy^3, y^5)}{1 + kx + \frac{\gamma+1}{2}k^2y^2 + \mathcal{O}(x^2, xy^2, y^5)}. \end{aligned} \quad (8.116)$$

Now we attempt to find the shape of that particular streamline that forms a throat at $T(x_T, y_T)$, see figure 8.6. Since $u(x, y)$ and $v(x, y)$ are almost known approximately it is not possible to find the exact shape of the streamline. Only an approximation that is consistent with the order estimation of $u(x, y)$ and $v(x, y)$ can be obtained.

The streamline going through y_T is a perturbation of the streamline $y = y_T$ being the unperturbed streamline of the uniform sonic flow ($u = a^*, v = 0$) going through T . Obviously in this unperturbed flow the flow direction is zero everywhere. In the perturbed situation the streamline going through T attains its minimum y -value at T and therefore it may be approximated by the expression

$$y - y_T = \alpha(x - x_T)^2 + H.O.T. \quad (8.117)$$

The coefficient α can be determined by requiring that (8.117) is an approximate solution of the streamline equation (8.116). This yields:

$$y - y_T = (\gamma + 1) \frac{k^2ky_T}{2} (x - x_T)^2 + H.O.T. \quad (8.118)$$

Since every inviscid streamline may be replaced by a solid wall, (8.118) gives an expression for the wall contour of a converging-diverging nozzle with a throat height $y_T = H$. The local parameter k is related to the radius of curvature R of the wall contour at the throat.

From (8.118) the radius of curvature of the nozzle contour follows as

$$\frac{1}{R} = (\gamma + 1)k^2H. \quad (8.119)$$

Remember that the parameter k is a measure for the streamline velocity gradient $\frac{\partial}{\partial x}(u/a^*)$ at the throat. Combining (8.115) and (8.119) we get the result

$$\frac{\partial}{\partial x} \left(\frac{u}{a^*} \right) = \pm \sqrt{\frac{1}{RH(\gamma + 1)}}. \quad (8.120)$$

The streamwise velocity gradient in the throat depends on the radius of the curvature and on the height of the throat; two parameters very typical for the throat geometry! A small throat height and a highly curved nozzle contour result into a high velocity gradient in the throat.

The flow properties and especially the velocity distribution in the Laval nozzle may now be obtained in a non-dimensional form if x/H and y/H are used as spatial variables. Furthermore, if k is expressed in terms of the throat height H and the radius of curvature R then the expressions, originally presented by Oswatitch and Rothstein are obtained:

$$\frac{u}{a^*} = 1 + \sqrt{\frac{H}{R}} \frac{1}{\sqrt{\gamma+1}} \left(\frac{H}{R}\right) \left(\frac{x}{H}\right) + \frac{1}{2} \left(\frac{H}{R}\right) \left(\frac{y}{H}\right)^2 \quad (8.121)$$

$$\frac{v}{u^*} = \left(\frac{H}{R}\right) \left(\frac{x}{H}\right) \left(\frac{y}{H}\right) + \frac{\sqrt{\gamma+1}}{6} \left(\frac{H}{R}\right)^{\frac{1}{2}} \left(\frac{y}{H}\right)^3 \quad (8.122)$$

Observe the appearance of the dimensionless parameter H/R in this representation of the velocity field.

8.4.1 Mass flow through a two-dimensional nozzle

Consider the mass flow through the upper half of a symmetric nozzle having a throat height H and a nozzle wall curvature R , see figure 8.7.

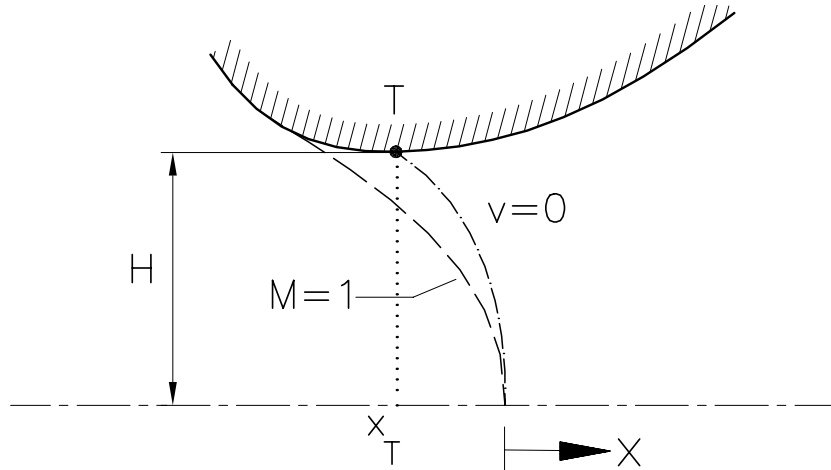


Figure 8.7: Two-dimensional nozzle

The mass flow through the throat at $x = x_T$ is defined as

$$\dot{m} = \int_0^H \rho u \, dy = \rho^* a^* \int_0^H \frac{\rho}{\rho^*} \frac{u}{a^*} \, dy \quad (8.123)$$

where $\rho u(x, y) = \rho u(x_T, y)$. From equation (8.107):

$$\frac{u}{a^*} = 1 + \frac{u'}{a^*} = 1 + kx + \frac{\gamma+1}{2} k^2 y^2 + H.O.T.$$

The ratio ρ/ρ^* follows from

$$\begin{aligned}\rho/\rho^* &= \left(\frac{a}{a^*}\right)^{\frac{2}{\gamma-1}} \\ &= \left\{1 - \frac{\gamma-1}{2} \left(2\frac{u'}{a^*} + \left(\frac{u'}{a^*}\right)^2 + \left(\frac{v'}{a^*}\right)^2\right)\right\}^{\frac{1}{\gamma-1}}.\end{aligned}$$

Since $\frac{u'}{a^*}$ and $\frac{v'}{a^*}$ are small with respect to one, a binomial expression ¹ can be applied to get the result:

$$\frac{\rho}{\rho^*} = 1 - \frac{u'}{a^*} - \frac{1}{2} \left(\frac{u'}{a^*}\right)^2 - \frac{1}{2} \left(\frac{v'}{a^*}\right)^2 + \frac{2-\gamma}{2} (u')^2 + H.O.T.$$

The mass flux ρu may be approximated as

$$\begin{aligned}\frac{\rho u}{\rho^* u^*} &= \left(1 + \frac{u'}{a^*}\right) \left(1 - \frac{u'}{a^*} - \frac{\gamma-1}{2} \left(\frac{u'}{a^*}\right)^2 - \frac{1}{2} \left(\frac{v'}{a^*}\right)^2 + \dots\right) \\ &= 1 - \frac{\gamma+1}{2} \left(\frac{u'}{a^*}\right)^2 - \frac{1}{2} \left(\frac{v'}{a^*}\right)^2 + \dots\end{aligned}$$

Inserting $\frac{u'}{a^*}$ and $\frac{v'}{a^*}$ from (8.107) and (8.108) and taking into account the proper order estimation, we find:

$$\frac{\rho u}{\rho^* u^*} = 1 - \frac{\gamma+1}{2} \left\{ k^2 x^2 + k^3 (\gamma+1) x y^2 + \left(\frac{\gamma+1}{2}\right)^2 k^4 y^4 \right\}. \quad (8.124)$$

The mass flow through the nozzle follows by integrating the mass flux ρu along the nozzle height at the throat where $x = x_T$; x_T itself is a function of the throat height H and the radius of curvature R :

$$x_T = -\frac{\gamma+1}{6} k H^2 = -\frac{H}{6} \sqrt{\gamma+1} \sqrt{\frac{H}{R}}. \quad (8.125)$$

The mass flow through a two-dimensional nozzle with throat height H and radius of curvature R may now be written as

$$\dot{m}_{2D} = \rho^* a^* H \left(1 - \frac{H^2}{R^2} \frac{\gamma+1}{90}\right). \quad (8.126)$$

Notice the difference with the mass flow according to the one-dimensional theory which predicts:

$$\dot{m}_{1D} = \rho^* a^* H. \quad (8.127)$$

There is a two-dimensional effect which reduces the mass flow with an amount that increases with the ratio H/R , see figure 8.8. For example: at $H/R = 1$ the mass flow reduction is 2.66 % but as $H/R = 4$ a mass flow reduction of 42.66 % has to be accepted.

¹Binomial expansion of $(1+\varepsilon)^\alpha = 1 + \alpha\varepsilon + \alpha(\alpha-1)\frac{\varepsilon^2}{2!} \dots$

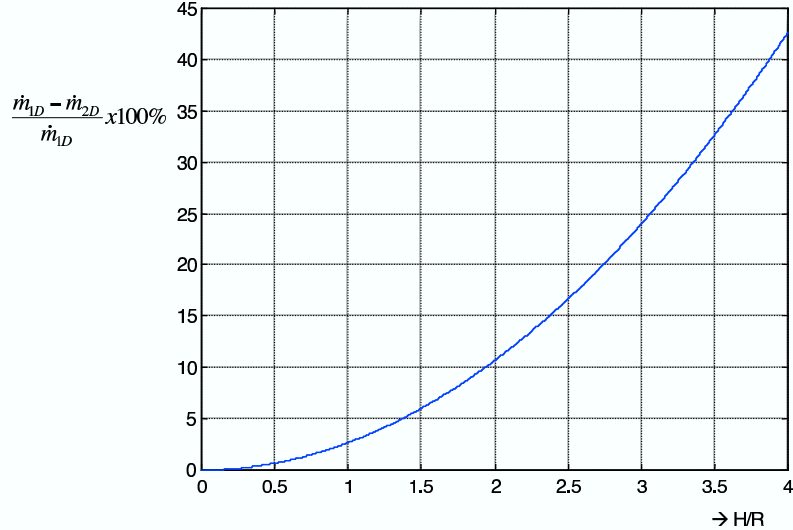


Figure 8.8: Mass flow reduction in a two-dimensional nozzle

The reduction of the mass flow is a direct consequence of the variable mass flux ρu in the throat. The mass flux distribution in the throat can be obtained from equation (8.124) by taking $x = x_T = -\frac{\gamma+1}{6}H^2$; this yields:

$$\begin{aligned} \left(\frac{\rho u}{\rho^* u^*} \right)_{\text{throat}} &= 1 - \frac{(\gamma+1)^2}{72} k^4 (H^4 - 6H^2y + 9y^4) \\ &= 1 - \left(\frac{\gamma+1}{72} \right) \frac{(H^2 - 3y^2)^2}{H^2 R^2}. \end{aligned} \quad (8.128)$$

A sketch of the mass flux distribution (according to equation (8.128)) is given in figure 8.9.

Observe that the mass flux attains its maximum one-dimensional value $\rho u = \rho^* a^*$ just at the sonic point ($y = y^* = H/\sqrt{3}$). At $y = 0$ (at the center line of the nozzle) the mass flux takes the value

$$(\rho u)_{\text{center line}} = \rho^* a^* \left(1 - \frac{\gamma+1}{72} \frac{H^2}{R^2} \right) \quad (8.129)$$

and at the nozzle wall $y = H$ we find a mass flux

$$(\rho u)_{\text{nozzle wall}} = \rho^* a^* \left(1 - \frac{4}{72} (\gamma+1) \frac{H^2}{R^2} \right) \quad (8.130)$$

The mass flux defect at the nozzle wall appears four times larger than that at the center line. Moreover, the subsonic part of the nozzle throat transports a higher amount of mass flow than the supersonic part does. This can be verified by calculating the mass ratio

$$\frac{\dot{m}_{\text{subsonic}}}{\dot{m}_{\text{total}}} = \frac{1}{\sqrt{3}} \frac{1 - \frac{\gamma+1}{135} \left(\frac{H}{R} \right)^2}{1 - \frac{\gamma+1}{90} \left(\frac{H}{R} \right)^2} \quad (8.131)$$

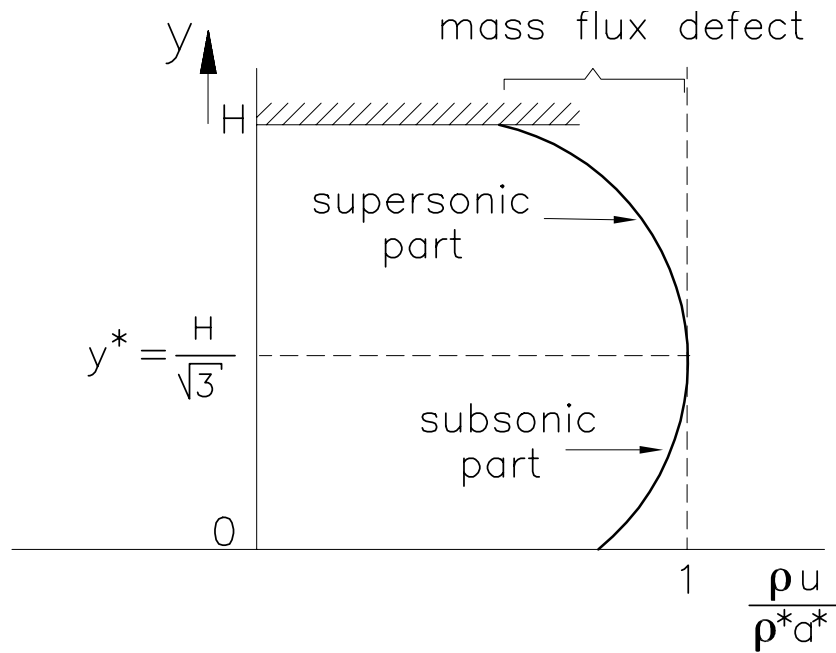


Figure 8.9: Mass flux distribution in the throat.

For example, if $H/R = 1$ the mass ratio takes a value 0.583 and if $H/R = 3$ this ratio becomes 0.639. Indeed the subsonic part of the throat transports a higher mass flow than the supersonic part does.

8.4.2 Literature on the subject

Relevant information on this subject can be found in the following references:

1. Oswatitsch & Rothstein: "Das Strömungsfield in einer Laval Düse", Deutsche Lufo I, 91-102, 1942.
2. Hall, I.M.: "Transonic Flow in Two-dimensional and Axi-Symmetric Nozzles", Quarterly Journal on Mechanics and Applied Mathematics 15, 487-508, 1962.
3. Oswatitsch, K.: "Spezialgebiete der Gasdynamik", Springer Verlag; pp. 94

Chapter 9

The 'first non linear' description of steady two dimensional supersonic flow

9.1 Inviscid Burgers equation

It is possible to derive an inviscid Burgers equation for simple waves in steady 2D supersonic flow. Let us assume that simple waves are created in the upper half plane by a bottom wall. This wall may have a more or less arbitrary shape but far upstream the wall is plane and parallel to the oncoming free stream with Mach number $M_\infty > 1$, see figure 9.1. We assume a homentropic and isenthalpic flow meaning that s and H are uniform. Above the wall a simple wave will be formed.

This created simple wave field is characterized by the condition that the invariant V^- is constant in the whole flow domain. Due to the uniformity of s and H this yields that

$$V^- = \nu + \varphi = \text{constant} = V_\infty^-, \quad (9.1)$$

hold in the whole field. This simple-wave field is still governed by the characteristic equation

$$\frac{\partial}{\partial x} (\nu - \varphi) + \tan(\varphi + \mu) \frac{\partial}{\partial y} (\nu - \varphi) = 0. \quad (9.2)$$

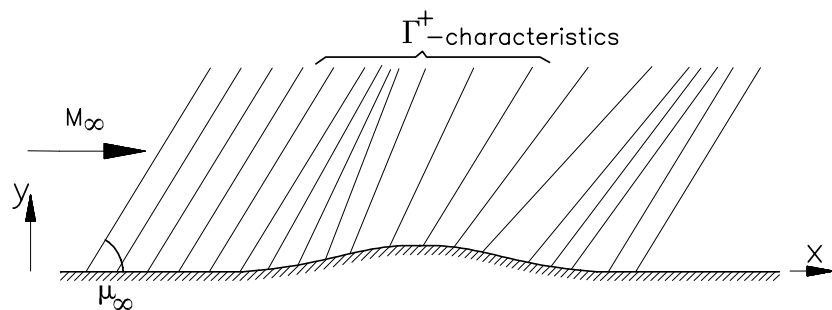


Figure 9.1: Simple waves created by a bottom wall in a supersonic flow

The invariant $V^+ = \nu - \varphi$ is constant along the Γ^+ characteristics having the slope $\frac{dy}{dx} = \tan(\varphi + \mu)$. But if this result is combined with the fact that $\nu + \varphi = \text{constant}$ everywhere it is clear that each variable ν or φ at its own is constant along Γ^+ ; and furthermore, $\nu = \text{constant}$ implies $\mu = \text{constant}$ and thus also the slope $\tan(\varphi + \mu)$ is constant along Γ^+ : the Γ^+ characteristics are straight lines.

From equation (9.1) it is obvious that in the simple wave domain the flow angle φ is only a function of the Mach number, formally written as

$$\varphi = V_\infty^- - \nu(M). \quad (9.3)$$

The function is monotonic in M because $\nu(M)$ is monotonic in M . But from equation (9.3) we must conclude that also the variables $(\nu - \varphi)$ and $\tan(\mu + \varphi)$ are purely monotonic functions of the Mach number M , thus formally written:

$$\nu - \varphi = 2\nu(M) - V_\infty^- = F(M), \quad (9.4)$$

and

$$\tan(\varphi + \mu(M)) = \tan(V_\infty^- - \nu(M) + \mu(M)) = V(M). \quad (9.5)$$

In principal it is now possible to eliminate the Mach number in (9.4) and (9.5) to obtain a direct expression for $(\nu - \varphi)$ in terms of $v = \tan(\varphi + \mu)$ yielding

$$(\nu - \varphi) = F^*(v) = F^*(\tan(\varphi + \mu)).$$

Equation (9.2) may be rewritten as:

$$\frac{\partial}{\partial x}(F^*(v)) + v \frac{\partial}{\partial y}(F^*(v)) = 0,$$

or

$$\frac{dF^*}{dv} \frac{\partial v}{\partial x} + v \frac{dF^*}{dv} \frac{\partial v}{\partial y} = 0. \quad (9.6)$$

Now get rid of $\frac{dF^*}{dv}$ in both terms of (9.6), yielding

$$\frac{\partial v}{\partial x} + v \frac{\partial v}{\partial y} = 0, \quad (9.7)$$

with $v = \tan(\varphi + \mu)$. Equation (9.7) is the desired form, it is the inviscid Burgers equation valid for simple waves (pointing upwards) in a two dimensional steady supersonic flow.

The characteristics of the Burgers equation

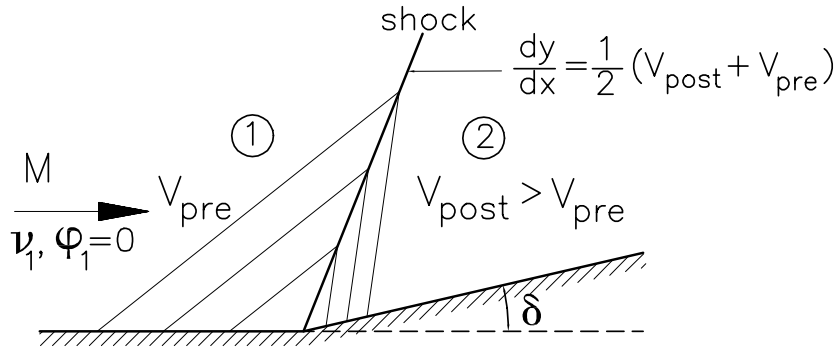
$$\frac{dy}{dx} = v = \tan(\varphi + \mu), \quad (9.8)$$

are just the Γ^+ characteristics in the simple wave.

In conservative form the inviscid Burgers equation becomes

$$\frac{\partial v}{\partial x} + \frac{\partial}{\partial y} \left(\frac{1}{2} v^2 \right) = 0. \quad (9.9)$$

This form is suitable in finding weak solutions to model discontinuities (see next section).

Figure 9.2: Shock formed at ramp with angle δ

9.2 Discontinuities of the inviscid Burgers equation

Equation (9.7) is applicable in the continuous part of the flow; once a shock is formed the solutions break down because the assumption that both entropy (s) and the invariant V^- are uniform is violated. For weak shocks however the error in the solution is small because shock jumps are of the order $(\Delta p)^3$.

Weak solutions of the Burgers equation in conservative form:

$$\frac{\partial v}{\partial x} + \frac{\partial}{\partial y} \left(\frac{1}{2} v^2 \right) = 0,$$

are given by

$$\left(\frac{dy}{dx} \right)_{\text{shock}} = \frac{[1/2v^2]}{[v]} = \frac{1}{2} (v_{\text{post}} + v_{\text{pre}}), \quad (9.10)$$

or in terms of $\varphi + \mu$:

$$\left(\frac{dy}{dx} \right)_{\text{shock}} = \frac{1}{2} \{ \tan(\varphi + \mu)_{\text{post}} + \tan(\varphi + \mu)_{\text{pre}} \}. \quad (9.11)$$

In words: the slope of the shock is the average of the slopes of the characteristics merging into the shock, see figure 9.2.

In this figure the supersonic flow along a ramp with ramp angle δ is considered. Upstream of the ramp there is a uniform supersonic flow with Mach number M_1 and corresponding Prandtl-Meyer angle ν_1 . Let the (x,y) -frame be chosen such that the flow angle $\varphi_1 = 0$. Referring to the simple wave condition (9.1) the flow properties downstream on the ramp are again uniform with Mach number M_2 , flow angle $\varphi_2 = \delta$ and Prandtl-Meyer angle $\nu_2 = \nu_1 - \delta$. Apparently $\nu_2 < \nu_1$ and therefore $M_2 < M_1$ and $\mu_2 > \mu_1$. The slope of the characteristics obey the inequality

$$\tan(\varphi_2 + \mu_2) > \tan(\varphi_1 + \mu_1),$$

or

$$v_{\text{post}} > v_{\text{pre}}.$$

Obviously the characteristics merge and terminate at the shock having the slope

$$\left(\frac{dy}{dx} \right)_{\text{shock}} = \frac{1}{2} \{ \tan(\varphi_2 + \mu_2) + \tan(\varphi_1 + \mu_1) \}.$$

Shock formation Shock formation appears if characteristics start to intersect. In order to study the shock formation process, consider an arbitrary non-linear distribution of $v(x, y)$ prescribed as boundary data along $y = 0$. Let the distribution be given by

$$v(x, 0) = v_B(x).$$

To find the location where the shock formation starts, consider an arbitrary point x_j and its neighbour $x_j + \Delta x$ on the line $y = 0$. The characteristics going through x_j and $x_j + \Delta x$ are given by:

$$y = v_B(x_j)(x - x_j),$$

and

$$y = v_B(x_j + \Delta x)(x - x_j - \Delta x),$$

respectively. Both characteristics intersect at (x_I, y_I) , for $\Delta x \rightarrow 0$ we find:

$$x_I - x_j = \frac{v_B(x_j)}{\left(\frac{dv_B}{dx}\right)_{x=x_j}} = \left(\frac{v_B}{v'_B}\right)_{x=x_j}, \quad y_I = \left(\frac{v_B^2}{v'_B}\right)_{x=x_j}. \quad (9.12)$$

Obviously, there are only intersecting characteristics in the upper half plane ($y > 0$) if $v'_B > 0$. Shock formation may be expected where $v_B(x)$ increases in streamwise direction. Equation (9.12) contains x_j being the x -location on the boundary value line ($y = 0$) of the characteristic running to (x_I, y_I) where neighbouring characteristics intersect.

Intersecting characteristics announce the possibility of shock development which really happens where y_I is minimal. This value of y_I is called y_s , the corresponding value of x_I is similarly called x_s . Let $x_{j_{min}}$ be the value of x_j where v_B^2/v'_B is minimal, then shock formation starts at (x_s, y_s) :

$$x_s - x_{j_{min}} = \left(\frac{v_B}{v'_B}\right), \quad y_s = \left(\frac{v_B^2}{v'_B}\right), \quad (9.13)$$

where $x_{j_{min}}$ has to be solved from

$$2v_B'^2(x_{j_{min}}) - v_B v''_B(x_{j_{min}}) = 0, \quad (9.14)$$

(primes indicate differentiation).

Example of a shock development Assume a boundary-value distribution $v_B(x)$ at $y = 0$ as follows

$$\begin{aligned} x < 0 & : v_B = 1, \\ 0 < x < 1 & : v_B = 1 + x, \\ x > 1 & : v_B = 2. \end{aligned}$$

Along interval $0 < x < 1$, $v_B(x)$ is increasing so that shock formation may be expected. Using equation (9.14) yields $x_{j_{min}} = 0$; shock formation starts at $(x_s, y_s) = (1, 1)$, see figure 9.3.

From the boundary value line ($y = 0$), $x < 0$, characteristics emanate and run into the upper half plane. They are parallel and have a slope $\frac{dy}{dx} = 1$; a uniform domain with $v(x, y) =$

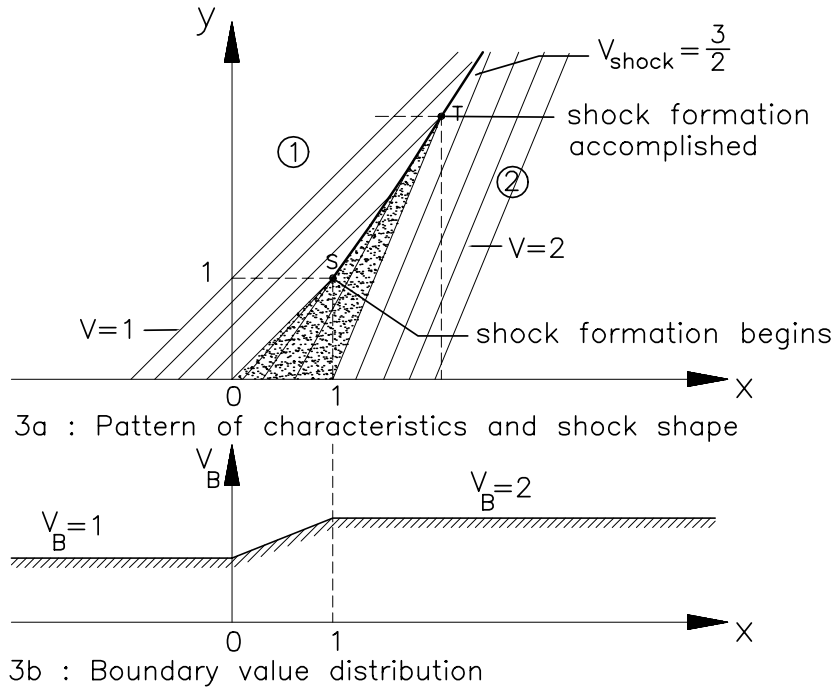


Figure 9.3: Shock formation process

constant($= 1$) results. If we further assume in domain ①a parallel flow with $\varphi_1 = 0$, then $v = 1$ implies a uniform supersonic flow with Mach number $M_1 = \sqrt{2}$ ($\tan \mu_1 = 1$).

The characteristics originating from $x > 1$, $y = 0$ are also parallel, they have a slope $\frac{dy}{dx} = 2$. A uniform domain ②is formed with $M_2 = 1.19$ and $\varphi_2 = 5.9^\circ$. In the shaded area between domains ①and ②characteristics converge, the flow variables are constant along a characteristic but they vary if one crosses a Γ^+ characteristic, so a real simple wave is formed. All characteristics terminate at the shock, the characteristics in domain ①terminate at the front part of the shock, those in the shaded area and in domain ②terminate at the rear part of the shock.

Let us try to find the shock shape from the O.D.E.

$$\left(\frac{dy}{dx} \right)_{\text{shock}} = \frac{1}{2} (v_{\text{post}} + v_{\text{pre}}).$$

Take an arbitrary point (x, y) on the shock, then

$$\begin{aligned} v_{\text{pre}} &= 1, \\ v_{\text{post}} &= v_B \left(x - \frac{y}{v_{\text{post}}} \right). \end{aligned}$$

For the *curved part* of the shock the expression for v_{post} becomes

$$v_{\text{post}} = 1 + x - \frac{y}{v_{\text{post}}},$$

or

$$v_{\text{post}}^2 - v_{\text{post}}(1 + x) + y = 0. \quad (9.15)$$

The O.D.E. that has to be solved becomes

$$\frac{dy}{dx} = \frac{1}{2} (1 + v_{\text{post}}), \quad (9.16)$$

where v_{post} is determined by equation (9.15).

The boundary condition that has to be satisfied is: $v_{\text{post}} = 1$ at $(x, y) = (1, 1)$; this condition guarantees that the shock starts to develop at the point $(x_s, y_s) = (1, 1)$ with the correct slope $\frac{dy}{dx} = 1$.

The solution procedure will be accomplished in two steps; in the first step v_{post} will be determined as a function of x , in the second step the R.H.S. of equation (9.16) is then a known function of x and integral calculus enables us to find the shock shape $y_s = y_s(x)$.

In order to set up the first step, equation (9.15) has to be differentiated w.r.t. x , this yields (using $v_p = v_{\text{post}}$)

$$2v_p \frac{dv_p}{dx} - (1 + x) \frac{dv_p}{dx} - v_p + \frac{dy}{dx} = 0.$$

The shock slope $\frac{dy}{dx}$ can be eliminated from equation (9.16) and expressed in terms of the variable v_p . Then the post shock value of v (i.e. v_p) is found as the solution of the O.D.E

$$\frac{dv_p}{dx} = \frac{v_p - 1}{2(2v_p - 1 - x)}, \quad (9.17)$$

with boundary condition: $x = 1, v_p = 1$.

The solution for $x > 1$ is the linear graph

$$v_p = \frac{3x + 1}{4}. \quad (9.18)$$

Shock development is accomplished when $v_p = 2$. This happens at $x = 7/3$. The shape of the shock follows from the O.D.E. (equation(9.16))

$$\frac{dy}{dx} = \frac{1}{2} \left(1 + \frac{3x + 1}{4} \right) = \frac{5 + 3x}{8}.$$

Taking into account the boundary conditions $x_s = 1, y_s = 1$ the shock shape is found as

$$y_{\text{shock}} = \frac{1}{16} (3x^2 + 10x + 3). \quad (9.19)$$

It is a parabolic curve that steepens when moving downstream until $x = \frac{7}{3}, y = \frac{8}{3}$. Here the shock formation is accomplished; point T in figure 9.3. For $x > \frac{7}{3}$ the shock maintains a constant slope $\frac{dy}{dx} = 2$.

As in the unsteady case the shock strength is measured as the difference $\Delta v = v_{\text{post}} - v_{\text{pre}}$. The shock strength varies along the shock curve as

$$\Delta v = \frac{3}{4} (x - 1),$$

which shows that the shock strengthens linearly from $\Delta v = 0$ at $x = 1$ to $\Delta v = 1$ at $x \geq \frac{7}{3}$. Streamlines in the steady two dimensional flow field are governed by the equation

$$\left(\frac{dy}{dx} \right)_{\text{streamline}} = \tan \varphi.$$

Writing $\tan \varphi = \tan(\varphi + \mu - \mu)$, the streamline equation can be arranged into

$$\left(\frac{dy}{dx} \right)_{\text{streamline}} = \frac{\beta v - 1}{\beta + v}, \quad (9.20)$$

where $\beta = \sqrt{M^2 - 1} = \cot \mu$.

Equation (9.20) is hard to solve, at least analytically because β is a complicated expression in terms of the variable v and v itself depends on x and y according to:

$$v(x, y) = v_B \left(x - \frac{y}{v} \right) = 1 + x - \frac{y}{v},$$

leading to

$$v^2 - v(1 + x) + y = 0, \quad (9.21)$$

valid in the simple wave region.

On a particular streamline, y depends on x and with equation (9.21) also v depends on x . The v distribution along a streamline satisfies the O.D.E. (differentiate equation (9.21) w.r.t. x !)

$$2v \frac{dv}{dx} - (1 + x) \frac{dv}{dx} - v \frac{dy}{dx} = 0.$$

Now $\frac{dy}{dx}$ can be substituted from equation (9.20) yielding

$$\left(\frac{dv}{dx} \right)_{\text{streamline}} = \frac{1 + v^2}{(\beta + v)(2v - 1 - x)}. \quad (9.22)$$

This expression, when solved, yields the v -distribution along a streamline.

In order to detect the course of a particular streamline, e.g. the extension of the streamline that starts in domain ① at level $y = h$, into the simple wave, we have to apply one of the following boundary conditions:

$$\begin{aligned} - & \text{ underneath } s & : & v = 1 (\beta = 1) , \quad x = h, \\ - & \text{ behind curved part of shock} & : & v = \frac{3x+1}{4} , \quad 16h = 3x^2 + 10x + 3. \end{aligned} \quad \left. \right\} \quad (9.23)$$

Once $v(x)$ is determined from equation (9.22) then *essentially* $\beta(x)$ is known along the streamline and equation (9.20) can be integrated yielding the shape of the streamline in the simple wave domain.

For the particular problem, defined in figure 9.3, with oncoming flow properties: $\beta = 1$, $v = 1$, the characteristic variable v lies in the interval $1 \leq v \leq 2$. The flow variable $(\beta + v)$ in equation (9.22) may be approximated as

$$(\beta + v) \approx (\beta + v)_a = 2 + \frac{(v - 1)}{2} + \frac{(v - 1)^2}{10}.$$

Although, the comparison with the exact value (see figure 9.4) shows a fair agreement, its use in equation (9.22) does not help that much than an analytical solution of equation (9.22) could be found. Consequently, we have to resort to numerical integration of the equations (9.22) and (9.20) finally.

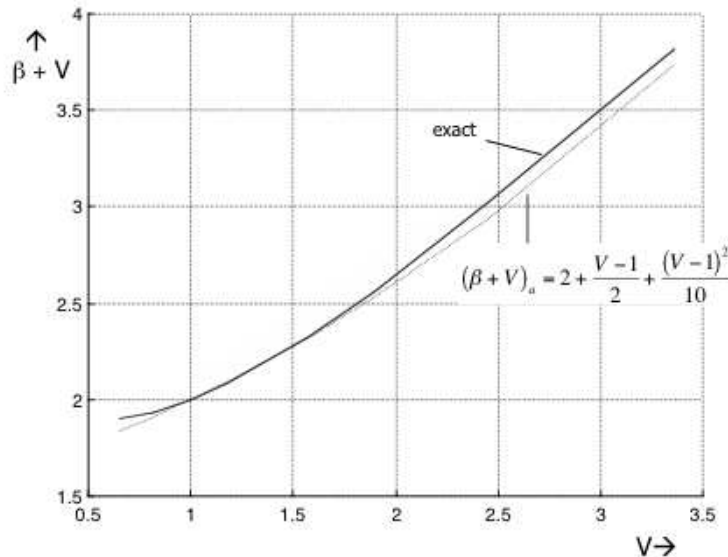


Figure 9.4: Approximation of $\beta + v$ in the neighbourhood $\beta = 1, v = 1$

9.3 Shock pattern created by a biconvex airfoil

A biconvex airfoil with symmetrical shape, a sharp leading edge (L.E.) and a sharp trailing edge (T.E.) is placed in a uniform supersonic flow (Mach number M_∞) at zero incidence ($\alpha = 0$), as shown in figure 9.5. Only the upper half of the flow is shown.

The strength of the shocks are assumed sufficiently weak, they are attached to the edges of the airfoil so that simple wave theory, e.g. presented by the inviscid Burgers equation is applicable. Using the simple wave conditions (see equation (9.1)):

$$V_\infty^- = \nu + \varphi,$$

the Prandtl-Meyer angle $\nu(x)$ along the airfoil contour $y = f(x)$ results. Once the distribution $\nu(x)$ is known also other variables as the Mach number $M(x)$, Mach angle $\mu(x)$ and characteristic direction $v(x)$ can be determined without much effort. Hence for a given airfoil contour the v -distribution on the contour: $v(x, f(x))$ is known and the (straight) characteristics emanating from the contour $y = f(x)$ can be drawn. A characteristic pattern results and shock appear if characteristics intersect.

To study the shock pattern let us consider the *inverse* problem where $v(x)$ is prescribed and the corresponding airfoil contour has to be derived. Furthermore we assume that $v(x)$ is prescribed on the x -axis ($y = 0$) rather than on the contour (yet unknown) itself. Since characteristics are straight lines and v is constant along a characteristic a simple extrapolation of the straight characteristic from airfoil contour onto the x -axis allows us to do so; see figure 9.6.

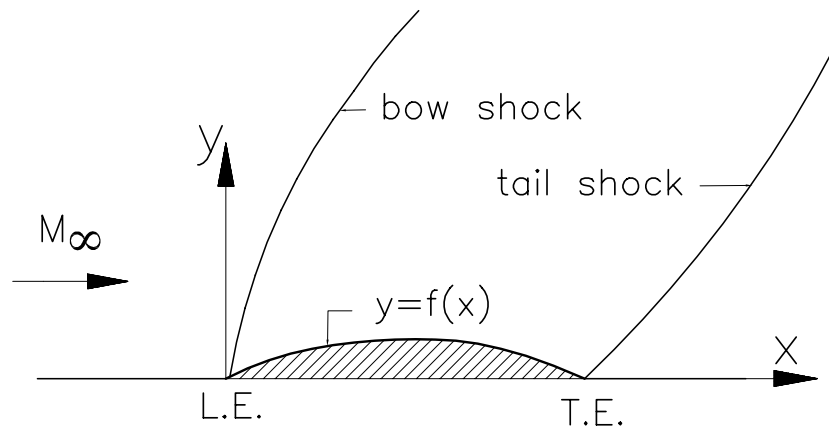
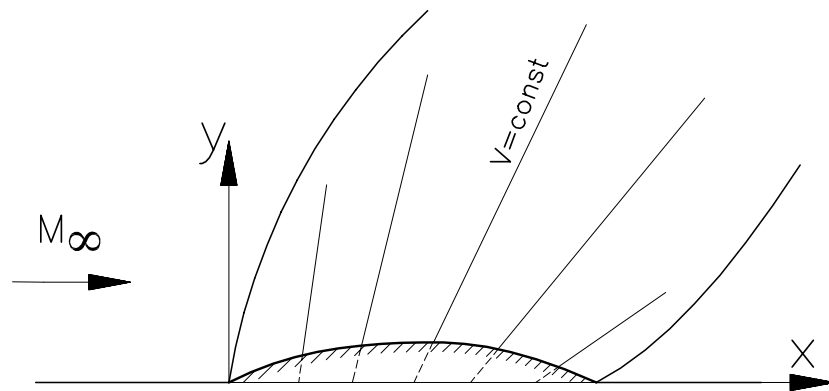


Figure 9.5: Shock pattern about a pointed airfoil

Figure 9.6: Projection of boundary data on x -axis

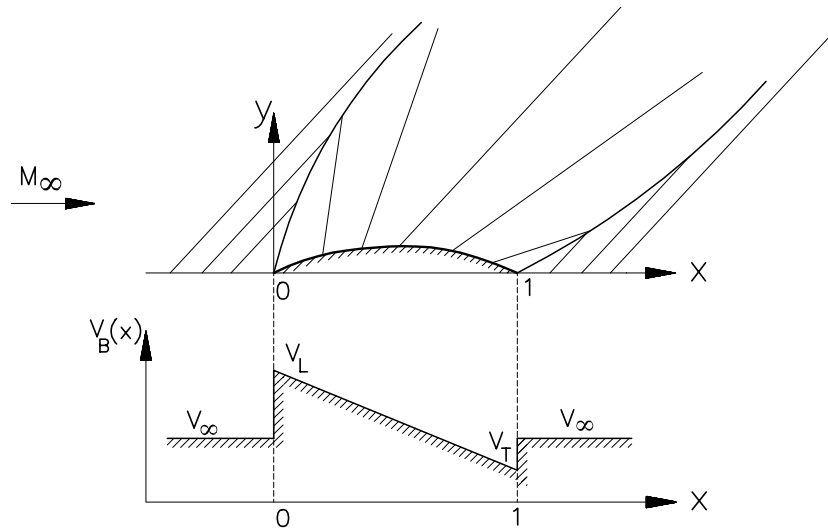


Figure 9.7: N-wave boundary value distribution at $y = 0$

By this procedure $v(x, f(x))$ on the contour is projected onto $y = 0$ resulting into a corresponding and equivalent distribution: $v_B(x)$ on $y = 0$. Thus $v_B(x)$ generates exactly the same wave pattern as the actual airfoil contour: $y = f(x)$, with prescribed $v(x, f(x))$ does. Consider the following boundary value distribution $v_B(x)$ at $y = 0$:

$$\left. \begin{array}{ll} x < 0 & v_B = v_\infty > 0, \\ 0 < x < 1 & v_B = v_L - (v_L - v_T)x, \\ x > 1 & v_B = v_\infty > 0, \end{array} \right\} \quad (9.24)$$

shown in figure 9.7 and being a typical N-wave.

In the oncoming uniform flow field all characteristics have the slope $v_\infty = \tan(\mu_\infty) > 0$. Across the leading edge shock the Mach number drops and the characteristic slope jumps to $v_L > v_\infty$. Over the airfoil the flow expands and v decreases linearly to $v_T < v_\infty$ being the pre-shock value of the trailing edge shock. Across the trailing edge shock v jumps to the free stream value v_∞ and keeps this value further downstream. The main objective is twofold; first find the shock wave pattern and its behaviour (e.g. shock delay) in the farfield ($y \rightarrow \infty$); secondly find the airfoil shape ($y = f(x)$) that generates that wave pattern.

Bow shock The bow shock shape is governed by the O.D.E.

$$\left(\frac{dy}{dx} \right)_{\text{shock}} = \frac{1}{2} (v_{\text{pre}} + v_{\text{post}}). \quad (9.25)$$

Take an arbitrary point (x, y) on the bow shock then,

$$\left. \begin{array}{lcl} v_{\text{pre}} & = & v_\infty, \\ v_{\text{post}} & = & v_B \left(x - \frac{y}{v_{\text{post}}} \right). \end{array} \right\} \quad (9.26)$$

Using equation (9.24) and the shorter notation $v_p = v_{\text{post}}$ there results

$$v_p(x, y) = v_L - (v_L - v_T) \left(x - \frac{y}{v_p(x, y)} \right),$$

or

$$v_p^2 - \{v_L - (v_L - v_T)x\} v_p = y(v_L - v_T). \quad (9.27)$$

The O.D.E. that has to be solved becomes

$$\left(\frac{dy}{dx} \right)_{\text{shock}} = \frac{1}{2} (v_\infty + v_p), \quad (9.28)$$

where v_p follows from equation (9.27).

The boundary conditions that must be fulfilled care that the bow shock starts at the leading edge, so at $(x, y,) = (0, 0)$, $v_p = v_L$. The solution procedure that results into the shock shape contains two steps; first v_p will be determined as a function of x , in the second step the R.H.S. of equation (9.28) is a known function of x and integral calculus enables us to get the shock shape $y_s = y_s(x)$. To set up the first step equation (9.27) is differentiated w.r.t. x , this yields

$$2v_p \frac{dv_p}{dx} - \{v_L - \Delta \cdot x\} \frac{dv_p}{dx} + \Delta \cdot v_p = \Delta \cdot \frac{dy}{dx},$$

here $\Delta = v_L - v_T$ being the total drop of v along the airfoil contour from leading edge to trailing edge. The shock slope may be substituted from equation (9.28). Then the v_p -distribution along the bow shock is governed by the O.D.E.:

$$\frac{dv_p}{dx} = \frac{\Delta (v_\infty - v_p)}{2(2v_p - v_L + \Delta \cdot x)}, \quad (9.29)$$

supplemented with the boundary conditions: $x = 0, v_p = v_L$. Standard solution techniques for O.D.E.'s teach us that the solution of equation (9.29) becomes

$$\frac{\Delta}{2} (v_p - v_\infty)^2 x + \frac{2v_p^3}{3} - \frac{v_p^2}{2} (2v_\infty + v_L) + v_p v_L v_\infty = \frac{v_L^3}{6}, \quad (9.30)$$

$v_p(x)$ is a monotonic *decreasing* function of x , see figure 9.8. For large x ($x \rightarrow \infty$) v_p approaches the free stream value v_∞ .

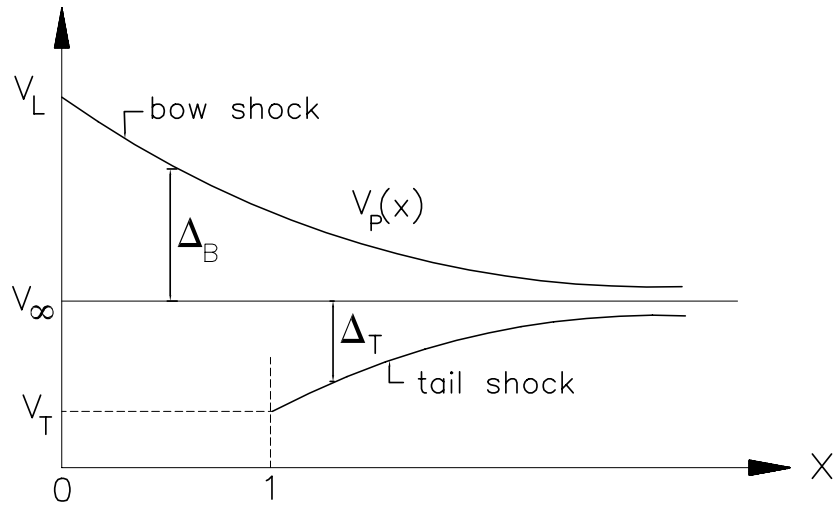
Let us define the strength of the bow shock by $\Delta_B = v_p - v_\infty$; figure 9.8 shows that the strength of the shock goes to zero for large x .

The asymptotic behaviour of the shock strength for $x \rightarrow \infty$ may be obtained from (9.30) as (take $v_p \rightarrow v_\infty$):

$$\frac{\Delta}{2} (\Delta_B)^2 x \propto \frac{v_L^3}{6} + \frac{v_\infty^3}{3} - \frac{v_L v_\infty^2}{2}.$$

Introducing the non-dimensional variables

$$\tilde{\Delta} = \frac{\Delta}{v_\infty}, \quad \tilde{\Delta}_B = \frac{\Delta_B}{v_\infty}, \quad \tilde{v}_L = \frac{v_L}{v_\infty},$$

Figure 9.8: Shock strength vs x

a suitable form follows

$$\tilde{\Delta}_B \propto (\tilde{v}_L - 1) \sqrt{\frac{2 + \tilde{v}_L}{3\tilde{\Delta}}} \sqrt{\frac{1}{x}}.$$

Since $\tilde{v}_L - 1$ can be interpreted as the non-dimensional shock strength at the leading edge the asymptotic behaviour of the shock strength gets the form:

$$\tilde{\Delta}_{B,x \rightarrow \infty} \propto \tilde{\Delta}_B(0) \sqrt{\frac{3 + \tilde{\Delta}_B(0)}{3\tilde{\Delta}}} \frac{1}{\sqrt{x}}. \quad (9.31)$$

So we observe shock decay with increasing x as $\frac{1}{\sqrt{x}}$.

The precise shock shape in the physical plane can be determined, at least in principle, by integrating equation (9.28) with $v_p(x)$ solved from equation (9.30). This is left as a homework exercise in numerical analysis.

Since $v_p(x)$ decreases monotonically to the limiting value $v_p = v_\infty$ at $x = \infty$, it is obvious that the shock has a curved shape with decreasing slope for increasing x . For $x \rightarrow \infty$ the shock attains the slope of the characteristics of the oncoming flow.

Tail shock The tail shock is determined by the O.D.E.

$$\left(\frac{dy}{dx} \right)_{\text{shock}} = \frac{1}{2} (v_{\text{pre}} + v_{\text{post}}). \quad (9.32)$$

If (x, y) is an arbitrary point on the tail shock then

$$\left. \begin{aligned} v_{\text{pre}} &= v_B \left(x - \frac{y}{v_{\text{pre}}} \right), \\ v_{\text{post}} &= v_\infty. \end{aligned} \right\} \quad (9.33)$$

Let us now compare this set of equations with those derived in (9.25) and (9.26) determining the bow shock. Evidently they are exactly the same! Both bow shock and tail shock are governed by the same O.D.E. namely equation (9.29). In case of the tail shock v_p refers to v_{pre} . Although bow and tail shock are governed by the same O.D.E. they have different shapes because their boundary conditions differ.

For the tail shock the boundary condition warrants that this shock starts at the trailing edge of the airfoil: $(x, y) = (1, 0)$, $v_p = v_T$. The solution of equation (9.29) that fulfills these boundary conditions reads:

$$\frac{\Delta}{2} (v_p - v_\infty)^2 x + \frac{2v_p^3}{3} - \frac{v_p^2}{2} (2v_\infty + v_L) + v_p v_L v_\infty = \frac{v_T^3}{6} + \frac{\Delta}{2} v_\infty^2, \quad (9.34)$$

where $v_p(x)$ is the pre-shock v -distribution along the tail shock.

$v_p(x)$ is monotonic increasing with x , for large x ($x \rightarrow \infty$) it approaches the free stream value v_∞ , see figure 9.8. The monotonic increase from $v_p = v_T$ to the limiting value $v_p = v_\infty$ (at $x \rightarrow \infty$) indicates a curved trailing edge shock with increasing slope for increasing x . For $x \rightarrow \infty$ the shock gets the slope of the characteristics of the free stream. Let the shock strength of the tail shock be defined as $\Delta_T = v_\infty - v_p$; from figure 9.8 we observe shock decay at larger distances from the airfoil.

Physically, shock decay is caused by the interaction of expansion characteristics emanating from the aft part of the airfoil with the trailing edge shock.

The asymptotic behaviour of the shock strength for $x \rightarrow \infty$ may be obtained from equation (9.34) as (take $v_p \rightarrow v_\infty$):

$$\frac{\Delta}{2} (\Delta_T)^2 x \propto \frac{v_T^3}{6} + \frac{v_\infty^3}{3} - \frac{v_T v_\infty^2}{2}.$$

Introducing the non-dimensional variables:

$$\tilde{\Delta} = \frac{\Delta}{v_\infty}, \quad \tilde{\Delta}_T = \frac{\Delta_T}{v_\infty}, \quad \tilde{v}_T = \frac{v_T}{v_\infty},$$

we find the form:

$$\tilde{\Delta}_T \propto (1 - \tilde{v}_T) \sqrt{\frac{2 + \tilde{v}_T}{3\tilde{\Delta}}} \frac{1}{\sqrt{x}}. \quad (9.35)$$

We observe shock decay with increasing x as $\frac{1}{\sqrt{x}}$; a result very similar to what happens with the bow shock (see equation (9.31)).

9.4 Wave interactions

As we have done in the unsteady 1-D case, the Burgers model for simple waves enables us to study non-linear wave interaction.

The biconvex airfoil, treated in section 9.3 is an example of this phenomenon. The bow wave is weakened due to the interaction with expansion waves that come from the front part of the airfoil; similarly the trailing edge shock wave is weakened by expansion waves coming from the aft part of the airfoil. In this section two other examples of wave interaction will be presented: shock-expansion interaction and the backward facing slope.

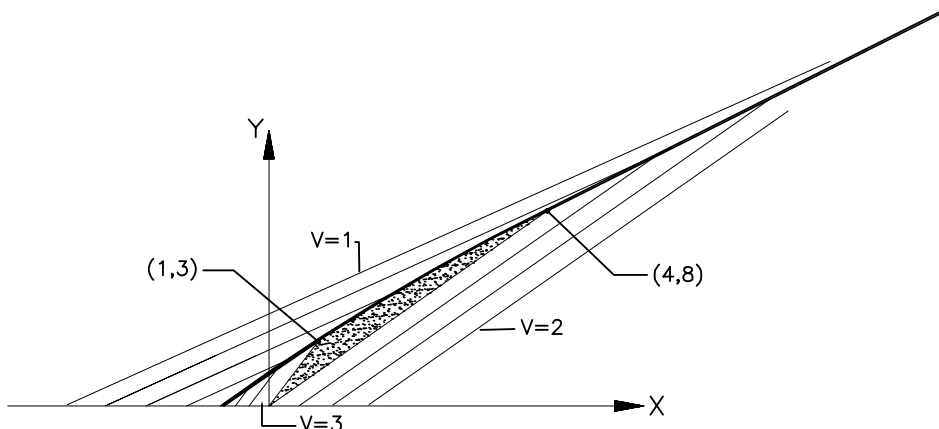


fig 9.9a : Shock and characteristics

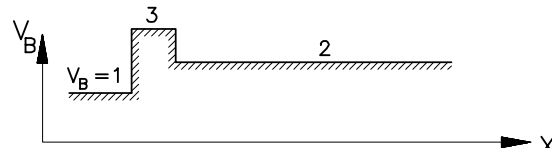


fig 9.9b : Boundary values

Figure 9.9: Shock-expansion interaction

9.4.1 Shock-expansion interaction

Assume boundary conditions on the x -axis: $v_B(x)$ given as:

$$\begin{aligned} x < -\frac{1}{2} & \quad v_B = 1, \\ -\frac{1}{2} < x < 0 & \quad v_B = 3, \\ x > 0 & \quad v_B = 2. \end{aligned}$$

This distribution represents a shock at $x = -\frac{1}{2}$ and a centered expansion at $x = 0$, see figure 9.9. The shock emanating from $x = -\frac{1}{2}$ has a slope $\frac{dy}{dx} = 2$. The first characteristic of the expansion fan hits the shock at $(1, 3)$. Then, for larger y , the shock gets curved. The shock shape is governed by the O.D.E.

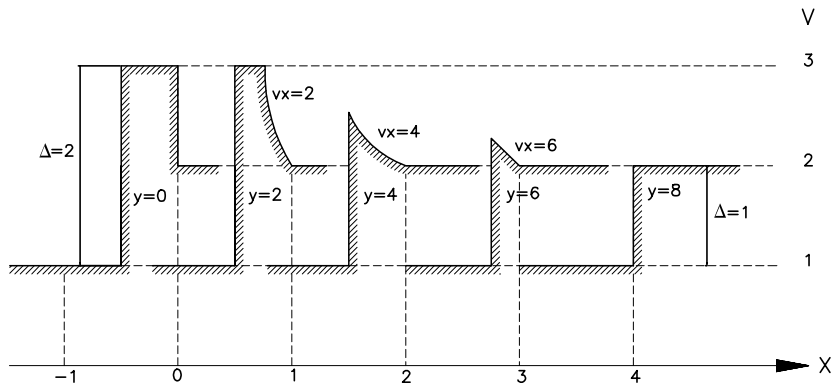
$$\left(\frac{dy}{dx} \right)_{\text{shock}} = \frac{1}{2} \left(1 + \frac{y}{x} \right),$$

supplemented with the boundary condition that it runs through $(x, y) = (1, 3)$. The solution that fulfills this boundary condition reads

$$y_s = 2\sqrt{x} + x.$$

The last characteristic of the fan ($v = 2$) hits the shock when the shock has the slope $\frac{dy}{dx} = \frac{3}{2}$. This happens at the point $(4, 8)$. For $x > 4$ the shock is straight keeping the slope $\frac{dy}{dx} = \frac{3}{2}$. The shock strength in the interval $1 \leq x \leq 4$ can be calculated as

$$\Delta = v_{\text{post}} - v_{\text{pre}} = \frac{2\sqrt{x} + x}{x} - 1 = \frac{2}{\sqrt{x}},$$

Figure 9.10: v distribution at different y levels

indicating shock decay from $\Delta = 2$ at $x = 1$ to $\Delta = 1$ at $x = 4$. The v -distribution at different y levels is drawn in figure 9.10.

The stronger shock with $\Delta = 2$ present at $y = 0$, is partially 'eaten' by the expansion, and a less stronger shock having $\Delta = 1$ remains at $y \geq 8$.

Notice the *non-linear* v decrease from $v = 3$ to $v = 2$. Its graph is the orthogonal hyperbolae: $vx = y$.

9.4.2 Backward facing slope

A uniform stream with Mach number 1.4 flows downhill of a 30° backward facing slope, then it is compressed back into the original direction, see figure 9.11. At the shoulder (O) a centered expansion appears which further downstream interacts with the shock wave generated at the compression corner (P). The free stream (domain ①) conditions with $\varphi_1 = 0$ are: $M_1 = 1.4$, $\mu_1 = 45.58^\circ$ and $v_1 = 1.020$. The flow conditions in the uniform domain ② along the backward facing slope may be calculated as $M_2 = 2.494$, $\mu_2 = 23.64^\circ$ and $v_2 = -0.111$. Downstream of the shock wave the flow is turned back to the original flow direction ($\varphi_3 = 0^\circ$), the flow conditions here (domain ③) are the same as those in domain ①(explain why?). To calculate the shock shape take the shoulder (O) as the origin of (x, y) coordinate system. The v distribution in the expansion fan then reads $v = \frac{y}{x}$.

The shock separating domains ② and ③ is straight and has a slope $\frac{dy}{dx} = \frac{1}{2}(v_2 + v_3) = 0.454$. It hits the last characteristic ($v = -0.111$) in the point Q $(3.161, -0.351)$. From this point a curved shock runs downstream. It is governed by the O.D.E.

$$\frac{dy}{dx} = \frac{1}{2} \left(\frac{x}{y} + v_3 \right) = \frac{1}{2} \left(\frac{x}{y} + 1.020 \right),$$

and it has to fulfill the boundary condition that it runs through the point Q .

The shock shape that satisfies all these requirements has the form:

$$y_s = A\sqrt{x} + Bx, \quad (x > x_Q),$$

with $A = -2.011$, $B = v_3 = 1.020$.

The shock strength becomes

$$\Delta = v_{\text{post}} - v_{\text{pre}} = v_3 - \frac{y}{x},$$

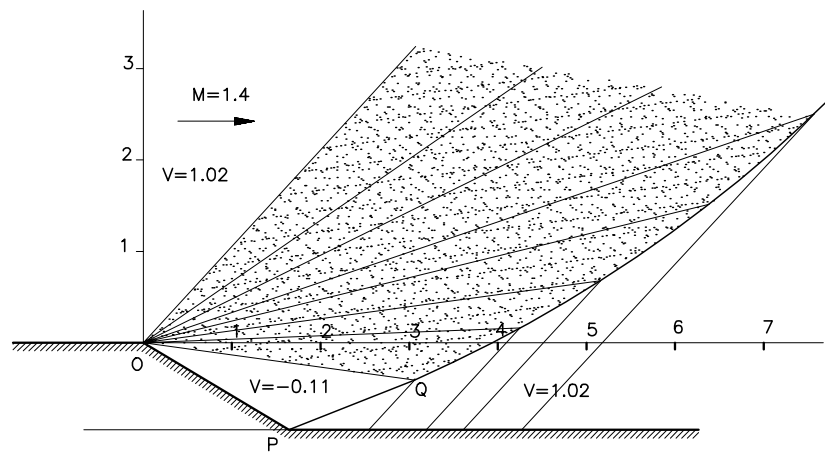


Figure 9.11: Flow downhill of a backward facing slope

or

$$\Delta = -\frac{A}{\sqrt{x}}.$$

The shock decays asymptotically to zero strength as $\frac{1}{\sqrt{x}}$.

Chapter 10

Steady one-dimensional viscous flow

10.1 Channel flow: assumptions and basic equations

If a gas travels with high speed through a channel of sufficient length the effects of viscosity and associated entropy change can not be neglected. We attempt to study these flows and suppose that the channel has a variable area $A(x)$, that the fluid is a perfect gas with constant specific heats and that the walls of the channel are perfectly insulated (adiabatic wall conditions). The flow will be treated as one-dimensional and friction in the boundary layer will be accounted for by assuming a tangential stress τ acting on the circumference, and which is modelled by

$$\tau = \frac{1}{2} f \rho v^2.$$

Here f is a friction coefficient, depending mainly on the Reynolds number Re . Experiments from Keenan and Neumann¹ teach us that for pipes having a length/diameter ratio $10 < L/D < 50$ and $25.000 < Re_D < 700.000$ that the friction coefficient takes the values:

$$\begin{aligned} f_{\text{average}} &\approx 0.003 - 0.0065 && \text{incompressible flow} \\ f_{\text{average}} &\approx 0.002 - 0.003 && \text{compressible flow onto } M = 3 \end{aligned}$$

Regarding turbulent incompressible flows Nikuradse has presented the implicit relation:

$$\frac{1}{\sqrt{4f}} = -0.8 + 2 \log(Re \sqrt{4f}).$$

In this chapter f is taken constant along the channel. Finally it is assumed that internal heat sources (combustion, chemical reaction, condensation etc.) are absent.

Gas flows satisfying the conditions just spelled out are governed by the following set of equations that appear when the conservation laws for mass, momentum and energy are applied onto the control volume V as shown in figure 10.1.

Continuity:

$$\frac{\partial}{\partial t} \iiint_V \rho \, dV + \iint_{\partial V} \rho \bar{v} \, ds = 0. \quad (10.1)$$

¹Keenan, J.H. and Neumann: Friction in pipes at supersonic velocities, NACA TN 963, 1945.

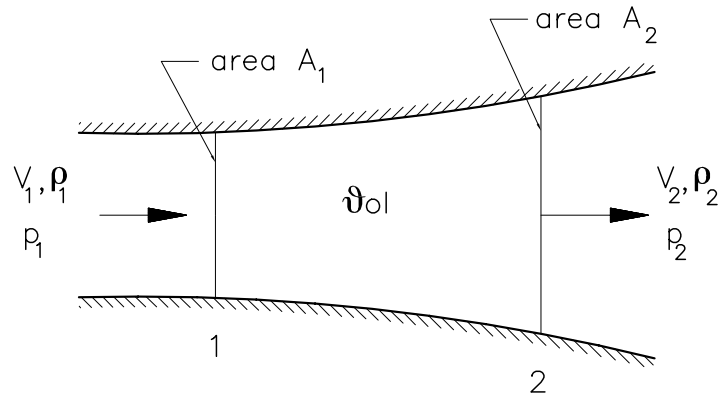


Figure 10.1: Control volume in quasi one-dimensional flow

For steady one-dimensional flow this yields:

$$\iint_{\partial V} \rho \bar{v} \, ds = \rho_2 v_2 A_2 - \rho_1 v_1 A_1 = 0. \quad (10.2)$$

The integral form of the continuity equation then becomes

$$\rho v A = \text{constant} \quad (10.3)$$

or in differential form

$$\frac{d\rho}{\rho} + \frac{dv}{v} + \frac{dA}{A} = 0. \quad (10.4)$$

Momentum:

The momentum equation without body force terms is:

$$\frac{\partial}{\partial t} \iiint_V \rho \bar{v} \, dV + \iint_{\partial V} \bar{v} (\rho \bar{v} \, d\bar{s}) = - \iint_{\partial V} p \, d\bar{s} + \iint_{\partial V} \bar{\tau} \, d\bar{s}. \quad (10.5)$$

For a steady one-dimensional flow between the stations 1 and 2 this reduces to

$$\rho v A (v_2 - v_1) = p_1 A_1 - p_2 A_2 + \int_1^2 p \, dA - \int_1^2 \tau \pi D_h \, dx, \quad (10.6)$$

where D_h is the hydraulic diameter of the channel (πD_h is the circumference of the channel cross-section).

Apparently the one-dimensional form of the viscous term $\iint_{\partial V} \bar{\tau} \, d\bar{s}$ in equation (10.6) is written as

$$\iint_{\partial V} \bar{\tau} \, d\bar{s} = - \int_1^2 \tau \pi D_h \, dx. \quad (10.7)$$

To understand this expression consider a small element with length dx of the control volume, see figure 10.2. The fluid inside this control volume experiences a friction force from the wall of the channel along its circumference.

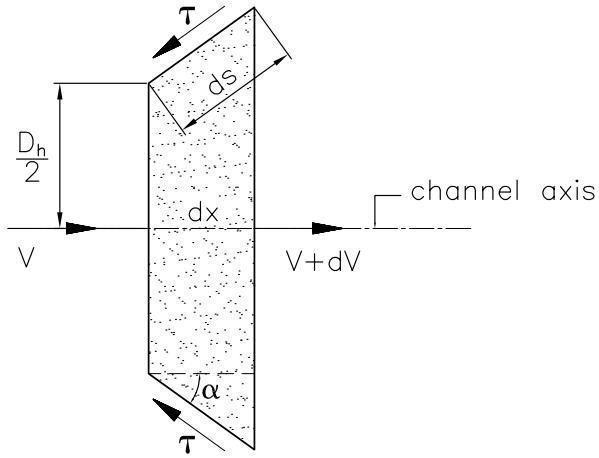


Figure 10.2: Friction force on a small fluid element

Let us write the circumference as πD_h with D_h as the hydraulic diameter. The friction force (in flow direction) on the fluid element is

$$\begin{aligned} dF_{vx} &= -\tau \pi D_h ds \cos \alpha \\ &= -\tau \pi D_h dx. \end{aligned}$$

Integrating from station 1 to station 2 yields equation (10.7).

The differential form of the momentum equation for one-dimensional viscous flow follows from (10.6) by taking stations 1 and 2 a distance dx apart; this results into

$$\rho v A \, du = -d(pA) + pdA - \tau \pi D_h \, dx,$$

or

$$\rho v A dv + Adp - \tau \pi D_h dx = 0. \quad (10.8)$$

Energy equation

Recall the energy equation without body forces:

$$\begin{aligned} \frac{\partial}{\partial t} \iiint_V \rho E \, dV + \iint_{\partial V} \rho E (\bar{v} \cdot d\bar{s}) &= \underbrace{- \iint_{\partial V} p(\bar{v} \cdot d\bar{s})}_{\text{work done by pressure forces}} + \underbrace{\iint_{\partial V} (\bar{\tau} \cdot \bar{v}) \cdot d\bar{s}}_{\text{work done by viscous forces}} \\ &\quad + \underbrace{\iiint_V \rho c \, dV}_{\text{volumetric heating}} - \underbrace{\iint_{\partial V} \bar{q} \cdot d\bar{s}}_{\text{conduction}}. \end{aligned} \quad (10.9)$$

For a steady one-dimensional adiabatic flow between the stations 1 and 2 this reduces to

$$\rho v A (E_2 - E_1) = -\rho v A \left(\frac{p_2}{\rho_2} - \frac{p_1}{\rho_1} \right),$$

or

$$E + \frac{p}{\rho} = e + \frac{p}{\rho} + \frac{v^2}{2} = h + \frac{v^2}{2} = H = \text{constant}. \quad (10.10)$$

In differential form with $dh = c_p \, dT$ (perfect gas) the energy equation reads

$$c_p \, dT + v \, dv = 0. \quad (10.11)$$

Equations (10.4), (10.8) and (10.11) form the basic set of equations that govern one-dimensional steady adiabatic flows.

Assume a variable area channel whose cross-sectional area $A(x)$ is a known function of x . So we have three equations for the unknowns $v(x)$, $\rho(x)$, $p(x)$ and $T(x)$. To close the system, we will use the perfect gas law in differential form:

$$\frac{dp}{p} = \frac{d\rho}{\rho} + \frac{dT}{T}. \quad (10.12)$$

To solve the system of equations the variables $\rho(x)$, $p(x)$ and $T(x)$ will be eliminated so that a single equation for the velocity $v(x)$ or the Mach number $M(x)$ results. First however some algebra is performed to attain a more suitable form of the system. Execute the following operations:

- Write cross-sectional area $A(x)$ in the momentum equation and in the continuity equation in terms of the hydraulic diameter $D_h = \sqrt{4A(x)/\pi}$.
- Divide the momentum equation (10.8) by the cross-sectional momentum $\rho v^2 A$ and substitute the friction coefficient f from equation (10.1).
- Divide the energy equation (10.11) by the enthalpy $c_p T$ and remember that $v^2/c_p T = (\gamma - 1)M^2$.

Then the following system of equations results:

$$\text{continuity: } \frac{d\rho}{\rho} + \frac{dv}{v} + \frac{2dD_h}{D_h} = 0, \quad (10.13a)$$

$$\text{momentum: } \frac{dp}{p} + \gamma M^2 \left(\frac{dv}{v} + \frac{2f}{D_h} dx \right) = 0, \quad (10.13b)$$

$$\text{energy: } \frac{dT}{T} + (\gamma - 1)M^2 \frac{dv}{v} = 0, \quad (10.13c)$$

$$\text{perfect gas law: } \frac{d\rho}{\rho} + \frac{dT}{T} = \frac{dp}{p} \quad (10.13d)$$

In order to solve this system a relation between the Mach number M and velocity v is still needed. For the specific case of a perfect gas the energy equation (10.9) reduces to

$$\frac{a^2}{\gamma - 1} + \frac{v^2}{2} = \text{constant},$$

which gives the following relation connecting the Mach number and velocity:

$$\frac{dv}{v} = \frac{1}{\left(1 + \frac{\gamma-1}{2}M^2\right)} \frac{dM}{M}. \quad (10.14)$$

Using the set of equations (10.13a)–(10.13d), the variables dp/p , $d\rho/\rho$ and dT/T may be eliminated and finally we obtain

$$\frac{dM}{dx} = \frac{2M(1 + \frac{\gamma-1}{2}M^2)(D'_h - \gamma f M^2)}{D_h(M^2 - 1)}, \quad (10.15)$$

where $D'_h = \frac{dD_h}{dx}$. For a known channel shape $D_h(x)$, (10.15) may be solved to get the corresponding mach number distribution along the channel. Equation (10.15) will now be analysed to understand the physics of one-dimensional viscous flow in a variable area channel. First we address the special case of flow through a constant area channel.

10.2 Constant-area channel flow; Fanno line

Consider a constant-area channel having its entrance at $x = 0$ and having a certain length L . The entrance conditions are specified as M_0 , v_0 and h_0 . The Mach number distribution along the channel is governed by the O.D.E.:

$$\frac{dM}{dx} = -\frac{2M^3(1 + \frac{\gamma-1}{2}M^2)\gamma f}{D_h(M^2 - 1)}. \quad (10.16)$$

This equation tells already the important but also paradoxical message that friction ($f \neq 0$) causes a Mach number distribution in a constant area channel.

Before analyzing equation (10.16) further some interesting properties of the flow can be discovered already by considering the integral forms of the continuity equation and the energy equation e.g.

$$J = \rho v = \text{constant},$$

and

$$H = h + \frac{v^2}{2} = \text{constant}.$$

Combining both equations yields

$$h + \frac{1}{2}J^2 \left(\frac{1}{\rho}\right)^2 = H, \quad (10.17)$$

J being the mass flux through the channel. Equation (10.17) is an algebraic relation between the thermodynamic variables h (enthalpy) and $\frac{1}{\rho}$ (specific volume). This relation defines a family of curves (a particular curve depends on the choice of J and H) in the $(h, \frac{1}{\rho})$ -plane, see figure (10.3). These parabolic curves are well known as Fanno lines.

The entrance conditions v_0 , h_0 and ρ_{00} fix the particular Fanno curve that describe all possible states $(h, \frac{1}{\rho})$ in the channel flow. Since we have assumed adiabatic flow the second law states that the entropy cannot decrease following a particle; thus a gas that moves in positive x -direction obeys the entropy condition:

$$\text{entropy condition: } \frac{ds}{dx} \geq 0. \quad (10.18)$$

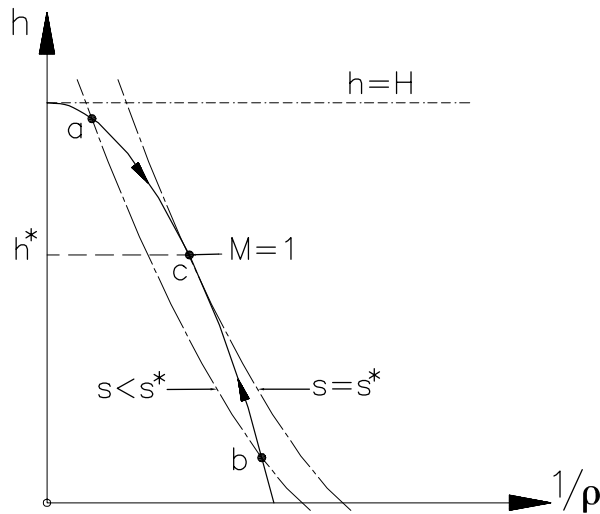


Figure 10.3: Fanno line in the $(h, \frac{1}{\rho})$ -plane

Following a fluid particle there can only be an increase of entropy. So it seems a good idea to study the graph of entropy level curves in the $(h, \frac{1}{\rho})$ -plane. From the entropy formula:

$$\frac{T}{T_0} \left(\frac{\rho_0}{\rho} \right)^{\gamma-1} = e^{s-s_0}/c_v,$$

it follows that iso-entropy lines in the $(h, \frac{1}{\rho})$ -plane have the form

$$h \left(\frac{1}{\rho} \right)^{\gamma-1} = \text{constant}.$$

The qualitative behaviour of these lines are shown in figure 10.3. For a particular value of the entropy $s = s^*$ the iso-entropy curve just touches the Fanno line in point **c**. An iso-entropy curve having $s < s^*$ intersects the Fanno line twice, in fact in the points **a** and **b**. Iso-entropy curves with $s > s^*$ nowhere intersect the Fanno line.

The entropy condition (10.18) implies that in a constant area flow the Fanno line is followed in a way corresponding to the arrows in figure 10.3 when following a particle. This means that irrespective the particular choice of the entrance conditions the channel develops in such a way that it tends to attain the flow conditions of point **c** ($h = h^*$, $\rho = \rho^*$) where entropy becomes as large as possible ($s = s^*$). It will be shown that in this point the Mach number is unity ($M = 1$). To that end observe that at point **c** the Fanno curve and the iso-entropy curve have the same slope.

The slope of the Fanno curve is

$$\left(\frac{dh}{d\frac{1}{\rho}} \right)_{\text{Fanno}} = -J^2 \left(\frac{1}{\rho} \right),$$

the slope of an iso-entropy curve is

$$\left(\frac{\partial h}{\partial \frac{1}{\rho}} \right)_s = -(\gamma - 1)\rho h = -\rho a^2,$$

equating both yields

$$J^2 = \rho^2 a^2$$

or

$$v^2 = a^2$$

which shows that $M = 1$. Thus in point **c** the flow becomes just sonic. ‘Above’ **c** the flow is subsonic ($M < 1$) because the density increases and consequently ($J = \text{constant}$) the velocity decreases. In a similar way it may be concluded that ‘below’ **c** the flow is supersonic ($M > 1$). The two distinct branches of the Fanno line thus represent subsonic flow ($h > h^*$) and supersonic flow ($h < h^*$). In the absence of discontinuities there is no possibility of passing from one branch to another because that would imply crossing point **c** and the condition of $ds/dx > 0$ would be violated. Thus an initially supersonic flow remains supersonic but slows down to $M = 1$; an initially subsonic flow remains subsonic but accelerates to $M = 1$. *The effect of friction is that it drives the Mach number to unity.* This is an interesting conclusion having the consequence that an initially subsonic flow defines a particular channel length L_{\max} at which exit the sonic conditions are just attained: this phenomenon is referred to as *frictional choking*; it will be discussed later.

Let us return to the O.D.E. (10.16), which governs the Mach number distribution along the channel and let us construct a qualitative sketch of the integral curves in the (M, x) -plane. The friction coefficient f is a positive quantity, so from (10.16) we conclude:

$$\begin{aligned} \frac{dM}{dx} &> 0, \quad \text{for } M < 1, \\ \frac{dM}{dx} &= \infty, \quad \text{for } M = 1, \\ \frac{dM}{dx} &< 0, \quad \text{for } M > 1. \end{aligned}$$

The graph $\frac{dM}{dx}$ as a function of M , shown in figure 10.4, illustrates a monotonic increase of $\frac{dM}{dx}$ if the flow is subsonic. In supersonic flow $\frac{dM}{dx}$ attains a negative maximum value.

The corresponding particular Mach number satisfies the relation:

$$3(\gamma - 1)M^4 - (5\gamma - 7)M^2 - 6 = 0;$$

for $\gamma = 7/5$ this particular Mach number takes the value $M = \sqrt[4]{5}$.

Based on the graph $\frac{dM}{dx}$ as a function of M the integral curves in the (M, x) -plane have a pattern as is shown in figure 10.5.

A particular curve depends on the choice of the entrance Mach number M_0 . The arrows indicate the direction in which an integral curve is followed when following a gas particle. Obviously the Mach number goes to unity. With every entrance Mach number M_0 there corresponds a maximum tube length L_{\max} beyond which choking occurs. From figure 10.5 we expect a zero tube length when $M_0 = 1$.

Equation (10.16) will now be integrated from the entrance $x = 0$ with entrance Mach number M_0 to an arbitrary section x with Mach number $M(x)$ in order to get an expression for the maximum tube length. Integration yields:

$$\frac{4\gamma f}{D_h} x = \frac{M^2(x) - M_0^2}{M^2(x)M_0^2} + \frac{\gamma + 1}{2} \ln \frac{M_0^2 \left(1 + \frac{\gamma-1}{2}M^2(x)\right)}{M^2(x) \left(1 + \frac{\gamma-1}{2}M_0^2\right)}. \quad (10.19)$$

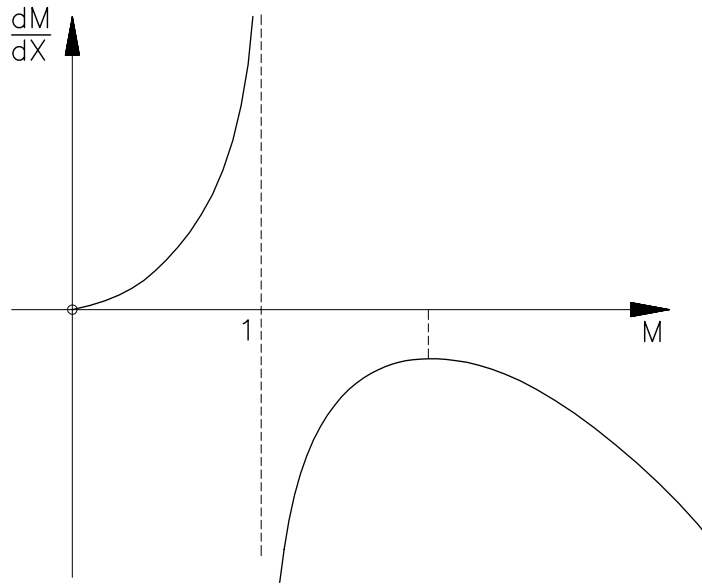
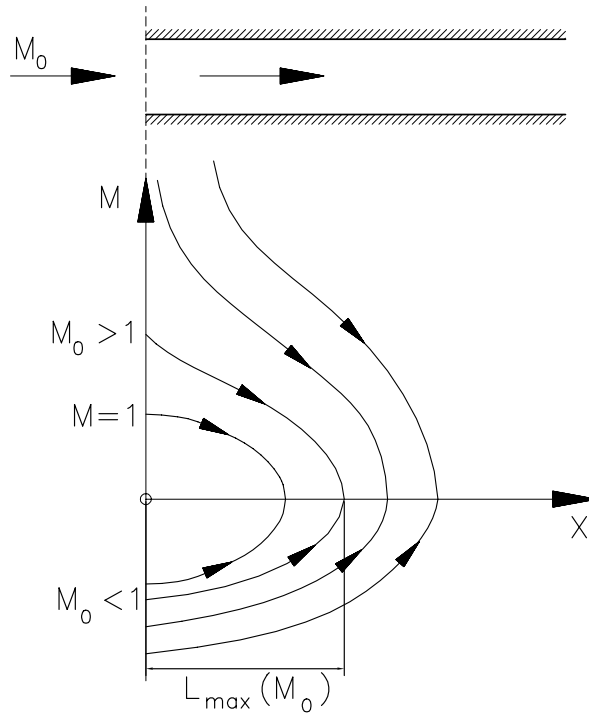
Figure 10.4: Graph of $\frac{dM}{dx}$ vs M .

Figure 10.5: Mach number distribution in a constant area tube.

The maximum tube length occurs at $x = L_{\max}$ with $M(x) = 1$, so there is obtained

$$\frac{4\gamma f}{D_h} L_{\max} = \frac{1 - M_0^2}{M_0^2} + \frac{\gamma + 1}{2} \ln \frac{(\gamma + 1)M_0^2}{2(1 + \frac{\gamma - 1}{2}M_0^2)}. \quad (10.20)$$

The maximum tube length depends on the entrance Mach number M_0 . Evidently for $M_0 = 1$

this length is zero; for $M_0 \rightarrow 0$, $L_{\max} \rightarrow \infty$ but $M_0 \rightarrow \infty$, L_{\max} tends to the limiting value (see figure 10.6):

$$\frac{L_{\max}}{D_h} = \frac{(\gamma + 1) \ln \frac{\gamma+1}{\gamma-1} - 2}{4\gamma f}.$$

For $\gamma = 1.4$ and $f = 0.003$ we find $L_{\max} \approx 68.5 D_h$. The phenomena that a maximum tube

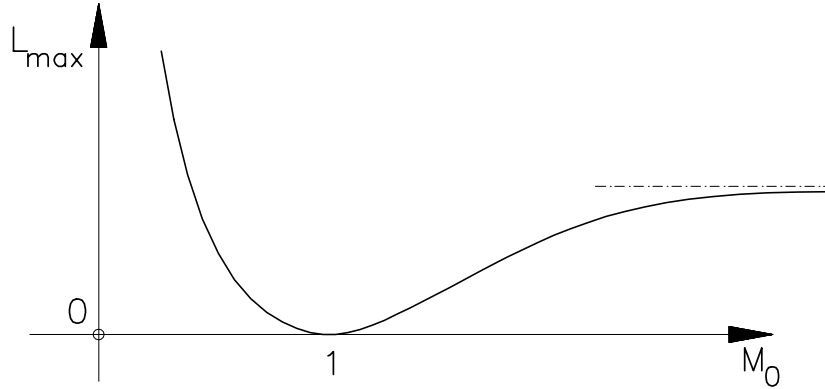


Figure 10.6: Maximum tube length.

length exists for a specified entrance Mach number is usually referred to as frictional choking. Friction reduces the effective cross-sectional area of the tube and drives the Mach number towards unity. Let us now conclude now by inviting the reader to comment on the interesting question: “What will happen if a uniform free stream with Mach number M_0 enters a tube with length L where L exceeds the maximum tube length $L_{\max}(M_0)$?” Distinguish the two cases $M_0 > 1$ and $M_0 < 1$ and be aware of the possibility that in the supersonic case shocks may appear.

10.3 A channel with a variable cross-sectional area

The Mach number distribution in a variable area channel is governed by the O.D.E.:

$$\frac{dM}{dx} = \frac{2M(1 + \frac{\gamma-1}{2}M^2)(D'_h - \gamma f M^2)}{D_h(M^2 - 1)}, \quad (10.15)$$

where the channel shape is defined by the variation of its hydraulic diameter

$$D_h = F(x). \quad (10.21)$$

To study the properties of the solution curves $M(x)$, equation (10.15) will be viewed as a nonlinear system of two ordinary differential equations having the formal shape:

$$\frac{dM}{d\lambda} = P(M, x), \quad (10.22a)$$

$$\frac{dx}{d\lambda} = Q(M, x), \quad (10.22b)$$

where functions $P(M, x)$ and $Q(M, x)$ are defined as

$$\begin{aligned} P(M, x) &= 2M\left(1 + \frac{\gamma - 1}{2}M^2\right)(F'(x) - \gamma f M^2), \\ Q(M, x) &= F(x)(M^2 - 1), \end{aligned}$$

and where λ is a parameter running along solution curves. System (10.22a),(10.22b) is nonlinear because its right-hand side depends nonlinearly on the variables M and x . The variables M and x are seen as depending on λ , the (M, x) -plane is referred to as the phase plane of the system.

Standard theory regarding nonlinear systems² will be applied to get the qualitative behaviour of solution curves (integral curves) in the phase plane.

Integral curves in the phase plane have a slope

$$\frac{dM}{dx} = \frac{P(M, x)}{Q(M, x)}. \quad (10.23)$$

Obviously these slopes are uniquely defined if $P(M, x) \neq 0$ or $Q(M, x) \neq 0$. However if we have $P = 0$ and $Q = 0$ at a common point this point becomes singular in the sense that the slope of the integral curves is not defined there. System (10.22a)-(10.22b) features singular points if:

$$M = 1, \quad \text{and} \quad F'(x) = \gamma f. \quad (10.24)$$

Let this happen in the phase plane at $x = x^*$. Since γ and f are both positive, singular points only appear in the diverging parts of a channel, where $F' > 0$. To analyse integral curves near the singularity, it is standard to linearize the system near $(M, x) = (1, x^*)$ where x^* satisfies equation (10.24). The linearized system that follows reads:

$$\begin{pmatrix} \frac{dM}{dx} \\ \frac{dM}{d\lambda} \end{pmatrix} = \begin{pmatrix} \frac{\partial P}{\partial M} & \frac{\partial P}{\partial x} \\ \frac{\partial Q}{\partial M} & \frac{\partial Q}{\partial x} \end{pmatrix} \begin{pmatrix} M - 1 \\ x - x^* \end{pmatrix} \quad (10.25)$$

where the matrix has to be evaluated at $M = 1$ and $x = x^*$; this yields:

$$\begin{pmatrix} P_M & P_x \\ Q_M & Q_x \end{pmatrix}_{\substack{M=1 \\ x=x^*}} = \begin{pmatrix} -2\gamma(\gamma+1)f & (\gamma+1)F'' \\ 2F & 0 \end{pmatrix}. \quad (10.26)$$

Important parameters for further analysis are the trace (T) and the Jacobian (J) of the matrix. Here they take the form

$$\begin{aligned} T &= -2\gamma(\gamma+1)f, \\ J &= -2(\gamma+1)FF'' \end{aligned} \quad (10.27)$$

Converging-diverging nozzle

Let us apply the theory of the specific situation of a converging-diverging nozzle. The shape of the contour and the corresponding phase plane (with solution curves $M = M(x)$) is shown in figure 10.7.

²See for example: Jordan, D.W. & P. Smith, Nonlinear Ordinary Differential equations, Clarendon Press, Oxford 1979

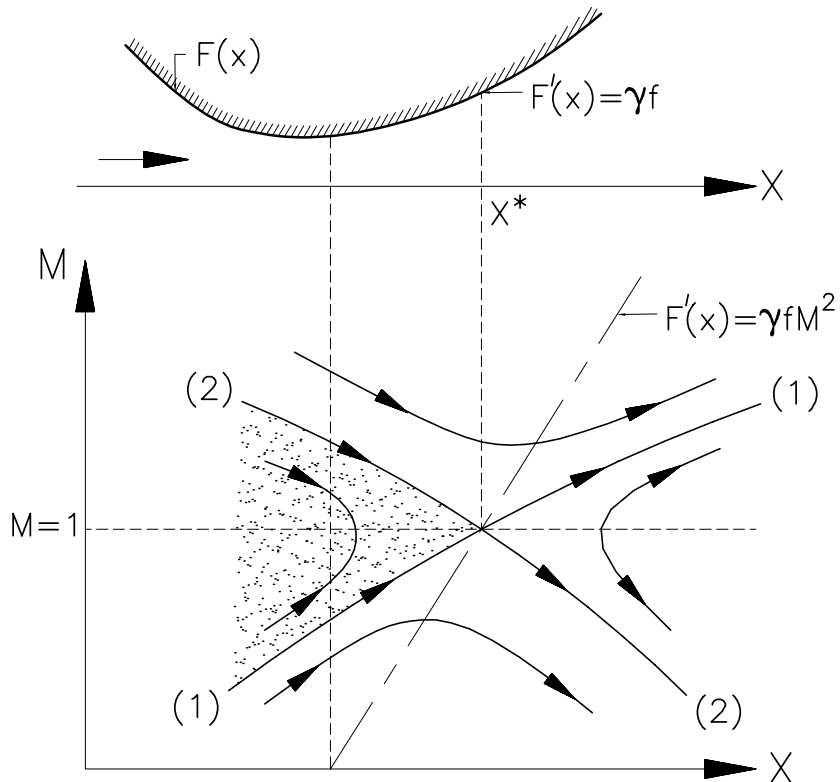


Figure 10.7: Viscous effects near the throat of a nozzle

Behind the throat in the diverging part the condition $F'(x) = \gamma f$ is fulfilled at $x = x^*$. The area behind the throat is increasing with x so that at $x = x^*$ also $F''(x^*) > 0$. Thus at $x = x^*$ the Jacobian is negative and the solution curves form a saddle-point there, the two separatrices of the saddle, labelled in figure 10.7 as (1) and (2), have slopes determined by

$$\left(\frac{dM}{dx}\right)_{1,2} = \frac{-\gamma(\gamma+1)f \pm \sqrt{\gamma^2(\gamma+1)^2f^2 - 2(\gamma+1)FF''}}{2F}. \quad (10.28)$$

Separatrix (1) has a positive slope and separatrix (2) has a negative slope.

The transition from subsonic to supersonic flow or vice versa is made possible by the presence of the saddle point and takes place *downstream* of the throat in the divergent part of the channel. Observe the contrast with inviscid flow where transition always happens *in* the throat. Due to viscous effects a subsonic flow in the throat section is accelerated and a supersonic flow is slowed down. The positive slope $(\frac{dM}{dx})_1$ tends to zero if $F''(x^*) \rightarrow 0$ and the negative slope $(\frac{dM}{dx})_2$ tends to $-\gamma(\gamma+1)f/F(x^*)$ which means that the transition from subsonic to supersonic flow can be made as slow as we please but the transition from supersonic to subsonic flow has a limiting value.

From figure 10.7 we observe that an increase of entrance Mach number in the subsonic domain moves the position of the highest Mach number from the throat downstream towards the sonic section. Similarly a decrease of a supersonic entrance Mach number moves the position of the minimum Mach number upstream onto the sonic section. Entrance Mach numbers defining integral curves in the shaded region will terminate at $M = 1$. A sonic section

upstream of x^* is predicted but transition through sonic conditions is not possible. The nozzle is *choked* and the corresponding range of entrance Mach numbers cannot be realized unless the nozzle is terminated before the sonic section or a shock (only for a supersonic entrance) appears.

Because x^* lies downstream of the throat *frictional choking* is possible even in the diverging part of the nozzle if the influence of friction dominates that of the area increase.

Converging-diverging nozzle with inflection point

Usually a supersonic wind tunnel is equipped with a converging-diverging nozzle having an inflection point ($F'' = 0$) downstream of the throat. The shape of such a contour together with the corresponding phase plane portrait is shown in figure 10.8.

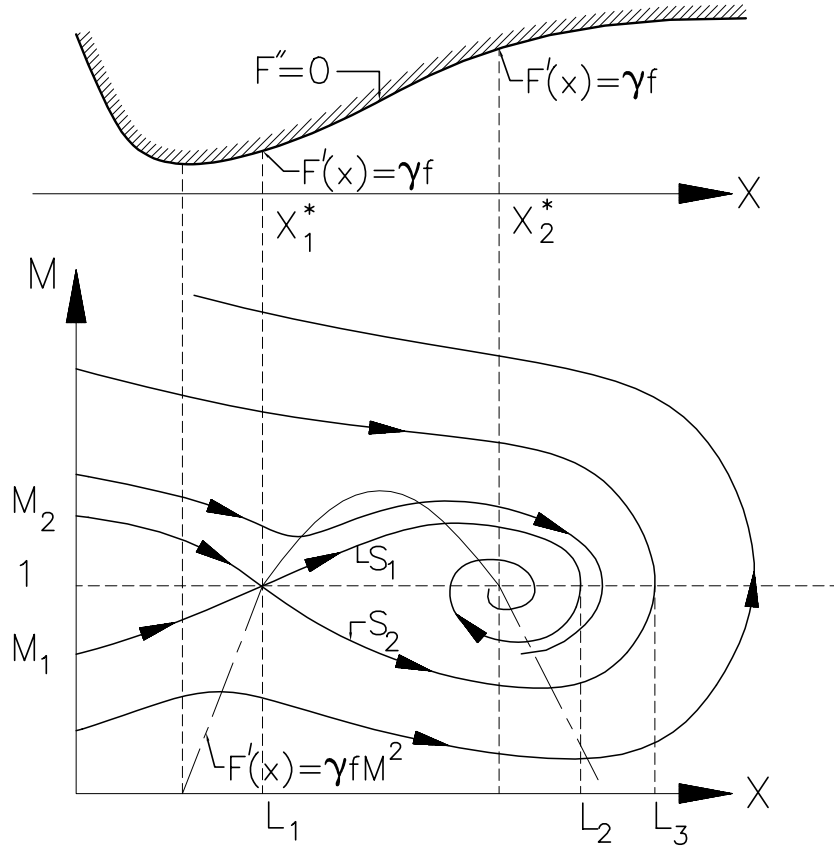


Figure 10.8: Typical nozzle contour with a corresponding phase plane

Assume a nozzle contour with a point of inflection between locations x_1^* and x_2^* where the condition $F'(x) = \gamma f$ holds. At x_1^* and x_2^* singular points occur in the phase plane on the line $M = 1$. The presence of an inflection point between x_1^* and x_2^* implies $F(x_1^*) > 0$ and $F(x_2^*) < 0$. Using equation (10.27) the Jacobians in these points have opposite signs, i.e. $J(x_1^*) < 0$ and $J(x_2^*) > 0$. So the singular point at $x = x_1^*$ is a saddle point. Standard theory about nonlinear systems of differential equations teaches us that $J > 0$ represents either a node if $4J - T^2 < 0$ or a spiral (focus) if $4J - T^2 > 0$. Evaluating equation (10.27) in $x = x_2^*$,

$M = 1$ yields

$$(4J - T^2)_{x_2^*, M=1} = (\gamma + 1) \{ 2FF'' + (\gamma + 1)(F')^2 \}. \quad (10.29)$$

Let us discuss here in more detail the spiral case (the nodal case is left as an exercise), thus we consider

$$FF'' < \frac{-\gamma + 1}{2}(F')^2$$

in x_2^* . Figure 10.8 already gives a qualitative picture of some integral curves. Observe that all integral curves have a vertical slope at the line $M = 1$ and a horizontal slope on the curve $F'(x) = \gamma f M^2$. This curve passes through the singularities $(x_1^*, 1)$ and $(x_2^*, 2)$ and must have a maximum somewhere between x_1^* and x_2^* . Because the trace T in $x_2^*, M = 1$ is negative the spiral singularity is asymptotically stable which means that trajectories spiral into the singularity if the parameter λ increases. But if the spiral is stable then separatrix S_1 runs into the spiral whereas separatrix S_2 bypasses the spiral singularity.

Set aside the local details near the singularities the trajectory pattern looks very similar one that corresponds to a constant area channel (shown in figure 10.5). For every entrance Mach number the flow in the variable area channel is driven to sonic conditions. So for every entrance Mach number there corresponds a maximum tube length L_{\max} . We do not attempt to find an analytic relation between L_{\max} and M_0 but we perform a qualitative research; the result is shown in figure 10.9.

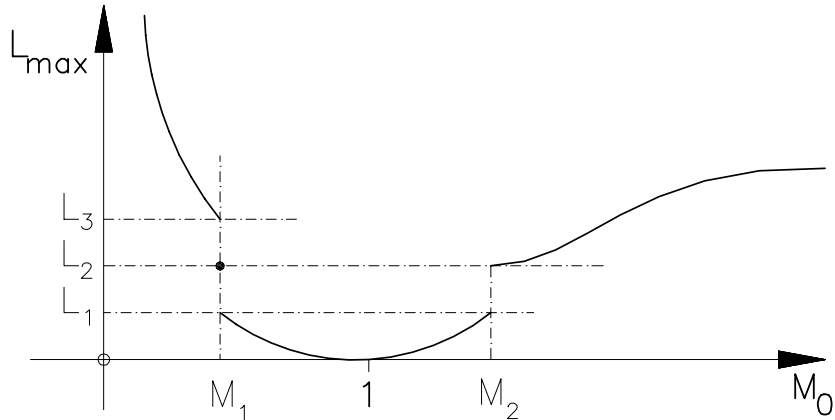


Figure 10.9: Maximum tube length for a converging-diverging nozzle with an inflection point

For increasing subsonic entrance Mach number $M_0 < M_1$ the L_{\max} decreases gradually. At $M_0 = M_1$ L_{\max} jumps from the large value L_3 to the much smaller length L_1 . For $M_1 < M_0 \leq 1$ the L_{\max} decreases to zero at $M_0 = 1$. For supersonic entrance Mach numbers there is a gradual increase of L_{\max} from zero to L_2 if M_0 increases to M_2 . At $M_0 = M_2$, L_{\max} jumps from the short value L_1 to a larger value $L_2 < L_3$. Beyond $M_0 = M_2$, L_{\max} increases continuously with increasing M_0 .

10.4 Internal structure of a shock wave

10.4.1 Introductory comments

The thickness of a shock wave refers to the spatial region in the flow field where the variation of flow properties is irreversible and where entropy increases. In most practical cases this region is very thin (comparable to the mean free path of molecules) causing high spatial gradients of temperature, pressure, density and velocity. In many applications the shock thickness is neglected and shocks are modelled as a true discontinuity. But doing so the velocity and temperature gradients become infinite causing infinite viscous stress and infinite heat flux. This ambiguity is resolved by introducing a shock or shock layer with a finite thickness. Notice the analogue with the boundary layer, both feature thin regions of large viscous stress and high heat flux.

The Navier-Stokes model will be applied to resolve the internal structure of a normal shock wave. Therefore we assume a perfect one-dimensional flow with a flow direction normal to the shock wave. Let this direction be the x -direction. Further let us assume the shock to be stationary, so we expect that acceleration is not of prime importance; nevertheless a detailed study on the structure of accelerating (or decelerating) shocks would be welcome. Finally, thermal radiation and diffusion are not taken into account.

10.4.2 Navier-Stokes equations for one-dimensional flow

To derive the Navier-Stokes equations in differential form for one-dimensional flow let us recall the conservation laws (in integral form) from chapter 1. The influence of body forces and volumetric heating is not taken into account so the terms accounting for these influences are dropped.

$$\begin{aligned} \text{Continuity: } & \frac{\partial}{\partial t} \iiint_V \rho \, dV + \iint_{\partial V} \rho \bar{v} \cdot \bar{n} \, ds = 0, \\ \text{Momentum: } & \frac{\partial}{\partial t} \iiint_V \rho \bar{v} \, dV + \iint_{\partial V} \rho \bar{v} \bar{v} \cdot \bar{n} \, ds + \iint_{\partial V} p \bar{n} \, ds = \iint_{\partial V} \bar{\tau} \cdot \bar{n} \, ds, \\ \text{Energy: } & \frac{\partial}{\partial t} \iiint_V \rho E \, dV + \iint_{\partial V} \rho E \bar{v} \cdot \bar{n} \, ds + \iint_{\partial V} p \bar{v} \cdot \bar{n} \, ds = \\ & \iint_{\partial V} (\bar{\tau} \cdot \bar{v}) \bar{n} \, ds - \iint_{\partial V} \bar{q} \cdot \bar{n} \, ds \end{aligned}$$

Here $\bar{\tau}$ is the viscous stress tensor and \bar{q} is the heat flux due to conduction.

For a Newtonian fluid:

$$\tau_{ij} = \lambda \nabla \cdot \bar{v} + \mu \left(\frac{\partial u_i}{\partial x_j} + \frac{\partial u_j}{\partial x_i} \right).$$

Fourier's law:

$$\bar{q} = -k \nabla T.$$

The divergence theorem and the gradient theorem are applied to transfer surface integrals to volume integrals. Combining the volume integrals and recalling that V is fixed in space but

otherwise arbitrarily chosen the integrand has to be zero for all points in space. This yields the differential form:

$$\frac{\partial \rho}{\partial t} + \nabla \cdot \rho \bar{v} = 0, \quad (10.30)$$

$$\frac{\partial \rho \bar{v}}{\partial t} + \nabla \cdot \rho \bar{v} \bar{v} + \nabla p = \nabla \bar{\tau}, \quad (10.31)$$

$$\frac{\partial}{\partial t}(\rho E) + \nabla \cdot \rho \bar{v} E = -\nabla \cdot (p \bar{v}) + \nabla (\bar{\tau} \cdot \bar{v}) - \nabla \cdot \bar{q}. \quad (10.32)$$

For a one-dimensional steady flow this reduces to

$$\begin{aligned} \frac{\partial}{\partial x}(\rho u) &= 0, \\ \rho u \frac{\partial u}{\partial x} + \frac{\partial p}{\partial x} &= \frac{\partial}{\partial x} \tau_{xx}, \\ \rho u \frac{\partial E}{\partial x} + \frac{\partial}{\partial x}(\rho u) &= \frac{\partial T}{\partial x} \left(k \frac{\partial T}{\partial x} \right) + \frac{\partial}{\partial x}(u \tau_{xx}), \end{aligned}$$

with $\tau_{xx} = \lambda \frac{\partial u}{\partial x} + 2\mu \frac{\partial u}{\partial x}$ the set of equations becomes

$$\frac{\partial}{\partial x}(\rho u) = 0, \quad (10.33)$$

$$\rho u \frac{\partial u}{\partial x} = -\frac{\partial p}{\partial x} + \frac{\partial}{\partial x} \left((\lambda + 2\mu) \frac{\partial u}{\partial x} \right), \quad (10.34)$$

$$\rho u \frac{\partial H}{\partial x} = \frac{\partial}{\partial x} \left((\lambda + 2\mu) u \frac{\partial u}{\partial x} \right) + \frac{\partial}{\partial x} \left(k \frac{\partial T}{\partial x} \right). \quad (10.35)$$

10.4.3 Equations of shock structure

Due to the one-dimensionality of the problem (there are only variations in x -direction), the effects of viscosity come from the normal viscous stress τ_{xx} and from heat conduction in x -direction. Shear stresses are absent here.

The viscous coefficients λ and μ appear in the combination $\hat{u} = \lambda + 2\mu$; taking the Stokes' hypotheses for granted ($\lambda = -\frac{2}{3}\hat{u}$) we assume that $\lambda + 2\mu = \frac{3}{4}\mu$. The set of equations can be integrated once giving the shock structure:

$$J = \rho u, \quad (10.36)$$

$$K = p + \rho u^2 - (\lambda + 2\mu) \frac{du}{dx}, \quad (10.37)$$

$$L = \rho u H - (\lambda + 2\mu) u \frac{du}{dx} - k \frac{dT}{dx}, \quad (10.38)$$

where J , K and L are integration constants representing the mass flux, momentum flux and energy respectively. Note that the viscosity coefficients λ and μ have not been assumed to be constant. Assuming flow to the right the upstream and downstream conditions are:

$$x = -\infty : \quad u = u_1, \quad p = p_1, \quad \rho = \rho_1, \quad T = T_1, \quad \hat{\mu} = \hat{\mu}_1,$$

$$x = +\infty : \quad u = u_2, \quad p = p_2, \quad \rho = \rho_2, \quad T = T_2, \quad \hat{\mu} = \hat{\mu}_2.$$

Far upstream ($x \rightarrow -\infty$) and far downstream ($x \rightarrow +\infty$) the derivatives $\frac{\partial u}{\partial x}$ and $\frac{\partial T}{\partial x}$ vanish. The system (10.36)–(10.38) reduces to the well-known Rankine-Hugoniot equations

$$\begin{aligned}\rho_1 u_1 &= \rho_2 u_2 \\ p_1 + \rho_1 u_1^2 &= p_2 + \rho_2 u_2^2 \\ H_1 = h_1 + \frac{1}{2} u_1^2 &= h_2 + \frac{1}{2} u_2^2 = H_2\end{aligned}$$

describing the shock discontinuity. The Rankine-Hugoniot equations are invariant under the transformation $u_1 = -u_1$ and $u_2 = -u_2$; the Rankine-Hugoniot equations are not decisive regarding the direction of the flow. Expansion shocks and compression shocks are both allowed by the Rankine-Hugoniot conditions.

10.4.4 An estimate for the shock-thickness

The momentum equation (10.37) contains only the derivative $\frac{du}{dx}$ and this fact enables us to make an estimate of the shock thickness. In the interior of the shock the velocity u decreases from u_1 (pre-shock value) to u_2 (post-shock value), see figure 10.10.

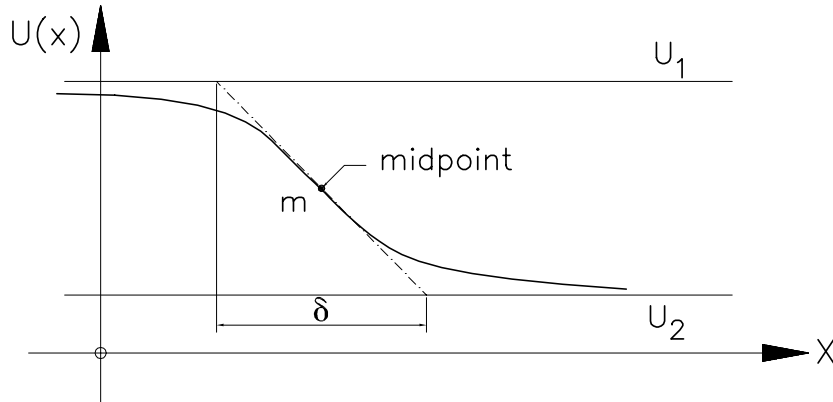


Figure 10.10: Internal velocity distribution

The differential equation that describes this behaviour reads

$$(\mu + 2\lambda) \frac{du}{dx} = p + \rho u^2 - K.$$

Let K be evaluated at $x = -\infty$, this yields

$$K = p_1 + \rho_1 u_1^2,$$

and the O.D.E. governing the velocity distribution in the shock reads

$$(\mu 2\lambda) \frac{du}{dx} = (p - p_1) + J(u - u_1). \quad (10.39)$$

The O.D.E. cannot be solved yet because the pressure $p(x)$ is still unknown. In order to get an estimate of the shock thickness we evaluate the derivative $\frac{du}{dx}$ at the midpoint of the velocity distribution. At the midpoint (subscript m) the velocity has the value:

$$u_m = u_1 + \frac{1}{2}(u_2 - u_1) = u_1 + \frac{1}{2}\Delta u. \quad (10.40)$$

The shock thickness δ is defined as, see figure 10.10:

$$\left(\frac{du}{dx} \right)_m = + \frac{(u_2 - u_1)}{\delta} = + \frac{\Delta u}{\delta}. \quad (10.41)$$

The pressure at the midpoint is obtained by performing a Taylor expansion of $p = p(\rho, s)$

$$p = p_1 + \left(\frac{\partial p}{\partial \rho} \right)_s (\rho - \rho_1) + \left(\frac{\partial^2 p}{\partial \rho^2} \right)_s \frac{(\rho - \rho_1)^2}{2} + \dots + \left(\frac{\partial p}{\partial s} \right)_\rho (s - s_1) + \dots$$

For weak shocks $(s - s_1)$ is at least of the order $(\rho - \rho_1)^3$ and if the analysis is restricted to second order terms $(\rho - \rho_1)^2$, the pressure can be calculated as

$$p = p_1 + a_1^2 (\rho - \rho_1) + (\gamma - 1) \frac{a_1^2}{\rho_1} \frac{(\rho - \rho_1)^2}{2}.$$

Using equation (10.36) in the form $\rho_1 u_1 = \rho_m u_m = J$ the density ρ_m at the midpoint is related to the velocity u_m as

$$\rho_m - \rho_1 = - \frac{\rho_1 \Delta u}{2u_1 + \Delta u}. \quad (10.42)$$

The pressure at the midpoint is

$$p_m - p_1 = - \frac{\rho_1 a_1^2}{2u_1} \Delta u + \rho_1 a_1^2 \frac{(\gamma + 1)}{2} \left(\frac{\Delta u}{2u_1} \right)^2 + O(\Delta u^3). \quad (10.43)$$

Evaluating equation (10.39) in the midpoint for the shock thickness δ :

$$\frac{(\mu + 2\lambda)}{\delta} = - \frac{\rho_1 a_1^2}{2u_1} + \rho_1 a_1^2 \frac{(\gamma + 1)}{2} \frac{(\Delta u)}{4u_1^2} + \frac{\rho_1 u_1^2}{2u_1},$$

or

$$2 \frac{(\mu + 2\lambda)}{\delta} = \rho_1 a_1^2 \left(M_1 - \frac{1}{M_1} \right) + \frac{\gamma + 1}{4} \rho_1 a_1 \frac{\Delta u}{a_1 M_1^2}, \quad (10.44)$$

where M_1 is the Mach number $M_1 = \frac{u_1}{a_1}$. The velocity jump Δu depends on the shock Mach number according to

$$\frac{\Delta u}{a_1} = - \frac{2(M_1^2 - 1)}{(\gamma + 1)M_1}.$$

If this relation is inserted into equation (10.44) the shock thickness δ follows from

$$\frac{2(\mu + 2\lambda)}{\delta} = \rho_1 a_1 \left(M_1 - \frac{1}{M_1} - \frac{M_1^2 - 1}{2M_1^3} \right).$$

Taking the weak shock limit ($M_1 \rightarrow 1$), the estimate for the shock thickness becomes:

$$\delta = \frac{2(\mu + 2\lambda)}{\rho_1 a_1 (M_1 - 1)}.$$

Notice that the shock thickness becomes large if the Mach number approaches $M = 1$; the weaker the shock the larger its thickness.

10.4.5 Entropy production in the shock zone

From inviscid theory it's known that passing a shock is a non-isentropic process; entropy increases across a shock discontinuity.

Let us now take the viscous model of the shock to study the entropy production in the shock zone. From the first law of thermodynamics

$$Tds = dh - \frac{dp}{\rho},$$

we write

$$\rho u T \frac{ds}{dx} = \rho u \frac{dH}{dx} - \rho u^2 \frac{du}{dx} - u \frac{dp}{dx}.$$

Inserting $\frac{dp}{dx}$ and $\rho u \frac{dH}{dx}$ from equations (10.34) and (10.35) and introducing $\hat{\mu} = \mu + 2\lambda$ we find

$$\rho u \frac{ds}{dx} = \frac{1}{T} \left\{ \frac{d}{dx} \left(\hat{\mu} u \frac{du}{dx} \right) + \frac{d}{dx} \left(k \frac{dT}{dx} \right) - u \frac{d}{dx} \left(\hat{\mu} \frac{du}{dx} \right) \right\}. \quad (10.45)$$

The first and second term in the right hand side may be worked out as follows

$$\begin{aligned} \frac{d}{dx} \left(\hat{\mu} u \frac{du}{dx} \right) &= u \frac{d}{dx} \left(\hat{\mu} \frac{du}{dx} \right) + \hat{\mu} \left(\frac{du}{dx} \right)^2, \\ \frac{1}{T} \frac{d}{dx} \left(k \frac{dT}{dx} \right) &= \frac{d}{dx} \left(\frac{k}{T} \frac{du}{dx} \right) + \frac{k}{T^2} \left(\frac{dT}{dx} \right)^2, \end{aligned}$$

and the expression for the entropy gradient becomes

$$\rho u \frac{ds}{dx} = \frac{\hat{\mu}}{T} \left(\frac{du}{dx} \right)^2 + \frac{k}{T^2} \left(\frac{dT}{dx} \right)^2 + \frac{d}{dx} \left(\frac{k}{T} \frac{dT}{dx} \right). \quad (10.46)$$

The first two terms in the R.H.S. are always positive, they will increase the entropy when moving downstream. The last term vanishes at the boundaries $x = -\infty$ and $x = +\infty$; integration w.r.t. x yields

$$\rho u (s_2 - s_1) = \int_1^2 \left[\frac{\hat{\mu}}{T} \left(\frac{du}{dx} \right)^2 + \frac{k}{T^2} \left(\frac{dT}{dx} \right)^2 \right] dx, \quad (10.47)$$

which clearly shows that passing a shock in down stream direction increases the entropy.

10.4.6 More about the shock structure

The internal structure of the shock region will now be discussed in more detail.
The equations (10.36), (10.37) and (10.38):

$$J = \rho u,$$

$$K = p + \rho u^2 - \hat{\mu} \frac{du}{dx},$$

$$L = \rho u H - \hat{\mu} u \frac{du}{dx} - k \frac{dT}{dx},$$

are the starting point for such a discussion.

They have to be integrated to get the variation of $u(x)$ and $T(x)$ in the shock zone between the upstream state ①($u = u_1, T = T_1$) and the downstream state ②($u = u_2, T = T_2$) where $\frac{du}{dx} = 0$ and $\frac{dT}{dx} = 0$.

Using $\rho u = J = \text{constant}$, the equations (10.37) and (10.38) may be written in the form:

$$\hat{\mu} \frac{du}{dx} = -K + Ju + \frac{JRT}{u}, \quad (10.48)$$

$$k \frac{dT}{dx} = -L + Ku + J \left(c_v T - \frac{1}{2} u^2 \right), \quad (10.49)$$

a set of O.D.E.'s with $u(x)$ and $T(x)$ as the two unknowns and J, K and L as constants. The ratios K/J and L/J may be interpreted in terms of the variables defining state ①. From:

$$K = p_1 + \rho_1 u_1^2 = \rho_1 RT_1 + Ju_1 = J \left(\frac{RT_1}{u_1} + u_1 \right),$$

$$L = \rho_1 u_1 H_1 = J \left(c_p T_1 + \frac{u_1^2}{2} \right),$$

is obtained that

$$K/J = \frac{RT_1 + u_1^2}{u_1}, \quad L/J = c_p T_1 + \frac{u_1^2}{2}.$$

Introduce the scaled variables $\tilde{u} = \frac{u}{u_1}$, $\theta = \frac{T}{T_1}$, into equations (10.48) and (10.49), this results into the system:

$$\frac{\hat{\mu}}{J} \tilde{u} \frac{d\tilde{u}}{dx} = \tilde{u} (\tilde{u} - 1) + \alpha (\theta - \tilde{u}), \quad (10.50)$$

and

$$\frac{k\alpha}{JR} \frac{d\theta}{dx} = \frac{\alpha}{\gamma - 1} (\theta - 1) + \alpha (\tilde{u} - 1) - \frac{1}{2} (\tilde{u} - 1)^2, \quad (10.51)$$

where α is a parameter defined as:

$$\alpha = RT_1/u_1^2 = (\gamma M_1^2)^{-1}. \quad (10.52)$$

The equations (10.50) and (10.51) form a dynamical system for the variables $\tilde{u}(x)$ and $\theta(x)$. The system is autonomous because the independent variable x is not explicitly present. The various solutions may be viewed as integral paths in the phase plane (\tilde{u}, θ) . For the shock structure problem a solution curve has to be sought that starts in the point $(\tilde{u}, \theta) = (1, 1)$ where $\frac{d\tilde{u}}{dx}$ and $\frac{d\theta}{dx}$ have to be zero and indeed this condition is fulfilled by the equations (10.50) and (10.51).

Our next question will be: starting from uniform state ①: $(\tilde{u}, \theta)_1 = (1, 1)$ is it possible that the flow may change onto another uniform state ②: $(\tilde{u}, \theta)_2 = (\tilde{u}_2, \theta_2)$ which is different from state ①?

To find such a uniform state we take $\frac{d\tilde{u}}{dx} = 0$ and $\frac{d\theta}{dx} = 0$ in equations (10.50) and (10.51) and have to solve:

$$\tilde{u} (\tilde{u} - 1) + \alpha (\theta - \tilde{u}) = 0, \quad (10.53)$$

$$\frac{\alpha}{\gamma - 1} (\theta - 1) + \alpha (\tilde{u} - 1) - \frac{1}{2} (\tilde{u} - 1)^2 = 0. \quad (10.54)$$

There are two solutions: $\tilde{u} = 1$ and $\tilde{u} = \tilde{u}_2$; $\tilde{u} = 1$ represents the original flow (state ①) and $\tilde{u} = \tilde{u}_2$ (state ②) with

$$\tilde{u}_2 = \frac{\gamma - 1 + 2\gamma\alpha}{\gamma + 1}, \quad (10.55)$$

represents a normal shock. Equation (10.55) is equivalent with the well known normal shock relation

$$\frac{u_2}{u_1} = \frac{(\gamma - 1) M_1^2 + 2}{(\gamma + 1) M_1^2}.$$

In the (\tilde{u}, θ) phase plane a solution curve has to be found which runs from state ①: $(\tilde{u}, \theta) = (1, 1)$ to state ②: $(\tilde{u}, \theta) = (\tilde{u}_2, \theta_2)$.

To see whether such a solution curve indeed exists let us do a plane analysis of equations (10.50) and (10.51). To obtain a qualitative impression of the phase portrait the singular points of equations (10.50) and (10.51) are considered.

They appear at:

$$\tilde{u} = 1, \theta = 1 \quad \text{and} \quad \tilde{u} = \tilde{u}_1, \theta = \theta_2.$$

Notice that they represent the uniform states ① and ② between which the solution for the shock structure problem has to be sought. Since state ② is a post-shock state we know that $\tilde{u}_2 < 1$ and $\theta_2 > 1$, implying that point 2 lies above and left from point 1 in the (\tilde{u}, θ) -plane; see figure 10.11.

The points 1 and 2 have Jacobians

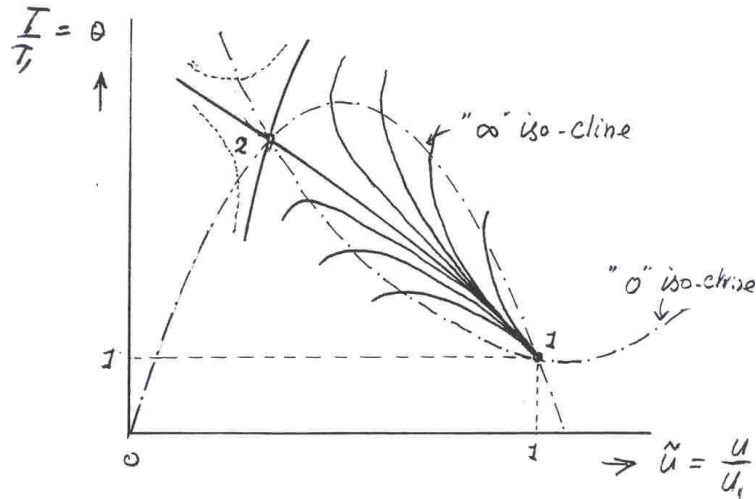


Figure 10.11: Phase plane with some integral curves

$$J_1 = \frac{k\alpha^2 \hat{\mu} R}{\gamma - 1} (1 - \gamma\alpha), \quad J_2 = \frac{k\alpha^2 \hat{\mu} R \tilde{u}_2}{\gamma - 1} (\gamma\alpha - 1)$$

respectively.

Since $0 < \gamma\alpha < 1$ it appears that the uniform state ① is represented by a node and that uniform state ② is represented by a saddle in the phase plane.

The iso-lines $\frac{d\theta}{d\tilde{u}} = 0, \infty$ are parabolas:

$$\begin{aligned}\frac{d\theta}{d\tilde{u}} = 0 & : \theta = \frac{\gamma-1}{2\alpha} (\tilde{u} - 1)^2 - (\gamma - 1)(\tilde{u} - 1) + 1 \quad , \\ \frac{d\theta}{d\tilde{u}} = \infty & : \theta = -\frac{\tilde{u}^2}{\alpha} + \frac{1+\alpha}{\alpha}\tilde{u}\end{aligned}$$

They are depicted in figure 10.11 which also shows some integral curves emanating from the singularity at $\tilde{u} = 1, \theta = 1$. The phase portrait as it is built up with integral curves reveals that an infinite number of integral curves start from uniform state ① but that only one of them terminates at the uniform state ②. So there is just one unique solution describing the shock structure between pre-state ① and post-state ②.

To find this unique solution analytically we have to solve equations (10.50) and (10.51) together with the boundary conditions $\tilde{u} = 1, \theta = 1$ and $\tilde{u} = \tilde{u}_2, \theta = \theta_2$. This problem is hard to solve and a solution for the general problem where $\hat{\mu}$ and k are still functions of the temperature is still not available. However various attempts have led to some interesting solutions valid for special cases. Two examples of special solutions: the Taylor solution and the Becker solution will be introduced (briefly) in the next section (10.4.7). More interesting details about the shock structure problem may be found in the excellent text: Von Mises (1958)³ ch. III, art. 11.

When an attempt is made to construct a numerical approximation of the shock structure it is very likely that the numerical iteration procedure does not converge if the pre-shock state ① is taken as starting point of the numerical process.

The nodal character of state ① implies that an infinite number of integral curves emanate from the starting point and all these curves diverge when they leave the neighbourhood of state ①. This divergent behaviour causes a growing deviation of the numerical path with respect to the exact path which connects states ① and ②.

The saddle character of state ② let the numerical path bypass state ② so that the boundary condition which states that the integral path should terminate in state ② is not (approximately) fulfilled by the numerical computation.

A careful look at figure 10.11 suggests that a smooth and converged solution is expected if the post-shock state ② is taken as starting point in the numerical process. The integral path followed by the numerical marching procedure converges to the exact integral curve because the integral curves converge in marching direction so that small deviations between the computational and exact path are suppressed naturally.

Figure 10.12 shows a typical curve for the shock structure region obtained by numerical calculation for $M_1 = 2.0$, $\gamma = 1.4$ and $Pr = \frac{\mu c_p}{k} = \frac{3}{4}$. The dependence of the viscosity with temperature is modelled with the power-law assumption $\mu = \mu_1(\theta)^{0.76}$.

10.4.7 Special solutions for the shock structure problem

Two special solutions of equations (10.50) and (10.51) may attract our attention. The first one is discussed by Taylor who took the assumption of zero heat conduction.

³Richard von Mises (1958), Mathematical Theory of Compressible Fluid Flow, Academic Press, Inc.

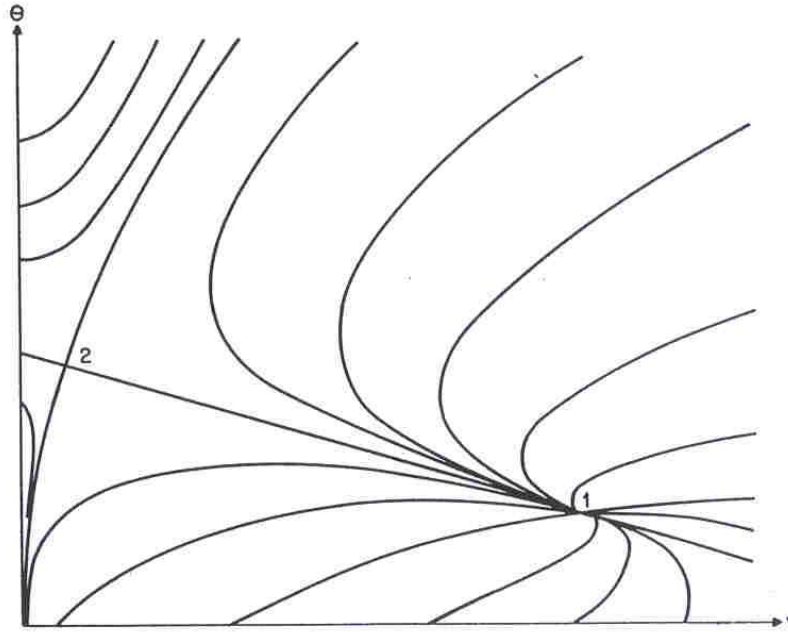


Figure 10.12: Integral curves for Mach number $M_1 = 2.0$, $\gamma = 1.4$ and Prandtl number $Pr = \frac{3}{4}$. The transition curve from 1 to 2 is a straight line (from von Mises (1958)).

Taylor's solution (no heat conduction, $k = 0$)

G.I. Taylor has shown that equations (10.50) and (10.51) can be integrated in closed form when the thermal conductivity k is set to zero. This is not a realistic assumption, since it is known that the ratio μ/k varies with temperature. However the solution is of interest because some principle flow features are already present under the assumption $k = 0$. Taking $k = 0$, equations (10.50) and (10.51) become:

$$\frac{\hat{\mu}}{J} \tilde{u} \frac{d\tilde{u}}{dx} = \tilde{u}(\tilde{u} - 1) - \alpha\tilde{u} + \alpha\theta, \quad (10.56)$$

with

$$\theta = 1 + \frac{\gamma - 1}{\alpha} \frac{(\tilde{u} - 1)^2}{2} - (\gamma - 1)(\tilde{u} - 1). \quad (10.57)$$

Eliminating θ there follows

$$\frac{\hat{\mu}}{J} \tilde{u} \frac{d\tilde{u}}{dx} = \frac{(\gamma + 1)}{2} \tilde{u}^2 - \gamma(1 + \alpha)\tilde{u}^2 - \gamma(1 + \alpha)\tilde{u} + \frac{1}{2}(\gamma - 1) + \gamma\alpha. \quad (10.58)$$

Except from a scale factor J and a translation of x , the solution of this equation only depends on the parameter α .

From equation (10.53) and (10.54) it is obvious that the uniform states $\tilde{u} = \tilde{u}_1 = 1$ and $\tilde{u} = \tilde{u}_2$ are roots of the right-hand side of equation (10.58) implying that it can be written as

$$\frac{\hat{\mu}}{J} \tilde{u} \frac{d\tilde{u}}{dx} = -\frac{(\gamma + 1)}{2}(1 - \tilde{u})(\tilde{u} - \tilde{u}_2). \quad (10.59)$$

When $\hat{\mu}$ can be taken constant, equation (10.59) can be integrated leading to the analytical solution as introduced by Taylor:

$$x = \frac{2}{\gamma + 1} \frac{\hat{\mu} \ln(1 - \tilde{u}) - \tilde{u}_2 \ln(\tilde{u} - \tilde{u}_2)}{J} \frac{(1 - \tilde{u}_2)}{(1 - \tilde{u})}. \quad (10.60)$$

Notice that for $x \rightarrow -\infty$, $\tilde{u} \rightarrow \tilde{u}_1 = 1$ and for $x \rightarrow \infty$, $\tilde{u} \rightarrow \tilde{u}_2$; consequently equation (10.60) describes transition from the pre-shock state onto the post-shock state which occurs in the interval $(-\infty, \infty)$.

In studying the transition and in particular a shock thickness estimate, consider two intermediate values u_ϵ^- and u_ϵ^+ defined as $u_\epsilon^- = 1 - \epsilon(1 - \tilde{u}_2)$ and $u_\epsilon^+ = \tilde{u}_2 + \epsilon(1 - \tilde{u}_2)$. ϵ is any number satisfying $0 < \epsilon < 1/2$.

The x -locations where u_ϵ^- and u_ϵ^+ appear in the transition region are x^- and x^+ respectively; they follow from

$$x^\pm = \frac{2}{\gamma + 1} \frac{\hat{\mu} \ln(1 - \tilde{u}_\epsilon^\pm) - \tilde{u}_2 \ln(\tilde{u}_\epsilon^\pm - \tilde{u}_2)}{J} \frac{(1 - \tilde{u}_2)}{(1 - \tilde{u})},$$

and differ by the amount

$$\Delta x = x^+ - x^- = \frac{2}{\gamma + 1} \frac{\hat{\mu}}{J} \frac{1 + \tilde{u}_2}{1 - \tilde{u}_2} \ln \frac{1 - \epsilon}{\epsilon}.$$

For given values of the flux J and the shock strength as expressed in terms of \tilde{u}_2 , the right-hand side tends to zero as $\hat{\mu}$ decreases no matter how small ϵ may be.

Let us for example calculate the shock thickness in air in a windtunnel experiment. Assume the tunnel is driven with settling chamber conditions $p_t = 5$ bar, $T_t = 228$ K. Assume a normal shock appears at $M = 2$. The pre-shock conditions are: $p_1 = 0.639$ bar, $\rho_1 = 1.39$ kg/m³ and $T_1 = 160$ K; the post-shock conditions are: $p_2 = 2.88$ bar, $\rho_2 = 3.71$ kg/m³ and $T_2 = 270$ K. The velocities in front of and behind the shock are respectively $u_1 = 507.14$ m/s and $u_2 = 190.15$ m/s.

If we take $\epsilon = 0.05$ then we find $\Delta x = 0.14 \times 10^{-3}$ mm. Thus, since the total velocity drop $u_1 - u_2 = 317$ m/s, then 90 percent of this drop is effected within a distance of 0.00014 mm! This is a significant result: the thickness of the layer within which the major part of the transition from pre-state ①to post-state ②occurs tends towards zero with $\hat{\mu} \rightarrow 0$ and is actually extremely small in air under normal conditions.

Becker's solution Becker has found an exact solution of the complete problem, equations (10.50) and (10.51), in the case that the Prandtl number: $Pr = \frac{\mu c_p}{k} = \frac{3}{4}$. The complete problem is described by the system of first order O.D.E.'s, given in equations (10.50) and (10.51) given in the unknowns \tilde{u} and θ . One could eliminate either \tilde{u} or θ to obtain a second-order differential equation for θ or \tilde{u} respectively. The resulting equation however would not be easy to handle and a better procedure is to eliminate x by dividing the two O.D.E.'s obtaining

$$\frac{d\theta}{\tilde{u} d\tilde{u}} = \frac{\hat{\mu} R}{k \alpha} \frac{\frac{\alpha}{\gamma-1} (\theta - 1) + \alpha (\tilde{u} - 1) - \frac{1}{2} (\tilde{u} - 1)^2}{\tilde{u} (\tilde{u} - 1) + \alpha (\theta - \tilde{u})}. \quad (10.61)$$

The coefficient $\frac{\hat{\mu} R}{k}$ is a dimensionless quantity very close related to the Prandtl number:

$$\frac{\hat{\mu} R}{k} = \frac{\hat{\mu} c_p}{k} \frac{\gamma - 1}{\gamma} = \frac{4}{3} \frac{\mu c_p}{k} \frac{\gamma - 1}{\gamma} = \frac{4}{3} \frac{\gamma - 1}{\gamma} Pr. \quad (10.62)$$

Observe that the Stokes hypothesis: $\lambda = -2/3\mu$ is used to write $\hat{\mu} = 2\mu + \lambda = \frac{4}{3}\mu$. For dry air under normal conditions the Prandtl number varies only slightly, roughly between 0.68 and 0.77.

Becker observed in 1922 that for $Pr = 3/4$ equation (10.61) results in an exact solution:

$$\theta - 1 = \frac{\gamma - 1}{2\gamma\alpha} (1 - \tilde{u}^2). \quad (10.63)$$

When this solution is expressed in terms of the dimensional variables u and T one finds

$$\frac{u^2}{2} + \frac{\gamma}{\gamma - 1} RT = \frac{u^2}{2} + c_p T = \text{constant}. \quad (10.64)$$

The total enthalpy is constant through the whole shock zone. But if that is true then one must conclude from equation (10.38) that $\frac{du}{dx}$ and $\frac{dT}{dx}$ are related such that

$$(\lambda + 2\mu) u \frac{du}{dx} + k \frac{dT}{dx} = 0,$$

or

$$\frac{dT}{udu} = -\frac{\hat{\mu}}{k} = \frac{\frac{3}{4}Pr}{c_p},$$

which corresponds exactly with the value of $\frac{1}{T} \frac{dT}{du}$ that is obtained from equation (10.63) with a Prandtl number of $\frac{3}{4}$.

In the Becker solution the viscous dissipation and heat conduction are in balance resulting into a constant total enthalpy in the entire shock zone.

10.4.8 Entropy behaviour in the shock zone

In this section we will investigate some properties of the behaviour of the entropy in the shock zone. One reason to do this investigation is that we want to know how the total entropy rise is built up in the shock zone. Are there parts in the shock zone that are almost isentropic and are there other parts in the shock zone that are responsible for the main part of the entropy rise? Regarding these questions let us take a particular example e.g. a shock wave in air ($\gamma = 1.4$) at a Mach number $M = 2$. Let us study the Taylor shock and the Becker shock as well.

In scaled variables the Taylor shock is governed by, (see equation (10.57))

$$\theta_{\text{Taylor}} = 1 + \frac{\gamma - 1}{\alpha} \frac{(\tilde{u} - 1)^2}{2} - (\gamma - 1)(\tilde{u} - 1),$$

and the Becker solution gives (equation (10.62))

$$\theta_{\text{Becker}} = 1 + \frac{\gamma - 1}{2\gamma\alpha} (1 - \tilde{u})^2.$$

For both shocks the transport coefficients μ and k are assumed to be constant. In the particular situation $M_1 = 2$ the parameter α takes the value $\alpha = 5/28$ and the post-shock conditions are $u_2 = 0.375u_1$ ($\tilde{u}_2 = 0.375$), $T_2 = 1.6875T_1$ ($\theta_2 = 1.6875$).

The velocity-temperature relation in the shock interior has graphs that may be viewed in figure

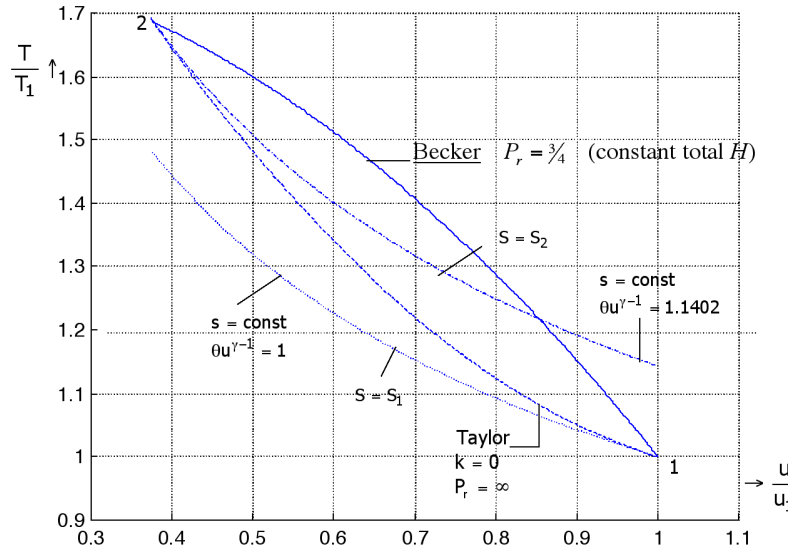


Figure 10.13: Taylor and Becker solution for the shock structure.

10.13. Obviously the Taylor shock and the Becker shock have states ① and ② in common but otherwise their behaviour differs substantially. A striking difference appears when considering the entropy. Figure 10.13 shows two entropy level curves; one carrying the pre-state value s_1 and the other carrying the post-state value s_2 . Taking the pre-state as reference, the entropy can be calculated from

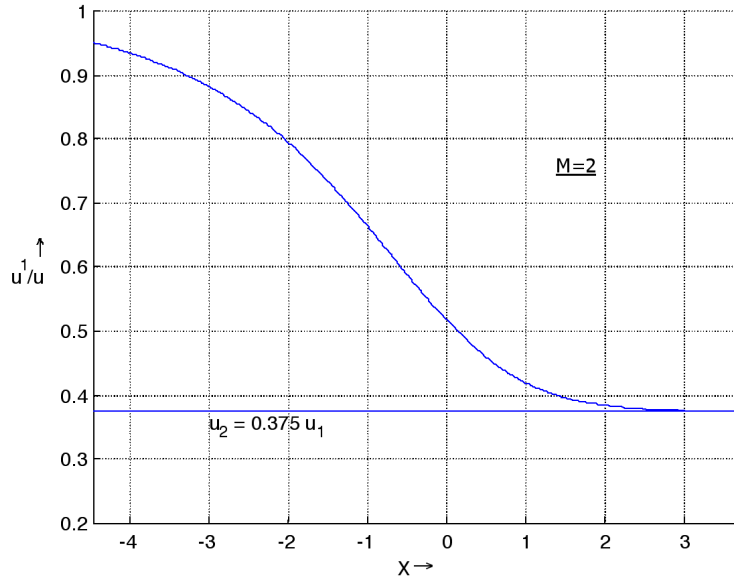
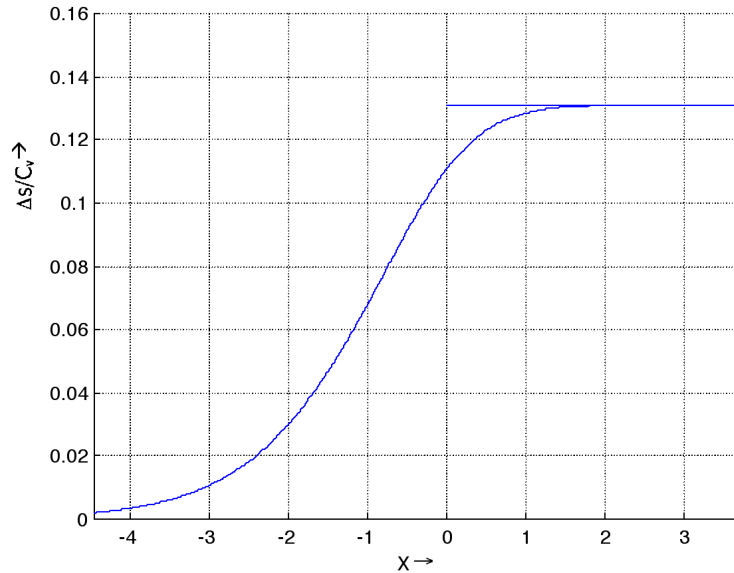
$$\frac{s - s_1}{c_v} = \ln \theta + (\gamma - 1) \ln \tilde{u}. \quad (10.65)$$

From figure 10.13 one observes that the curve representing the Taylor shock intersects each entropy level curve only once implying a monotonic increase of entropy when following a particle downstream. Since the Taylor curve is tangent (the proof is left to the reader) to the entropy level curves s_1 and s_2 the streamwise entropy gradient is zero far upstream ($x \rightarrow -\infty$) and far downstream ($x \rightarrow +\infty$). A numerical calculation of the entropy distribution in the shock zone of the Taylor shock (figure 10.15) reflects this observation. The most typical characteristic of the Taylor shock is the absence of heat conduction in the shock zone. Of course severe temperature gradients appear but due to the assumption $k = 0$ no heat will be transferred between adjacent fluid particles. So the energy content of a fluid element can only be changed by work; done by pressure forces and/or viscous (normal) forces. To get some physical insight in this process let us study the breakdown of energy into its constituting components like internal energy, kinetic energy, work done by viscous forces and work done by pressure forces. Let us start by considering the energy equation for 1-dimensional steady flow in the form of equation (10.38)

$$L = \rho u H - \hat{\mu} \frac{udu}{dx} - k \frac{dT}{dx} = \text{constant},$$

or with $k = 0$ (Taylor shock) and inserting $H = E + \frac{p}{\rho}$

$$L = \rho u E + pu - \hat{\mu} u \frac{du}{dx},$$

Figure 10.14: Velocity decrease in a Taylor shock at $M_1 = 2$.Figure 10.15: Entropy increase in a Taylor shock at $M_1 = 2$.

or

$$E + \frac{pu}{J} - \frac{\hat{\mu}u}{J} \frac{du}{dx} = \frac{L}{J} = \text{constant.} \quad (10.66)$$

The first term represents the total energy (E), being the sum of the internal energy (e) and the kinetic energy ($\frac{1}{2}u^2$). The second term is the energy needed to run against the adverse pressure gradient. The third term is the energy needed to overcome viscous normal stresses.

In case of the Taylor shock these terms may be calculated as follows:

internal energy:

$$E_i = \frac{c_v T}{u_1^2} = \frac{\alpha \theta}{\gamma - 1},$$

kinetic energy:

$$E_k = \frac{1}{2} \frac{u^2}{u_1^2} = \frac{1}{2} \tilde{u},$$

work done by pressure forces:

$$W_p = \frac{p u}{J u_1^2} = \alpha \theta,$$

work done by viscous forces:

$$W_v = -\frac{\mu u}{J u_1^2} \frac{du}{dx} = -\tilde{u} (\tilde{u} - 1) + \alpha \tilde{u} - \alpha \theta.$$

Note that the kinetic energy of the pre-state: u_1^2 is chosen as a reference.

The energy breakdown for a Taylor shock at $M_1 = 2$ is calculated in table 10.1 and depicted in figures 10.16 and 10.17. Due to the assumption of a Taylor shock, which gives a relation between velocity and temperature, the internal energy E_i and kinetic energy E_k are coupled. In figure 10.16 we see a monotonic increase of internal energy and mutually a monotonic decrease of kinetic energy when passing the shock in downstream direction. The energy needed to run against the adverse pressure gradient is also increasing monotonically.

The energy needed to overcome viscous forces is growing in the low pressure part of the

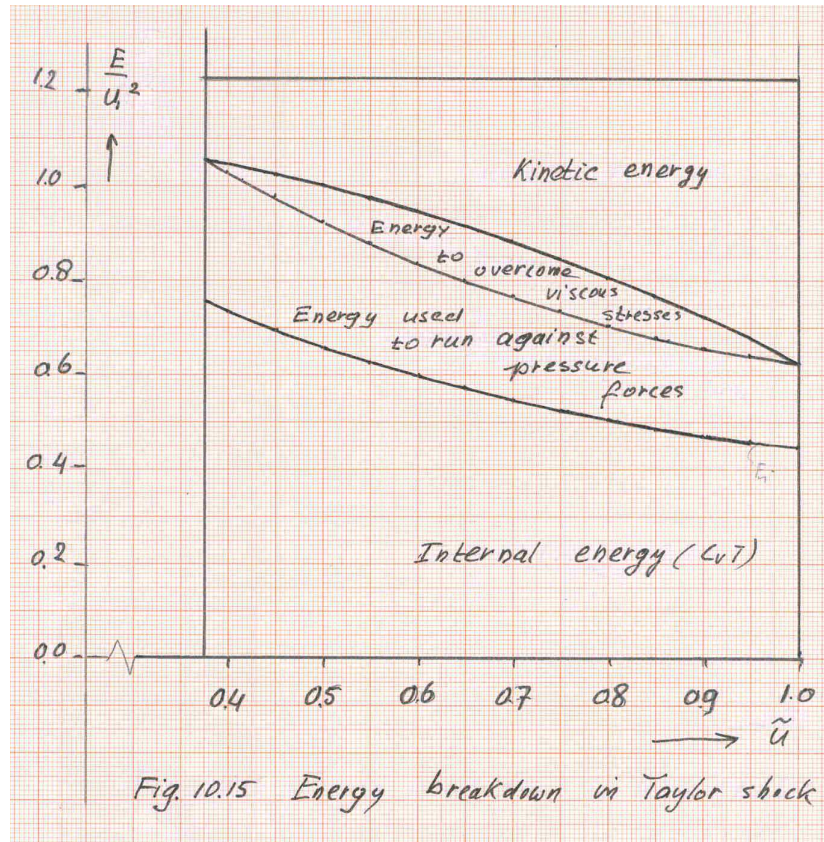


Figure 10.16: Energy breakdown in a Taylor shock.

shock, it reaches a maximum at about $\tilde{u} = 0.7$, then it decreases to zero at the post state. From figure 10.17 we conclude that a fluid element that passes a shock experiences a decrease of total energy (E) in the front part of the shock caused by the fact that the strong decrease of kinetic energy is not sufficiently compensated by the moderate increase of internal energy. In

\tilde{u}	θ	E_i	E_k	E	W_p	H	W_v
1.0	1.0	0.4464	0.5000	0.9464	0.1786	1.1250	0
0.95	1.023	0.4567	0.4513	0.9080	0.1827	1.0907	0.0343
0.90	1.051	0.4692	0.4050	0.8742	0.1877	1.0619	0.0631
0.85	1.085	0.4844	0.3613	0.8457	0.1938	1.0395	0.0755
0.80	1.125	0.5022	0.3200	0.8222	0.2009	1.0231	0.1019
0.75	1.170	0.5223	0.2813	0.8036	0.2089	1.0125	0.1125
0.70	1.221	0.5450	0.2450	0.7900	0.2180	1.0080	0.1170
0.65	1.277	0.5701	0.2113	0.7814	0.2280	1.0094	0.1156
0.60	1.339	0.5978	0.1800	0.7778	0.2391	1.0169	0.1081
0.55	1.407	0.6281	0.1513	0.7794	0.2513	1.0307	0.0943
0.50	1.480	0.6607	0.1250	0.7857	0.2643	1.0500	0.0750
0.45	1.559	0.6960	0.1013	0.7973	0.2784	1.0757	0.0493
0.40	1.643	0.7335	0.0800	0.8135	0.2934	1.1069	0.0181
0.375	1.6875	0.7533	0.0703	0.8236	0.3014	1.1250	0

Table 10.1: Energy breakdown in Taylor shock

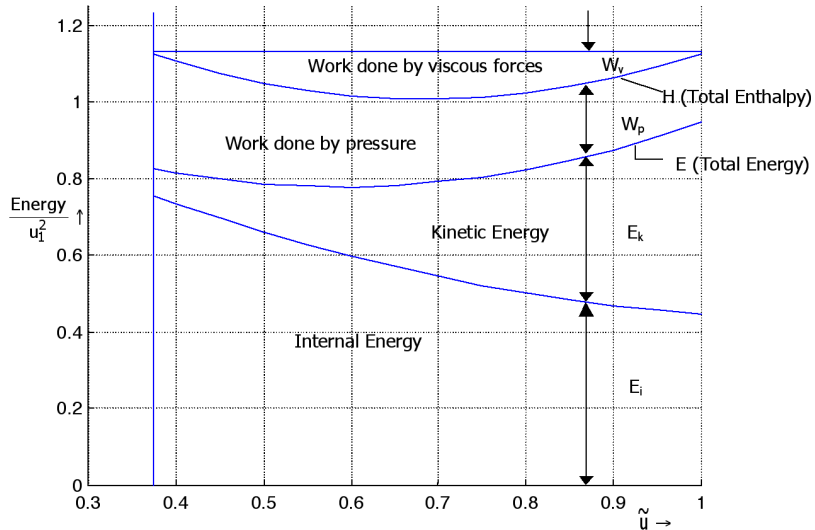


Figure 10.17: Energy breakdown in a Taylor shock.

this front part of the shock the loss of kinetic energy is used to overcome the adverse pressure gradient and the work against viscous normal stresses. In the aft part of the shock zone the total energy (E) starts recovering. Observe that due to viscous forces the total enthalpy is not constant here; passing the shock we see first a decrease of H and further downstream an increase of H .

Finally let us pay attention to the Becker shock and in particular to the entropy variation through the shock. First we remember that the Becker shock is characterized by a perfect balance between viscous dissipation and heat conduction resulting into a constant total enthalpy through the entire shock zone.

Concerning entropy it appears (figure 10.13) that this parameter attains a maximum value:

s_{\max} somewhere in the shock zone and being larger than its post-state value s_2 . To understand this entropy overshoot let us consider the entropy distribution as calculated for the Becker shock having $M_1 = 2$ and as shown in figure 10.18.

Obviously a maximum appears at $\tilde{u} \approx 0.6$. This maximum is about 1.6 times larger than its

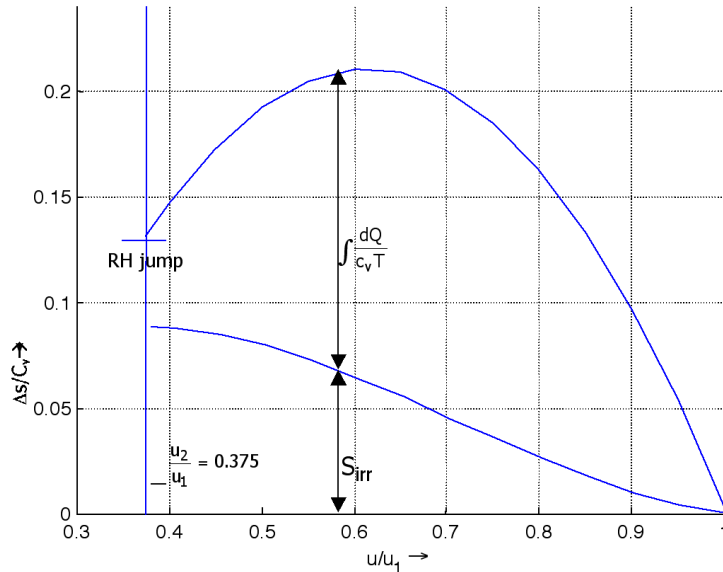


Figure 10.18: Breakdown of entropy in a Becker shock at $M_1 = 2$.

post-state value!

As we know, the heat flux is related to temperature gradients. Consider a small one-dimensional fluid element and in particular the heat flux through its upstream face and its downstream face. As long as this fluid element resides in the front part of the shock, the temperature gradient at the upstream face is higher than at the downstream face. So in the front part of the shock there is a net influx of heat into the fluid element. Fluid elements residing in the aft part of the shock experience higher temperature gradients at the downstream face than those at their upstream face. Therefore in the aft part of the shock fluid elements experience a net outflux of heat.

It is this changing behaviour of net heat flux that is responsible for the entropy overshoot we have discovered in figure 10.18.

In order to understand this more clearly let us breakdown the entropy according to its definition:

$$s = \int \frac{dQ}{T} + \int ds_{\text{irr}}, \quad (10.67)$$

into a part that comes from the heat flux and into the irreversible part.

Since dQ changes from positive to negative when moving downstream through the shock we expect a maximum of $\int \frac{dQ}{T}$ somewhere inside the shock. Let dQ be calculated as follows: consider a one-dimensional fluid element of unit mass and having a length ℓ , see figure 10.19. Due to mass conservation the length of the fluid element varies with the density as $\rho\ell = 1$. The heat flux into the fluid element through its upstream face is

$$d\dot{Q}_{\text{in}} = k \left(\frac{dT}{dx} \right)_{x+\ell} = k \left\{ \left(\frac{dT}{dx} \right)_x + \left(\frac{d^2T}{dx^2} \right)_x \ell \right\}.$$

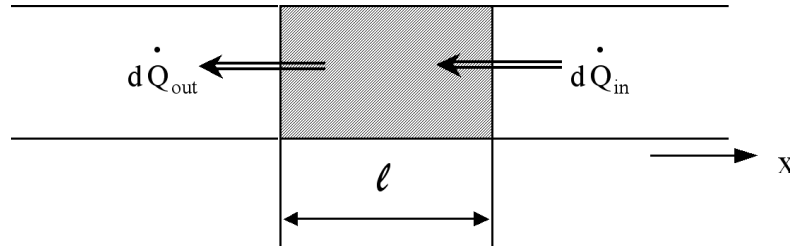


Figure 10.19: Heat flux into a one dimensional fluid element.

The heat flux that leaves the fluid element through its downstream face is

$$d\dot{Q}_{\text{out}} = k \left(\frac{dT}{dx} \right)_x .$$

The net heat flux during a time lapse dt then becomes:

$$dQ = \left(d\dot{Q}_{\text{in}} - d\dot{Q}_{\text{out}} \right) = k \left(\frac{dT}{dx} \right)_x \ell dt .$$

Since the fluid element itself moves with the velocity u the net heat influx during a traveling distance dx is:

$$dQ = k \left(\frac{d^2T}{dx^2} \right) \frac{\ell dx}{u} .$$

Finally using $\rho\ell = 1$ (conservation of mass) and $\rho u = J$ is constant we find

$$\frac{dQ}{T} = \frac{k}{JT} \frac{d^2T}{dx^2} dx = \frac{k}{JT} \frac{d^2T}{dx^2} \frac{du}{dx} . \quad (10.68)$$

This expression is now evaluated for the Becker shock by substituting:

$$k \frac{dT}{dx} = -J \frac{\gamma + 1}{2\gamma} u^2 + Ku - \frac{\gamma - 1}{\gamma} L ,$$

and

$$\hat{\mu} \frac{du}{dx} = J \frac{\gamma + 1}{2\gamma} u - K + \frac{\gamma - 1}{\gamma} \frac{L}{u} ,$$

which leads to the final expression

$$\frac{dQ}{c_v T} = \frac{\gamma - 1}{\gamma \alpha \theta} \{ \gamma (1 + \alpha) - (\gamma + 1) \tilde{u} \} d\tilde{u} . \quad (10.69)$$

Inserting the Becker solution:

$$\theta = 1 + \frac{\gamma - 1}{2\gamma \alpha} (1 - \tilde{u}^2) ,$$

equation (10.69) can be integrated giving the result

$$\int \frac{dQ}{c_v T} = \frac{\gamma (1 + \alpha)}{B} \ln \frac{(B + \tilde{u})(B - 1)}{(B - \tilde{u})(B + 1)} + (\gamma + 1) \ln \theta , \quad (10.70)$$

where $B^2 = 1 + \frac{2\gamma\alpha}{\gamma+1}$ and where the pre-state $\tilde{u} = 1$, $\theta = 1$ is chosen as the reference state.

Figure 10.18 is now completed by showing the behaviour of $\int \frac{dQ}{c_v T}$ through the shock zone. As was expected $\int \frac{dQ}{c_v T}$ attains a maximum value and causes the entropy overshoot which is already mentioned. Furthermore we see in figure 10.18 that the irreversible part of the entropy s_{irr} increases continuously when moving downstream. This irreversible part of the entropy can be attributed to the presence of viscous normal stresses. To verify this statement consider equation (10.45):

$$JT \frac{ds}{dx} = \frac{d}{dx} \left(\hat{\mu} u \frac{du}{dx} \right) + \frac{d}{dx} \left(k \frac{dT}{dx} \right) - u \frac{d}{dx} \left(\hat{\mu} \frac{du}{dx} \right).$$

Equation (10.68) can be used to eliminate $\frac{d}{dx} (k \frac{dT}{dx})$

$$JT \frac{ds}{dx} = \frac{d}{dx} \left(\hat{\mu} u \frac{du}{dx} \right) + J \frac{dQ}{dx} - u \frac{d}{dx} \left(\hat{\mu} \frac{du}{dx} \right),$$

or

$$J \frac{ds}{dx} = \frac{1}{T} \left\{ \hat{\mu} \left(\frac{du}{dx} \right)^2 \right\} + \frac{J dQ}{T dx}. \quad (10.71)$$

This equation may be compared to equation (10.67) where we have given the usual breakdown of entropy into a part that comes from the heat flux and into an irreversible part. Comparison shows that the viscous term $\hat{\mu} \left(\frac{du}{dx} \right)^2$ causes the irreversibility of the shock wave.